Son Of X-Shooter

SOXS

EXPOSURE TIME CALCULATOR DESIGN AND PERFORMANCE ESTIMATES

	NAME	SIGNATURE	DATE
PREPARED	M. Genoni	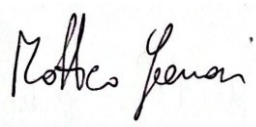	2026-03-30
APPROVED	P. Schipani		2026-03-30
RELEASED	S. Campana		2026-03-30

With contributions from: A. Scaudo (INAF-OAB), L. Cabona (INAF-OAB) - M. Landoni (INAF-OAB) – P. D'Avanzo (INAF-OAB).

CHANGE RECORD

ISSUE	DATE	SECTION/PARAGRAPH AFFECTED	REASON/INITIATION DOCUMENTS/REMARKS
1.0	2018-06-30	All	First issue for FDR
1.1	2019-09-30	3.5 – 3.6.1 – 3.8.1 – 3.8.2	Update for NIR detector acquisition
1.2	2021-05-30	All	Update for PAE documentation
1.3	2021-08-05	3.10	Unit tests section added
1.4	2021-08-31	APPENDIX 1 and 2	Details on all elements efficiency
1.5	2022-08-11	All	Minor corrections
1.6	2023-09-29	3.3.6 – 3.4.7 – 3.6.4 – 3.8	Imaging mode
1.7	2024-09-02	3.3.1 – 3.3.2 – 3.3.3 – 3.3.4 3.4.6 – 3.8.1	Updated UV-VIS detector read-out modes
		3.9	Thermal Noise included from real tests in AIT labs
1.8	2026-03-10	3.3.1 – 3.3.2 – 3.3.3 – 3.3.4	Updated UV-VIS detector read-out modes
		3.4.2	Clarification on the variation of Telescope efficiency values considered and the current one agreed with ESO.
		3.5.1 and 3.5.2 3.8.1 – 3.8.2 – 3.8.3	Update on the Input and Results from the ETC web-page
		4	New section 4 pointing to the Commissioning Report for on-sky ETC tests and verification

TABLE OF CONTENTS

1 Purpose and Scope of the Document

Purpose of this document is to provide a description of the current version of the ETC for SOXS, what it requires in terms of input from the user, and what will be produced as output. It also specifies the data relevant for the present status and future update and development of the ETC in the view of the forthcoming SOXS PAE milestone.

2 List of Reference Documents

2.1 Reference Documents

Ref.	Document title	Document ID
[RD1]	Data flow for VLT/VLTI instruments : Deliverables Specifications	VLT-SPE-ESO-19000-1618 Issue 3 - 2011-02-01
[RD2]	Common Pipeline Library	http://www.eso.org/sci/software/cpl/
[RD3]	SOXS Optical Design 1.4	SOXS-TRE-0001
[RD4]	SOXS Software Design 2.0	SOXS-SPE-0002
[RD5]	SOXS Operation Plan 2.0	SOXS-PLA-0002
[RD6]	VIS Detector System Design 1.1	SOXS-TRE-0005
[RD7]	NIR Detector System Design 1.1	SOXS-TRE-0006
[RD8]	Acquisition Camera	SOXS-TRE-0009
[RD9]	SOXS Commissioning Report	SOXS-TRE-0079
[RD10]	PESSTO: survey description and products from the first data release by the Public ESO Spectroscopic Survey of Transient Objects - Smartt, S. J. ; Valenti, S et al.	A&A 579, A40 (2015) DOI https://doi.org/10.1051/0004-6361/201425237

3 ETC Specifications

3.1 Overview

This section provides a description of how the ETC for SOXS should work, what it requires in terms of input from the user, and what will be produced as output. It also specifies the data relevant for the development of the ETC.

3.2 Instrument Summary

SOXS is a single-object wide-band spectrograph for the NTT (it will be installed at one of the Nasmyth foci of the NTT) covering in a single exposure the spectral range from the UV to the NIR (350-2000 nm). The instrument is designed to maximize the sensitivity in the spectral range through the splitting in two arms (paths) with optimised optics, coatings, dispersive elements and detectors. It operates at intermediate resolutions (R=3500-6000, depending on wavelength and slit width) sufficient to address quantitatively a vast number of astrophysical questions.

SOXS consists of a central structure (the backbone) that supports two distinct spectrographs, one operating in the UV-VIS 350-850 nm and the other in the NIR 800-2000 nm wavelength ranges. The two arms are fed by the light coming through a common opto-mechanical system (the Common Path). It redirects the light from the telescope focus to the spectrograph slits through relay optics reducing the F/number and compensating for the atmospheric dispersion (only in the UV-VIS, where the dispersion at large zenith angles is unacceptably large). The Common Path provides also the mechanism to drive the light to/from the other instrument subsystems, i.e. the acquisition camera and the calibration unit. Figure provides a functional schematic describing the system.

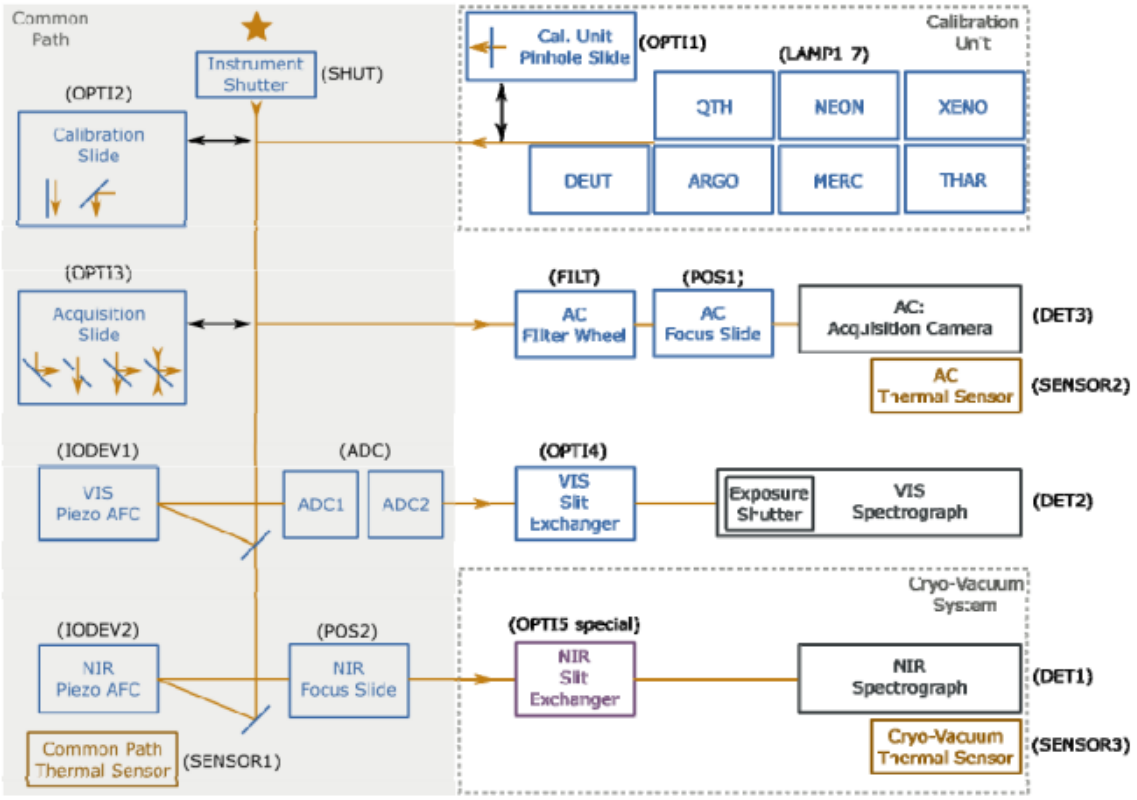

Figure 1. Functional schematic describing the system.

The light coming from the telescope goes through an instrument shutter used as a safety cover and for blocking any spurious light from the telescope side during calibrations. Two slides allow for the operations of the calibration unit and the acquisition camera. The calibration slide allows us to select between the light coming from the calibration and flat-field lamps, and the one from the telescope side. The UV-VIS spectrograph arm is based on a novel multi-grating concept (see [RD2]), in which the incoming beam is partitioned into four polychromatic beams using dichroic surfaces, each covering a waveband range of ~100 nm. Each quasi-order is diffracted by an ion-etched grating. The detector, located 4 mm behind the camera field flattener back surface, is an e2V CCD44-82 CCD (see [RD2] and [RD6] for details).

The near infrared spectrograph is a cross-dispersed echelle, with R~5000 (for 1 arcsec slit), covering the wavelength range from 800 to 2000nm with 15 orders. It is based on the 4C concept (see [RD2]), characterised by a very compact layout, reduced weight of optics and mechanics, good stiffness and high efficiency. The spectrograph is composed of a double pass collimator and a refractive camera, a grating disperser main and a prism-based cross disperser. The detector is a Teledyne H2RG array operated at 40K, i.e. below its nominal working temperature of 77K (see RD2 and [RD7] for details).

The main components of the acquisition camera (see [RD8] for details) are a CCD detector, the focal reducer optics, a re-focuser linear stage, a flat 45° folding mirror configurable in different positions (for different operative modes), a filter wheel with 6 LSST (u, g, r, i, z, y) + 1 V Johnson filters + 1 free position for the slit viewer. The camera detector will be the Andor iKon M934, using a CCD sensor BEX2-DD (Back Illuminated CCD, Deep Depletion with fringe suppression, extended range dual AR coating) 1024x1024 with 13 µm pixel size, low readout noise, negligible dark current with industry-leading thermoelectric cooling down to -100°C.

The calibration unit is designed to provide the calibration spectra to remove the instrument signatures and convert the observed spectrum into one with physical units (in wavelength and flux). The calibration spectra are generated using a synthetic light source, adopting an integrating sphere equipped with lamps suitable for wavelength and flux calibrations across the full wavelength range of the instrument (350-2000 nm). The following lamps are used:

- Quartz-tungsten-halogen (QTH) lamp, for flux calibration 500-2000 nm;
- Deuterium (D2) lamp, for flux calibration 350-500 nm (used simultaneously with QTH lamp for UV-VIS arm flux calibration);
- NeArHgXe pen-ray lamps bundled together, for NIR wavelength calibration. The individual lamps are controlled to operate together as one lamp;
- ThAr hollow cathode lamp, for UV-VIS wavelength calibration.

3.3 Instrument Configuration

The possible operative modes of the instrument in the 2 spectral channels (UV-VIS and NIR) are related to the 4 slit widths foreseen for each channel (see next subsections). In addition in the UV-VIS spectrograph, the CCD detector of has different possible read-out options. The optical path is different within the UV-VIS spectrograph according to the specific band (u, g, r, i).
The imaging mode is operated with the Acquisition Camera.

3.3.1 UV-VIS Spectrograph u-band

Spectral range: 3500 – 4400 Å.

Elements permanent:

- Common path: Dichoric (in reflection, CP_DCR, cut-off at 8300 Å), folding mirror (CP_FM_VIS), the ADC assembly (CP_LVIS_01 and CP_LVIS_02; the assembly is actually composed of two double prisms with two doublets, glued on the prisms), tip/tilt mirror (CP_TT_VIS) and a field lens (CP_LVIS_03).

- Spectrograph: folding mirror, off-axis parabola (OAP, reflection), first dichroic (reflection, cut-off at 5350 Å), folding mirror (u+g), second dichroic (reflection, cut-off at 4350 Å), disperser, Camera Corrector (2 x Refraction), Camera Mirror (reflection), CCD window (Field Flattener, 2 x Refraction).

Elements variable: slits of different widths: 0.5 – 1.0 – 1.5 – 5.0 arcsec.

CCD: 2048 x 4096 pixels, 30.7 x 61.4 mm; Pixel size 15 µm; Read-out modes binning(spatial x spectra) 1X1, 2x1, 2x2; Implemented Gain (e^- /ADU) High Gain 1.1, Low Gain: 2.0; Implemented Detector Read-out Noise (e- RMS) Low noise mode: <3.5e- rms^-, Fast mode: 5.1e- rms^-.
These info are also shown in the Web-Page as explained in subsection 3.8.1.
Other parameters and details are given in [RD6].

3.3.2 UV-VIS Spectrograph g-band

Spectral range: 4300 – 5450 Å.

Elements permanent:

- Common path: Dichoric (in reflection, CP_DCR, cut-off at 8300 Å), folding mirror (CP_FM_VIS), the ADC assembly (CP_LVIS_01 and CP_LVIS_02; the assembly is actually composed of two double prisms with two doublets, glued on the prisms), tip/tilt mirror (CP_TT_VIS) and a field lens (CP_LVIS_03).

- Spectrograph: folding mirror, off-axis parabola (OAP, reflection), first dichroic (reflection, cut-off at 5350 Å), folding mirror (u+g), second dichroic (transmission, cut-off at 4350 Å), folding mirror (g), disperser, Camera Corrector (2 x Refraction), Camera Mirror (reflection), CCD window (Field Flattener, 2 x Refraction).

Elements variable: slits of different widths: 0.5 – 1.0 – 1.5 – 5.0 arcsec.

CCD: see info in the CCD paragraph of subsection 3.3.1 above.

3.3.3 UV-VIS Spectrograph r-band

Spectral range: 5220 – 6800 Å.

Elements permanent:

- Common path: Dichoric (in reflection, CP_DCR, cut-off at 8300 Å), folding mirror (CP_FM_VIS), the ADC assembly (CP_LVIS_01 and CP_LVIS_02; the assembly is actually composed of two double prisms with two doublets, glued on the prisms), tip/tilt mirror (CP_TT_VIS) and a field lens (CP_LVIS_03).

- Spectrograph: folding mirror, off-axis parabola (OAP, reflection), first dichroic (transmission, cut-off at 5350 Å), second dichroic (reflection, cut-off at 6680 Å), disperser, Camera Corrector (2 x Refraction), Camera Mirror (reflection), CCD window (Field Flattener, 2 x Refraction).

Elements variable: slits of different widths: 0.5 − 1.0 − 1.5 – 5.0 arcsec.

CCD: see info in the CCD paragraph of subsection 3.3.1 above.

3.3.4 UV-VIS Spectrograph i-band

Spectral range: 6560 – 8500 Å.

Elements permanent:

- Common path: Dichoric (in reflection, CP_DCR, cut-off at 8300 Å), folding mirror (CP_FM_VIS), the ADC assembly (CP_LVIS_01 and CP_LVIS_02; the assembly is actually composed of two double prisms with two doublets, glued on the prisms), tip/tilt mirror (CP_TT_VIS) and a field lens (CP_LVIS_03).

- Spectrograph: folding mirror, off-axis parabola (OAP, reflection), first dichroic (transmission, cut-off at 5350 Å), second dichroic (transmission, cut-off at 6680 Å), folding mirror (i), disperser, Camera Corrector (2 x Refraction), Camera Mirror (reflection), CCD window (Field Flattener, 2 x Refraction).

Elements variable: slits of different widths: 0.5 − 1.0 − 1.5 – 5.0 arcsec.

CCD: see info in the CCD paragraph of subsection 3.3.1 above.

3.3.5 NIR Spectrograph

Spectral range: 8000 – 20000 Å.

Elements permanent:

- Common path: Dichoric (in refraction, CP_DCR, cut-off at 8300 Å), folding mirror (CP_FM_IR), tip/tilt mirror (CP_TT_IR), a doublet (CP_LIR_01), a flat window (CP_W_IR), a cold stop (CP_ST_IR), and a field lens (CP_LIR_02).
- Spectrograph: Folding Mirror (NIR-FM), Collimator mirror and collimator lens (NIR-CM and NIR-CL), three prisms, used in double pass (NIR-P1, NIR-P2, NIR-P3), Grating (NIR-G), Spherical Fold Mirror (NIR-SM), Camera a completely transmitting system, composed of three single lenses (NIR_L1, NIR_L2, NIR_L3) and a filter/window (NIR_W).

Elements variable: slits of different widths: 0.5 – 1.0 – 1.5 – 5.0 arcsec.

NIR Detector 2048 x 2048 pixels, Pixel size 18 µm; other parameters and details are given in [RD7].

3.3.6 Imaging with Acquisition Camera

Spectral range: 6 LSST (u, g, r, i, z, y) + 1 V Johnson filter bands. (See in section 3.4.7 the bands plot)

Filter	Central Wavelength (nm)	Cut-Off limits (nm)	Wavelength range (nm)
u'	356.95	305.30/408.60	103.3
g'	476.65	386.30/567.00	180.7
r'	621.45	536.90/706.00	169.1
i'	754.45	675.90/833.00	157.1
z'	870.75	802.90/938.60	135.7
y'	1003.95	908.30/1099.60	191.3

Elements permanent:

- Lens and Folding mirror to reimage the pupil
- Reimaging Camera made by 2 doublets and 2 lenses delivering a F/3.6 beam onto the detector.

Elements variable:

- Filter wheel to select the different filters mentioned above.

AC Detector 1024 x 1024 pixels, Pixel size 13 µm; total gain 2.3 e-/ADU; other parameters and details are given in [RD3].

3.4 ETC Characteristic Data

A spectrum will consist of two read-outs of the two detectors. The efficiency of the different components has been derived from measurement done during manufacturers' acceptance tests or simulated from theoretical predictions when measures are not available. No error is assumed at this current ETC version.

3.4.1 Sky Emission and Atmosphere Transmission

The modelling of the sky background emission and the scattering, absorption occurring in the Earth's atmosphere is done by directly calling the ESO SkyCalc tool (available at the web page), which is based on the Cerro Paranal Advanced Sky Model. The specific sky and atmosphere observing conditions are set by the following parameters: moon phase, air-mass (AM) and precipitable water vapor (PWV). The sky radiance spectrum loaded is in units of ph/s/m^2/µm/arcsec^2, thus it is first calculated for the on-sky area related to the slit length and selected slit width according to the simulation (both in arcsec) and then the units are converted in ph/s/cm^2/Å).

3.4.2 Telescope

The NTT telescope effective area considered for the computation is $S = 8.9\ m^2$. This is the value given in ESO documentation (here : The telescope surface).
For what concerns the NTT total efficiency, after FDR the value was set as 61% (constant over the full wavelength range), but during the AIV and Commissioning periods of 2025 it was set to 39% to match SOXS UV-VIS average on-sky performance measurements. This NTT throughout reduction is likely due to the mirror coating degradation over the years (effect also observed with EFOSC2 data (see RD10 – Fig 15)).
The mirrors have been washed at the beginning of 2026 and ESO plans to re-aluminize them in April 2026. Therefore, the agreed NTT-Nasmyth throughout value to be implemented in the SOXS-ETC is 66.5% (then also in the total efficiency presented in section 3.4.8); this value is an average over time and constant over the full wavelength range.

3.4.3 Dichroics

Dichroics efficiency has been calculated on the basis of the measurements and test reports from manufacturers, and adapted for the different consecutive band transition regions cut-off wavelength and spectral width of the optical design.

3.4.4 Common Paths Optics

The efficiencies of the CP (both UV-VIS and NIR channels) optics have been calculated by multiplying the efficiencies of each element.
The efficiency curves of each element have been computed on the basis of the measurements data from manufacturers test reports and on realistic assumptions in cases where no measures are available. For example this is the case of the glue considered in between the optical elements of each ADC quadruplet in the UV-VIS channel.
The details on the computation of the efficiencies of all the CP elements from available data can be found in APPENDIX 1.

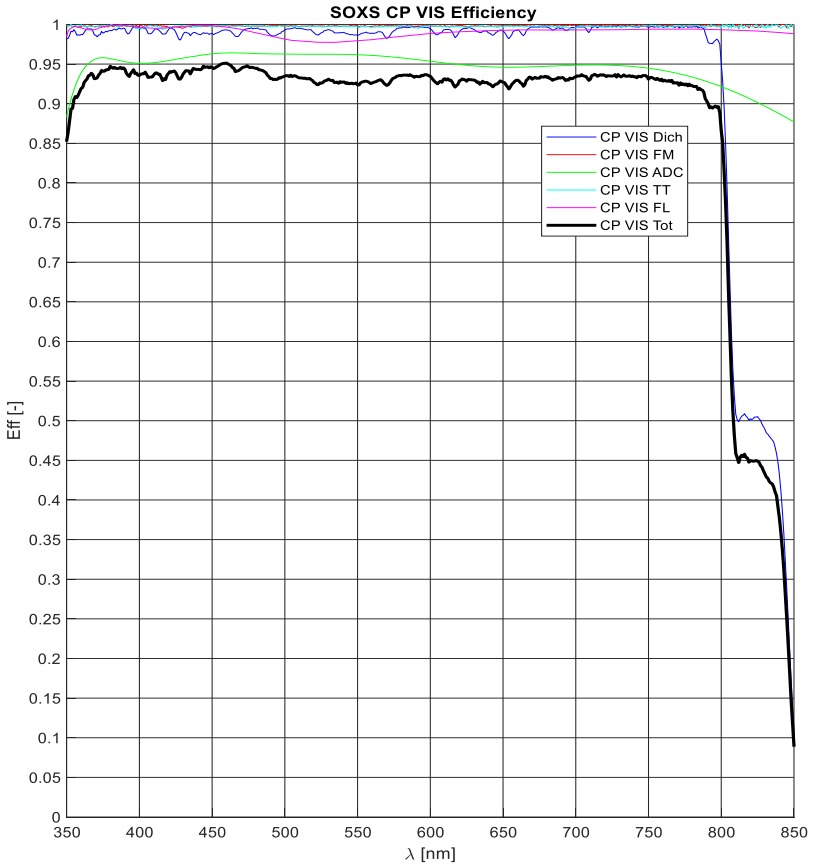

Figure 2. Total CP-throughput in the UV-VIS channel in black bold line. In colored lines the single Common-Path optical elements efficiency. Dich – Dichroic, FM – folding mirror, ADC – atmospheric dispersion corrector, TT – tip-tilt mirror, FL – field lens.

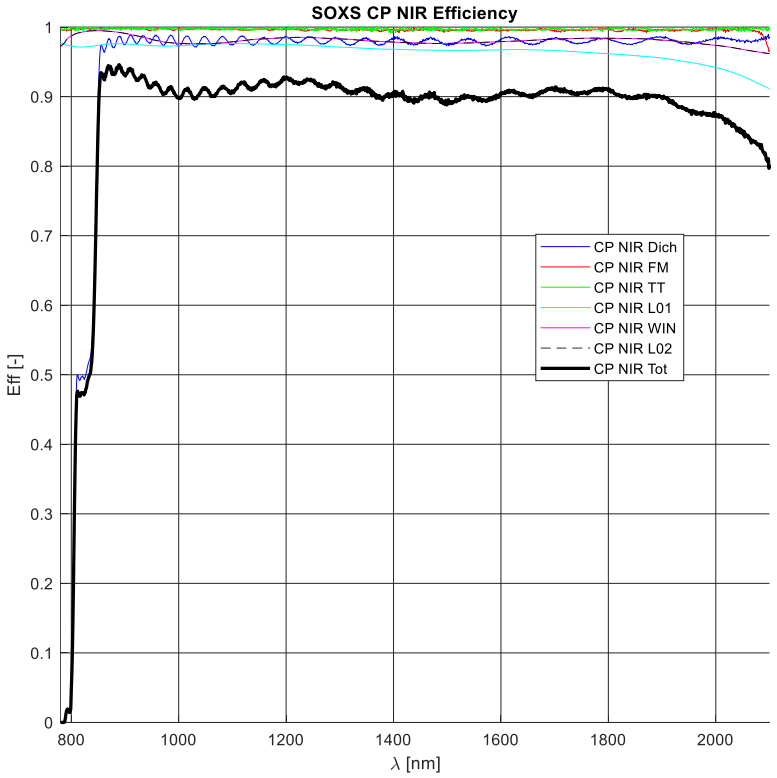

Figure 3. Total CP-throughput in the NIR channel in black bold line, while in colored lines the single Common-Path optical elements efficiency. Dich – Dichroic, FM – folding mirror, TT – tip-tilt mirror, L01 – lens 1 (refocuser), WIN – window, L02 – lens2 (field lens).

3.4.5 Spectrographs Optics

The efficiencies of the spectrograph optics have been calculated by multiplying the efficiencies of each element. The efficiency curves of each element have been computed on the basis of the measurements data from manufacturers test reports and on realistic assumptions in cases where no measures are available. The details on the computation of the efficiencies of all the spectrograph elements from available data can be found in APPENDIX 1.

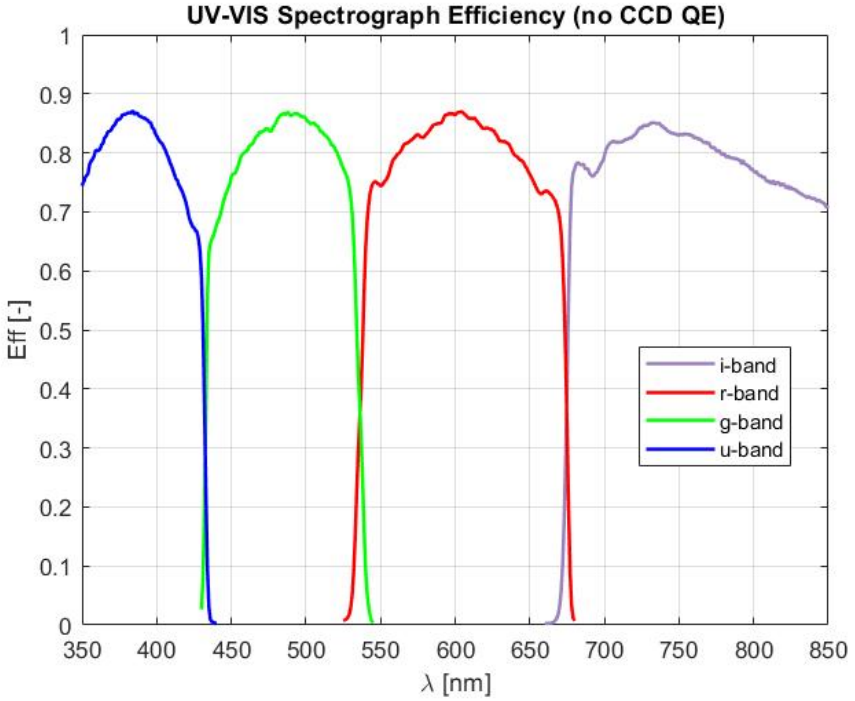

Figure 4. Total Spectrograph Optics throughput in the UV-VIS channel – All bands.

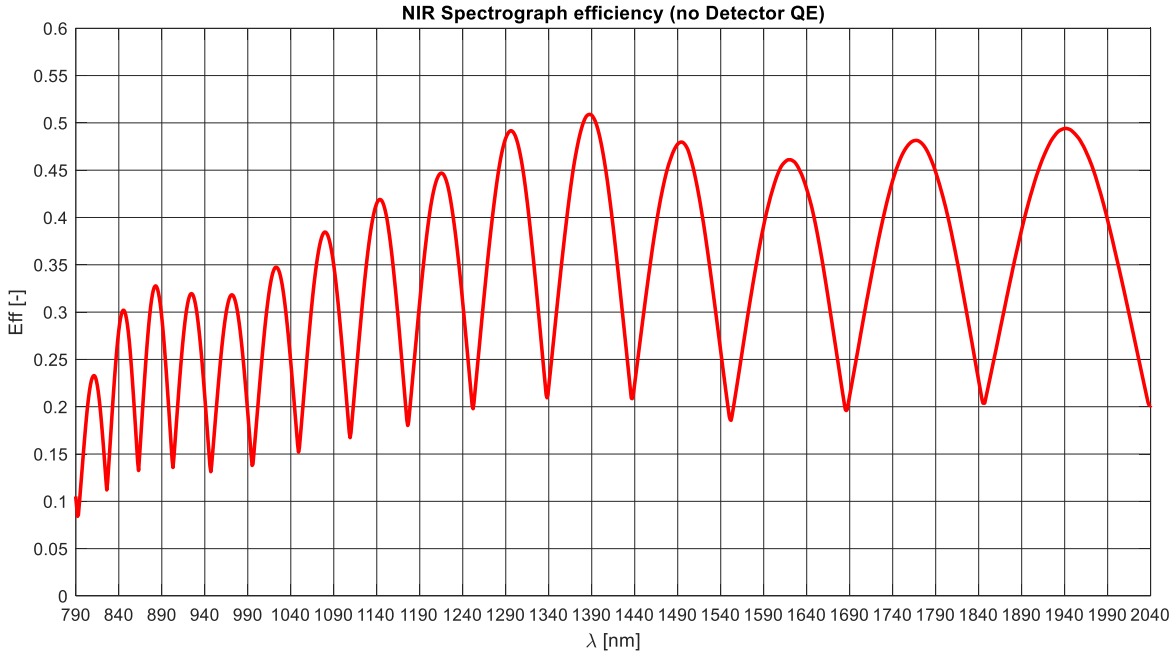

Figure 5. Total Spectrograph Optics throughput of the NIR channel.

3.4.6 Detectors

The parameters (read-out channels, binning, read-out noise, dark current, etc.) are taken from the E2V-Teledyne test reports and from the final configurations set by detector responsibles; these are listed in sections 3.3.1 and 3.3.5, for the UV-VIS CCD44-82 and NIR Hawaii H2RG Array, as well as summarized in section 3.8.1 (specifically in *Figure 14 and Figure 16*).

QE curves were derived through an extrapolation from measurement data summarized in the test reports (RD6 and RD7), but given the small amount of data available (just 4 points for each detector) the derived QE curves shown here below are considered not fully reliable and the difference between theoretical total efficiency and on-sky measurements could also be due to this uncertainty (see sec. 4).

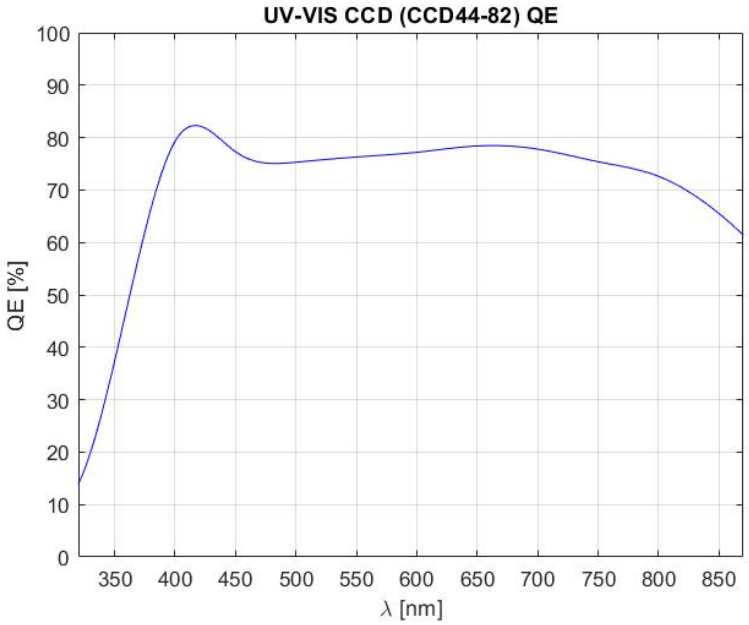

Figure 6. UV-VIS CCD quantum efficiency.

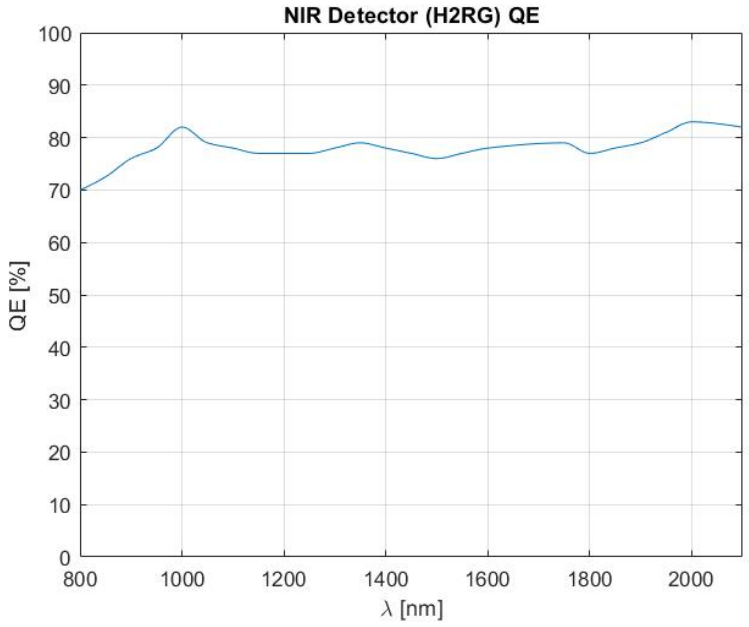

Figure 7. NIR array quantum efficiency.

3.4.7 Imaging Mode for the Acquisition Camera

The acquisition camera (AC) is briefly described in sec. 3.2. It can be used to perform photometry in 6 LSST (u, g, r, i, z, y) + 1 V Johnson filter bands. The AC throughput for the different filter bands, according to the optical element as-built data, is provided from the AC-workpackage and showed in the following.

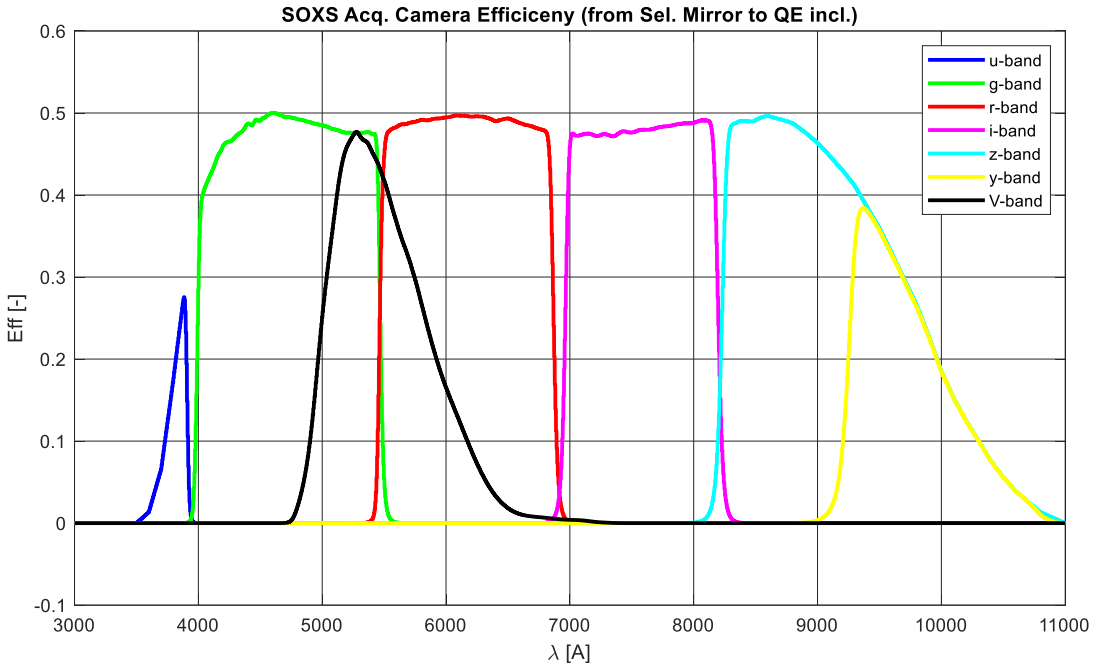

Figure 8. Acquisition-Camera efficiency from selector mirror to detector QE included. The diferent bands profile, related to the LSST and V filters, are listed in the legend.

3.4.8 Resulting Efficiency from Below Atmosphere to Detectors

Apart from atmosphere airmass and slit losses that depend on seeing, all the other components are permanently positioned in the beam. Therefore, there is essentially only one single global efficiency curve per each arm, which is used to predict the observed spectra. The curves shown in the following plots consider a telescope throughput of 66% as explained in section 3.4.2 .

A summarizing discussion on the comparison between the total efficiency used in the ETC and the one measured on-sky, as well as for SNR comparison and verification is given in section 4.

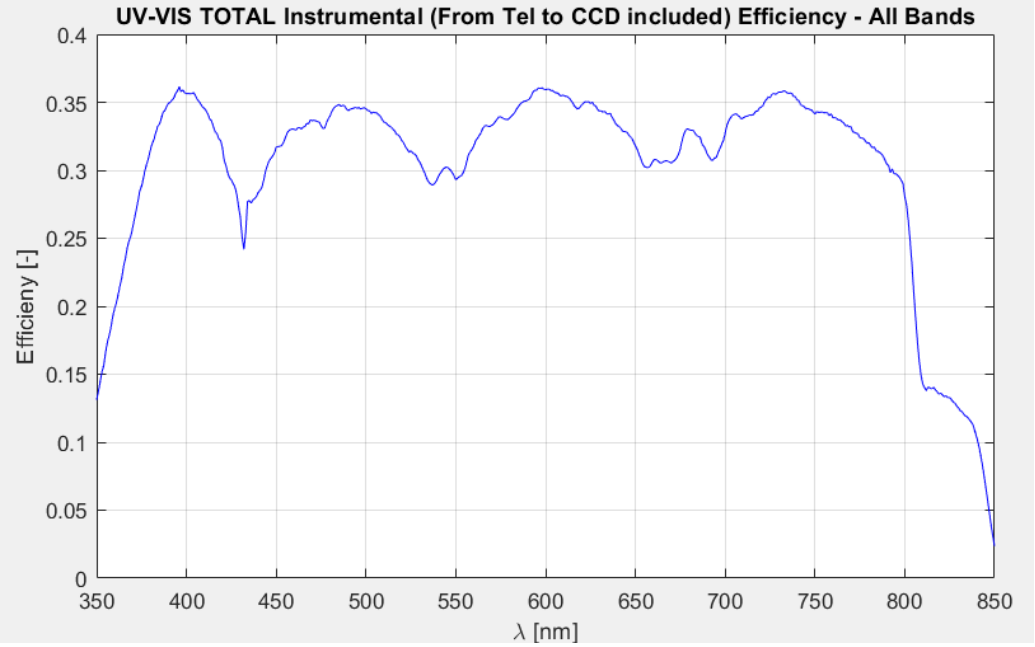

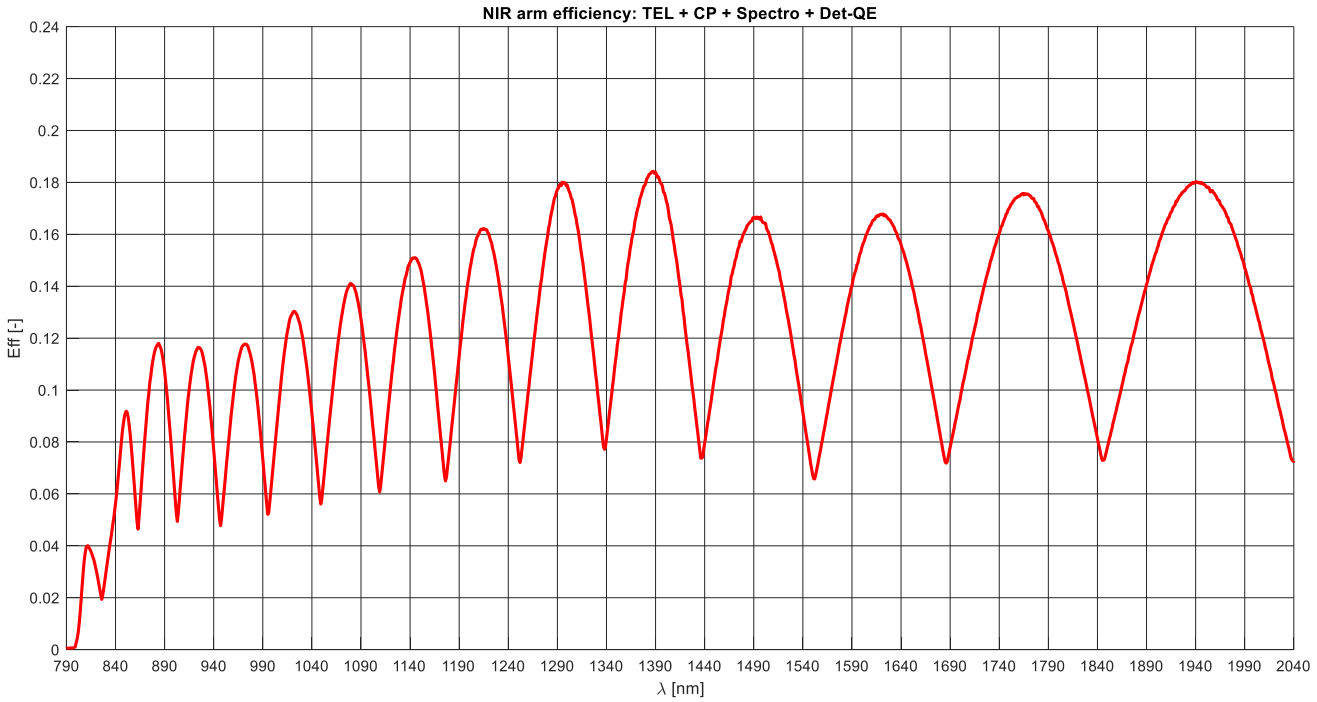

Figure 9. Overall efficiency (apart of airmass absorption and slit losses, these are taken into account but not here).

3.4.9 Error Budget

Considering the uncertainty on some instrumental parameter and features (like efficiencies, linear dispersion, detector noises) the current global uncertainty attributed to the ETC results (science object or sky photoelectrons, SNR , etcetc) is estimated to be of the order of 10%.

3.5 ETC User Interface

SOXS includes only a small number of moving functions and therefore instrument paths. In order to perform the S/N calculation, the user will be asked to enter a number of parameters, relevant for the observations, through a public HTML interface available at the following link: https://soxs-etc.brera.inaf.it/

3.5.1 The INPUT parameters are divided into different sections:

Science Object input parameters:

- type of input spectrum
  - black-body: temperature
  - power-law: spectral index
  - User-defined upload spectrum, as a .txt or .dat table in units [Å, erg/s/cm^2/ Å] – (Note the web-page allows the user to download some template spectra, which can then be loaded as U*ser-Defined Spectrum* – their format is already the proper one requested)
  - Single Emission Line: central wavelength [Å], FWHM [Å], Flux [ergs/s/cm^2]
- spatial distribution
  - point-like
  - extended source
- object magnitude (which for extended objects is give per arcsec^2), reference band and AB or Vega magnitude system
- Redshift

Sky and Atmospheric conditions input parameters:

- Fraction of Lunar Illumination (pure number in the range 0, i.e. New Moon, to 1, i.e. Full Moon)
- Airmass
- Precipitable Water Vapour (PWV)
- Seeing (reference value at zenith and 500 nm)

Instrument set-up input parameters.

- slit width (the 4 possible slit widths : 0.5 – 1.0 – 1.5 – 5.0 arcsec)
- Exposure time settings:
  - Exposure time (Single Exposure, t_EXP) and Number of Exposures (NEXP) for UV-VIS arm (the overall exposure time is the t-EXP (single exposure) multiplied by NEXP)
  - Detector Integration Time (DIT), Number of DIT (NDIT, non-destructive reads) and Number of Integrations (NINT) for NIR arm detector (the overall exposure time is the product of DIT, NDIT and NINT)
- UV-VIS Detector read-out mode, gain and binning in the form (gain) (spatial×spectral binning) (readmode) like done also in the XSHOOTER ESO ETC; NIR detector mode: Gain 2.3 e-/ADU, Binning 1x1 only

Input for calculation database:

- Wavelength database: number of wavelength per each order, 3, 15 (default value), 100
- SNR calculation: per Spectral Resolution Element (SRE) or per pixel-bin
- IF to include the derived exposure time for a specific User-Defined SNR

Output selection:

- Table: tabular results in a similar format as XSHOOTER ETC (see section3.8.3)
- Graph: selection of which kind of output plots among the list of subsection 3.5.2.

3.5.2 Results, for each instrument channel (UV-VIS & NIR)

The following list of plots are displayed, for a more detailed descriptions see section 3.8.2:

- S/N spectrum (per SRE or per PIX accordingly)
- Total efficiency – from top atmosphere to detector including slit-losses
- Source object spectrum in units of [ph/s/cm^2/ Å]
- Sky Radiance (units of [ph/s/cm^2/ Å]) after interpolation from the online calling to ESO-SkyCalc tool.
- expected photo-electrons: i) object; ii) sky; iii) object+sky (maximum intensity in single pixel)
- Noises (shot-noise, sky-noise, DC-noise and RON-noise)
- Table information for the Single Emission Line case
- The derived exposure time to reach a specific SNR set in input from the user, computed for 3 wavelengths per each quasi-order (in the UV-VIS) and per each diffraction order (in the NIR)

All plots/graph are downloadable as .txt files, coded in UTF-8, in the format of 2 columns:

- Wavelength in [Å]
- Specific parameters (SNR, Efficiency, photo-electrons, etcetc) according to the user selection.

Tables, if selected by the user displayed results for 3 wavelengths per each quasi-order (in the UV-VIS) and per each diffraction order (in the NIR) in a similar format as XSHOOTER ETC (see section 3.8.3).

3.6 Mathematical Model

3.6.1 General formula: Staring Mode

The formula used for the calculation of S/N (or SNR) at different wavelength is the detailed below (adapted from formula used in ESO ETC). This formula is referred to observation in staring mode and it assumes that, during reduction, the sky signal to be subtracted is measured on an area much larger than the area used to get the object signal. If this is not the case, other terms, which depend on the area used to measure the sky contribution, should be added.

$$\frac{S}{N} = \frac{\sqrt{C_1} * \mathrm{N_{Obj}}}{\sqrt{\mathrm{N_{Obj}} + \mathrm{N_{Sky}} + n_{\mathrm{bin}} \cdot \mathrm{RON}^2 \cdot C_2 + n_{\mathrm{pix}} \cdot \mathrm{dc} \cdot C_3}}$$

Where:

- N_{Obj} is the object counts in e$^-$ computed per SRE-bin or PIX-bin according to the required simulation by the user. $\mathrm{N_{Obj}}$ takes into account the spectral total efficiency, thus including slit-efficiency as described in sec. 3.6.2, and the effective telescope area value reported in sec. 3.4.2.
- N_{Sky} is the sky signal in e$^-$ computed per SRE-bin or PIX-bin according to the required simulation by the user. $\mathrm{N_{Sky}}$ does not take into account the slit-losses, since the sky background emission is homogeneously spatially distributed on the slit plane. The effective telescope area value reported is the one in sec. 3.4.2. The PSF extension in spatial direction, over which the signal is integrated, is converted in aperture-on-sky by the instrument plate scale (in $["/pixel]$).
- n_{bin} is the number of bins in the bin-element area where the SNR is computed. This is related to the number of pixels and binning option.
- n_{pix} is the number of pixels in the bin-element area where the SNR is computed. For point-like sources, in the spatial direction this is set as PSF extension as $1.5 \cdot FWHM_{IQ} \cdot plate\_scale$.
- RON is the readout noise in e$^-$/readout bin (according to UV-VIS or NIR the proper value is considered)
- dc is the dark current in in e$^-$/pixel/sec (according to UV-VIS or NIR the proper value is considered)
- C_1 = NEXP (for UV-VIS), NDIT x NINT (for NIR, non-destructive read out implemented)
- C_2 = 1 (for UV-VIS), 1/NDIT (for NIR, non-destructive read out implemented)
- C_3 = t_EXP (for UV-VIS), DIT (for NIR, non-destructive read out implemented)

3.6.2 Slit Losses

The slit efficiency is calculated through multiple steps, initially the Image Quality of the PSF FWHM is obtained by the quadrature sum of the atmosphere and the telescope FWHM:

$$FWHM_{IQ} = \sqrt{FWHM_{atm}^2 + FWHM_{tel}^2}$$

The specific adopted formulas are the ones described in the ESO ETC webpage; for what concern the atmospheric PSF is modeled as a Gaussian profile with terms introducing the effects of turbulence:

$$FWHM_{atm}(s,x,\lambda) = s \cdot x^{0.6} \cdot \left(\frac{\lambda}{5000}\right)^{0.2} \cdot \sqrt{1 + F_{Kolb} \cdot 2.183 \cdot \left(\frac{r_0}{L_0}\right)^{0.356}}$$

Where:

- $s =$ *Seeing at reference wavelength (*5000 Å*)*
- $x =$ *Airmass*
- $r_0 =$ *Fried parameter obtained by* $0.100 \cdot s^{-1} \cdot \left(\frac{\lambda}{5000}\right)^{1.2} \cdot x^{0.6}$
- $F_{Kolb} = \frac{1}{1+300\frac{D}{L_0}} - 1$, *where:* $D =$ *Telescope diameter,* $L_0 =$ *Wave-front outer scale*

The diffraction limited PSF FWHM for the telescope with diameter D at observing wavelength λ, in units of *arcsec*, is modeled as:

$$FWHM_{tel} = 0.000212\frac{\lambda}{D}$$

Finally, the slit efficiency is obtained by:

$$eff = \mathrm{erf}\left[\frac{a}{\sqrt{2}}\right] + \mathrm{erf}\left[\frac{b}{\sqrt{2}}\right]$$

Where: $a = \frac{w \cdot \sqrt{\log 4}}{FWHM_{IQ}}$ and $b = \frac{l \cdot \sqrt{\log 4}}{FWHM_{IQ}}$ *with* w and l *representing the width and length of the slit respectively.*

3.6.3 Thermal emissivity

No thermal emission from optical element is taken into account at this current ETC version.
The diffuse thermal noise on the NIR array is included in the model according to the measurements done in the NIR arms AIT as presented in sec. 3.9.

3.6.4 Imaging Mode for the Acquisition Camera

The acquisition camera (AC) is briefly described in sec. 3.2. It can be used to perform photometry in 6 LSST (u, g, r, i, z, y) + 1 V Johnson filter bands. The AC throughput for the different filter bands is provided from the AC-workpackage and showed in Figure 8.
The SNR computation using a classical aperture photometry approach involves the definition of a reference area around the object image in which the object, sky and detector noises contributions are evaluated. The reference area is dependent on:

- the image FWHM related seeing and telescope (as described in sec. 3.6.2, with the difference that in this case the implemented case is the pin-hole and not slit-through),
- the AC image scale, which is 0.205 arcsec/pixel,
- the AC optical PSF (set from PSF maps derived from the AC optical design),

- the contribution of the atmospheric dispersion which translates in image elongation effect along the vertical direction, due to the relative displacement and distortion in each filter w.r.t. the reference wavelength. Centroids shift and distortion maps, calculated following Filippenko 1982 (using T=10°C, P=770mb, H=44%), are provided by AC-WP and shown in here after.

z (deg)	u' (arcsec)	g' (arcsec)	r' (arcsec)	i' (arcsec)	z' (arcsec)	y' (arcsec)
30	1.12	0.55	0.27	0.14	0.07	0.02
45	1.94	0.96	0.46	0.24	0.13	0.04
60	3.36	1.65	0.80	0.42	0.22	0.07

Table 1. Acquisition Camera centroids shift with respect to 1100nm, at different zenith angle for the different LSST filters.

z (deg)	u' (arcsec)	g' (arcsec)	r' (arcsec)	i' (arcsec)	z' (arcsec)	y' (arcsec)
30	0.82	0.58	0.23	0.11	0.06	0.06
45	1.42	1.00	0.39	0.20	0.11	0.10
60	2.45	1.73	0.68	0.34	0.19	0.17

Table 2. Acquisition Camera distortion due to atmosphere, computed at different zenith angle for the different LSST filters.

The FWHM of atmosphere and telescope are summed in quadrature to the FWHM of the instrument, i.e. the acquisition camera optical PSF of the selected band. Then the atmospheric dispersion contribution is added in quadrature according to the specific considered zenith angle and band. Finally the reference area diameter, in units of pixels, is computed as $2 \cdot (FWHM_{IQ}/image\_scale)$.

3.7 User Templates

Different science object input spectral energy distributions (SEDs) can be simulated, as listed in sec. 0. The different SEDS are first generated in units of $[erg/(s \cdot cm^2 \cdot \text{Å})]$, then converted in units of $[ph/(s \cdot cm^2 \cdot \text{Å})]$. Then, the SEDs are rescaled according to the simulated magnitude and filter; the Zeropoints applied inside the ETC code have been taken from ESO at the following web page. As mentioned, the Zeropoints are thus obtained by integrating across each band pass filter transmission ($T(\lambda)$) and the Vega spectrum ($Vg(\lambda)$):

$$ZeroPoint \equiv \frac{\int T(\lambda) Vg(\lambda) d\lambda}{\int T(\lambda)\, d\lambda}$$

The magnitude is given per arcsec^2 in case of an extended source spatial distribution.

3.7.1 Black-Body

The blackbody profile is defined by its temperature and apparent magnitude at a given filter's band. Temperature is expected in Kelvin and the apparent magnitude in one of the band filters U, B, V, R, I, J, H and K.

3.7.2 Power-Law

The target model is a power law spectrum defined, at the wavelength *w*, from continuum flux level F0 a reference wavelength *wc* and the power low index p, a real number, as:

$$F(w) = F_0 \left[\frac{w}{w_c}\right]^p$$

where:

$$F_0 = 10^{-(0.4 \cdot M_v + Z)}$$

where Mv is the object magnitude and Z is the zero order point in the selected observing band.

3.7.3 Templates Spectra

A database of templates spectra was kindly provided by ESO. These spectra are the same that can be loaded in the Template Spectrum tab of ESO ETCs (like the one of X-SHOOTER or FORS2). In the current SOXS-ETC they can be downloaded from a link accessible through the web-page, just before the type of input flux distribution box list, and then loaded as User-Defined spectra.

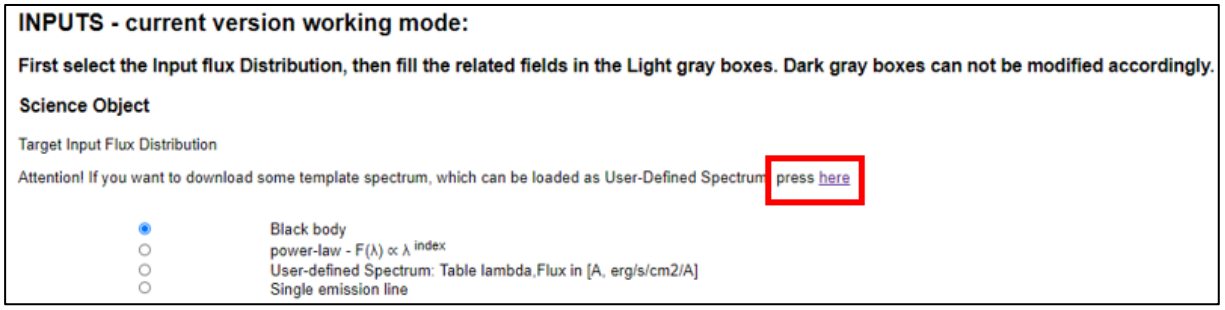

Figure 10. Link to access a repository containing the ESO Template Spectra Database in the red-box.

The following type of spectra are present in the database:

- *Stars spectra*: stellar Kurucz and Pickles models of different spectral classes.
- *Galaxy spectra*: Elliptical, Kinney S-type and Kinney Starbust (1-to-6).
- *A QSO spectrum*.
- *Supernova:* no spectra currently available

3.7.4 User-defined upload Spectra

The user will have, in the future version of the ETC, the possibility to upload a user-defined spectrum in a tabular layout with two columns: wavelength (in [Å]) and flux (in [erg/s/cm^2/ Å]). The table must be in ASCII format.

3.7.5 Single Emission Line

The user has the possibility to simulate a single line. In this case the source is a single emission line, having a Gaussian profile with a characteristic wavelength, FWHM, and Flux in erg/s/cm^2 for point sources or erg/s/cm^2/arcsec^2 for extended sources.

3.8 Examples of the Web-Page Layouts

In the following subsections, example of Input and Output pages for both Spectroscopic and Imaging mode are given. The selection of Spectroscopy versus Imaging can be done via the sliding toggle in the very top section of the web-page.

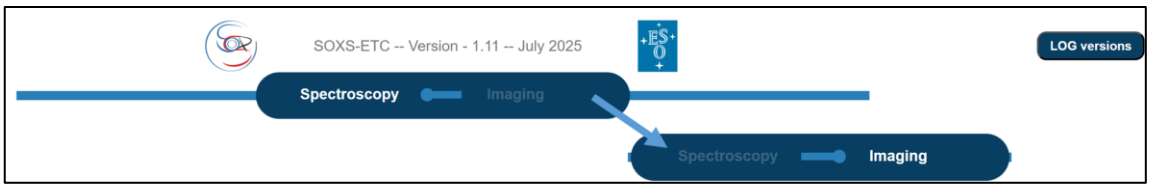

Figure 11. Graphical layout of the very top section of ETC Web-page to select between spectroscopy versus Imaging.

3.8.1 Example Input Page (Spectrograph mode)

The input page graphical layout of the current version is divided into sections as described in sec. 0. In the Science Object input flux distribution section, shown in *Figure 12*, the different parameters box are in light grey or dark grey according to the type of selected SED. Example, if the power-law is selected then only power-law index and mag parameters can be set, while others cannot be modified.

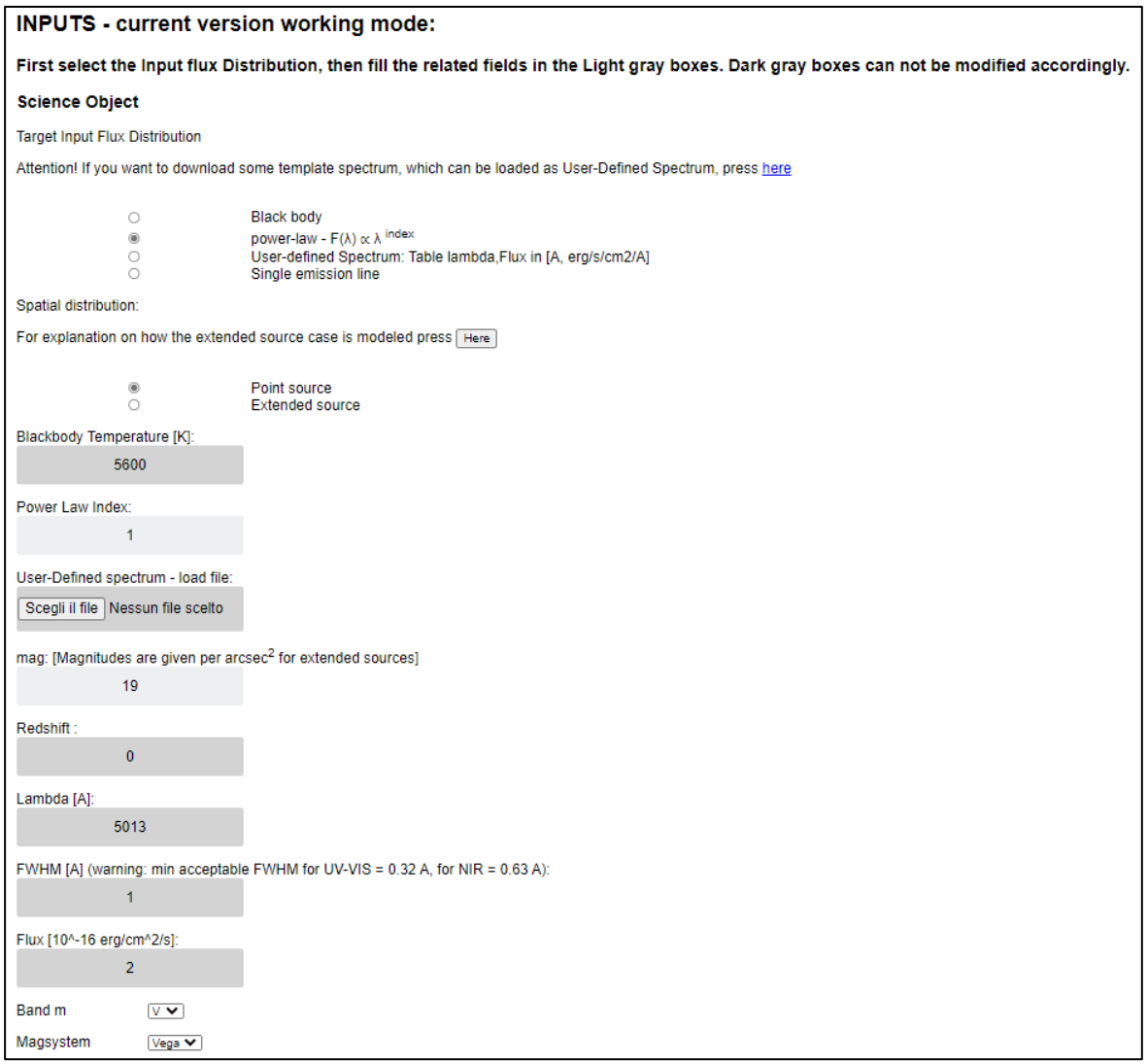

Figure 12. Graphical layout of the internal ETC simulator of SOXS. Science-Object input flux distribution.

The Sky and Atmospheric condition parameters section is shown in *Figure 13*.

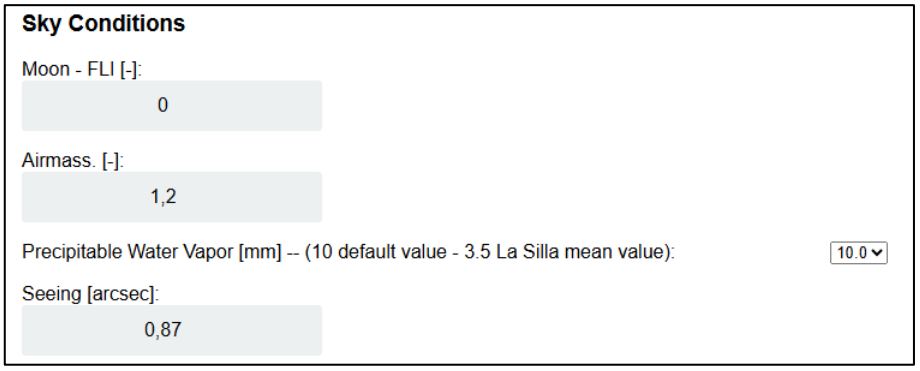

Figure 13. Graphical layout of the internal ETC simulator of SOXS. Sky and Atmospheric condition.

The instrument set-up section, together with the inputs for calculation database, is shown in *Figure 14*.

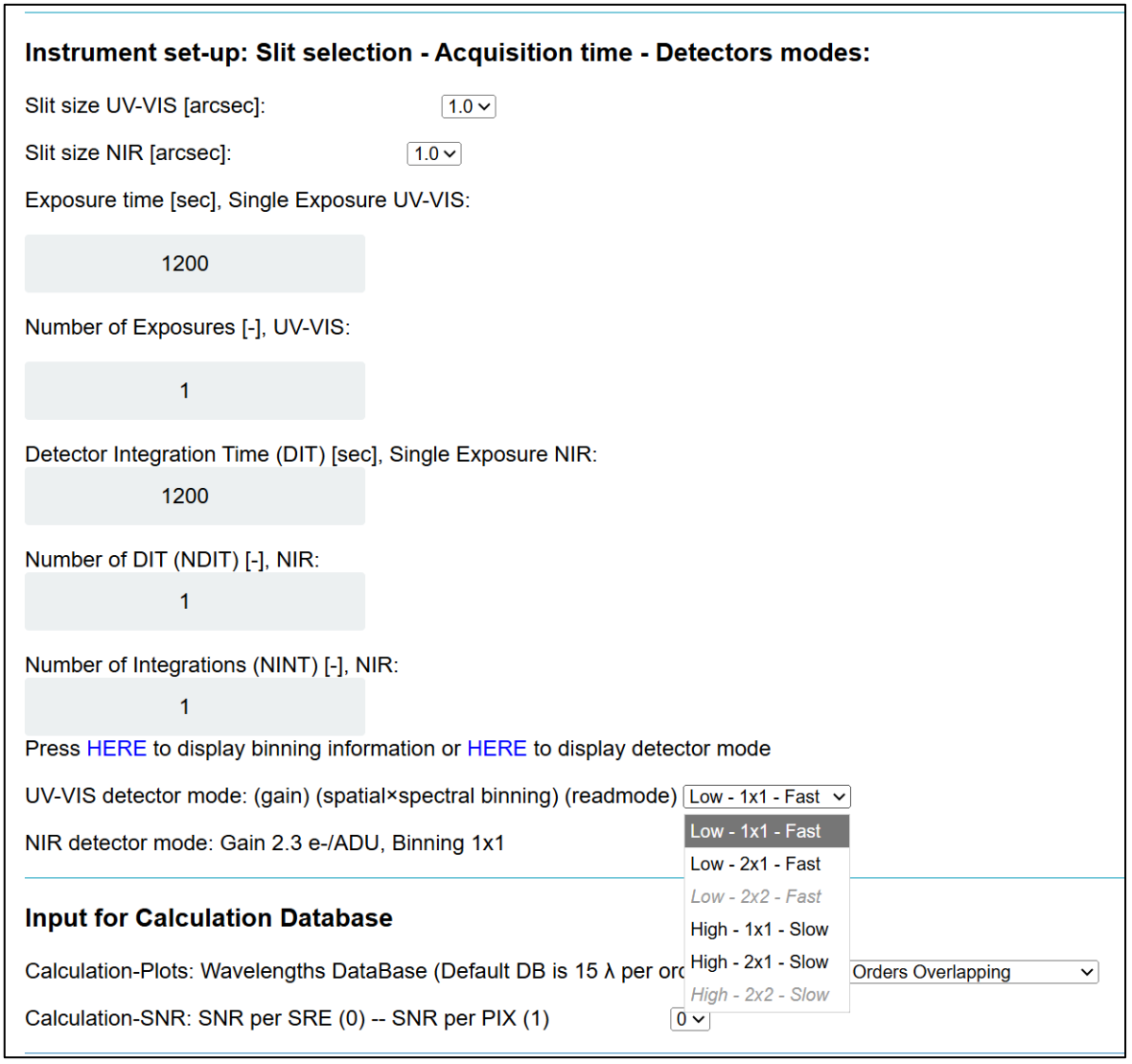

Figure 14. Graphical layout of the internal ETC simulator of SOXS. Instrument set-up input parameters.

Note that for the UV-VIS the detector read-out mode can be specified using the drop-down menu as indicated in *Figure 14*. Here the gain, binning and read-mode are visualized like done in many other ESO Instrument ETC web-pages (e.g. XSHOOTER, see here: X-SHOOTER Exposure Time Calculator).
Note that the different binning options are depended on the SNR computation required, if per SRE or per Pixel-bin; in the case of pixel-bin all binning options can be selected, while in the case of SRE-bin only spatial binning are available (i.e. the 2x2 binning is not offered – see that this is light-gray color in the example shown in *Figure 14*).
Gain and read-out values currently for the UV-VIS detector can be displayed by clicking the "**HERE** to display detector mode" as shown in *Figure 16.*

For what concerns the relevant binning information to be known and understood by users of the ETC, see the pop-up in *Figure 15*, which will display when clicking the "**HERE** to display binning information".

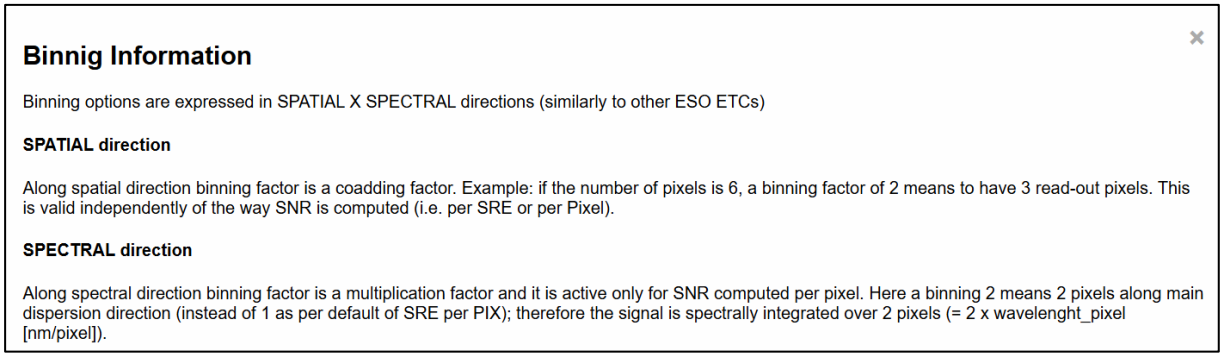

Figure 15 Binning information pop-up.

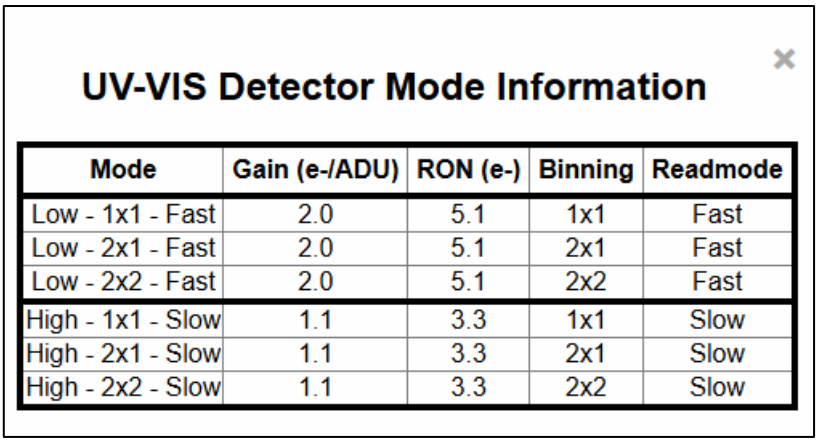

Figure 16. UV-VIS detector read-out mode information pop-*up*.

3.8.2 Example of Output plots (Spectrograph mode)

As described in sec 3.5.2, the output for the current version are:

- S/N spectrum (per SRE or per PIX accordingly)
- Total efficiency – from top atmosphere to detector including slit-losses
- Source object spectrum in units of [ph/s/cm^2/ Å]
- Sky Radiance (units of [ph/s/cm^2/ Å]) after interpolation from the online calling to ESO-SkyCalc tool.
- expected photo-electrons: i) object; ii) sky; iii) object+sky (maximum intensity in single pixel)
- Noises (shot-noise, sky-noise, DC-noise and RON-noise)
- Table information for the Single Emission Line case
- The derived exposure time to reach a specific SNR set in input from the user, computed for 3 wavelengths per each quasi-order (in the UV-VIS) and per each diffraction order (in the NIR)

All plots/graph are downloadable as .txt files, coded in UTF-8, in the format of 2 columns:

- Wavelength in [Å]
- Specific parameters (SNR, Efficiency, photo-electrons, etcetc) according to the user selection.

In the following, a simulation of a Kurucz G2V stars, with mag-V = 19 in Vega system. The observation is simulated with a FLI of 0.25 (i.e. 7 days from New-Moon) at AM = 1.16 with a PWV = 10 mm and a seeing at 500nm of 0.9 arcsec. The 1-arcsec slit width is used and single exposures of 1200 sec are set for both arms; binning is 1x1 in low gain fast red-out mode. The SNR is computed per pixel-bin, the plot is shown in *Figure 17*. Note that this is not computed per single pixel and in the subtitle the user has to possibility to click to see a schematic visualization example of the considered SNR Area with a simple explanation of Aperture and Spectral integration of the signal, *see Figure 18.*

Below the plot, the user has the possibility to download the .txt files containing the SNR data for both arms. Since the input source spectrum does not cover the whole spectral range of SOXS a warning message is properly displayed, and the plotted range is zoomed/scaled to match the source one.

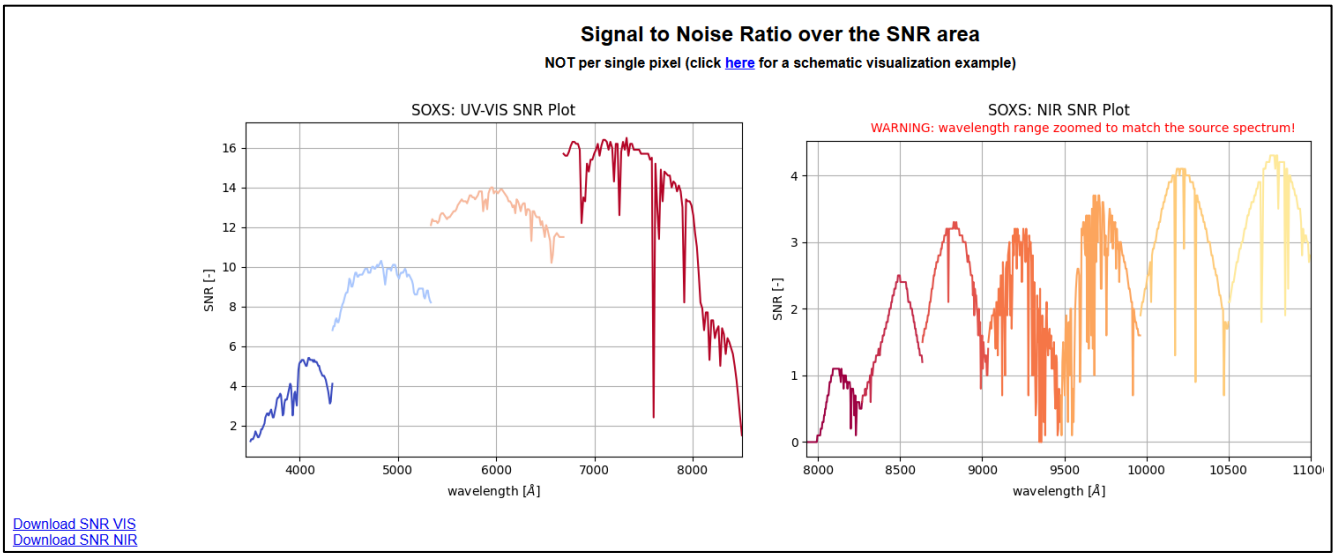

Figure 17. Graphical view of the SNR for the two arms.

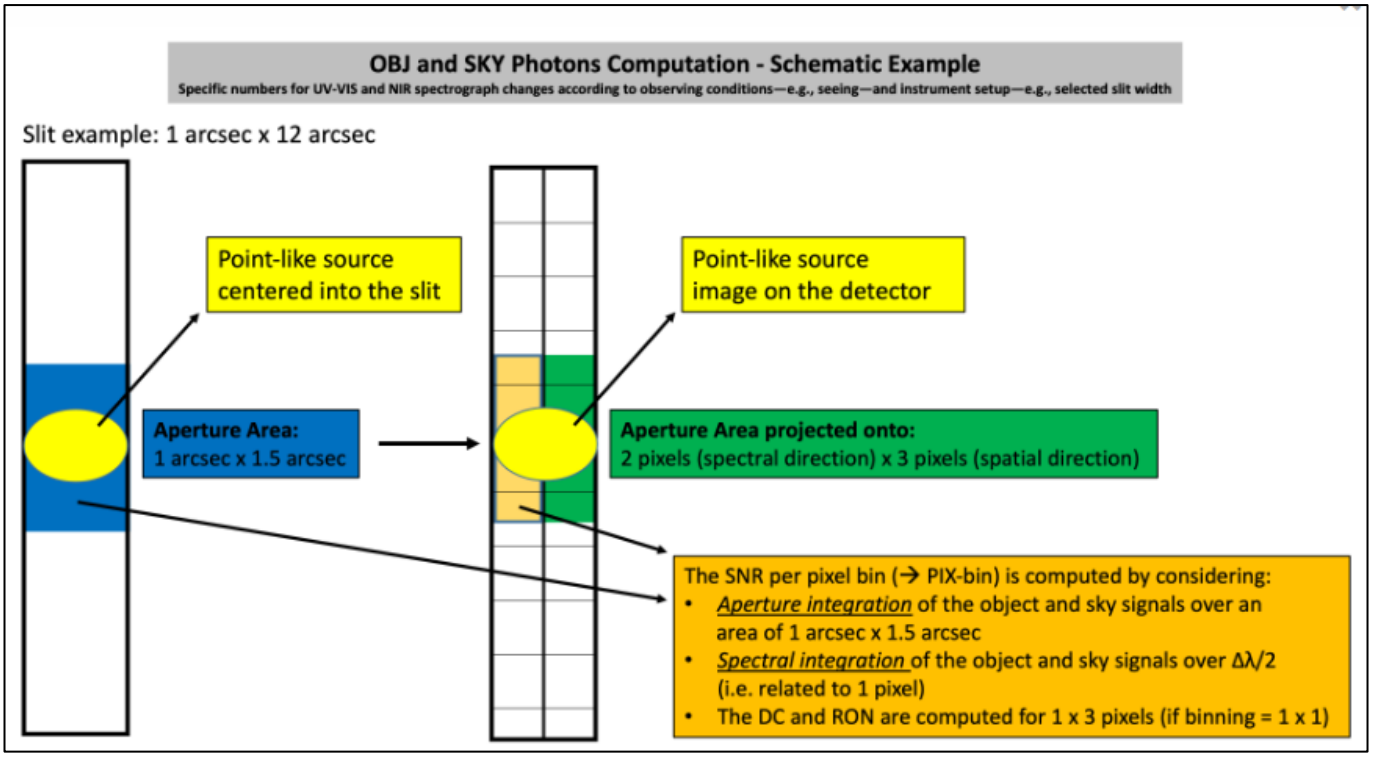

Figure 18. Schematic visualization example of the considered SNR Area.

The total efficiency plot, from top atmosphere to detectors including the slit efficiency, related to the simulated observing condition is shown *Figure 19*.

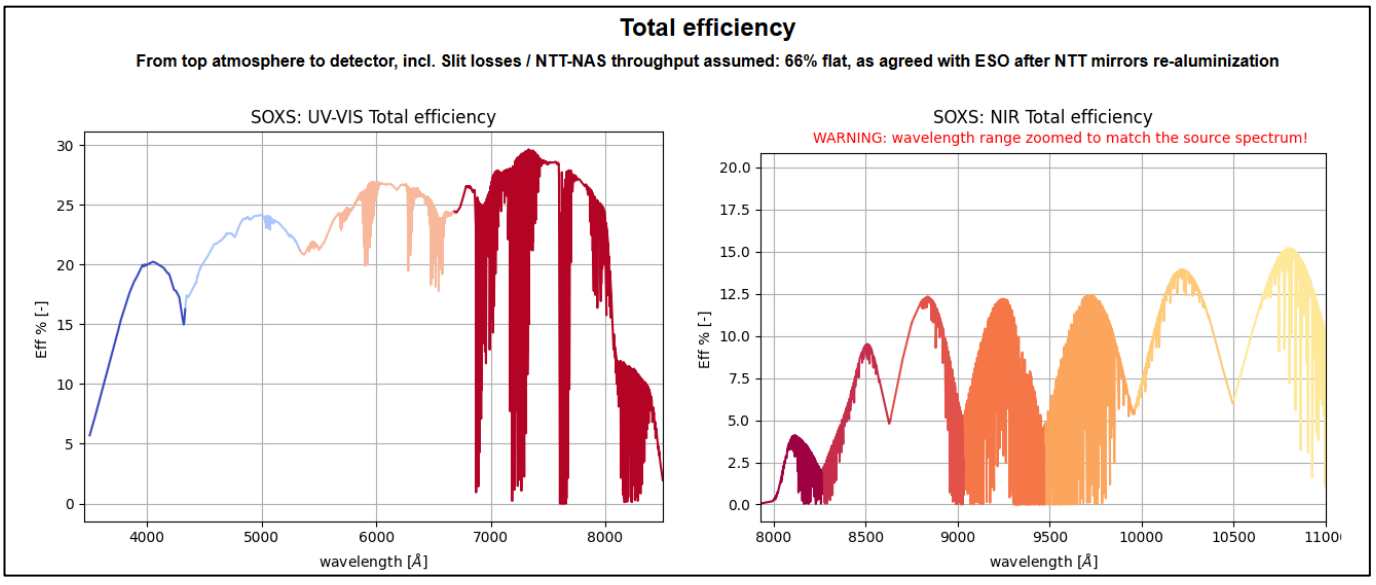

Figure 19. Overall efficiency for the simulated observation.

The Source input spectrum is plotted in units of $[ph/(s \cdot cm^2 \cdot Å)]$ at top of atmosphere, with the apparent magnitude and red-shift applied. Also in this case, if the source data do not cover the whole spectral range of SOXS a warning message is properly displayed.

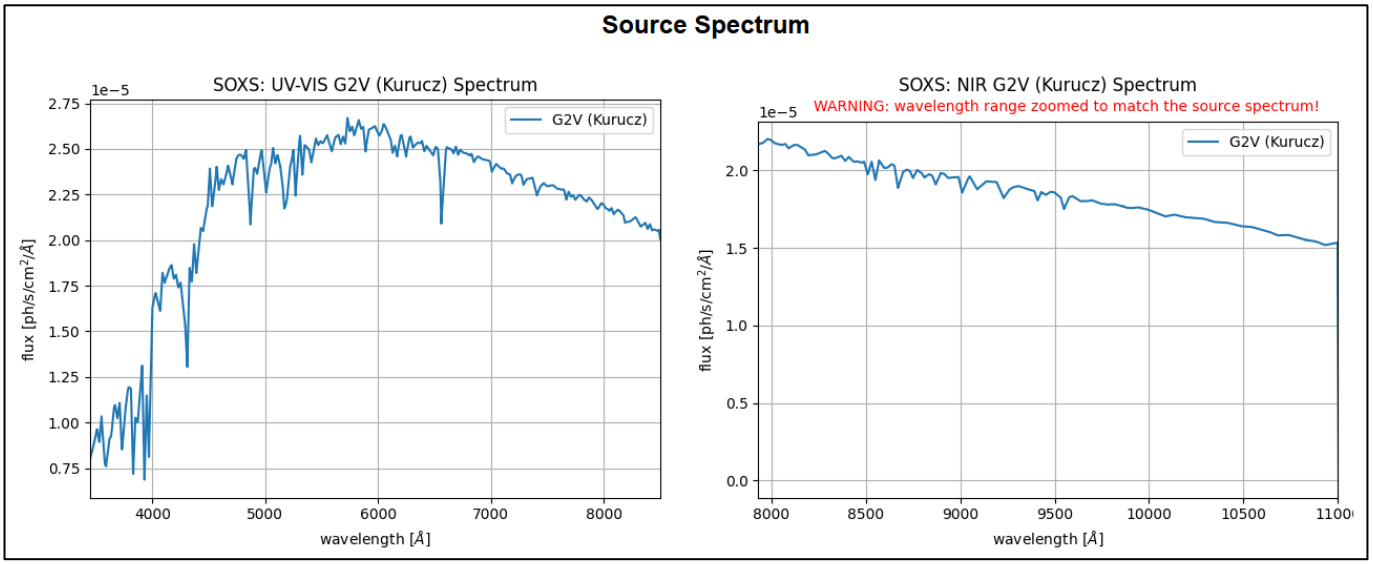

Figure 20. Source object input SED.

The Sky radiance spectrum, generated by calling ESO Sky-Calc tool according to the set input parameters, is properly converted in units of $[ph/(s \cdot cm^2 \cdot Å)]$ by multiplying for the effective slit area (in [arcsec^2] to be considered for the SNR calculation. In the following figure, both radiance and atmospheric transmission are presented.

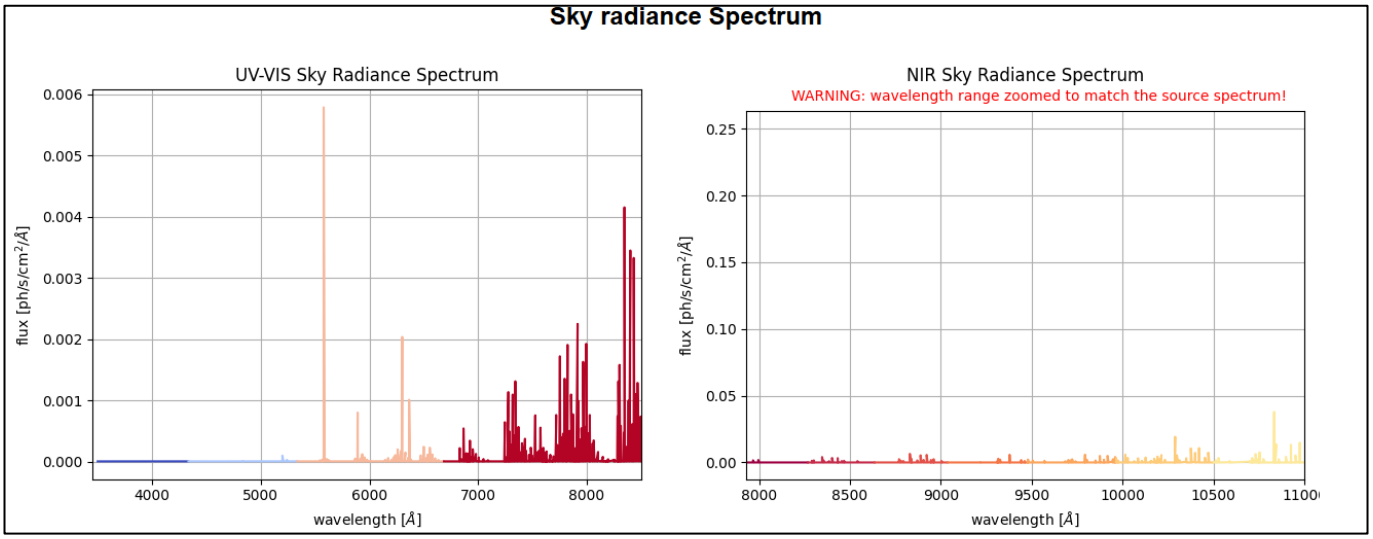

Figure 21. Sky radiance and Atmospheric transmission related to the simulated observing condition.

The Source and sky background photoelectrons are computed per SRE-bin or pixel-bin according to what selected by the user. The counts are computed taking into account the overall efficiency, effective telescope area, the exposure time of a single exposure (T-exp for UV-VIS and DIT for NIR). Also in this case, if the source data do not cover the whole spectral range of SOXS a warning message is properly displayed.

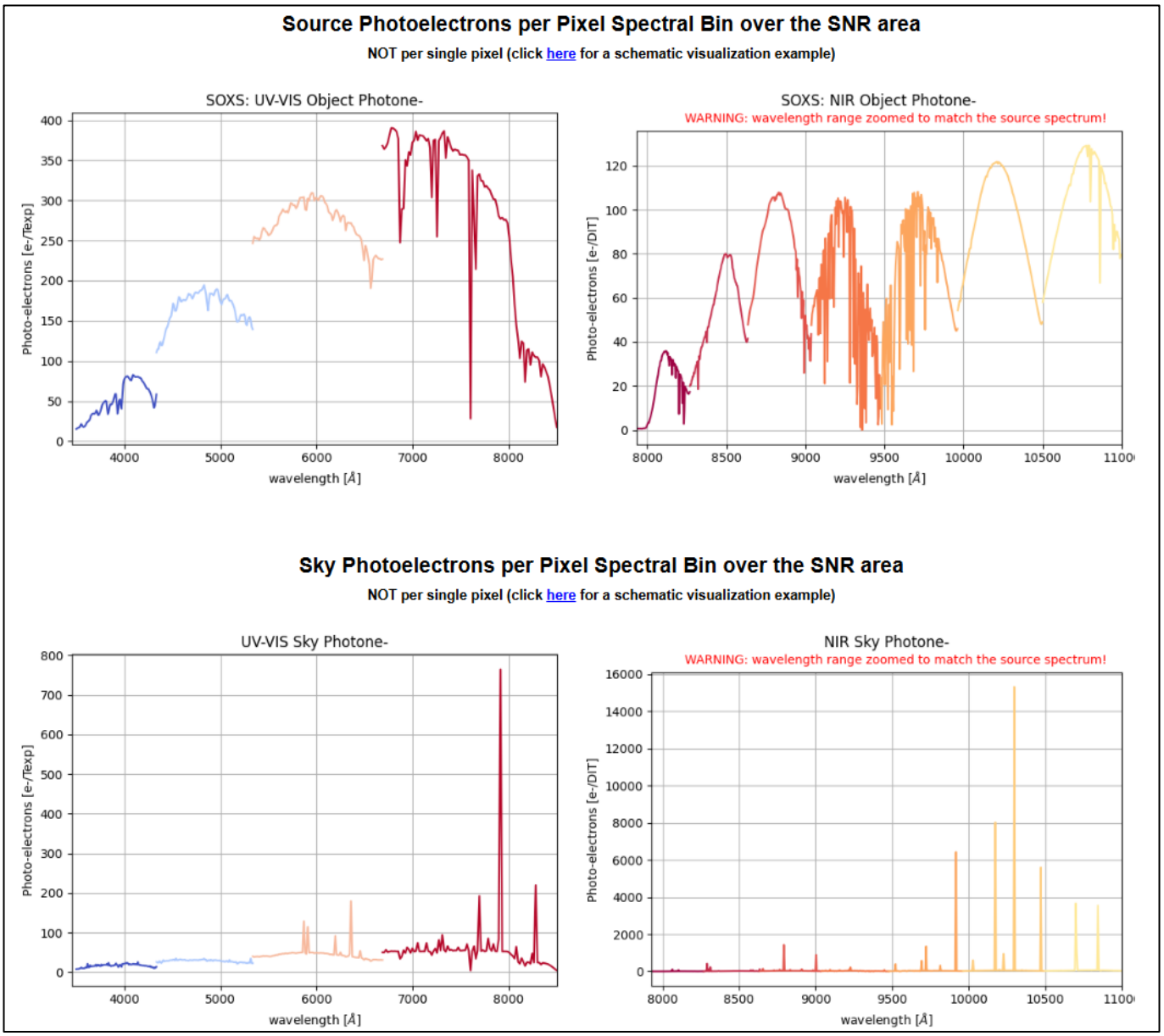

Figure 22. Object and Sky photoelectrons computed per selected spectral bin (pixel bin).

The maximum instensity (i.e. source + sky) per each single exposure (i.e. per T-exp in for UV-VIS and DIT for NIR) is computed not over a SNR area but in a single physical pixel. This is reported in units of photoelectrons/Texp (or /DIT for the NIR) and it is compared with the full-well capacity (converted from ADUs to photoelectrons, accounting for the proper detector gain value) to report possible saturation warnings. An example for the observations simulated, is shown in *Figure 23.*

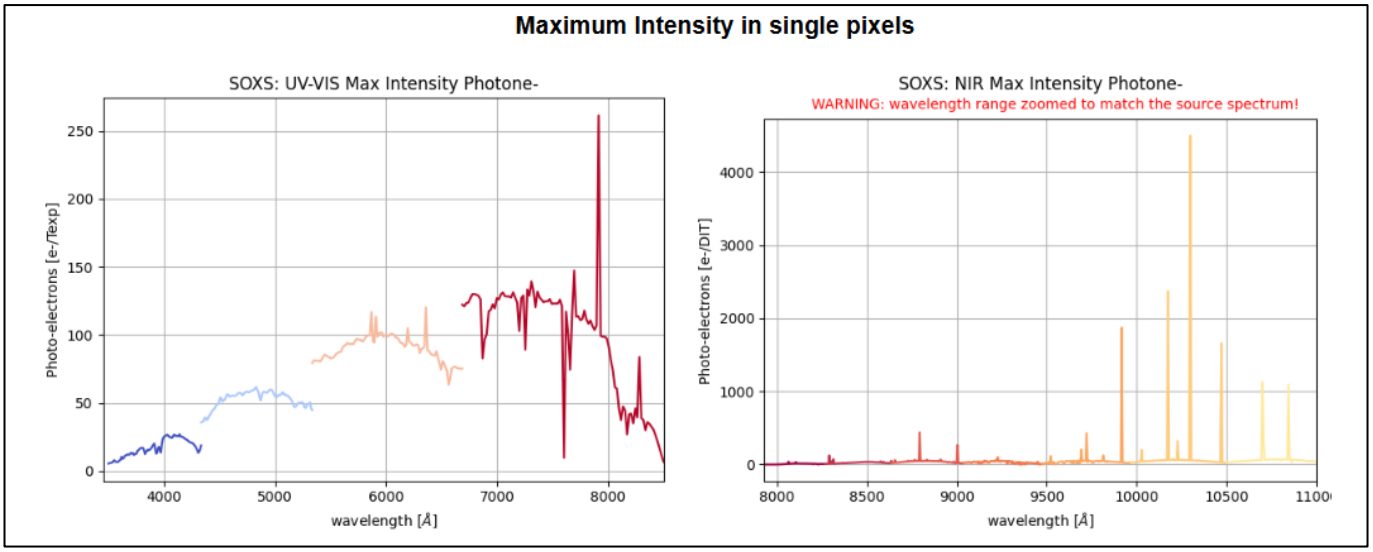

Figure 23. Maximum instensity per pixel plot.

Moreover, the different noise terms are plotted to give the user a fast and simple identification of the main limiting and dominating noise in an observation (i.e. if the observation is shot-noise or RON dominated). These are called as “squared noises” since are given in the plot as they appear in the denominator of the SNR formula (see 3.6.1). These are computed over the SNR area (see explanation above in *Figure 18*) to be coherent with their impact in the SNR.

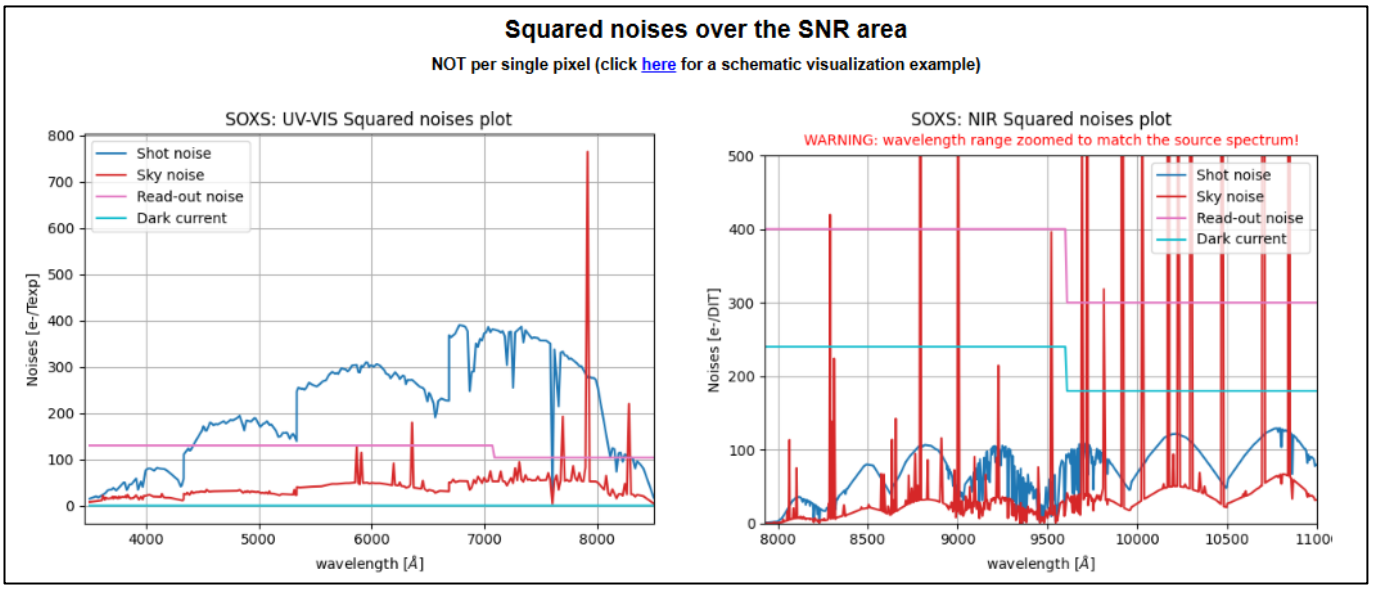

Figure 24. Squared-Noises plot over the SNR Area. The goal of this plot is to give the user a fast and simple identification of the main limiting and dominating noise in an observation. See the text for further details.

3.8.3 Example of Output Table (Spectrograph mode)

If the user selects also **Table** (by flagging it – see figure below), the ETC also returns results in a tabular format, similar to what is also done for the XSHOOTER ETC Webpage.

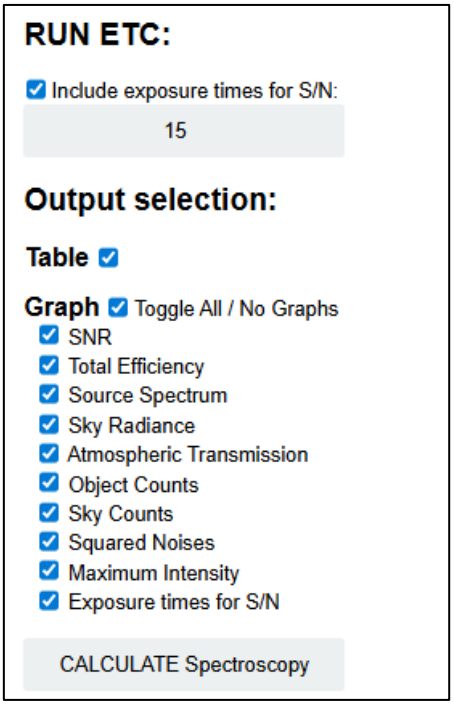

Figure 25. Selection of output results to be provided by the ETC. See in this case the Table flagged.

The tables are displayed for both UV-VIS and NIR arms.
Three wavelengths are reported for each diffraction order (or as called in the UV-VIS the 4 quasi-orders). For each wavelength the bin-size in Angstrom considered for the signal spectral integration (i.e. the pixel-bin or the SRE-bin according to user's selection) and the efficiency are given.
As shown in the subtitles of both tables (see examples in **Figure 26**) the signals Object, Sky and Max-Intensity (Imax) refer to one exposure (T. exp for UV-VIS, while DIT for NIR) but the S/N refers to all exposures that compose the observation (i.e. T. exp*N. exp for the UV-VIS, while the product DIT*NDIT*NINT for the NIR arm).
If the users also selected the option of deriving the exposure time to reach a defined SNR, this is also included in the table; this is computed assuming the same number of exposures set by the user (in the case of NIR arm, the same NDIT and NINT values).
Warnings are displayed in case where the time needed to reach the desired SNR is larger than 1 hours and also when the signal could be so low that the derived time would be unreasonable high (this may be caused by extremely low efficiency or by an object that is too faint).

UV-VIS

The signals **Obj**, **Sky** and **Imax** refer to one exposure (T. exp) but the **S/N** refers to all exposures (T. exp*N. exp)
* The exposure time required to reach the desired S/N is computed assuming the same number of exposures set by the user.

WARNING: For some wavelength the exposure time needed for reaching the desired S/N is greater than 1 hour.

Order	Lambda (Å)	Bin size (Å)	Eff. tot. (%)	Obj (e-/Texp)	Sky (e-/Texp)	Image Quality (arcsec)	Imax (e-/Texp)	S/N	T. exp(s) for S/N* = 15.0	FSR
1	3499.22	0.26	3.71	9.81	5.53	1.025	3.56	0.8	> 1 Hour	Min
1	3911.96	0.23	11.80	36.50	14.95	1.000	12.49	2.7	> 1 Hour	Blaze
1	4333.12	0.18	10.56	37.80	9.46	0.977	12.06	2.8	> 1 Hour	Max
2	4334.23	0.34	10.68	71.74	17.92	0.977	22.88	4.8	> 1 Hour	Min
2	4829.59	0.31	15.19	124.73	23.32	0.953	39.16	7.5	3374.75915	Blaze
2	5335.06	0.26	13.50	88.85	15.42	0.932	28.27	5.8	> 1 Hour	Max
3	5335.99	0.45	13.49	157.15	27.02	0.932	49.95	8.9	2657.366716	Min
3	6003.94	0.41	16.99	191.92	33.01	0.907	62.61	10.2	2175.826909	Blaze
3	6685.53	0.35	15.41	143.14	20.63	0.884	46.96	8.3	2875.543361	Max
4	6685.76	0.56	15.42	232.27	33.47	0.884	76.20	11.7	1771.592353	Min
4	7584.23	0.50	17.72	217.86	36.31	0.859	74.59	11.1	1911.297029	Blaze
4	8501.04	0.41	1.26	11.29	3.19	0.836	4.26	1.0	> 1 Hour	Max

NIR

The signals **Obj**, **Sky** and **Imax** refer to one exposure (DIT) but the **S/N** refers to all exposures (DIT*NDIT*NINT)
* The DIT required to reach the desired S/N is computed assuming the same NDIT and NINT values set by the user.

WARNING: For some wavelength the DIT needed for reaching the desired S/N is greater than 1 hour.
WARNING: Not enough signal indicates that the DIT required to achieve the desired S/N would take an unreasonable amount of time, this may be caused by extremely low efficiency or by an object that is too faint.

Order	Lambda (Å)	Bin size (Å)	Eff. tot. (%)	Obj (e-/DIT)	Sky (e-/DIT)	Image Quality (arcsec)	Imax (e-/DIT)	S/N	DIT(s) for S/N* = 15.0	FSR
24	7931.75	0.39	0.04	0.35	0.13	0.831	0.16	0.0	Not enough signal	Min
24	8098.10	0.38	2.56	22.35	4.75	0.826	9.46	0.7	> 1 Hour	Blaze
24	8267.85	0.36	1.36	11.26	2.66	0.822	4.86	0.4	> 1 Hour	Max
23	8268.71	0.41	1.37	12.95	3.06	0.822	5.59	0.4	> 1 Hour	Min
23	8450.11	0.40	5.10	44.53	12.07	0.818	19.73	1.4	> 1 Hour	Blaze
23	8635.22	0.38	3.25	26.90	78.34	0.813	31.39	0.8	> 1 Hour	Max
22	8636.30	0.43	3.29	31.03	9.26	0.813	14.05	1.0	> 1 Hour	Min
22	8834.12	0.41	7.98	69.92	59.27	0.809	42.38	2.1	> 1 Hour	Blaze
22	9035.99	0.39	3.44	28.24	9.48	0.804	13.21	0.9	> 1 Hour	Max
21	9037.17	0.45	3.41	30.86	10.34	0.804	14.43	1.0	> 1 Hour	Min
21	9254.69	0.43	7.82	66.88	23.89	0.800	31.87	2.1	> 1 Hour	Blaze
21	9476.66	0.41	0.60	12.42	4.57	0.795	5.98	0.4	> 1 Hour	Max
20	9478.13	0.48	2.31	14.95	5.5	0.795	7.21	0.5	> 1 Hour	Min
20	9717.32	0.45	7.38	65.66	25.7	0.790	32.27	2.0	> 1 Hour	Blaze
20	9961.39	0.43	3.67	29.84	12.3	0.785	14.93	0.9	> 1 Hour	Max
19	9963.59	0.50	3.72	35.21	14.52	0.785	17.62	1.1	> 1 Hour	Min
19	10228.62	0.48	9.03	78.71	649.48	0.780	215.39	1.9	> 1 Hour	Blaze
19	10499.06	0.45	4.00	31.85	15.14	0.775	16.70	1.2	> 1 Hour	Max
18	10500.97	0.53	4.04	37.69	18.43	0.775	19.92	1.4	> 1 Hour	Min
18	10796.71	0.50	9.88	83.75	45.58	0.770	45.87	2.9	> 1 Hour	Blaze
18	11098.49	0.48	3.56	0.00	9.03	0.764	2.62	0.0	Not enough signal	Max
17	11101.58	0.56	4.39	0.00	15.34	0.764	4.46	0.0	Not enough signal	Min
17	11431.64	0.53	9.58	0.00	33.08	0.759	9.69	0.0	Not enough signal	Blaze
17	11768.44	0.50	4.66	0.00	14.55	0.753	4.29	0.0	Not enough signal	Max
16	11772.72	0.60	4.72	0.00	17.51	0.753	5.17	0.0	Not enough signal	Min
16	12145.89	0.57	8.85	0.00	20.94	0.747	6.23	0.0	Not enough signal	Blaze
16	12526.68	0.53	5.10	0.00	1.12E+03	0.742	335.37	0.0	Not enough signal	Max
15	12530.92	0.64	5.23	0.00	11.3	0.742	3.39	0.0	Not enough signal	Min
15	12955.35	0.61	11.92	0.00	21.62	0.735	6.53	0.0	Not enough signal	Blaze
15	13388.44	0.56	4.17	0.00	9.11	0.729	2.78	0.0	Not enough signal	Max
14	13392.24	0.69	2.92	0.00	8.7	0.729	2.65	0.0	Not enough signal	Min
14	13880.39	0.65	0.00	0.00	0.08	0.723	0.03	0.0	Not enough signal	Blaze
14	14378.49	0.60	0.00	0.00	0.09	0.717	0.03	0.0	Not enough signal	Max
13	14383.28	0.75	2.53	0.00	8.8	0.716	2.73	0.0	Not enough signal	Min
13	14947.71	0.70	11.36	0.00	132.59	0.710	41.52	0.0	Not enough signal	Blaze
13	15523.66	0.64	4.85	0.00	31.78	0.703	10.05	0.0	Not enough signal	Max
12	15530.42	0.81	4.93	0.00	40.35	0.703	12.76	0.0	Not enough signal	Min
12	16192.84	0.76	12.25	0.00	120.33	0.696	38.44	0.0	Not enough signal	Blaze
12	16868.78	0.69	5.34	0.00	18.69	0.689	6.03	0.0	Not enough signal	Max
11	16876.21	0.89	5.43	0.00	25.01	0.689	8.07	0.0	Not enough signal	Min

Figure 26. Output results tables examples. UV-VIS arm top panel. NIR arm bottom panel.

3.8.4 Example Input Page (Imaging mode)

In addition to the science object input flux distribution and sky/atmosphere conditions already shown in previous section, when Imaging is selected, the related instrument set-up can be configured in terms of: filter, exposure time and number of exposures.

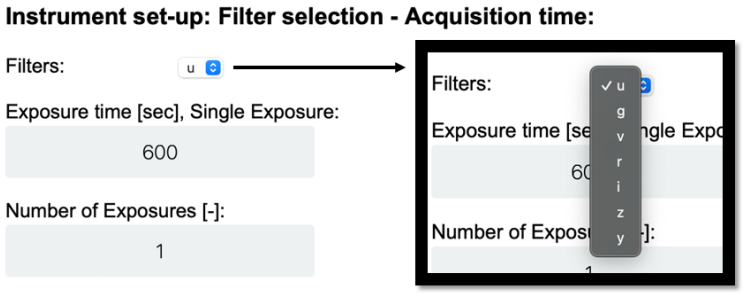

Figure 27. Graphical layout of the internal ETC simulator of SOXS. Instrument set-up input parameters for Imaging.

3.8.5 Example of Output plots (Imaging mode)

The main output plots in imaging mode are:

- Signal to Noise vs exposure time
- Noises vs exposure time
- Filter efficiency (incl. Acq. Camera Transmission)
- Total efficiency (composed by):
  - Acquisition Camera Transmission
  - Filter efficiency
  - Telescope efficiency
  - Atmospheric transmission

In the following, a simulation of a 5600K black body, with mag-V = 20 in AB system. The observation is simulated 1 day from New-Moon at AM = 1.16 with a PWV = 10 mm and a seeing at 500nm of 1.0 arcsec. The selected filter is V in a single exposure of 60 seconds.

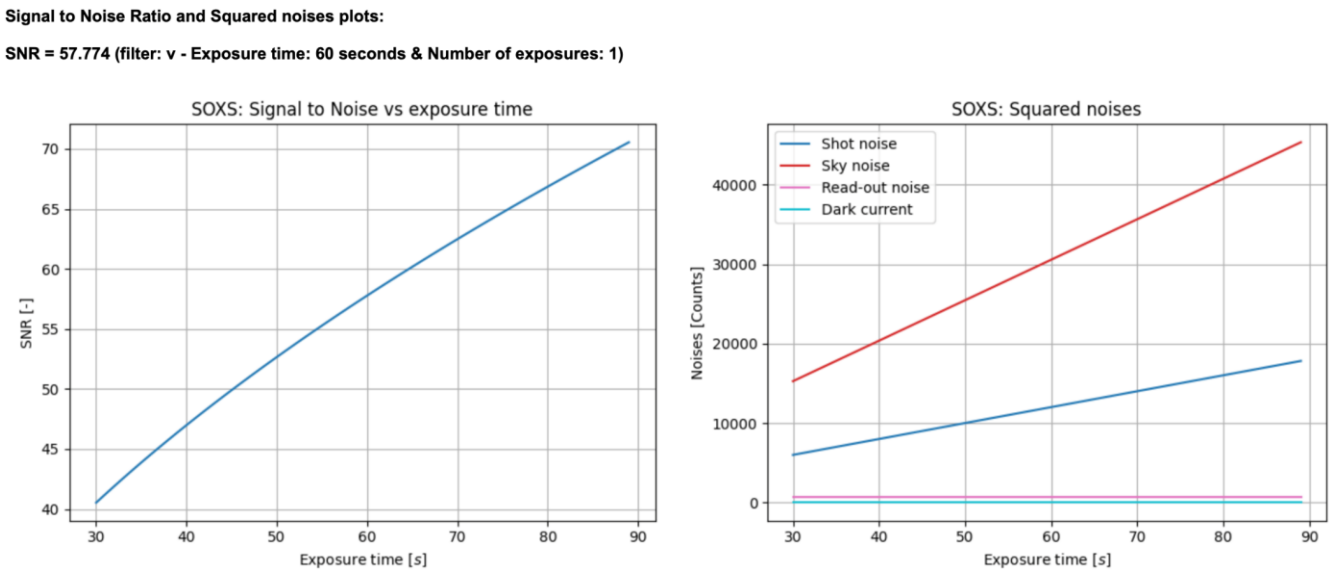

Figure 28. Imaging mode output plots example. SNR and Noises versus exposure time.

Filter and Total efficiency

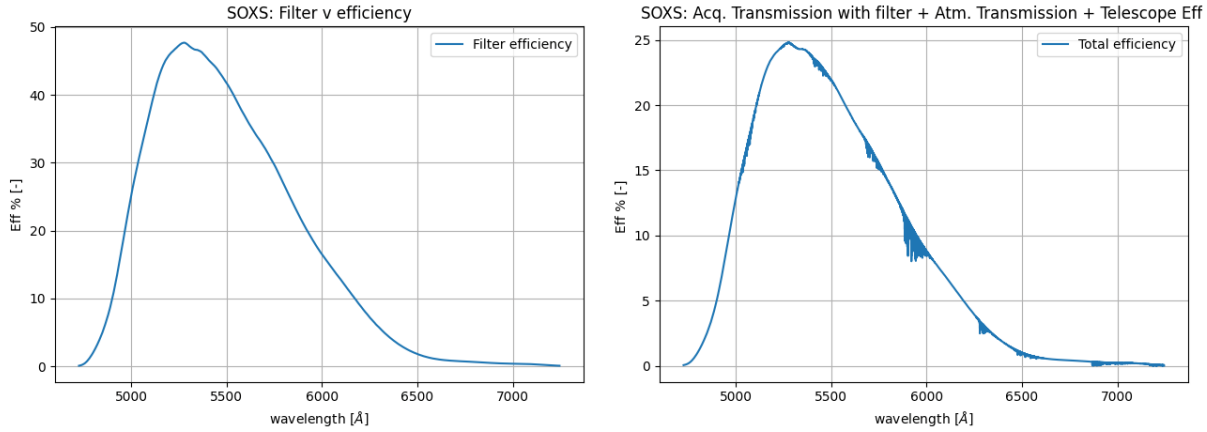

Figure 29. Imaging mode output plots example. Selected filter profile and total acquisition camera efficiency.

3.9 Thermal noise in NIR arm

During the full AIT phase of NIR spectrograph baffling installation was done to ensure that the total dark-current + thermal noise is below 0.05 e-/s/pixel, as required by the Instrument Scientist.

Figure 30 shows a plot of series of dark-current + thermal noise levels derived from a series of dark frames was obtained at different temperatures of the vacuum vessel (VV), spanning from 156 to 142 K, with the detector being always at T ~ 42 K. The detector read-out procedure was the Up-the-Ramp mode and the derived gain 2.3 e-/DN (digital number); the DIT was 1200 seconds for all frames.

The requirement is met for VV temperature below 148/147 K with a possibly final operating temperature (TBC during ongoing system tests in Padova) at 145 K.

The present implemented value in the ETC is 0.05 e-/s/pixel.

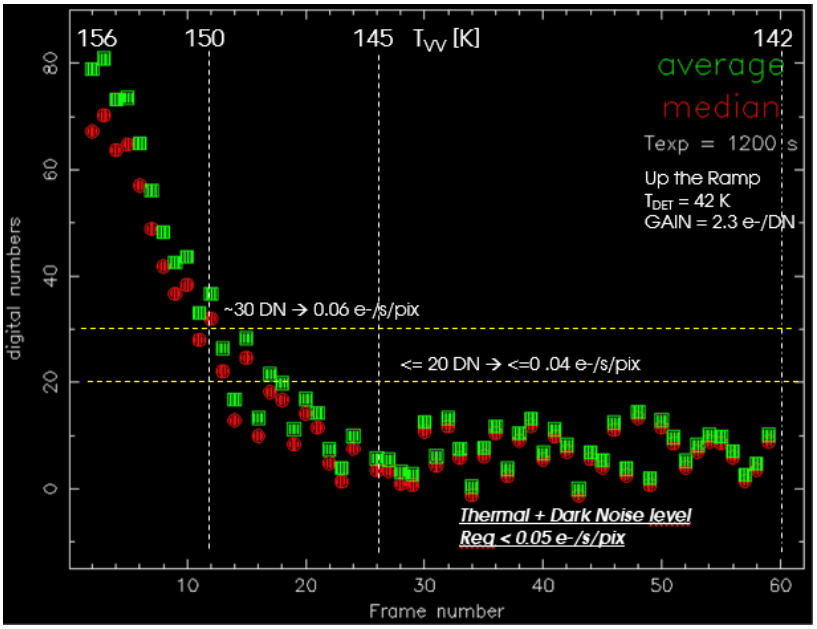

Figure 30. NIR thermal and dark noise level plot, for VV temperature range from 156 to 142 K and detector at about 42 K. Both average (green squares) and median (red circles) measures are shown. The requirement is met for the region below 148/147 K.

3.10 Test Unit

The ETC code and its specific units and functions were tested separately in order to verify the products of the different code steps. The Units tests were done by applying the features of different ESO VLT spectrographs. The results obtained by the different instruments were compared with the outputs generated by the respective ETC web pages. Below are the results, along with the methods used for each step, of the various comparisons performed.

3.10.1 Spectral Energy Distribution

The first test unit performed is related to the generation of the different input spectral energy distributions (SEDs). The ETC of X-SHOOTER has the same typologies of SED that will be present in the ETC of SOXS, for this reason it has been chosen to carry out this first test.

As explained in sec. 3.7, the different SEDS are first generated in units of $[erg/(s \cdot cm^2 \cdot \text{Å})]$, then converted in units of $[ph/(s \cdot cm^2 \cdot \text{Å})]$. Finally the SEDs are rescaled according to the simulated magnitude and filter; the Zeropoints applied inside the code have been taken from ESO at the following web page. As mentioned, the Zeropoints are thus obtained by integrating across each band pass filter transmission (T(λ)) and the Vega spectrum (Vg(λ)):

$$ZeroPoint \equiv \frac{\int T(\lambda) Vg(\lambda) d\lambda}{\int T(\lambda)\, d\lambda}$$

3.10.1.1 Black-Body

The test for the black-body was performed considering an equivalent reference temperature of 5600 K and using two magnitude values 13 and 17 for the U, B, V, R, I, J, H and K bands in both the Vega and AB reference systems.

In addition, each test was performed by applying the following redshift values: 0, 1 and 2.

An example of a comparison table for a SED in units of $[erg/(s \cdot cm^2 \cdot \text{Å})]$ is given in the following table as the ratio between X-SHOOTER values to the ones computed with our code.

ERGS	ESO (Vega) - T: 5600 K					
REDSHIFT	0		1		2	
BANDS/MAG	13	17	13	17	13	17
U	1,77%	1,79%	5,16%	5,18%	5,56%	5,58%
B	-3,27%	-3,25%	-0,01%	0,01%	2,09%	2,11%
V	0,33%	0,35%	2,98%	3,00%	4,93%	4,95%
R	1,74%	1,76%	6,25%	6,27%	10,88%	10,90%
I	-0,82%	-0,80%	0,40%	0,41%	0,92%	0,94%
J	1,18%	1,20%	2,20%	2,22%	2,52%	2,54%
H	0,25%	0,27%	0,75%	0,76%	0,55%	0,56%
K	-1,39%	-1,37%	-1,29%	-1,27%	-1,94%	-1,93%
					Mean:	2,47%

Table 3. Percentage variation of the black-body fluxes between the code and the ETC of X-SHOOTER, considering the former as the reference value (The flux values used as a comparison were extracted where maxima within their own spectrum).

Examples of the SED profiles compared are shown in the panels of *Figure 31*, where the considered filters, band-system, magnitude and applied red-shift is in the figures title.

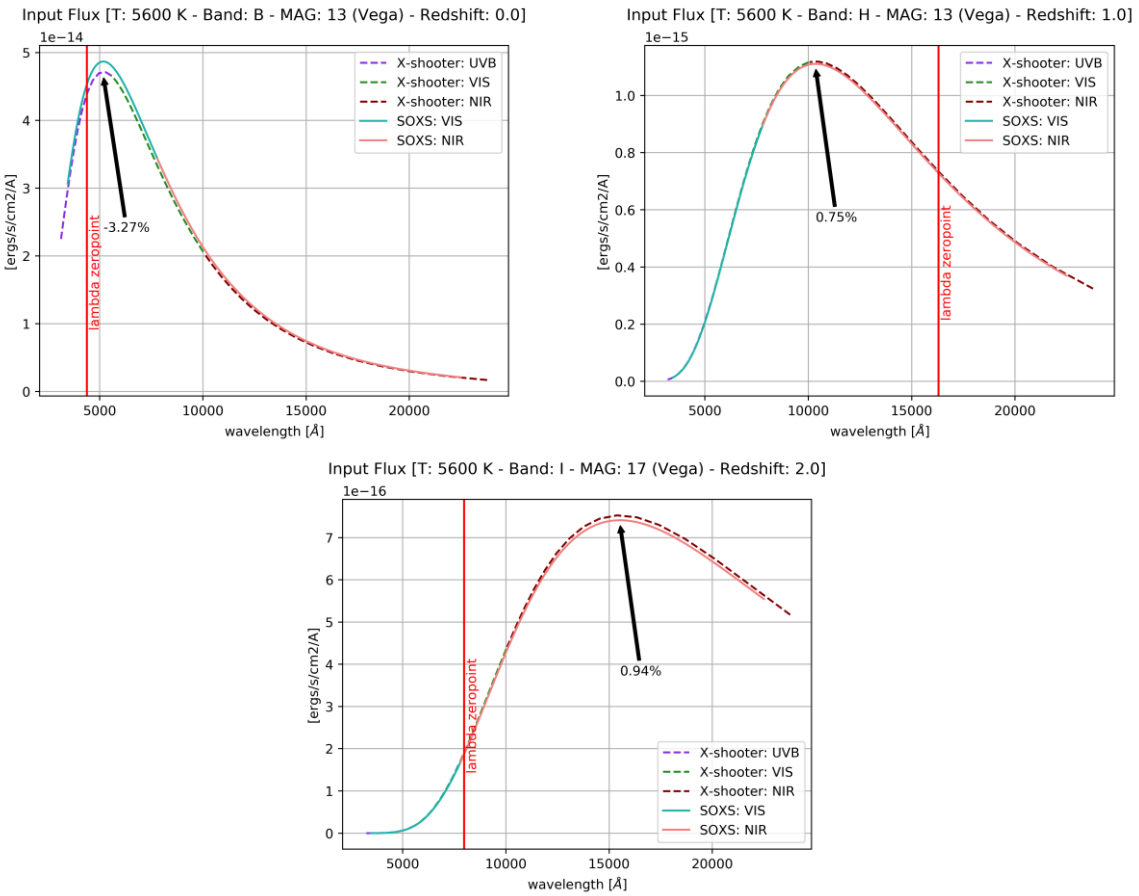

Figure 31. Three representative examples of Table 3.

The table and plot examples demonstrate that the agreement with the XSHOOTER and SOXS codes results is within 3% in most of the cases with some exception of 5-6% in visible bands. The mean difference is 2.47%. No exhaustive explanations are found to explain the 10% difference in R-band at z=2.

3.10.1.2 Power-Law

The applied formula for the power law has been described in section 3.7.2, while, as for the test on the blackbody, different configurations have been verified, such as indexes 2, 1, -1, -2 and -5. We also tested relatively extreme values, such as -5 (no matter the identification with specific astronomical objects) in order to check the code also in these conditions. An example of a comparison table for a SED in units of $[erg/(s \cdot cm^2 \cdot \text{Å})]$ is given in the following table at a single magnitude value of 17 in the Vega system.

ergs/s/cm2/A	ESO (Vega) - BANDPASS				
MAGNITUDE	17				
BANDS/INDEX	2	1	-1	-2	-5
U	0,84%	0,38%	-0,80%	-1,76%	-5,09%
B	-9,79%	-7,06%	-4,25%	-4,80%	-6,38%
V	2,05%	1,08%	0,14%	-0,39%	-1,85%
R	14,58%	8,03%	2,03%	0,98%	-1,67%
I	3,43%	1,53%	-0,42%	-0,77%	-1,79%
J	4,56%	3,36%	2,14%	1,66%	-0,22%
H	2,36%	1,69%	0,99%	0,71%	-0,11%
K	-1,26%	-1,42%	-1,38%	-1,29%	-1,18%
				Mean:	2,66%

Table 4. Percentage variation of the power-law fluxes between the code and the ETC of X-SHOOTER, considering the former as the reference value.

Examples of the SED profiles compared are shown in the panels of *Figure 32*, where the considered filters, band-system, magnitude and applied red-shift is in the figures' title.

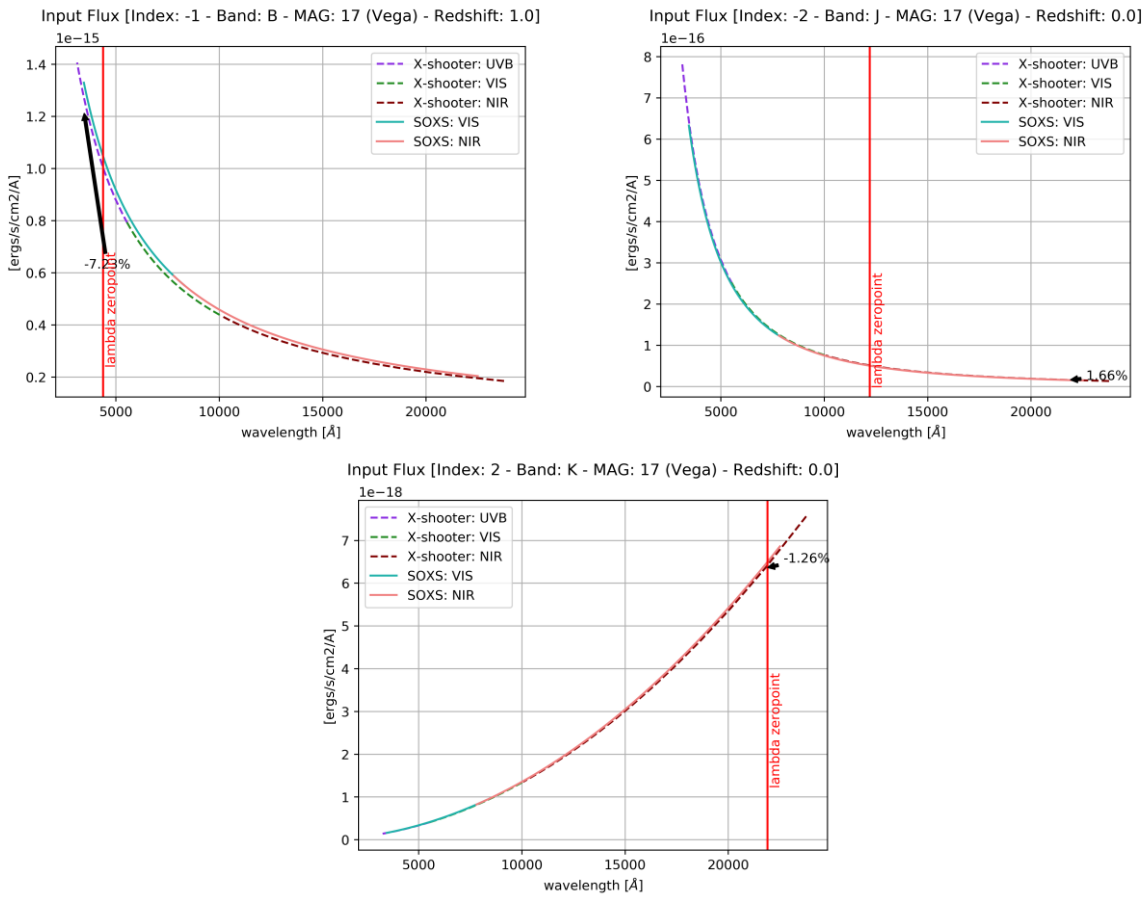

Figure 32. Three representative examples of Table 4.

The *Table 4* and plot examples demonstrate that the agreement with the XSHOOTER and SOXS codes results is within 3% in most of the cases with some exception of 5-10% in visible bands. The mean difference is 2.47%. No reliable explanations are found to explain the 14.58% difference in R-band at index=2.

3.10.1.3 Template Spectrum

Multiple template spectra were considered during this test unit, one for each different category: Pickles A0V, Kurcuz B1V, Sb Galaxy, Starburst Galaxy 1. Results in the following tables.

ergs/s/cm2/A	ESO (Vega) - BANDPASS		
MAGNITUDE	17		
BANDS/REDSHIFT	0	0.5	1
U	-0,01%	0,22%	-0,47%
B	-3,57%	-3,60%	-4,52%
V	-0,76%	3,17%	0,73%
R	0,07%	1,76%	4,97%
I	-1,12%	-0,97%	1,00%
J	0,91%	1,27%	1,15%
H	0,36%	0,36%	0,46%
K	-1,21%	-1,16%	-1,19%
		Mean:	1%

ergs/s/cm2/A	ESO (Vega) - BANDPASS		
MAGNITUDE	17		
BANDS/REDSHIFT	0	1	2
U	-3,10%	-3,26%	-1,40%
B	-5,24%	-4,90%	-5,56%
V	-1,17%	-0,92%	-0,78%
R	-0,59%	0,01%	0,53%
I	-1,39%	-0,91%	-1,19%
J	-11,47%	0,81%	1,25%
H		0,20%	0,18%
K			-1,28%
		Mean:	2%

ergs/s/cm2/A	ESO (Vega) - BANDPASS		
MAGNITUDE	17		
BANDS/REDSHIFT	0	1	2
U	0,42%	14,27%	0,47%
B	-1,94%	-3,86%	-3,81%
V	0,86%	3,04%	-1,09%
R	3,04%	5,56%	1,69%
I	-0,24%	1,33%	0,83%
J	2,54%	2,70%	4,15%
H	-9,94%	1,27%	1,35%
K		-1,50%	-1,04%
		Mean:	3%

ergs/s/cm2/A	ESO (Vega) - BANDPASS		
MAGNITUDE	17		
BANDS/REDSHIFT	0	1	2
U	1,36%	-1,20%	0,12%
B	-4,01%	-4,53%	-4,41%
V	-1,00%	-0,17%	-0,27%
R	1,75%	2,79%	1,37%
I	-0,99%	-0,21%	-0,80%
J	2,61%	2,53%	2,09%
H	-9,87%	0,83%	0,46%
K		-1,48%	-0,42%
		Mean:	2%

Table 5. Percentage of fluxes variation in different spectrum (Top: left Pickels A0V, right Kurucz B1V, Bottom: left Sb Galaxy, right starb1 Galaxy) between the code and the ETC of X-SHOOTER, considering the former as the reference value.

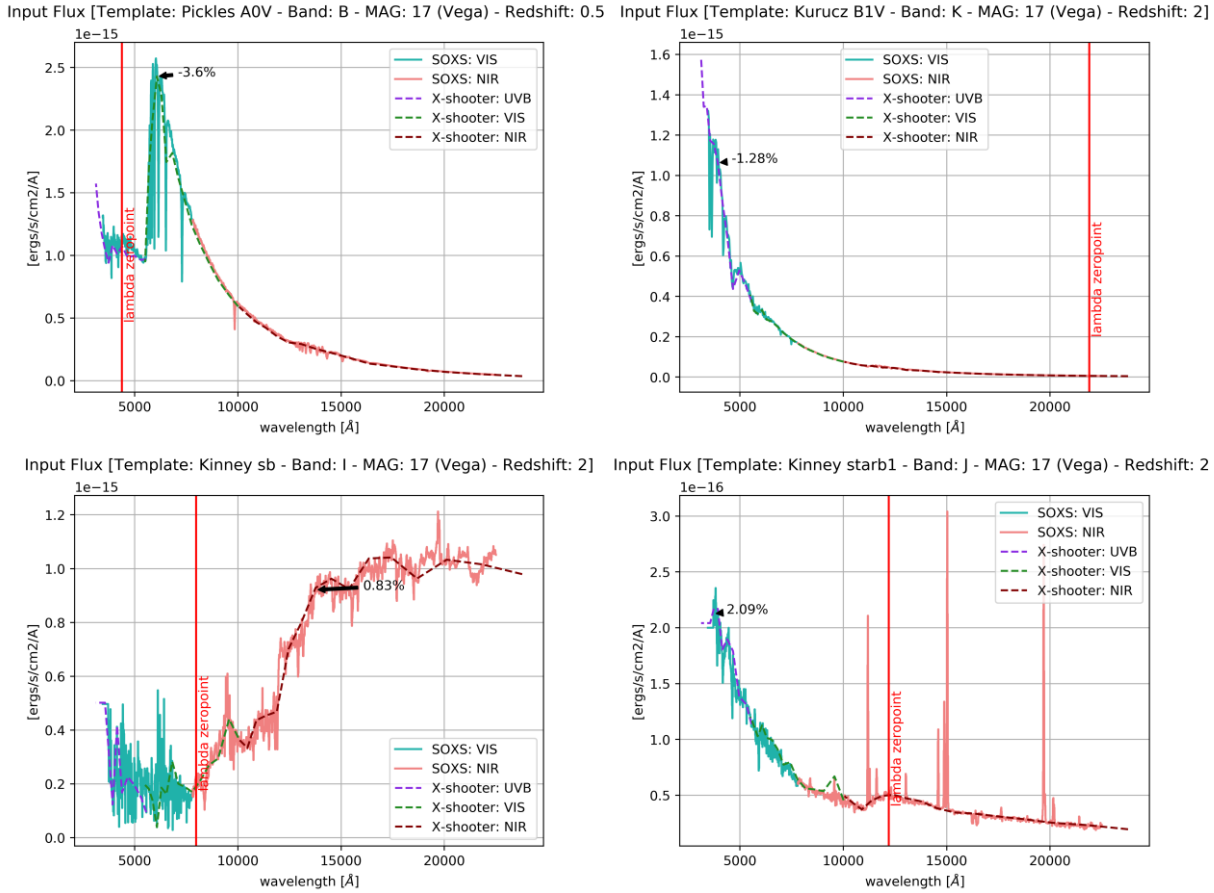

Figure 33. An example for each type of spectrum represented in Table 5.

Table 5 shows how the percentage difference between the SOXS code and the results obtained by the ETC of XSHOOTER is around an average of 1% for A0V, 2% for B1V and starb1, and up to a maximum of 3% for Sb galaxy. There are two singular cases in the J-band of B1V and in the U-band of Sb galaxy, of -11.47% and 14.27% respectively for which no adequate explanation has been found. In *Figure 33* there are 4 examples, one for each type tested, in which it is possible to verify how the shape of the spectra, as well as the emission and absorption lines, find correspondence between the code and the ETC of XSHOOTER.

3.10.1.4 Emission Line

The last test carried out for the SEDs concerned the single emission line, for this unit the code was compared with the ETC of the FORS2 Spectrograph and the results obtained by varying the FWHM are shown below.

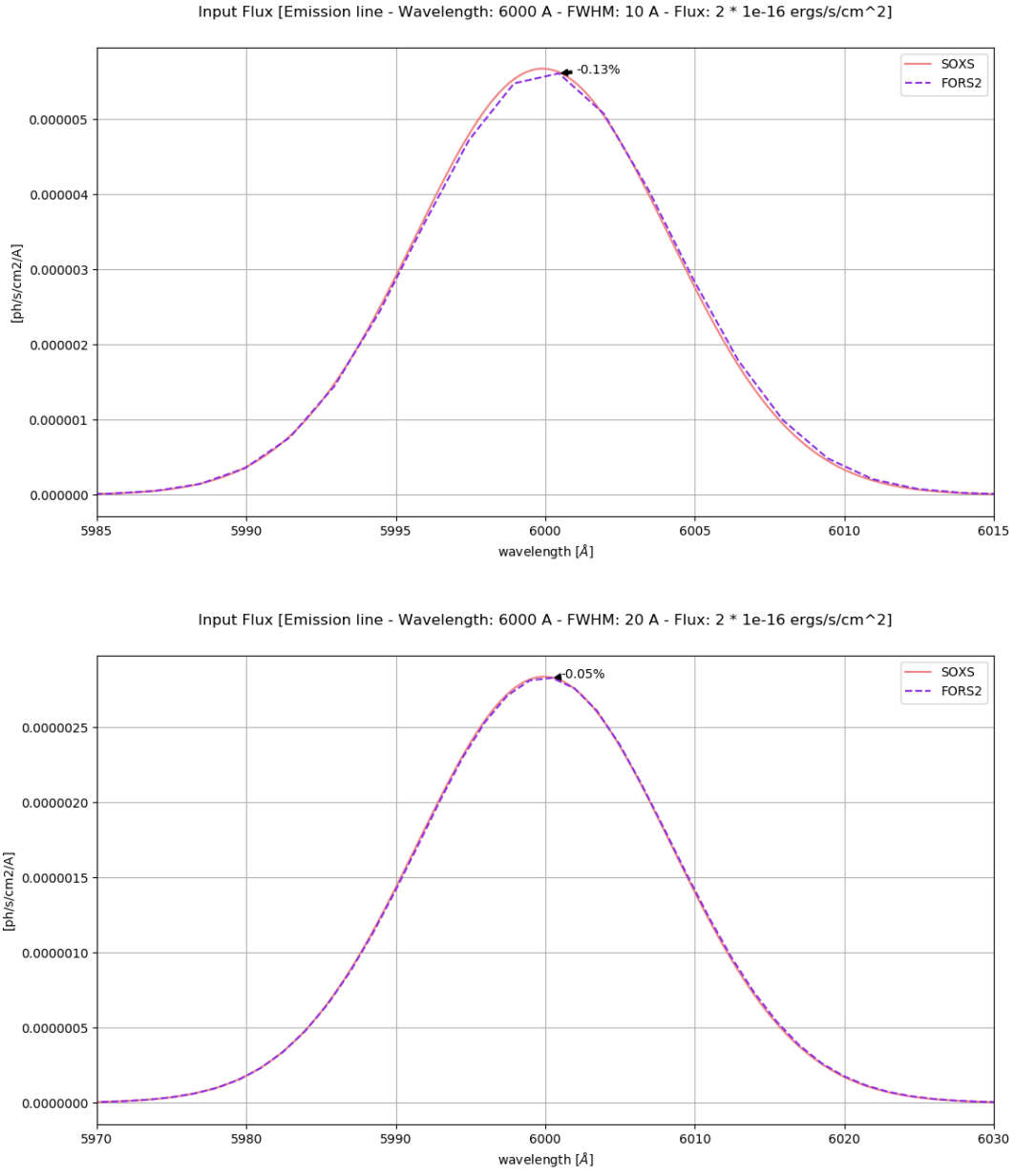

Figure 34. Single line emission fluxes compared with the ETC of FORS2.

3.10.2 Seeing and Slit efficiency

The impact of seeing and turbulence condition on the slit efficiency are modeled as explained in sec. 3.6.2. The example of the slit-through profile for SOXS UV-VIS and NIR arms, for a reference seeing at zenith of 1 arcsec at 5000 A, considering the 1 arcsec slit width is shown in plots of Figure 35.

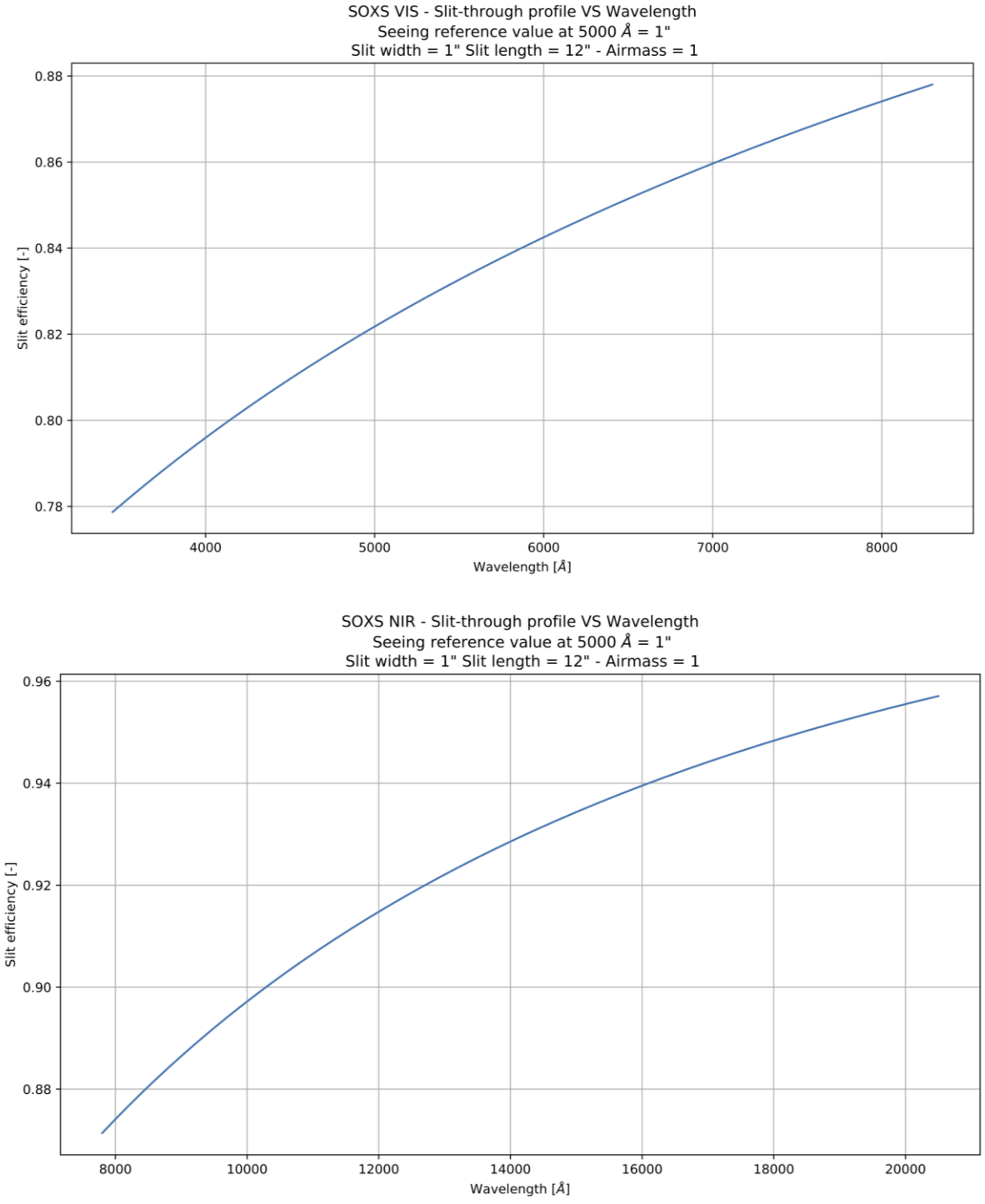

Figure 35. Slit Efficiency of SOXS in the UV-VIS and NIR arm.

In addition, considering the reference wavelength at 5000 A, it is possible to observe in Figure 36 how the efficiency of the SOXS slit varies as a function of the atmospheric seeing.

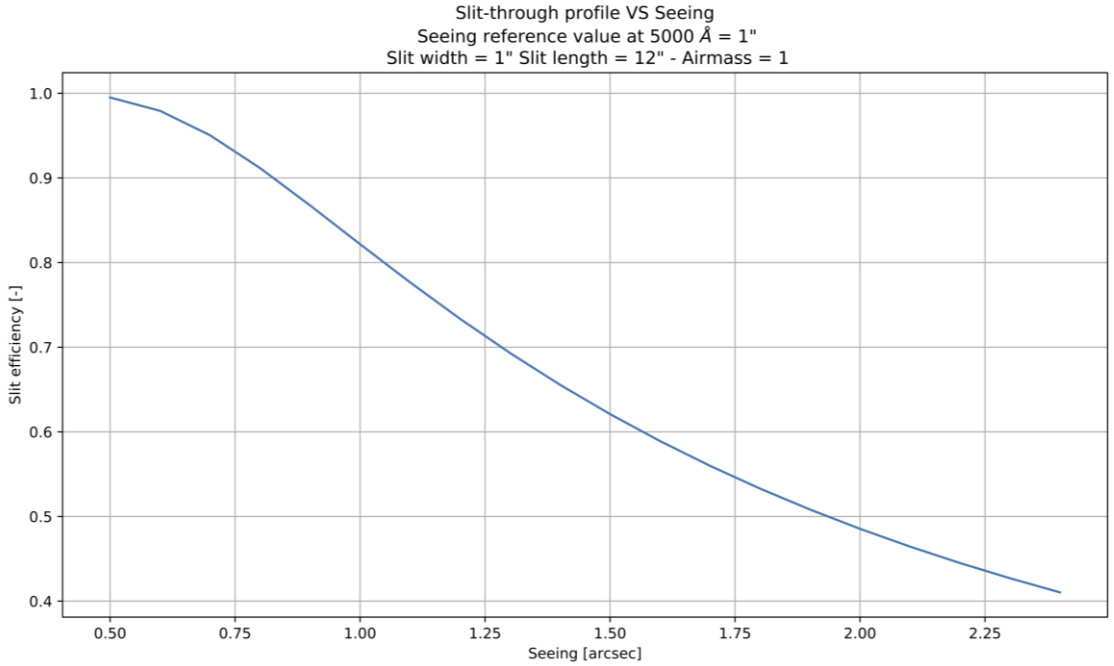

Figure 36. Slit Efficiency of SOXS vs Seeing.

Finally, a correct match, as shown in Figure 37, was verified using the code to evaluate the X-SHOOTER slit efficiency and then comparing it with the data obtained from the corresponding ETC webpage. All three arms of the spectrograph were verified (UVB, VIS and NIR) and different seeing values were also tested.

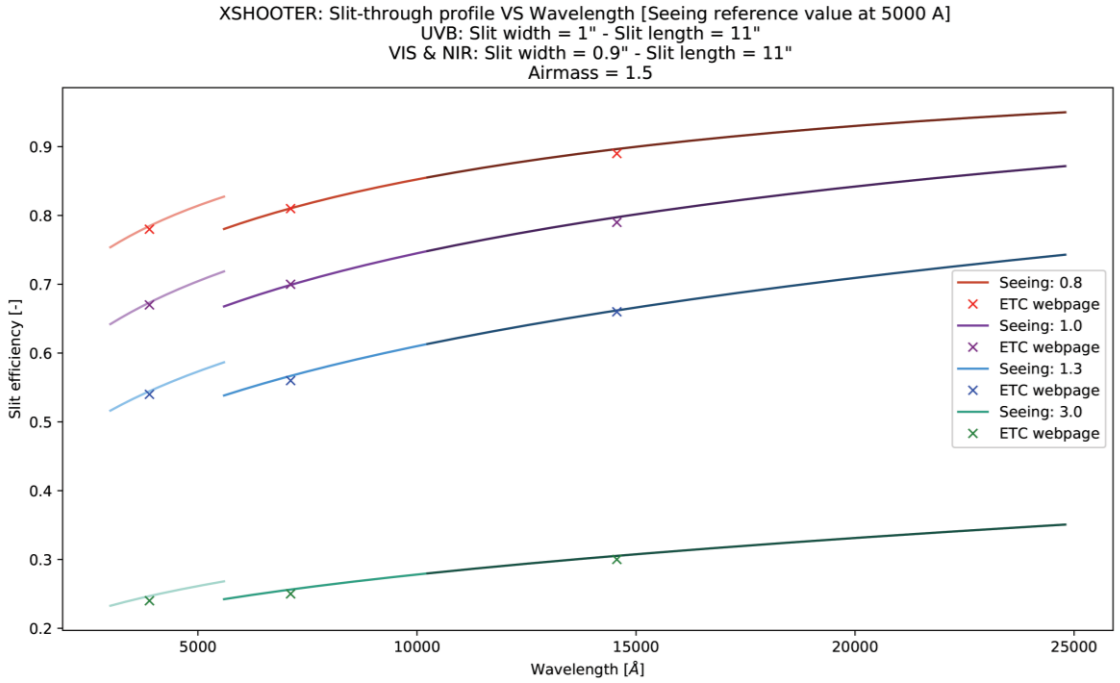

Figure 37. Slit Efficiency of X-SHOOTER obtained through the implemented code and compared with its ETC web page.

3.10.3 Sky Counts

Sky counts are calculated from the sky radiance obtained from the SkyCalc tool given in [ph/(s*m2*um*arcsec2)] and converted in units of [ph/(s*cm2*A*arcsec2)]. The radiance is then multiplied by the area [arcsec2] of the slit taken into consideration, by the seconds of exposure time and by the effective telescope area. The result in units of [ph/A] is finally integrated over the delta lambda [A] between pixels to get the Sky Counts in [e-/Texp], or, as reported below, some ETC spectrographs consider a single pixel in the spatial direction [e-/Pixel/Texp]. The efficiency of the instrument is applied to the final counts, while atmospheric transmission is already taken into account in the initial sky radiance (Slit loss are not to be considered for the sky signal).

The parameters used for the following tests are:

- Airmass: 1 (thus at zenith)
- Moon FLI: 1 (thus full moon)
- Seeing (at 5000 A): 1 arcsec
- T. exp or DIT: 900s

3.10.3.1 FORS2

For the visible part of the sky counts spectrum the ETC of FORS2 is used for comparison, since it gives in output the full spectrum over its wavelength band.

Characteristics:

- Slit Width: 1”
- Slit Length: 6.8”
- On-Sky area considered: Slit Width * Bin Scale = 0.125 arcsec2 [Sky counts from the ETC webpage are provided per pixel in the spatial direction and NOT by the PSF extension]
- VLT Telescope effective area considered also in the FORS2 ETC: 51.2 m2

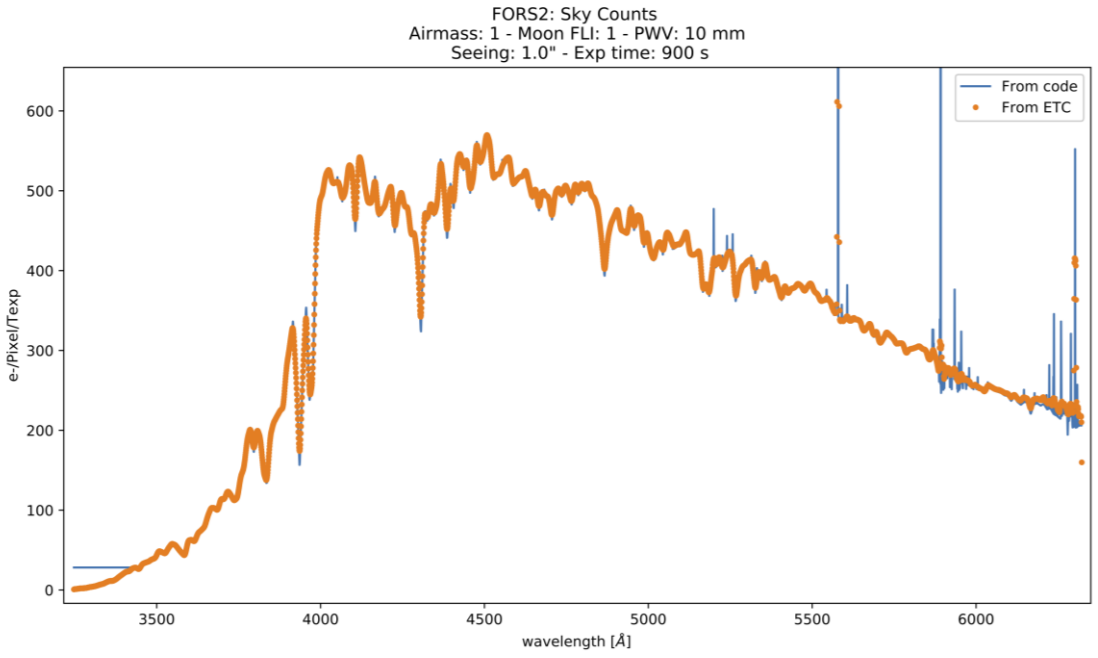

Figure 38. Comparison of sky counts obtained by code and by the ETC of FORS2.

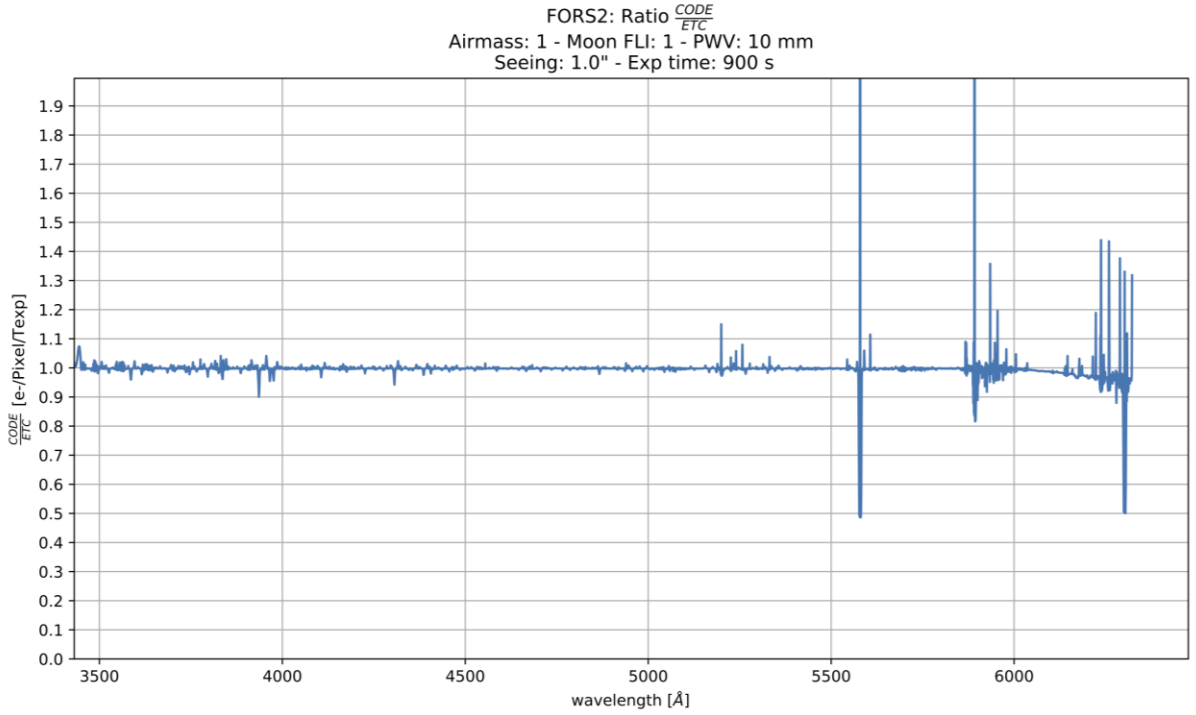

Figure 39. Ratio between the code and the ETC of FORS2.

From the plot of sky counts profile and ratio (between our code and FORS2-ETC), shown in Figure 38 and Figure 28, we verify that the computations are in very good accordance. The mean ratio is 1, while some variations larger than 10% are present above 5000 A are due to strong emission or absorption lines which affects the integral calculation over the wavelength step.

3.10.3.2 SOFI

For the NIR part of the sky counts spectrum the ETC of SOFI-NTT is used for comparison, since it gives in output the full spectrum over its wavelength band (two arms 9500-16500 A and 15000-20000 A).

Characteristics:

- Slit Width: 1”
- Slit Length: 290”
- On-Sky area considered: Slit Width * Bin Scale = 0.29 arcsec2 [Sky counts from the ETC webpage are provided per pixel in the spatial direction and NOT by the PSF extension]
- NTT Telescope effective area considered also in the SOFI ETC: 8.9 m2

Also, for the NIR part of the spectrum the test has positive results as can be seen in the next figures (29, 30, 31, 32). Obviously in the NIR, a larger presence of emission and absorption lines difference, again probably affecting the results of the integral calculation over the wavelength bin, can be seen in the ratio plots.

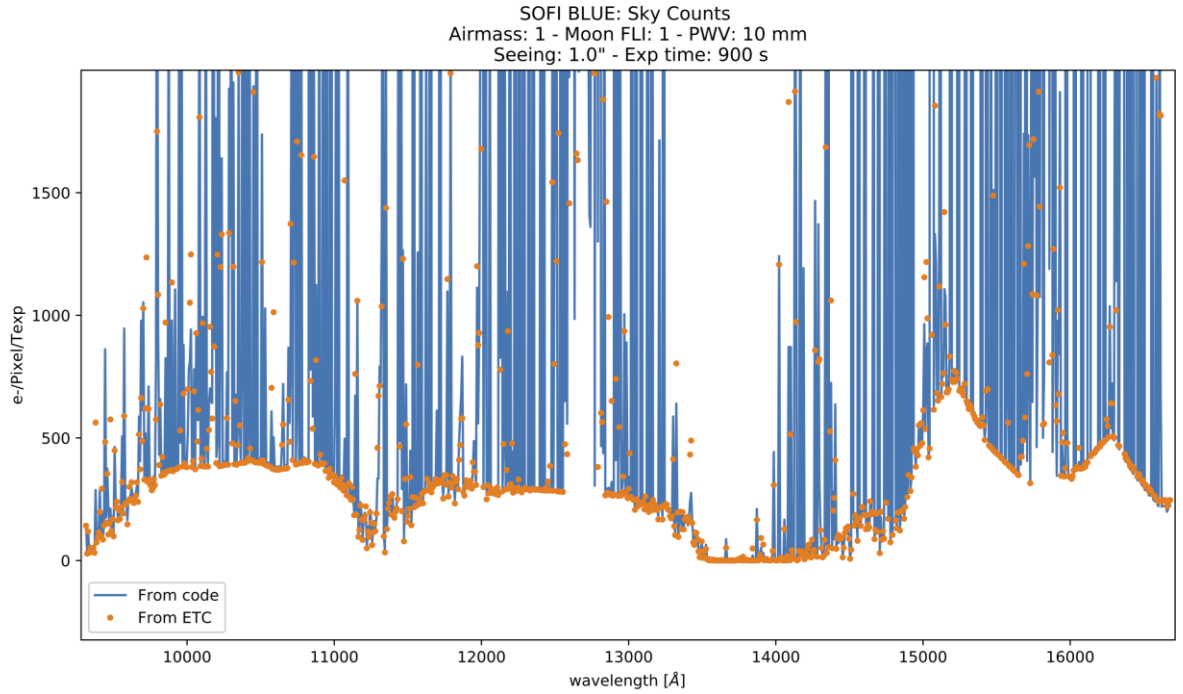

Figure 40. Comparison of sky counts obtained by code and by the ETC web page of SOFI the "BLUE" arm.

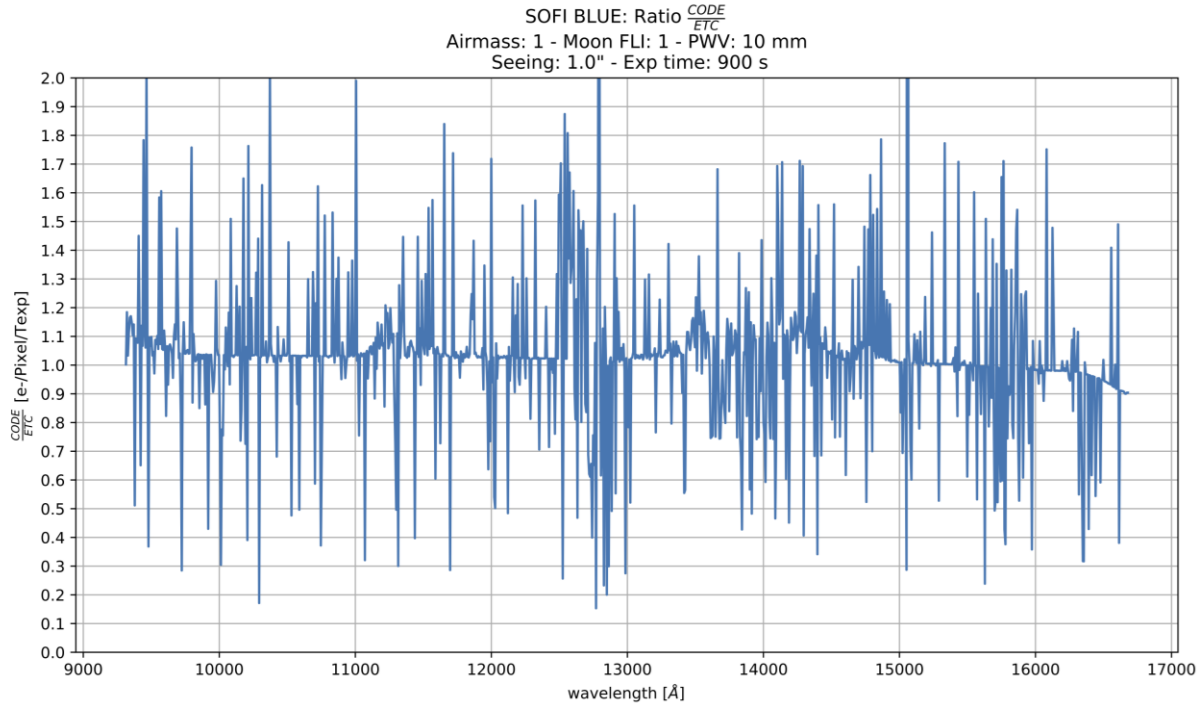

Figure 41. Ratio between the code and the ETC of SOFI in the "BLUE" arm.

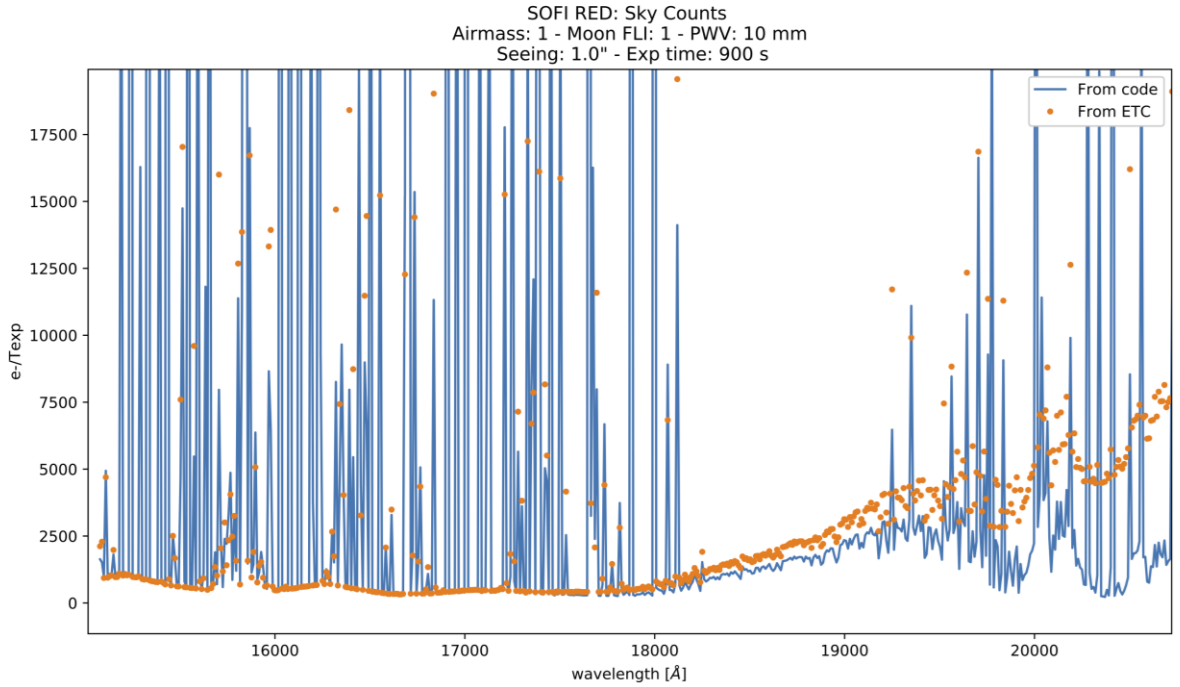

Figure 42. Comparison of sky counts obtained by code and by the ETC web page of SOFI in the "RED" arm.

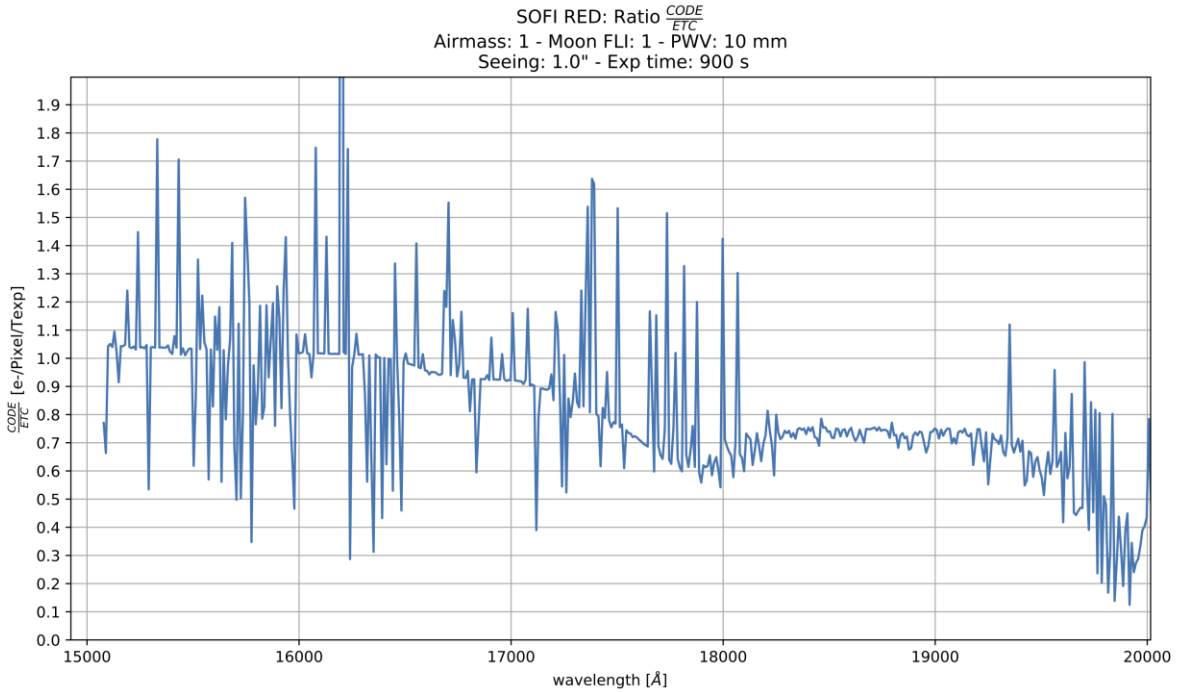

Figure 43. Ratio between the code and the ETC of SOFI in the "RED" arm.

3.10.4 Object Counts

Object counts in [e-/Texp] are obtained from the previously selected spectral energy distribution (SED), which from [ph/s/cm2/A] are multiplied by the effective telescope area in [cm2] and by the exposure time in [s]. The result in [ph/A], as performed for the sky counts, is integrated over the delta lambda [A] between pixels. Instrument efficiency and slit loss, along with atmospheric transmission are taken into account in the final counts. The following tests were carried out comparing the code with different instruments while considering an exposure time of 900 seconds, seeing of 1" (at 5000 A) and arimass equal to 1 (thus at zenith).

3.10.4.1 FORS2

The FORS2 ETC was chosen to test the code for the UV-VIS arm of the instrument and as shown below the comparison was performed with several SEDs.

Characteristics:

- Slit Width: 1”
- Slit Length: 6.8”
- VLT Telescope effective area considered also in the FORS2 ETC: 51.2 m2
- Total efficiency of FORS2 is shown in Figure 44.

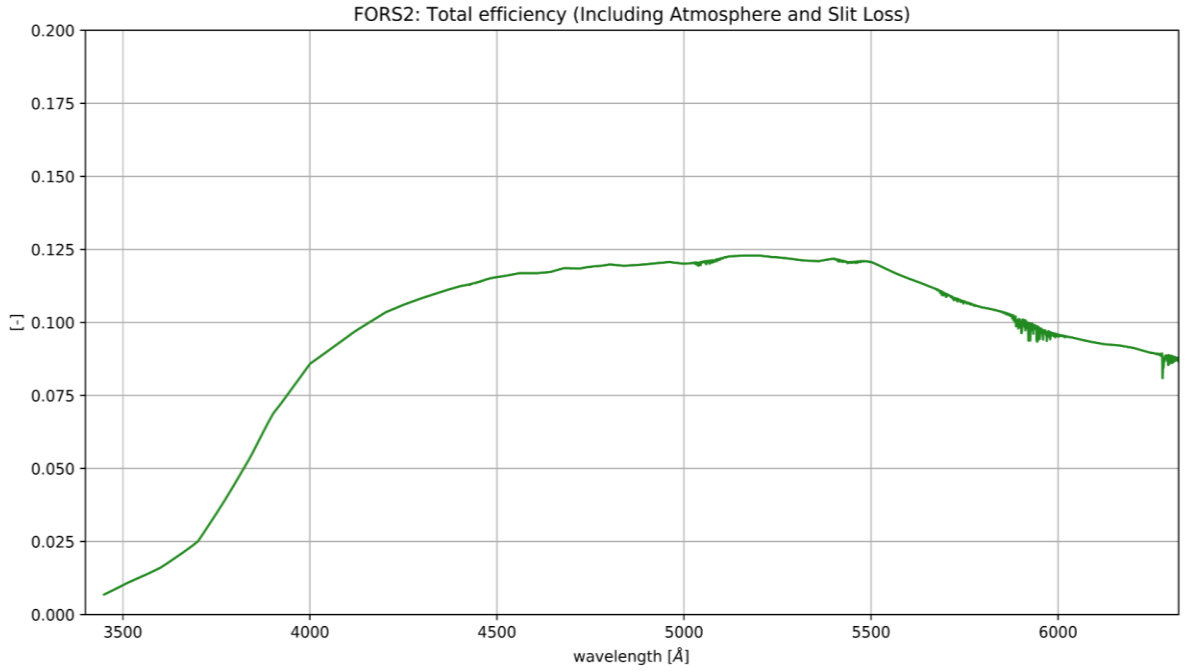

Figure 44. Total efficiency of FORS2, including Atmosphere transmission and Slit Loss.

Power-Law:

- Index: 1
- Magnitude: 20
- Band: V

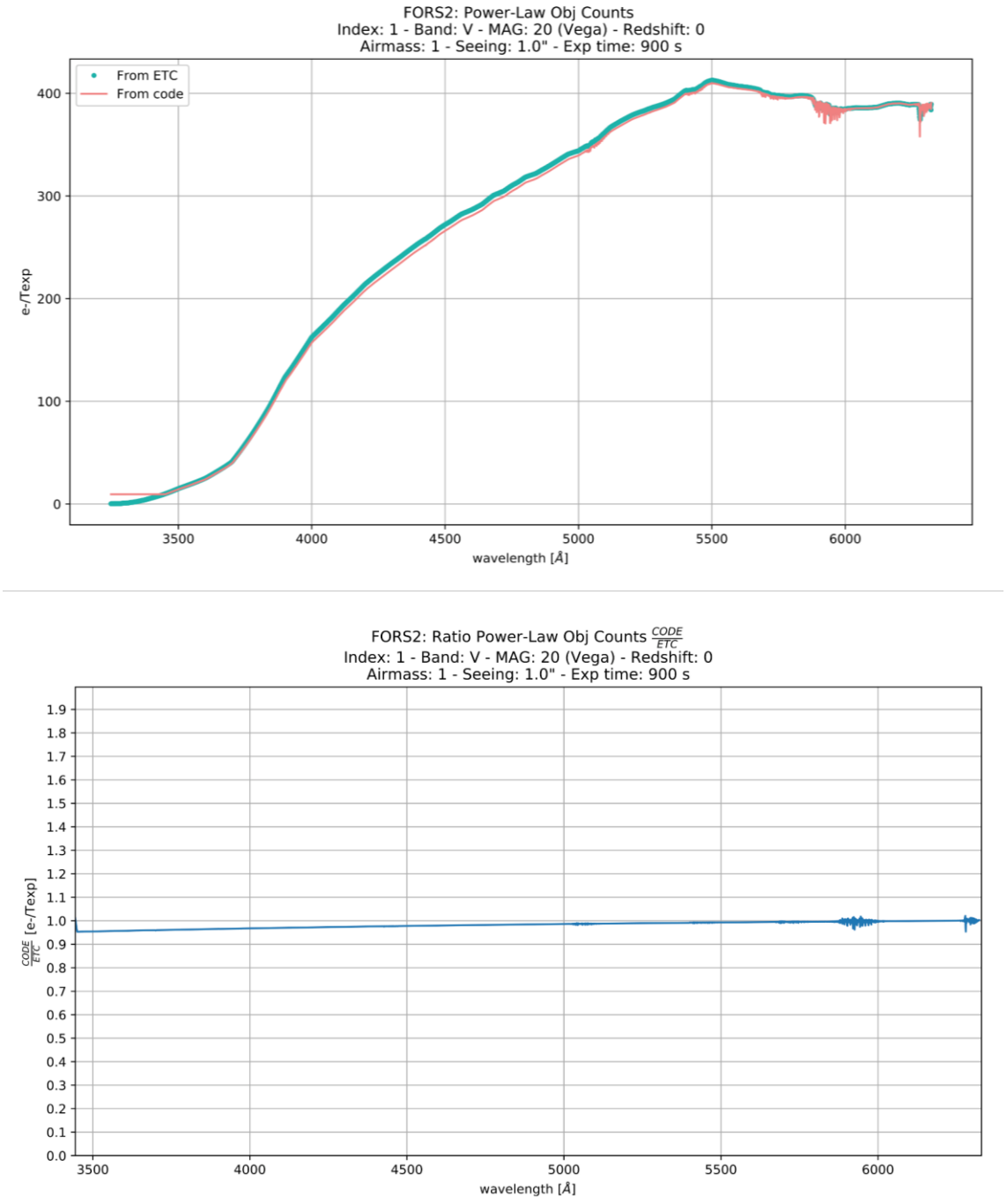

Figure 45. Power-Law spectra comparison (up) and RATIO (bottom) between the code and the ETC.

Black-Body

- Temperature: 5600 K
- Magnitude: 20
- Band: V

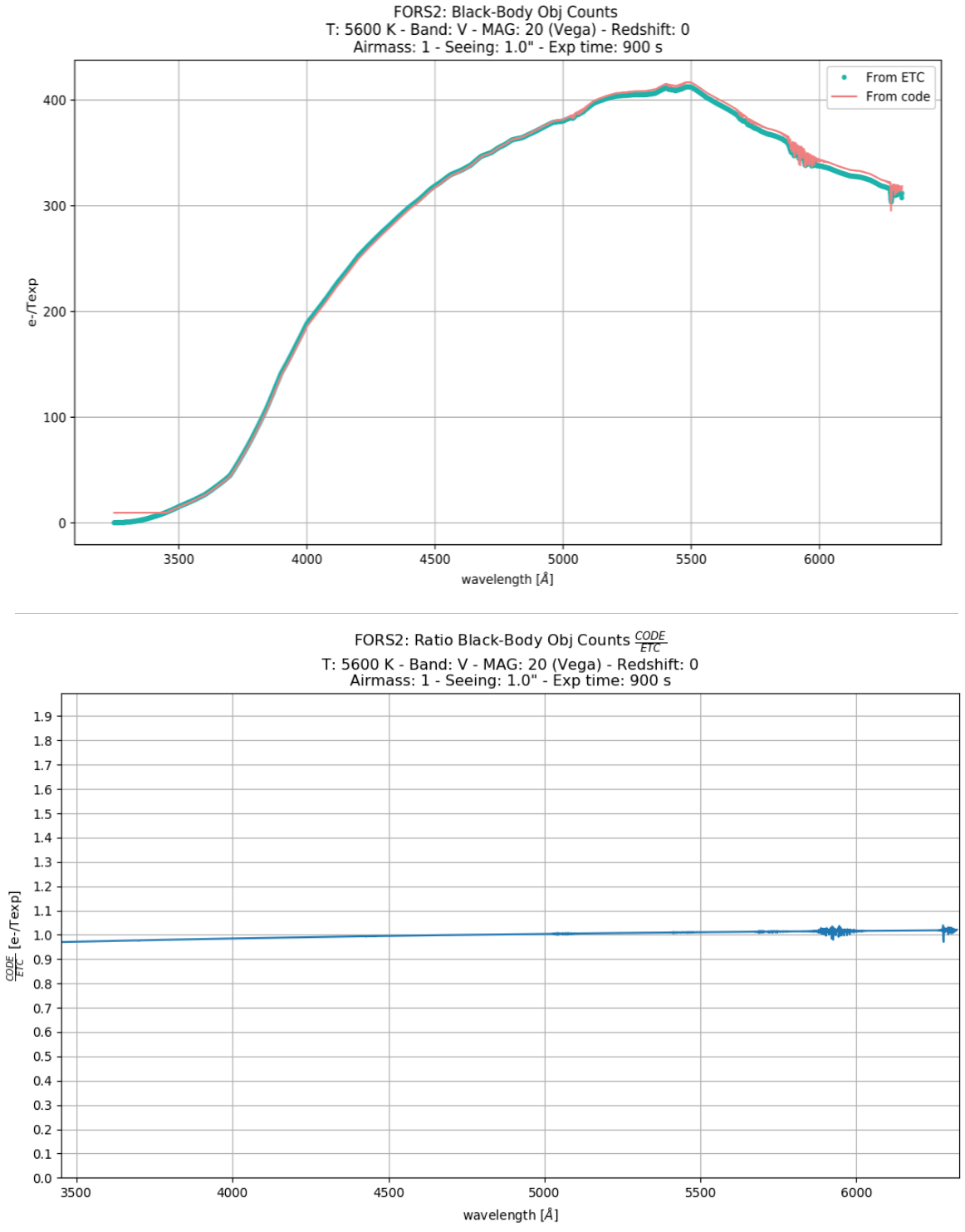

Figure 46. Black-Body spectra comparison (up) and RATIO (bottom) between the code and the ETC.

Kurucz B1V

- Magnitude: 20
- Band: V

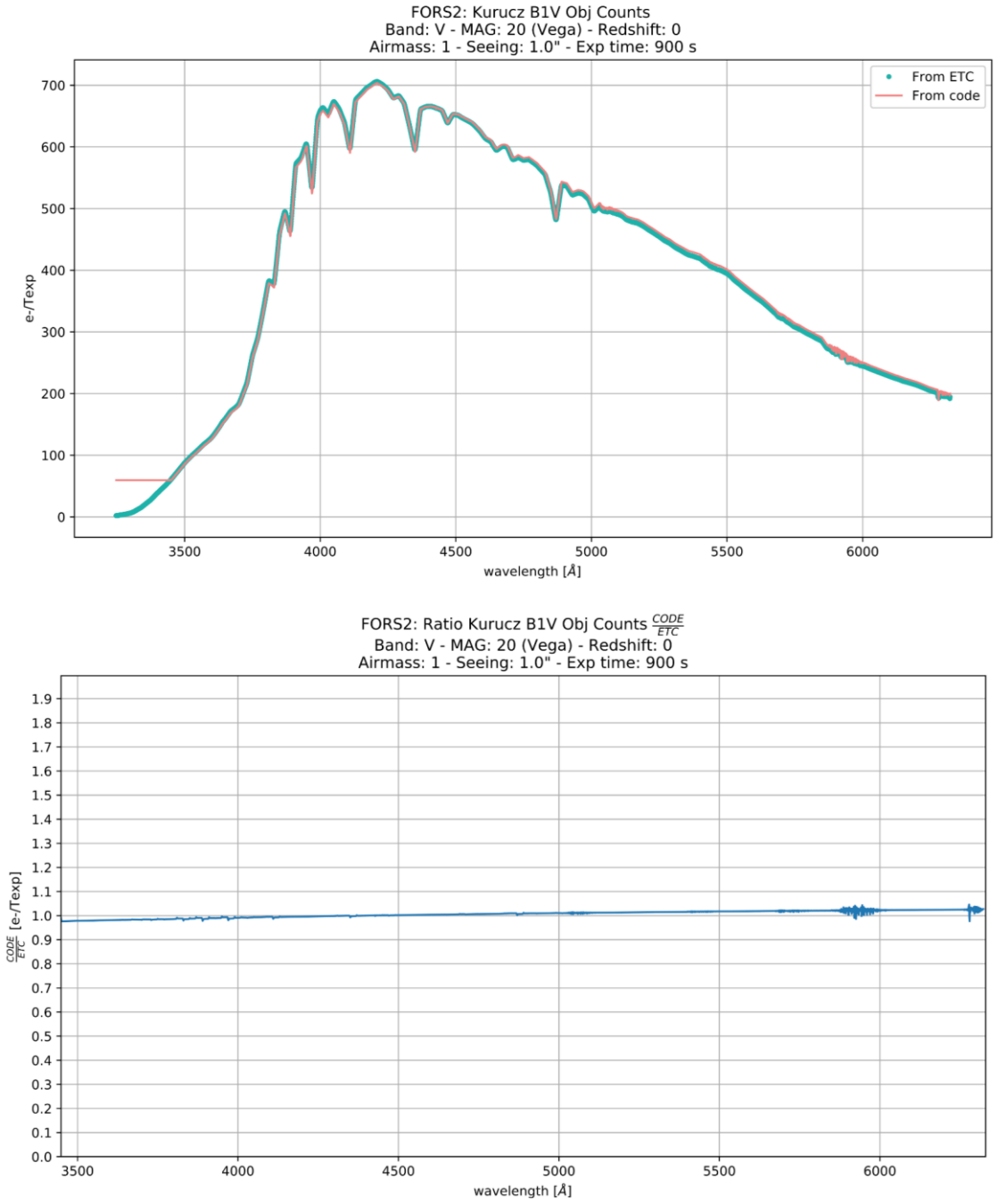

Figure 47. Kurucz B1V spectra comparison (up) and RATIO (bottom) between the code and the ETC.

The results obtained, as can be seen from all the SEDs tested (Figures 34, 35, 36), are in total agreement with each other, having a ratio almost constant at 1.0 and without presenting any relevant difference.

3.10.4.2 X-SHOOTER

The NIR arm of X-SHOOTER was used to test the code for the infrared arm of SOXS and, as for the previous test on the visible, the SEDs used are shown below.

Characteristics:

- Slit Width: 0.9”
- Slit Length: 11”
- VLT Telescope effective area considered also in the X-SHOOTER ETC: 48.7 m2
- Total efficiency of X-SHOOTER in the NIR arm is shown in Figure 48.

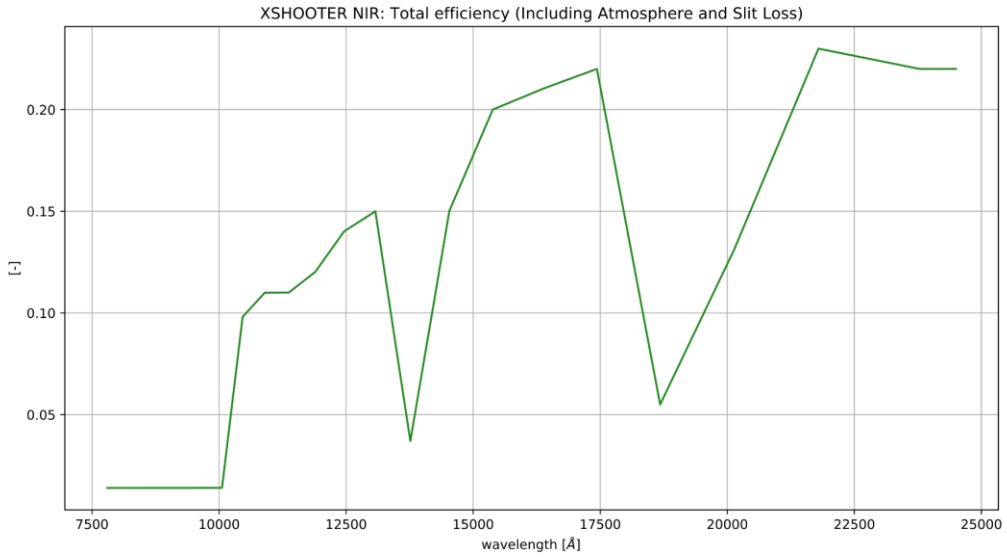

Figure 48. Total efficiency of XSHOOTER, including Atmosphere transmission and Slit Loss.

Power-Law

- Index: 1
- Magnitude: 20
- Band: V

Figure 49. Power-Law spectra comparison (up) and RATIO (bottom) between the code and the ETC.

Black-Body

- Temperature: 5600 K
- Magnitude: 20
- Band: V

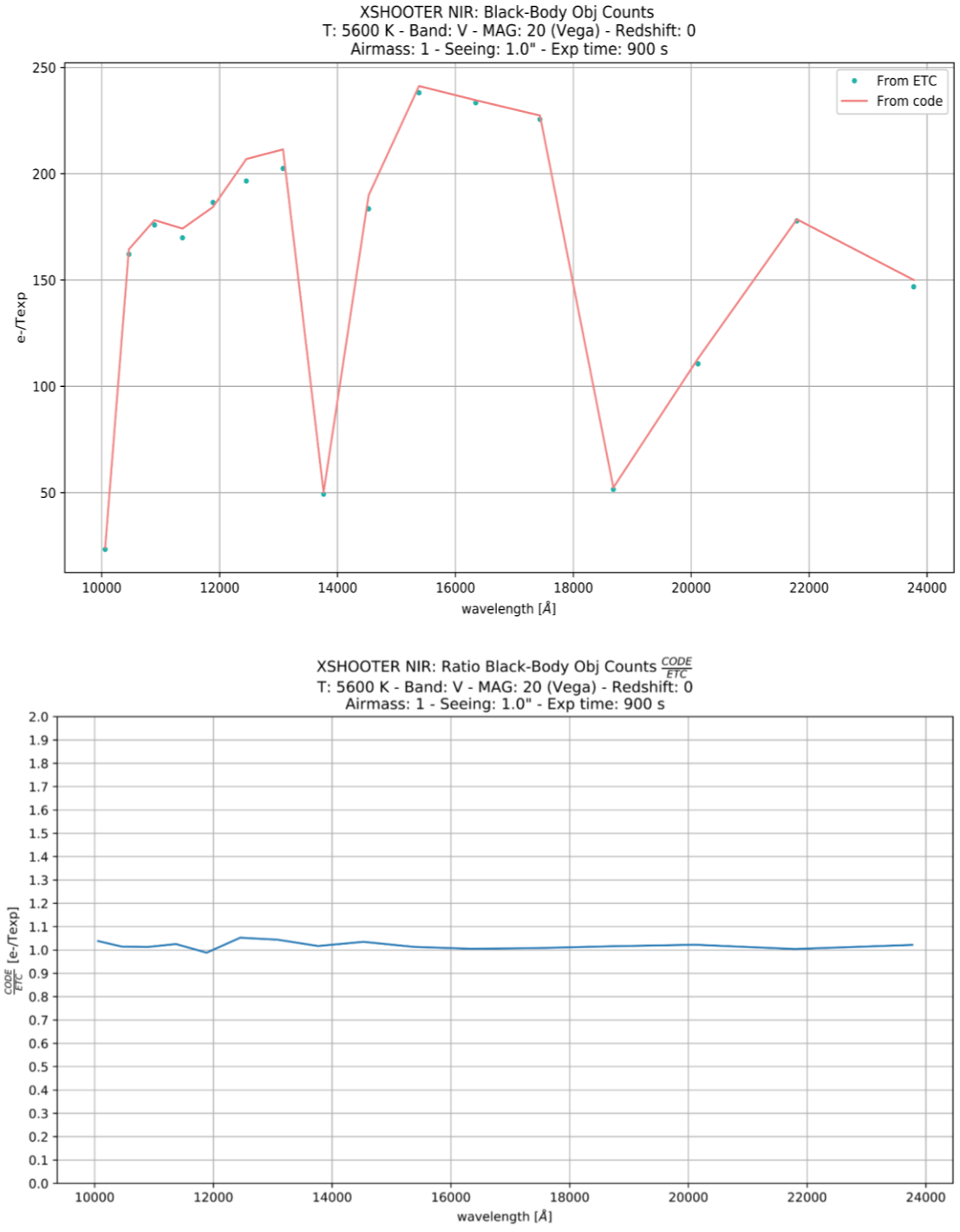

Figure 50. Black-Body spectra comparison (up) and RATIO (bottom) between the code and the ETC.

Pickles A0V

- Magnitude: 20
- Band: V

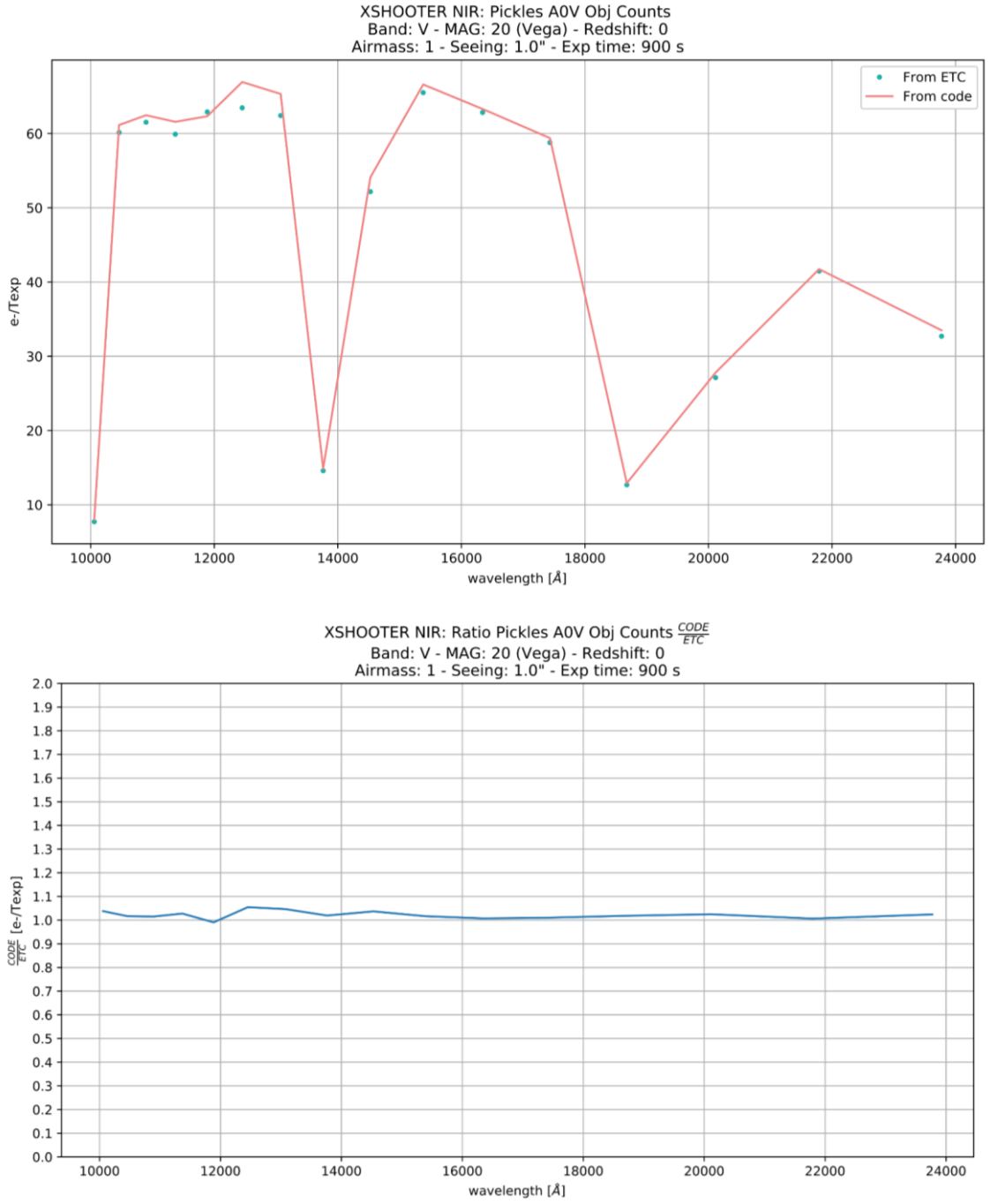

Figure 51. Pickles A0V spectra comparison (up) and RATIO (bottom) between the code and the ETC

Although the ETC of X-SHOOTER provides fewer points than other ETCs tested, the results obtained fit precisely with the code, having a maximum difference of 2-3%, as shown in the previous Figures.

3.10.4.3 SOFI

The NIR arm was also tested by comparing the results with the ETC of SOFI. The test was performed only with a Black-Body spectra, being the only compatible SED provided by the ETC.

Characteristics:

- Slit Width: 1”
- Slit Length: 290”
- NTT Telescope effective area considered also in the SOFI ETC: 8.9 m2
- Total efficiency of SOFI in the blue arm is shown in Figure 41.

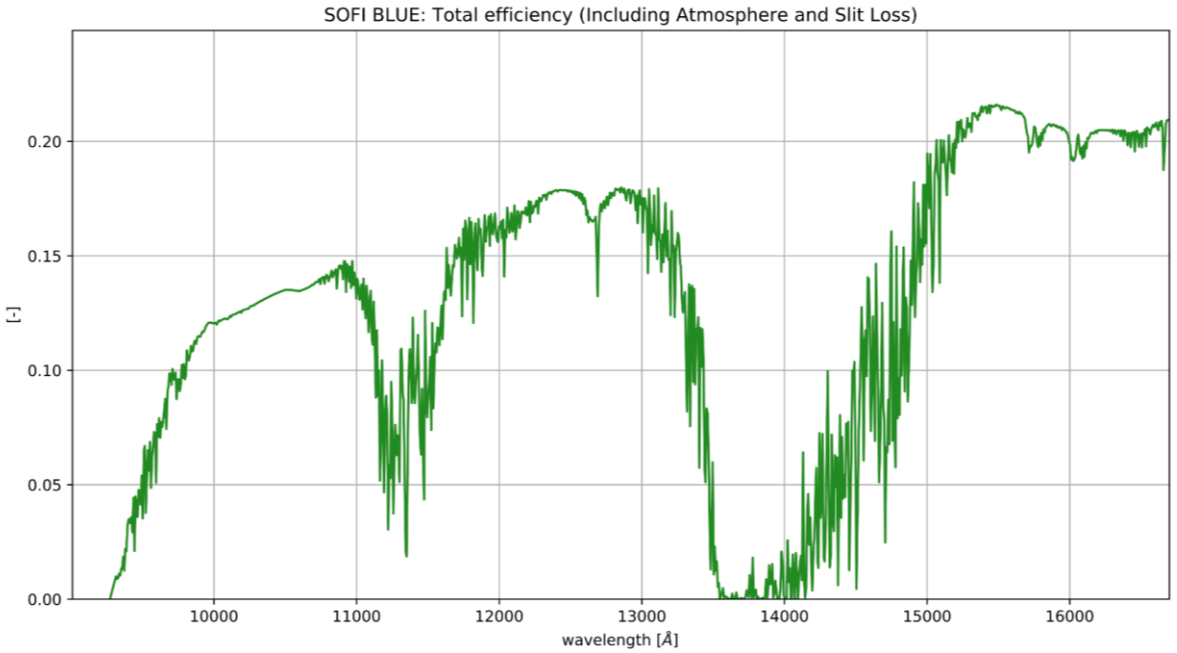

Figure 52. Total efficiency of SOFI, including Atmosphere transmission and Slit Loss.

Black-Body

- Temperature: 5600 K
- Magnitude: 20
- Band: J

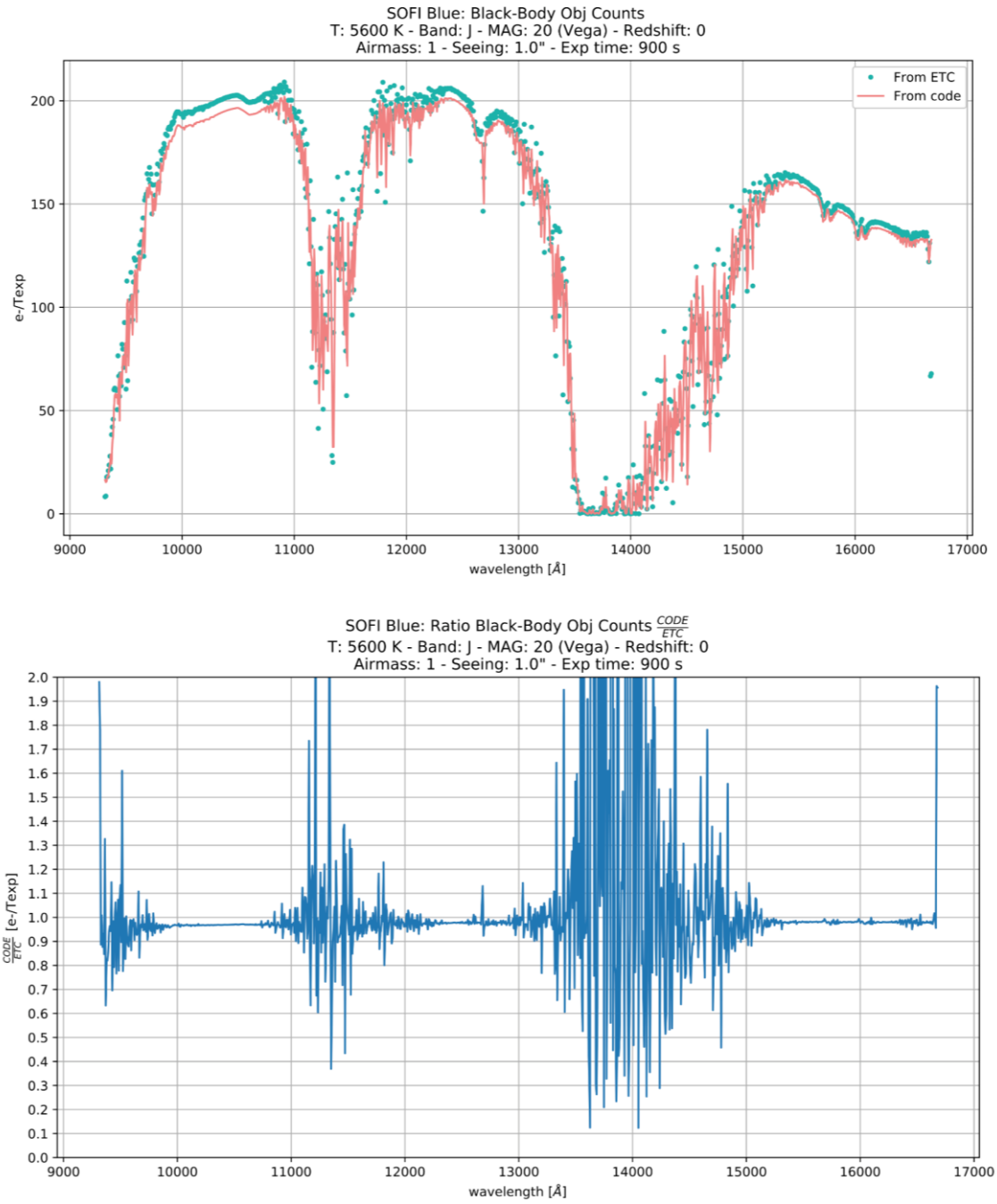

Figure 53. Black-Body spectra comparison (up) and RATIO (bottom) between the code and the ETC.

Despite some differences around 9500 A, 11500 A and 14000 A, probably due to an increased presence of absorption and emission lines, as shown in figure 42, the mean ratio is around 1.0 across all wavelengths and the two spectra are totally comparable.

3.10.5 Signal-to-Noise ratio computation

The S/N (or SNR) is computed according to the formula described in sec. 3.6.1, and combining the test-results presented in the previous sub-sections.
In the following, single exposure observations (thus NEXP, NDIT and NINT are equal to 1) and 1x1 binning acquisition are considered. The SNR is computed per pixel-bin along the dispersion direction (thus, not per SRE) and over the PSF extension along the slit direction coherently with what is set in the different instrument-ETC of ESO. The PSF extension impacts on the sky contribution and the number of pixel considered for the detector noises.

The common parameter for all the cases, as implemented in sec. 3.10.3, are:

- Red-shift: 0
- Airmass: 1 (thus at zenith)
- Moon FLI: 1 (thus full moon)
- Seeing (at 5000 A): 1 arcsec
- T. exp or DIT: 900s

3.10.5.1 FORS2

The following parameters are used for the test:

- **Power-Law:** Index = 1
- Magnitude: 20
- Band: V

- VLT Telescope effective area considered also in the FORS2 ETC: 51.2 m2
- Slit Width: 1”
- PSF extension: 14 pixels

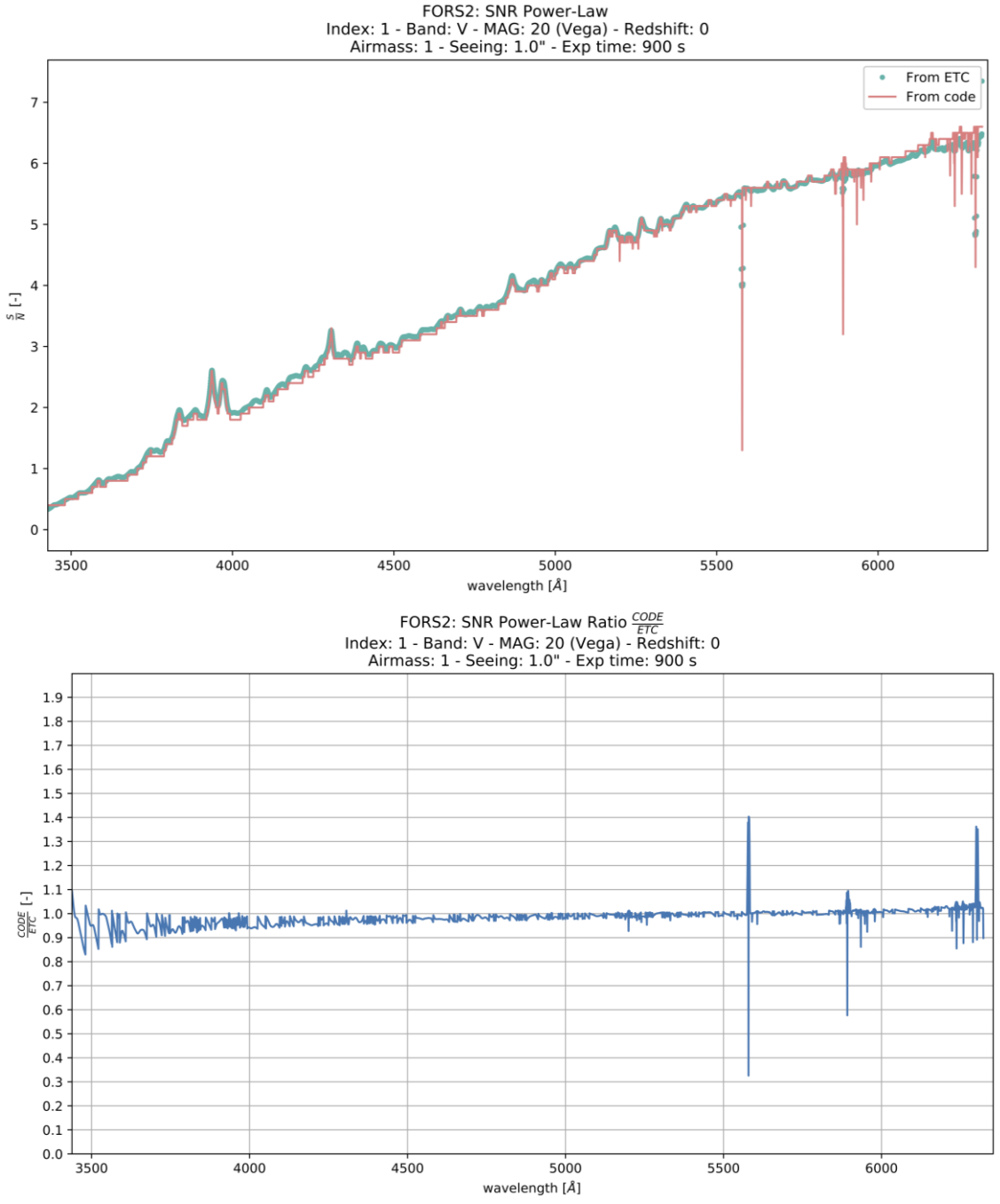

Figure 54. FORS2 SNR test on Power-Law input object distribution. Other used parameters value in the figure title.

3.10.5.2 XSHOOTER

The test using XSHOOTER ETC is done for all the wave-bands. The following parameters are used:

- **Pickels A0V model**
- Magnitude: 20
- Band: V

- VLT Telescope effective area considered also in the X-SHOOTER ETC: 48.7 m2
- Slit Width: 0.9”
- PSF extension: 14, 12, 8 pixels in the UVB, VIS, NIR arms respectively.

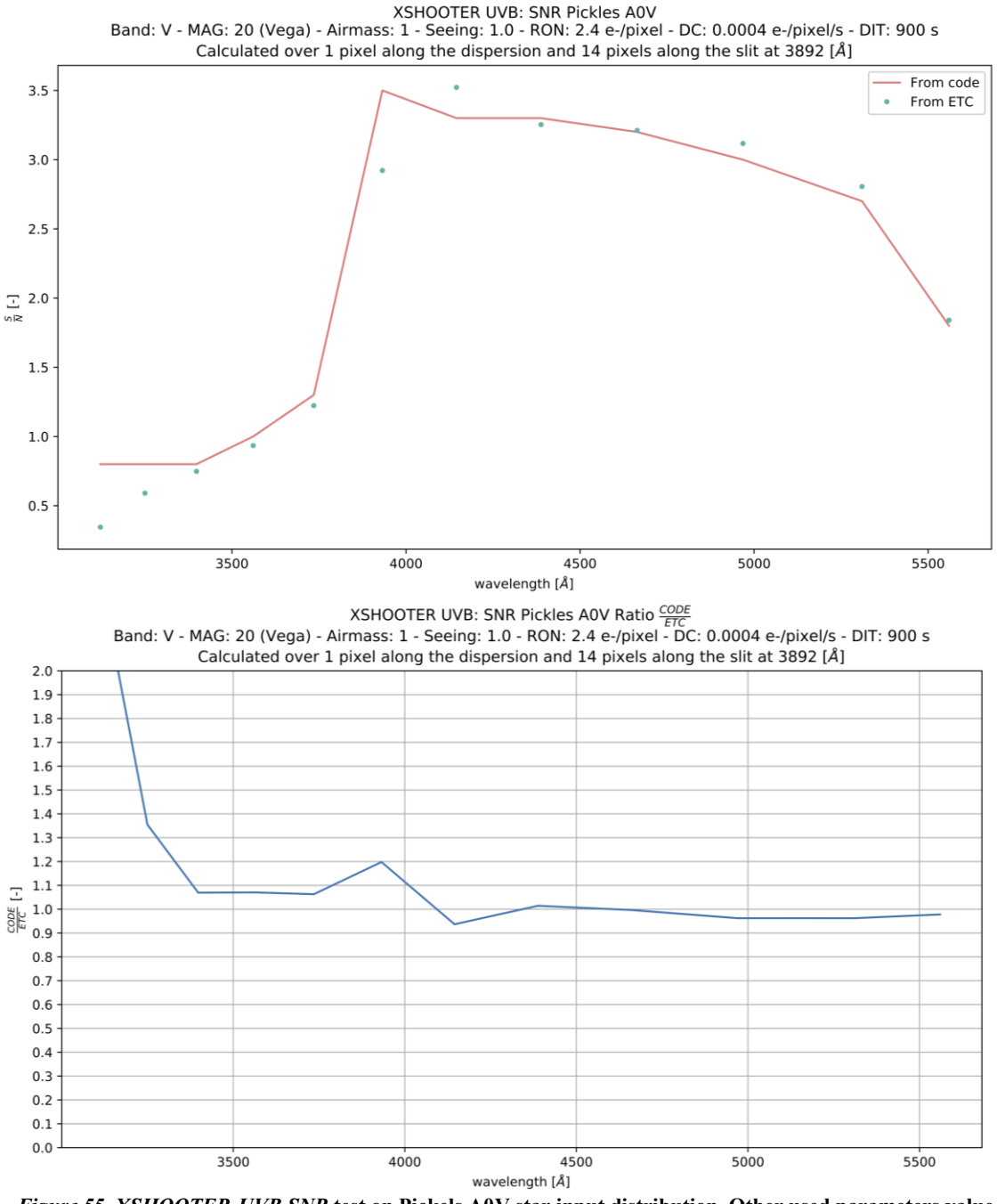

***Figure 55. XSHOOTER-UVB SNR* test on Pickels A0V star input distribution. Other used parameters value in the figure title. The PSF extension (14 pixels) is calculated at the reference wavelength 3892 Å.**

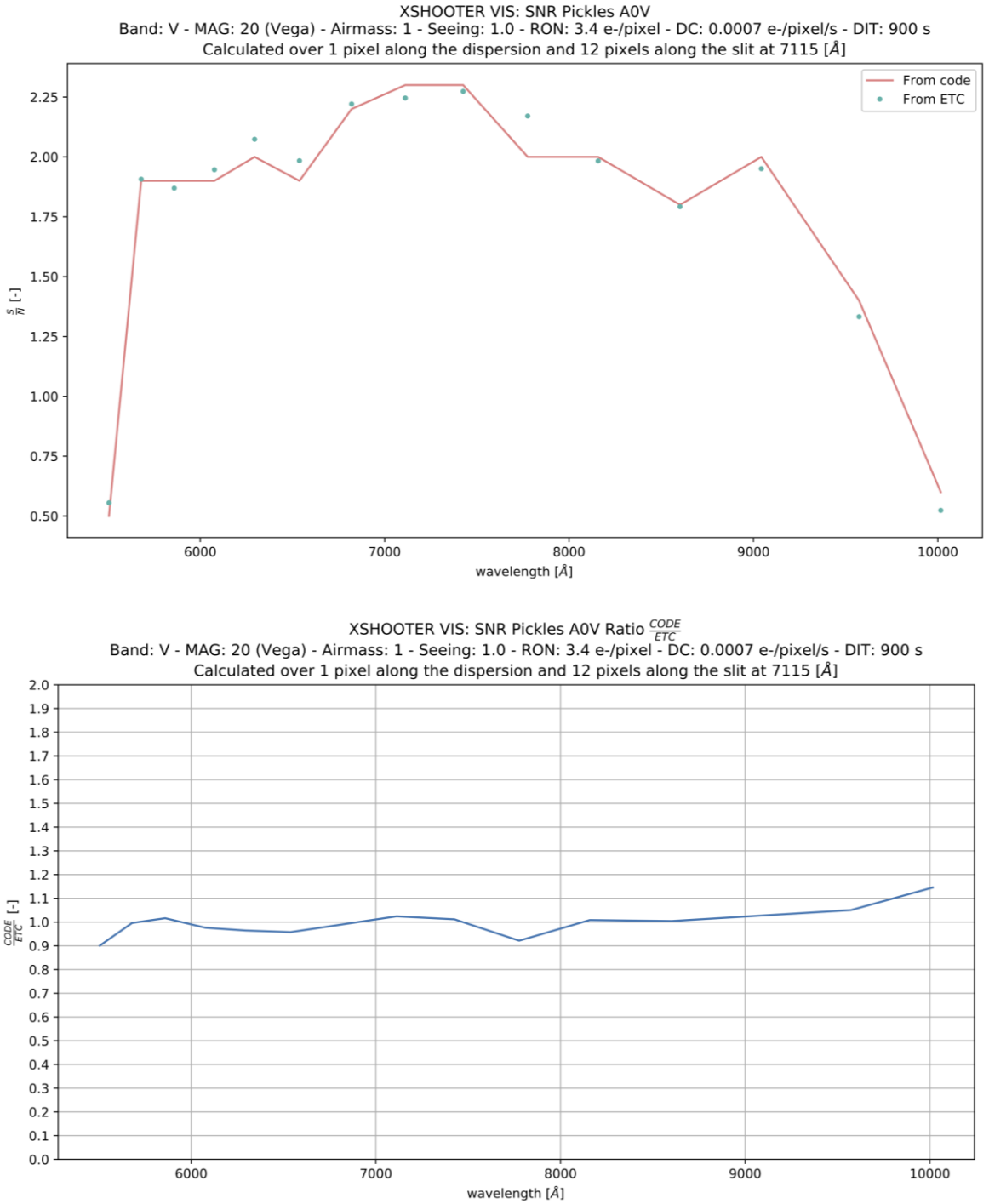

***Figure 56. XSHOOTER-VIS SNR* test on Pickels A0V star input distribution. Other used parameters value in the figure title. The PSF extension (12 pixels) is calculated at the reference wavelength 7115 Å.**

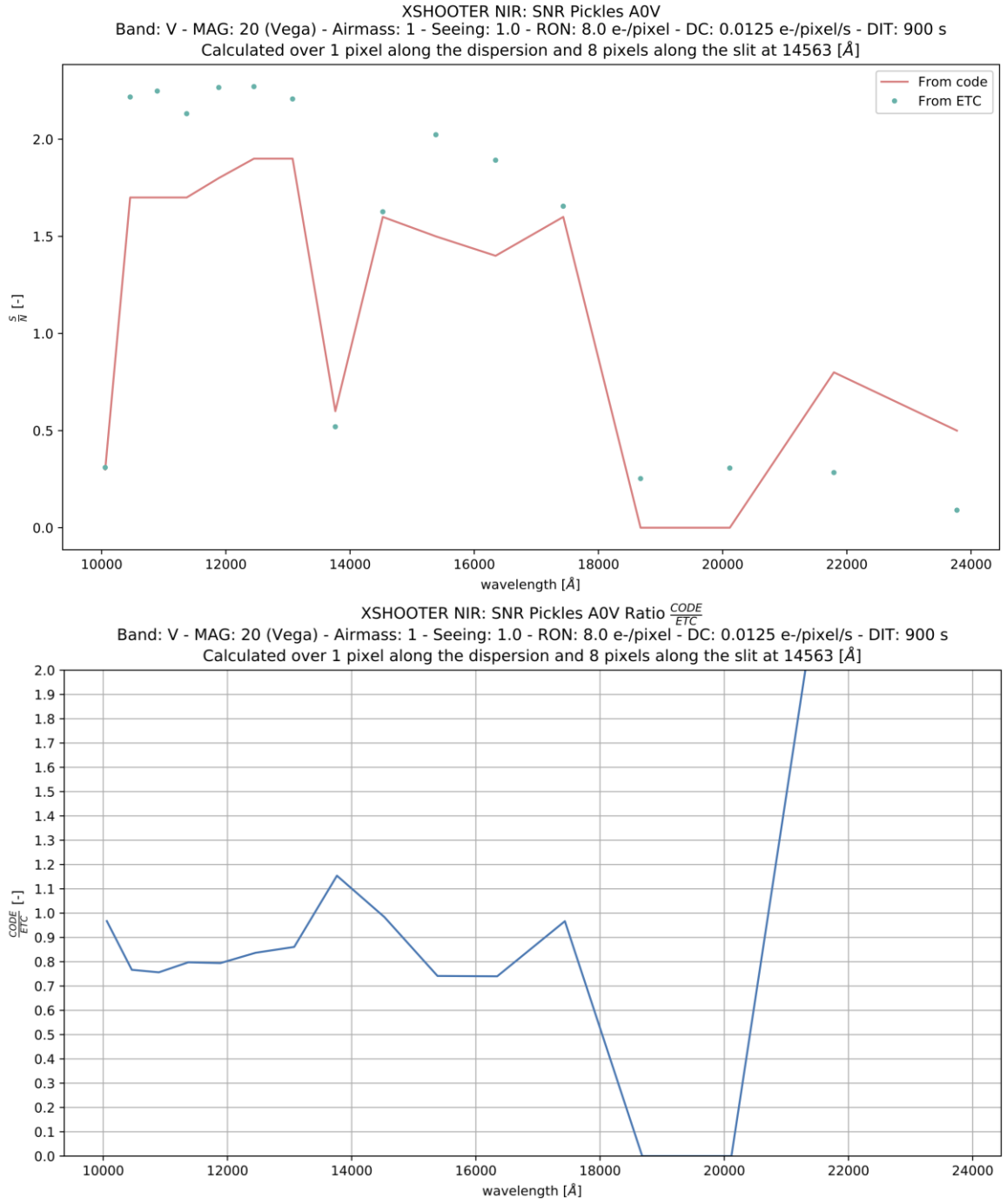

***Figure 57. XSHOOTER-NIR SNR* test on Pickels A0V star input distribution. Other used parameters value in the figure title. The PSF extension (8 pixels) is calculated at the reference wavelength 14563 Å.**

In the UVB and VIS arms the SNR computation with our code is very close to the results obtained from ESO XSHOOTER ETC, having ratio within 10% difference in the range 3500 – 10000 Å.
In the NIR arm up to 18000 Å a larger difference (up to 20-25 %) can be noticed; even though for an ETC estimation this is quite acceptable, this is due to difference in the sky contribution computation for the XSHOOTER NIR case.

3.10.5.3 SOFI

The following parameters are used for the test:

- **Black-body:** T = 5600 K
- Magnitude: 20
- Band: J

- VLT Telescope effective area considered also in the SOFI ETC: 8.9 m2
- Slit Width: 1”
- PSF extension: 7 and 6 pixels, in the “blue” and “red” band respectively

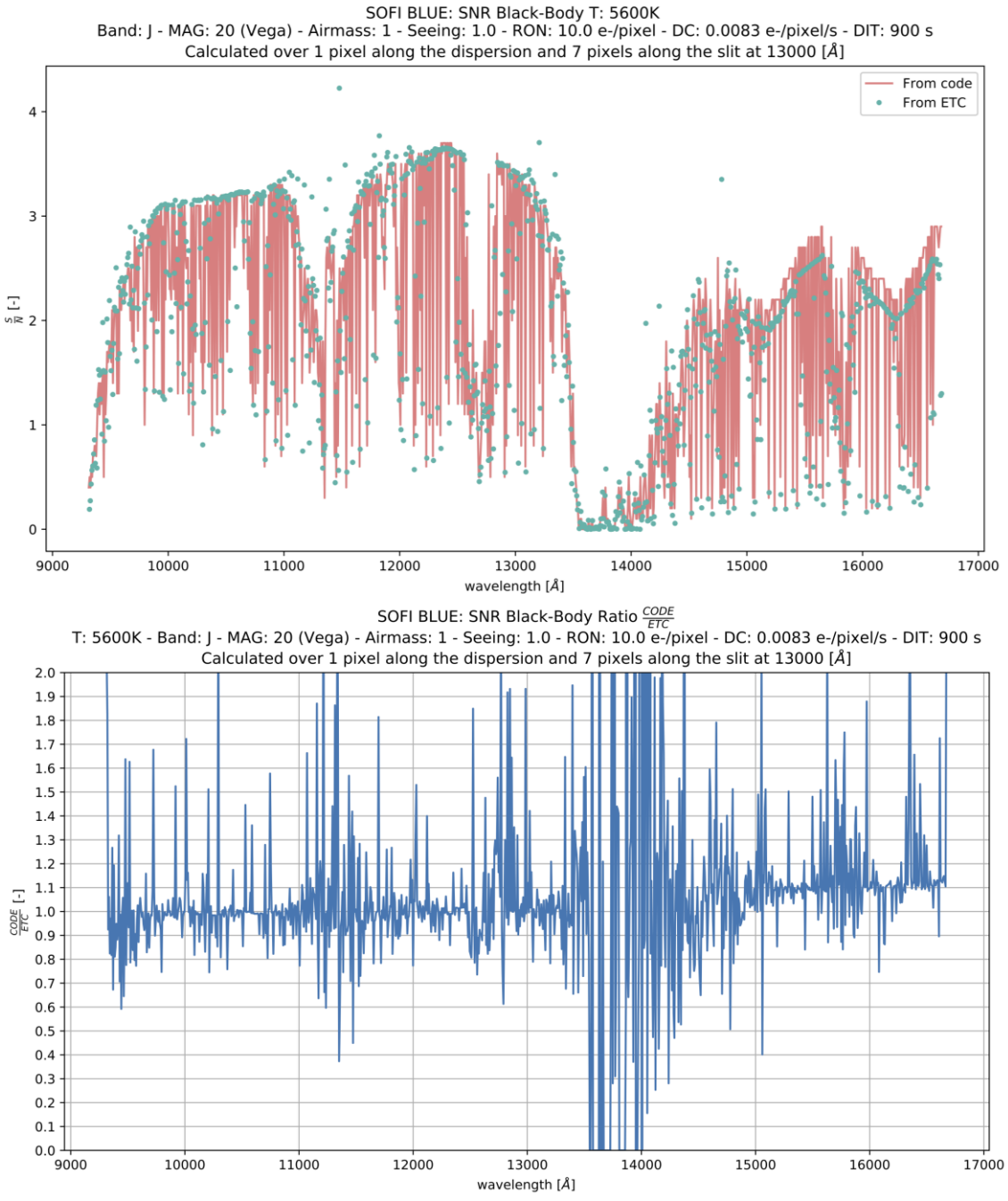

***Figure 58. SOFI-BLUE SNR* test on black-body input distribution. Other used parameters value in the figure title. The PSF extension (7 pixels) is calculated at the reference wavelength 13000 Å.**

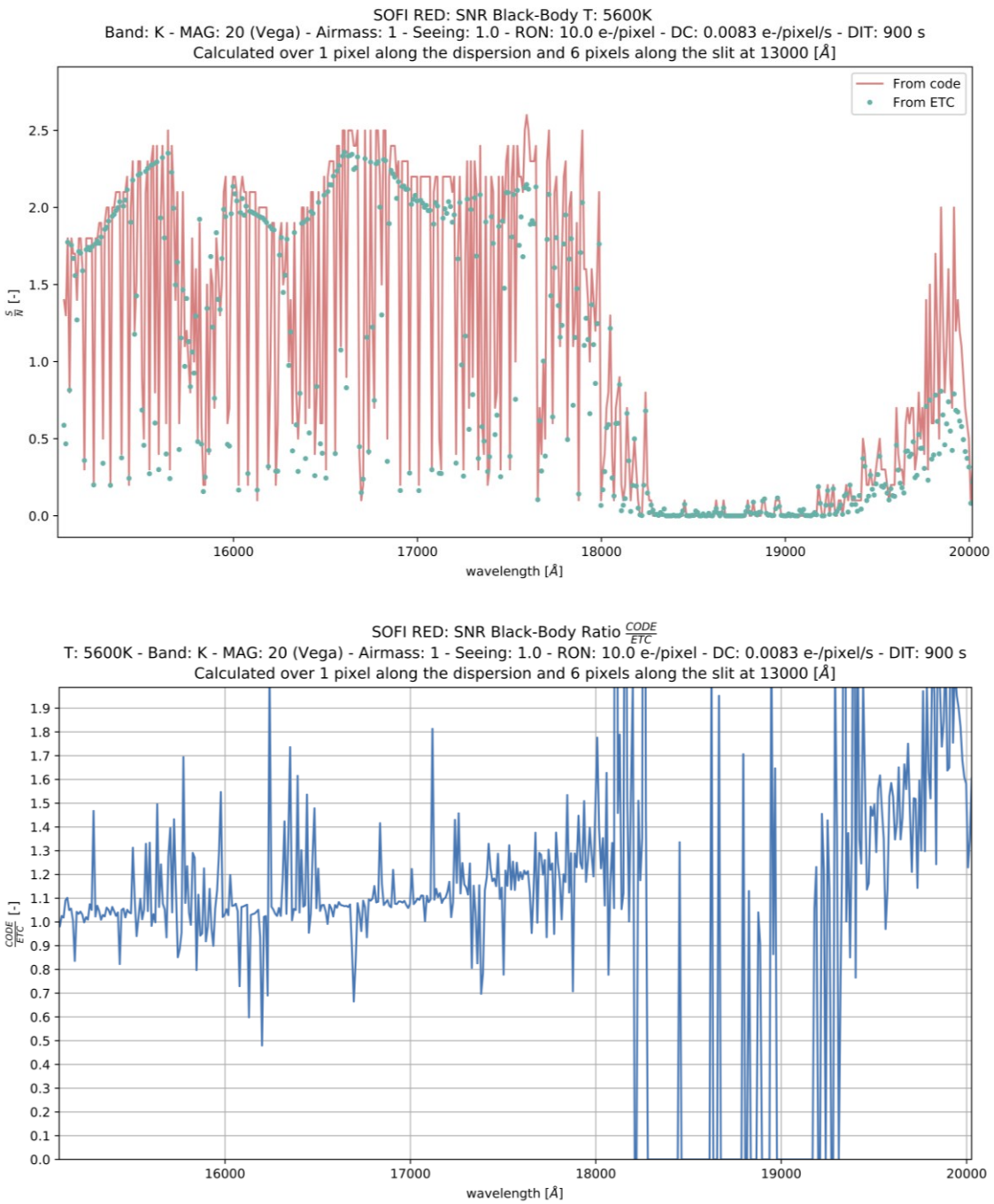

***Figure 59. SOFI-RED SNR* test on black-body input distribution. Other used parameters value in the figure title. The PSF extension (7 pixels) is calculated at the reference wavelength 13000 Å.**

Also in the case of SOFI, the SNR results obtained with our ETC-code are in agreement with the ones from the ESO ETC computation. In fact, in the "blue" band the mean ratio is close to 1 with larger variations only related to the strong atmospheric absorption bands (compare the zones around 11500, 12750 and 14000 Å with the figure 41). In the "red" band the large difference (>10%) is in the region around the atmospheric absorption band between H and K band.

4 ETC On-Sky Tests and Verifications

The ETC on-sky tests done during the different commission runs and verifications w.r.t. the DRS/Pipeline extractions from real SOXS data are described in section 4.14 of the Commission Report (RD9). There the data comparison is based on the ETC model which assumes the NTT telescope total efficiency to be flat average 39% over the SOXS wavelength range, as explained in section 3.4.2.

Scaling the NTT efficiency to 39% —based on June 2025 commissioning data— yields a strong match between the observed throughput and the ETC model in the bands R-I and orders up to 110nm (in the UVVIS and NIR arms respectively). This aligns with the theoretical reflectivity profile of bare aluminum. However, discrepancies of up to a factor of two emerge in the U-band and above 1300 nm (NIR). Specifically, we observe lower transmission in the UV and higher transmission in the red NIR orders compared to the ETC model.

This is qualitatively consistent with coating degradation, which typically impact the UV (much) more severely than the NIR (especially above 1400/1500 nm).

A more detailed quantification is currently unnecessary, as the mirrors will be recoated in April 2026; a new profile will be implemented in the ETC (the flat average at 66.5% as explained in section 3.4.2) and will be compared and validated against new commissioning data (as soon as NTT-SOXS will be fully operative).

5 APPENDIX 1: Common Path Efficiency estimation

Purpose of this appendix is to provide the data that are considered to compute the Efficiency of the SOXS-Common-Path UVVIS and NIR arms.

5.1 UV-VIS Common-Path Efficiency

5.1.1 Overview

The SOXS UC-VIS Common-Path is composed by the following optical elements:

- Dichroic
- Folding Mirror
- ADC-first quadruplet
- AD second quadruplet
- Tip-Tilt mirror
- Field lens

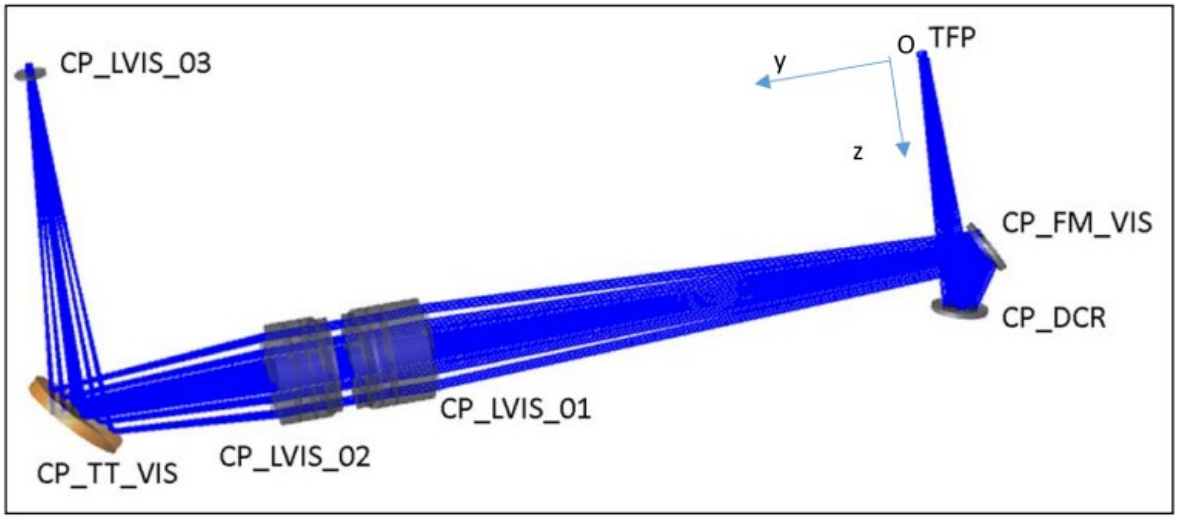

Figure 60. UV-VIS Common Path optical layout.

5.1.2 Dichroic (CP_DCR)

The dichroic in the UV-VIS works in reflection. This is the plot from the measures data from ASAHI-SPECTRA company.

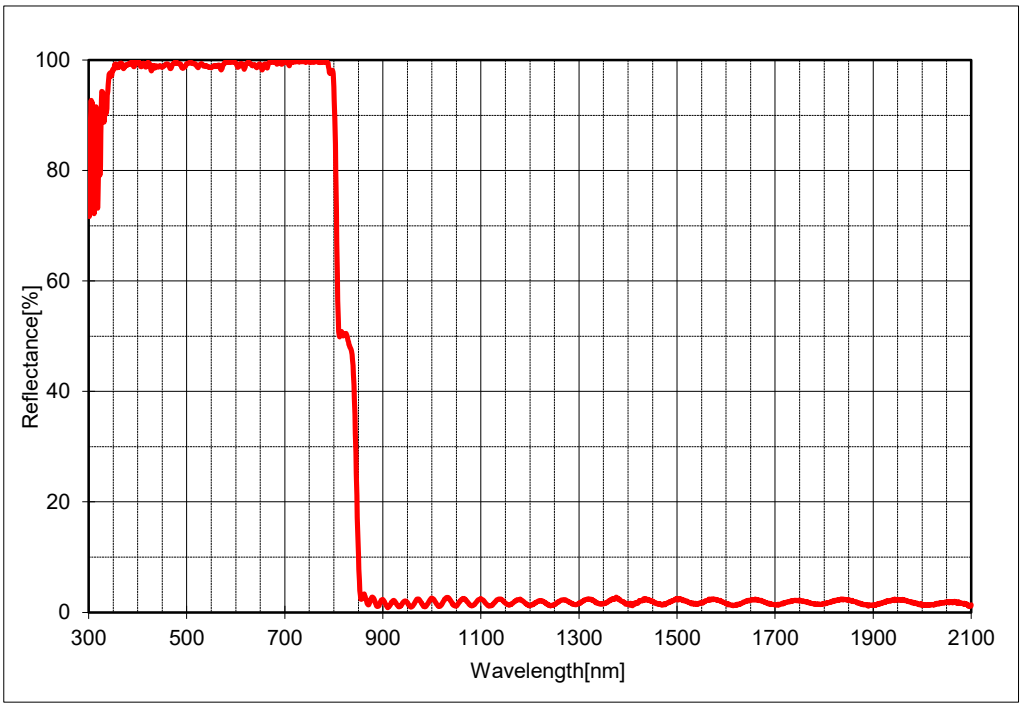

Figure 61. Common-Path Dichroic reflection curve.

Interpolation from 350 to 850 nm, with 1nm step. This is the curve used in the global CP-VIS efficiency.

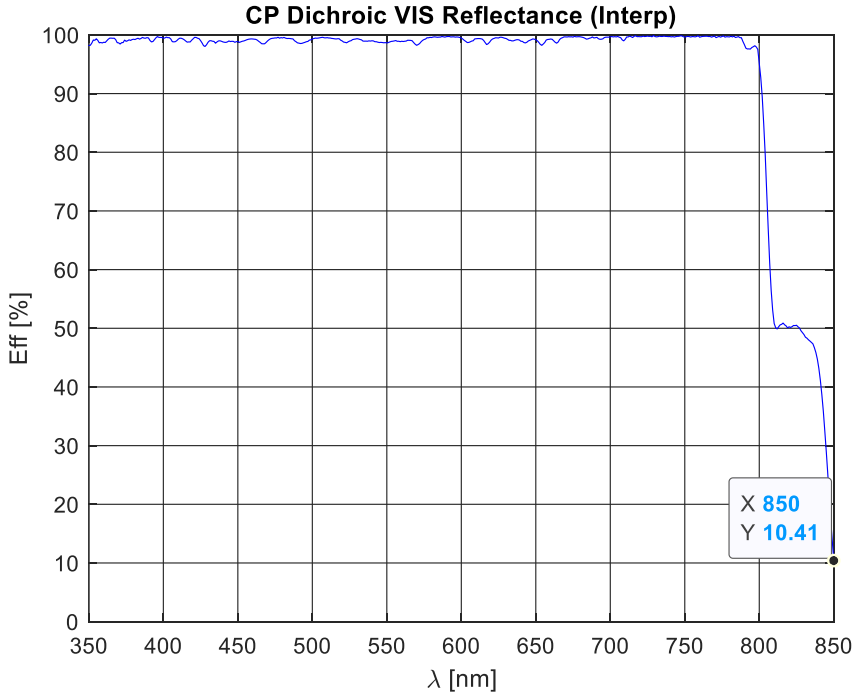

Figure 62. Common-Path Dichroic reflection curve interpolation used for the total CP UV-VIS transmission.

5.1.3 Folding Mirror (CP_FM_VIS)

PDF plot and excel data from ASAHI-SPECTRA. See the zoomed plot of data in 350-850 nm.

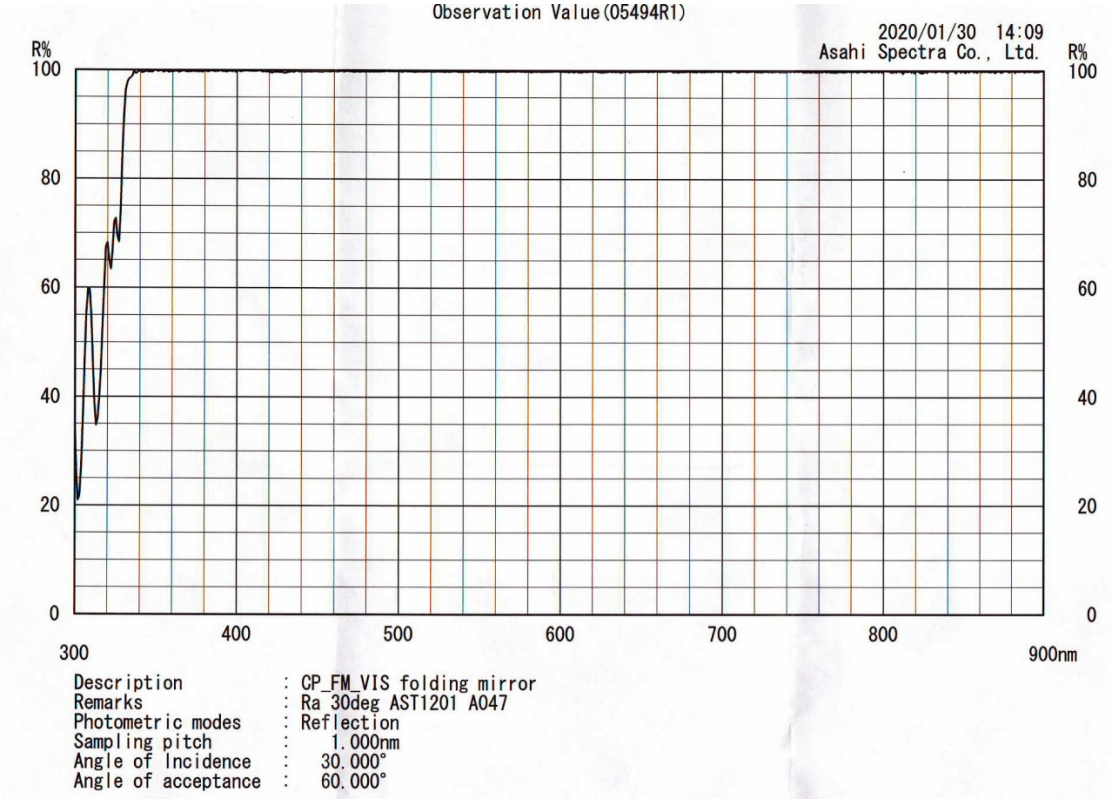

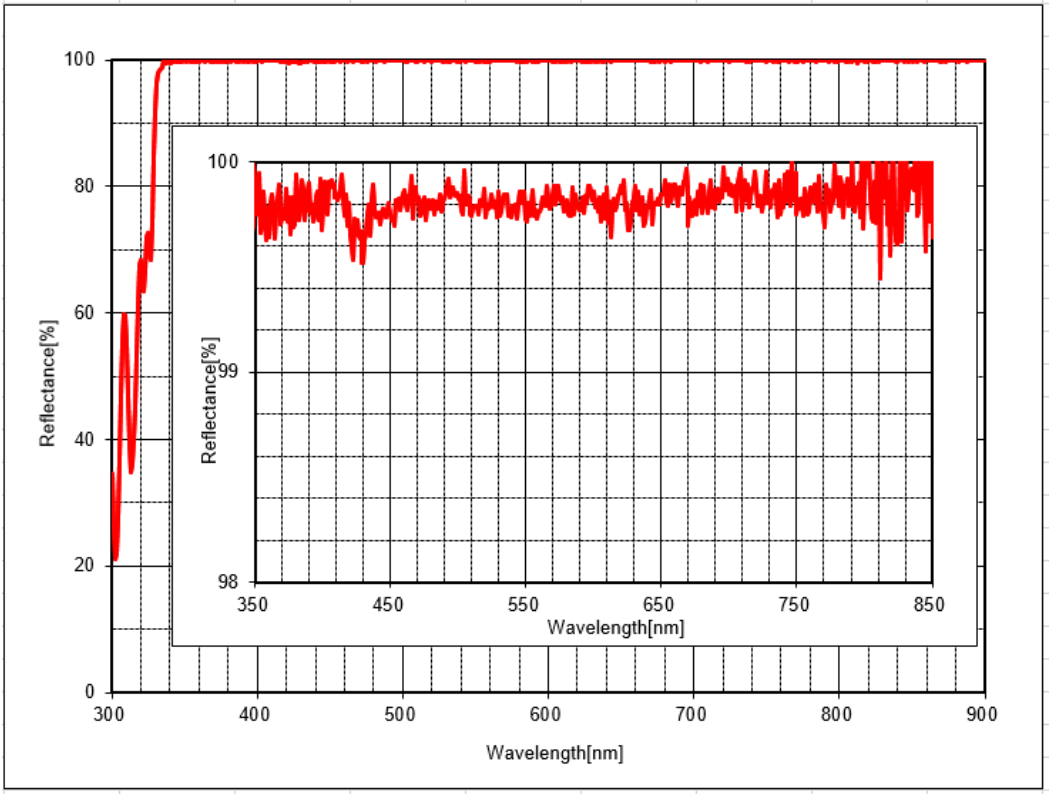

Figure 63.Common-Path UV-VIS folding mirror reflectivity profile. Top panel: PDF data. Bottom panel: excel data with zoom view.

Extracted data with MATLAB.

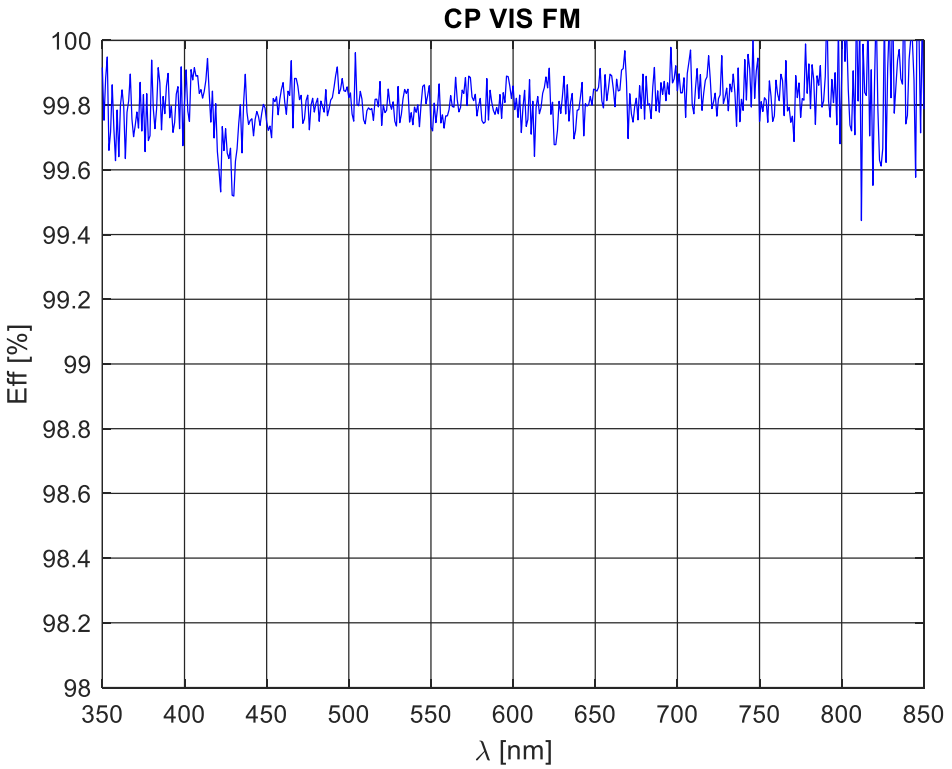

Interpolation from 350 to 850 nm, with 1nm step. This is the curve used in the global CP-VIS efficiency.

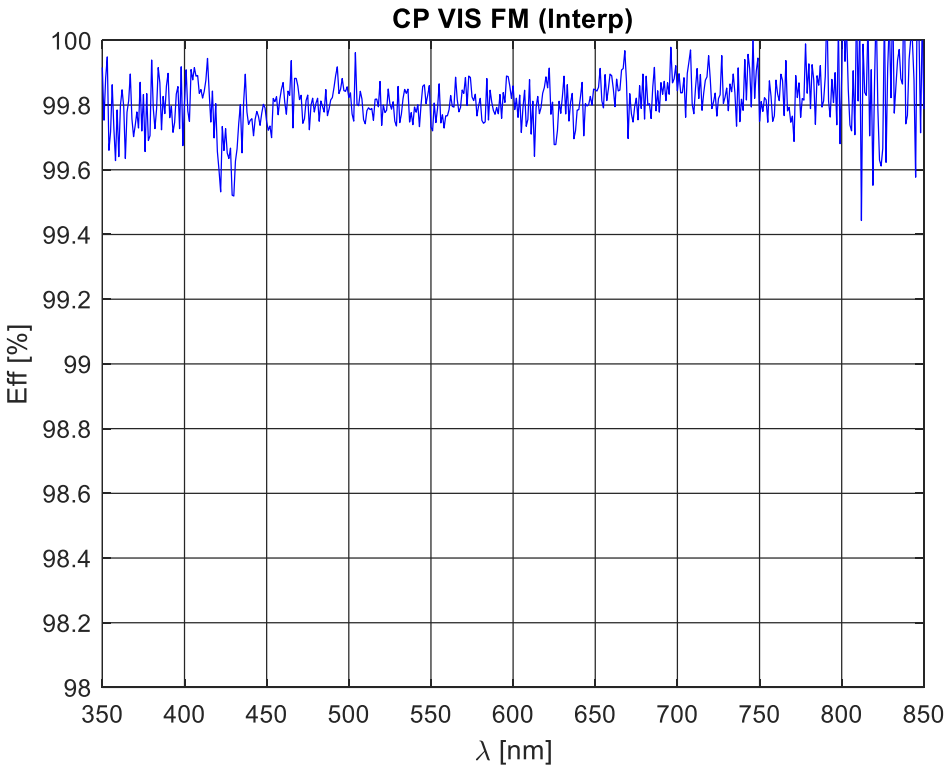

Figure 64. Common-Path UV-VIS folding mirror interpolated reflectivity profile used in the overall transmission computation.

5.1.4 ADC first quadruplet (CP_LVIS_01)

The ADC first quadruplet is made by: CAF2 (15mm), BAL35Y (3mm), BAL15Y (4mm), S-FPL51Y (4mm). Excel data points for the AR-Coating of the first and exit surface of the first ADC quadruplets.

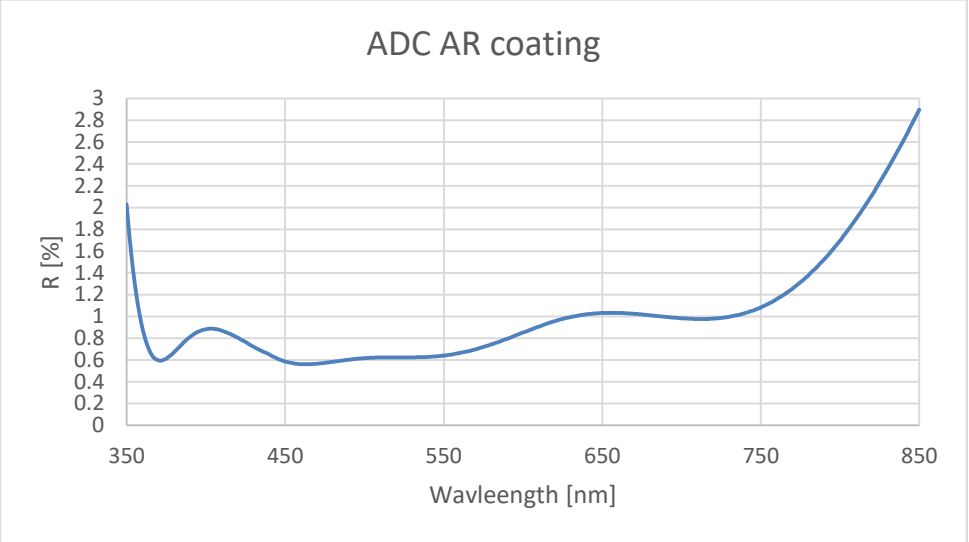

Figure 65. Common-Path UV-VIS first ADC quadruplet AR-coating curve.

Data on glasses: CAF2 (15mm). There are no fully coherent data among optical material producers about CAF2 in term of internal transmission, but considering data on the total transmission (including Fresnel losses at surfaces) and refractive index data, it is possible to retrieve that CAF2 has internal transmission >99% in the range 300-2000 nm. So flat CAF2 internal transmission of 99% is assumed here. For all other glasses data from Zemax archive are equal to the ones from RefractiveIndex.info.

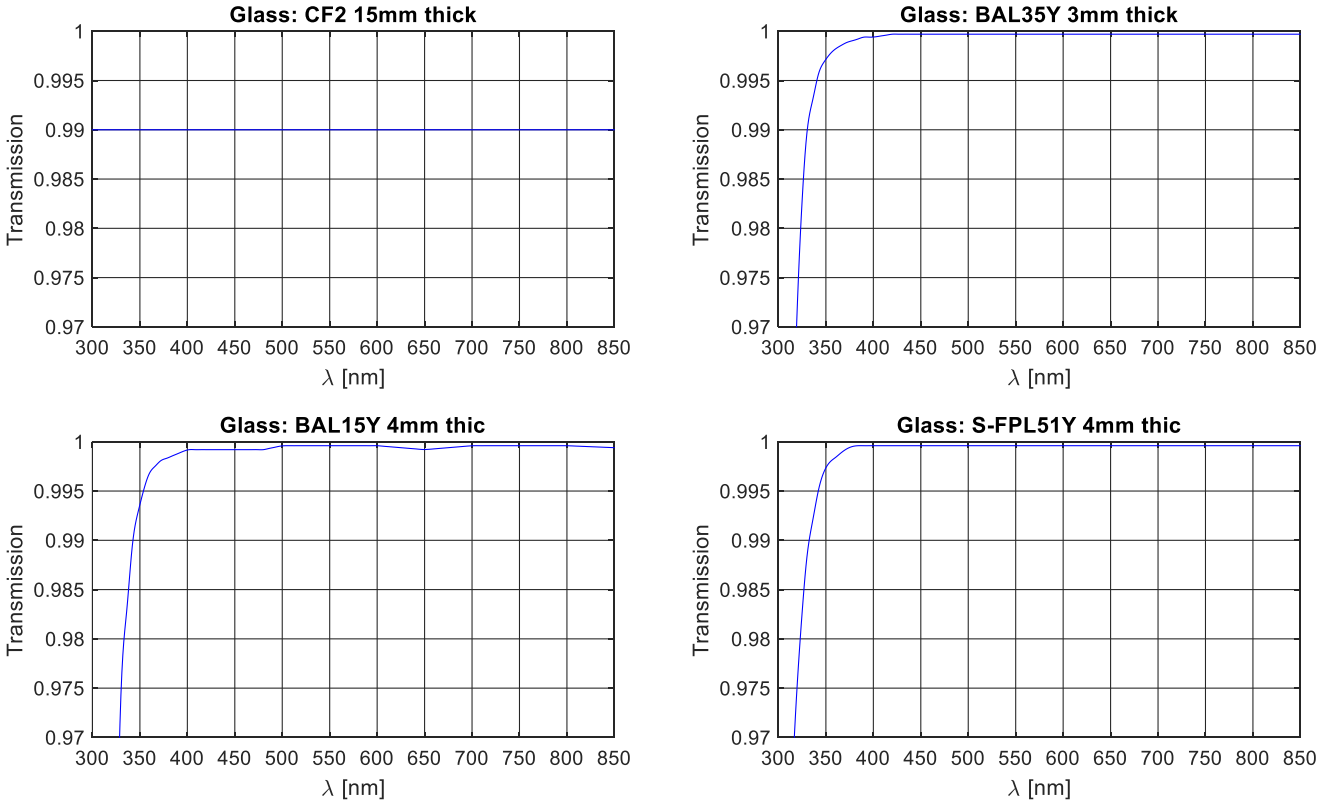

Figure 66. Common-Path UV-VIS first ADC quadruplet glasses internal transmission.

The total ADC-1 transmission, taking into account both AR-Coatings (on first and last surface) and glasses internal transmission. This is the curve used in the global CP-VIS-ADC efficiency.

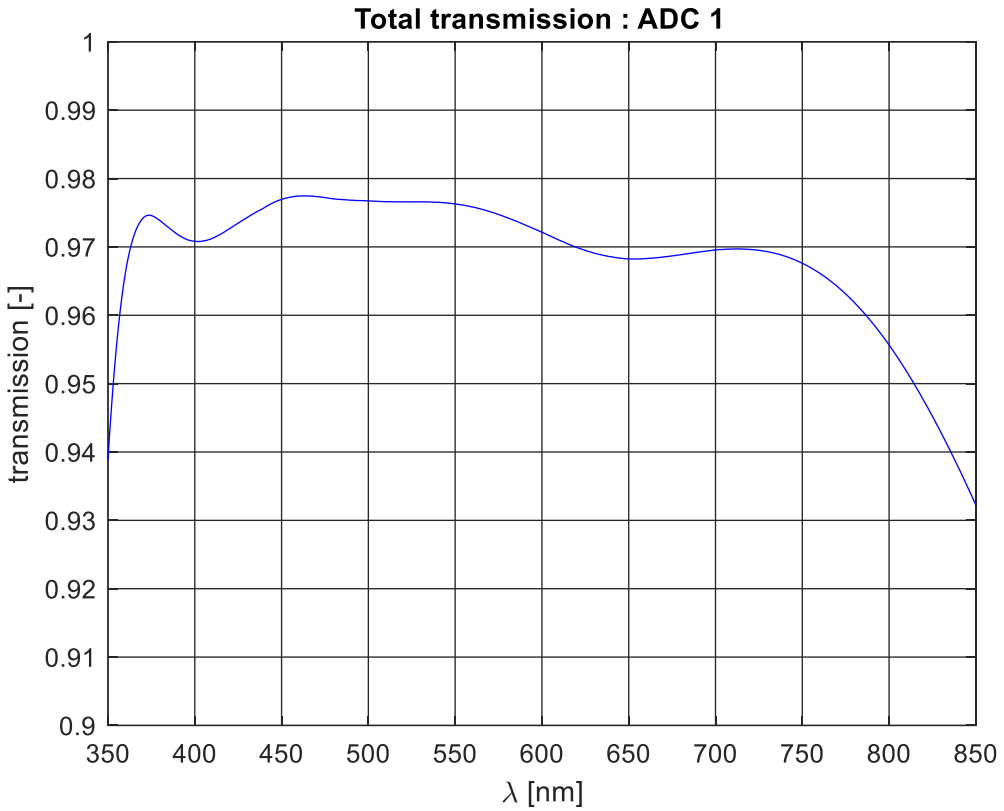

Figure 67. Common-Path UV-VIS first ADC quadruplet total transmission. This is the curve used in the global CP-VIS-ADC efficiency.

5.1.5 ADC second quadruplet (CP_LVIS_02)

The ADC 2nd quadruplet is made by: S-FPL51Y (4mm), BAL15Y (3mm), BSM15Y (4mm), S-FPL51Y (10mm).

Excel data points for the AR-Coating of the first and exit surface of the first ADC quadruplets.

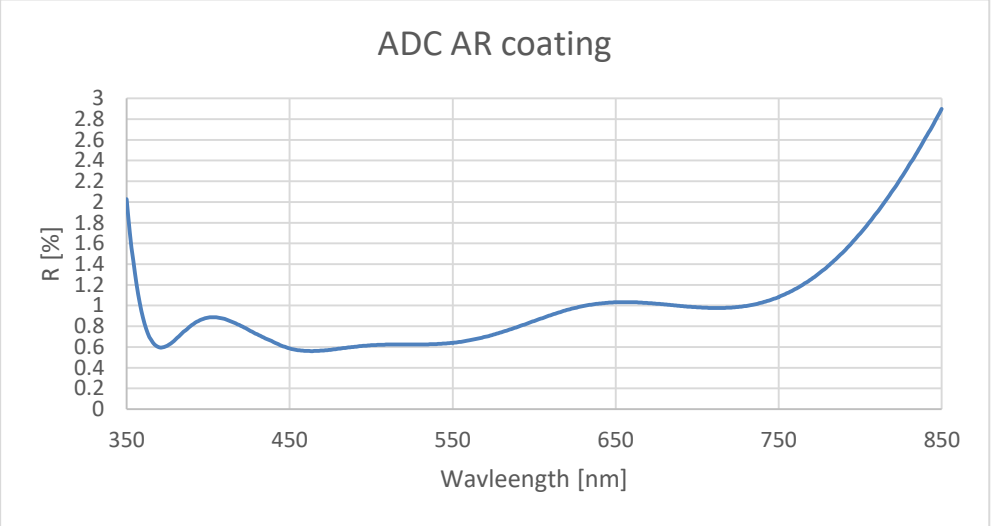

Figure 68. Common-Path UV-VIS second ADC quadruplet AR-coating curve.

For all glasses data from Zemax archive are equal to the ones from RefractiveIndex.info.

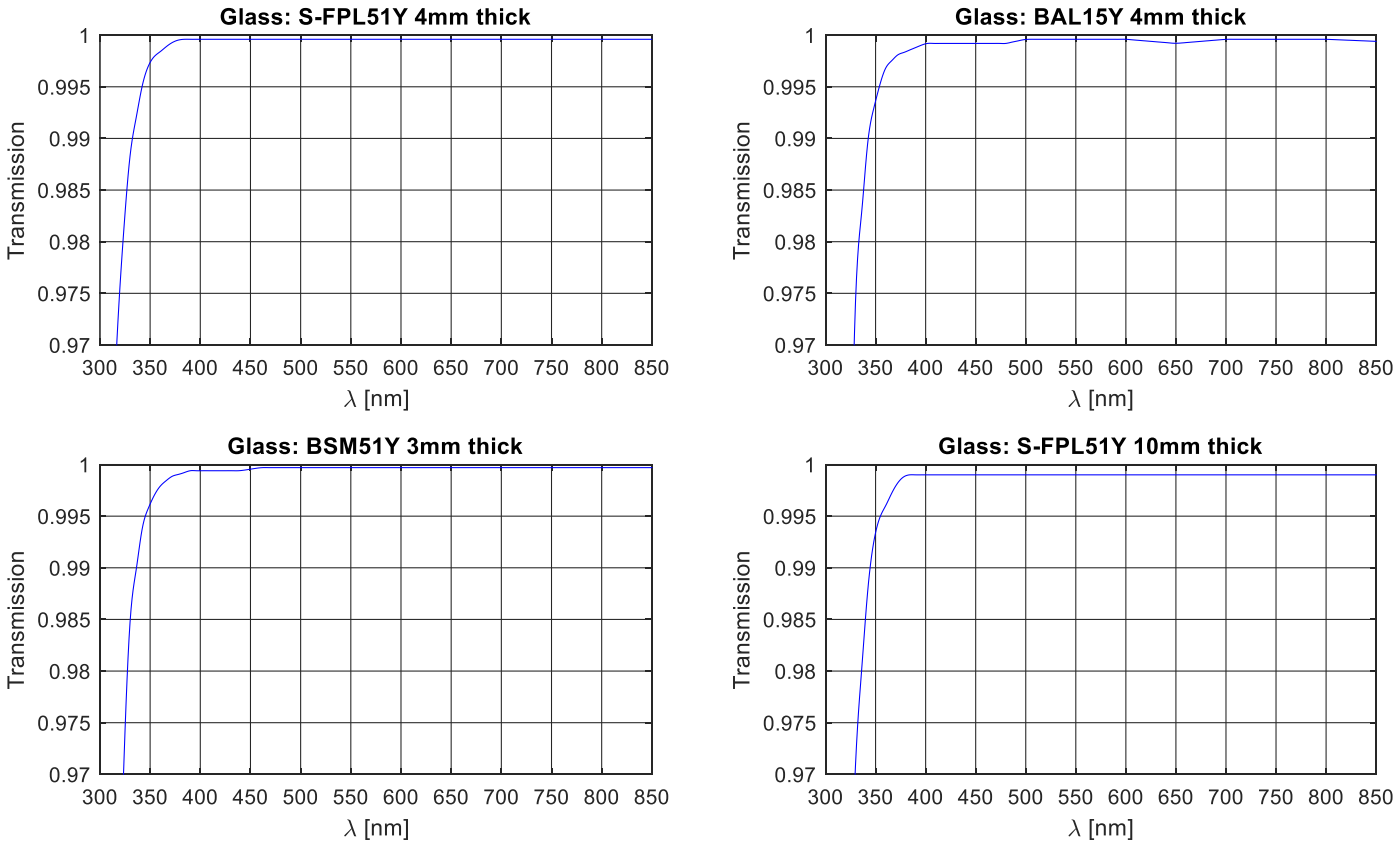

Figure 69. Common-Path UV-VIS second ADC quadruplet glasses internal transmission.

The total ADC-2 transmission, taking into account both AR-Coatings (on first and last surface) and glasses internal transmission. This is the curve used in the global CP-VIS-ADC efficiency.

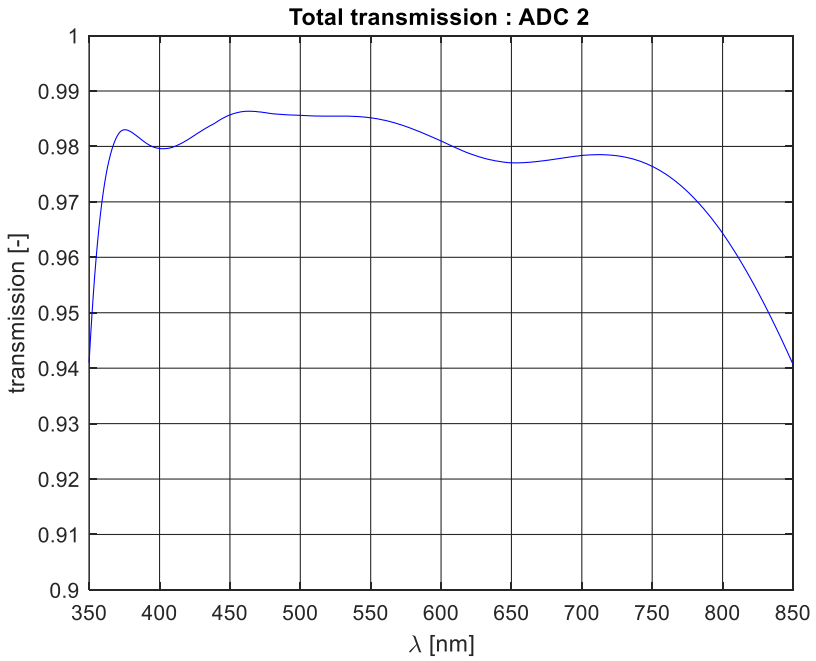

Figure 70. Common-Path UV-VIS second ADC quadruplet total transmission. This is the curve used in the global CP-VIS-ADC efficiency.

5.1.6 ADC total transmission/efficiency

The total ADC transmission is computed by multiplying the ADC-1 and ADC-2 transmissions. This is the curve used in the global CP-VIS efficiency.

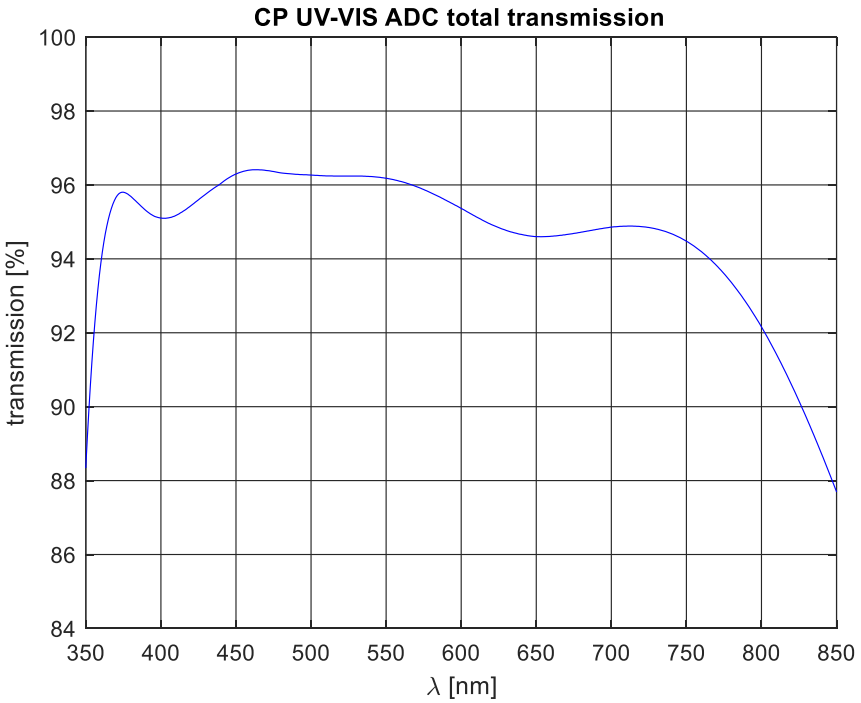

Figure 71. Common-Path UV-VIS ADC total transmission.

5.1.7 Tip-Tilt Mirror (CP_TT_VIS)

PDF plot and excel data from ASAHI-SPECTRA. See the zoomed plot of data in 350-850 nm.

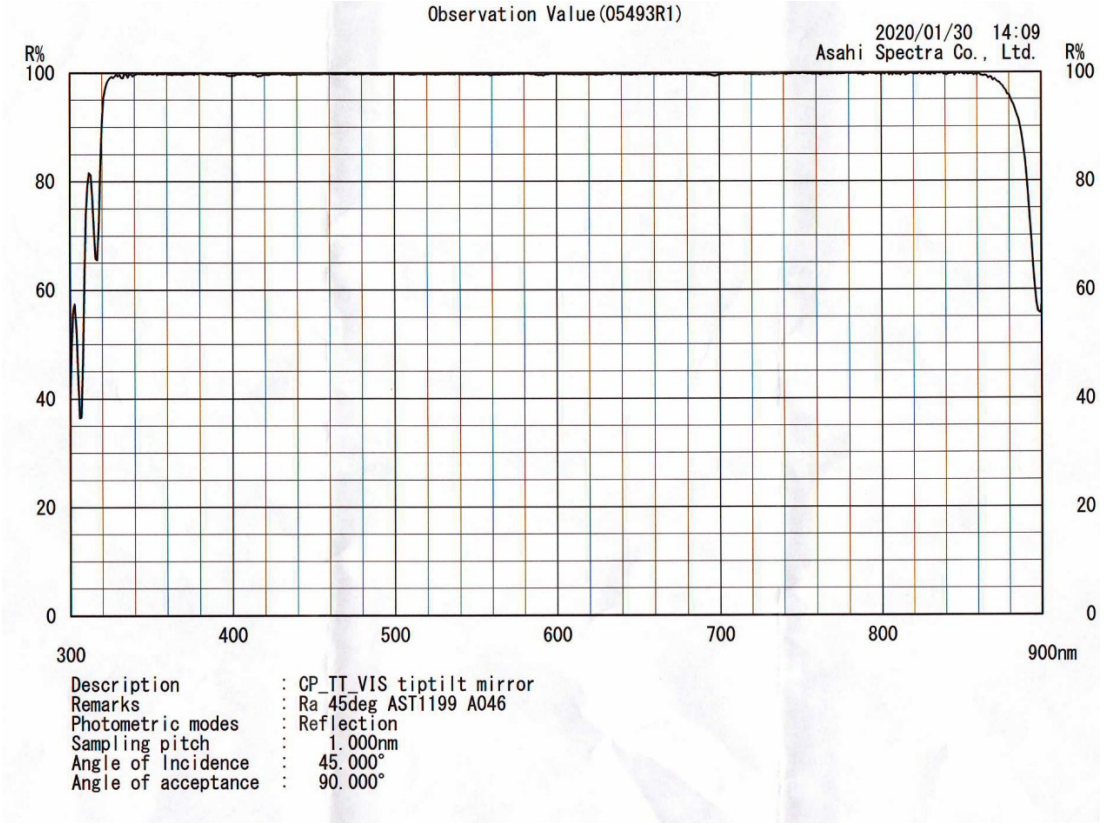

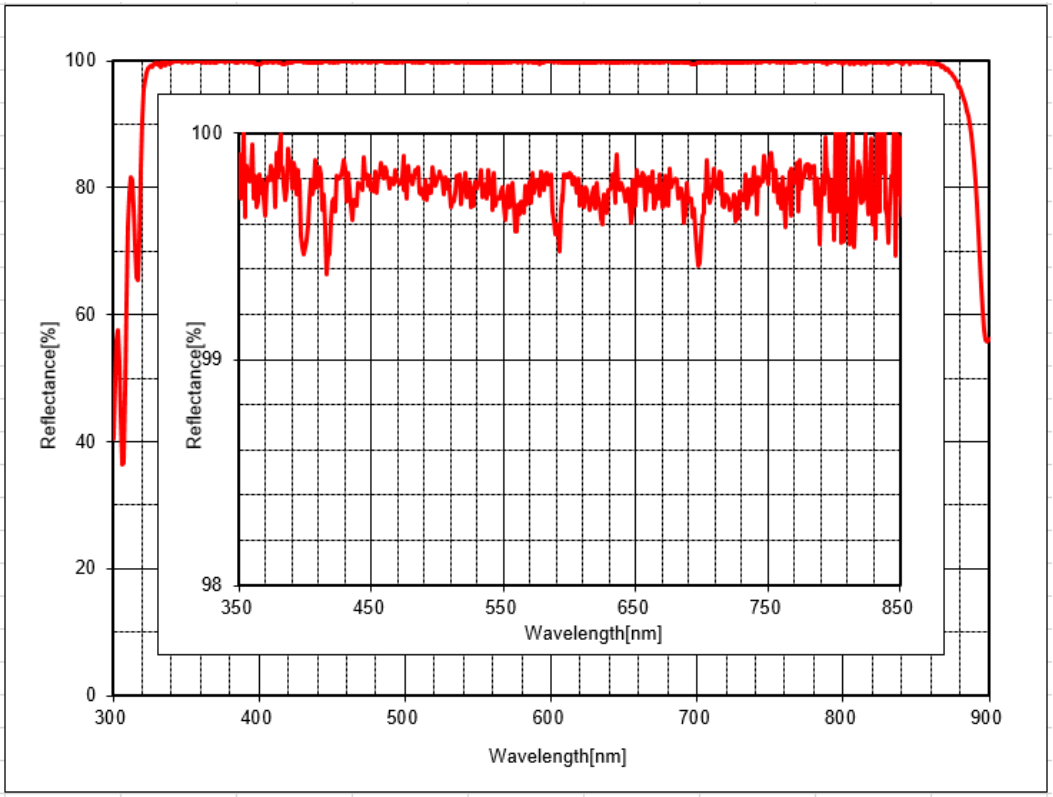

Figure 72.Common-Path UV-VIS tip-tilt mirror reflectivity profile. Top panel: PDF data. Bottom panel: excel data with zoom view.

Extracted data with MATLAB.

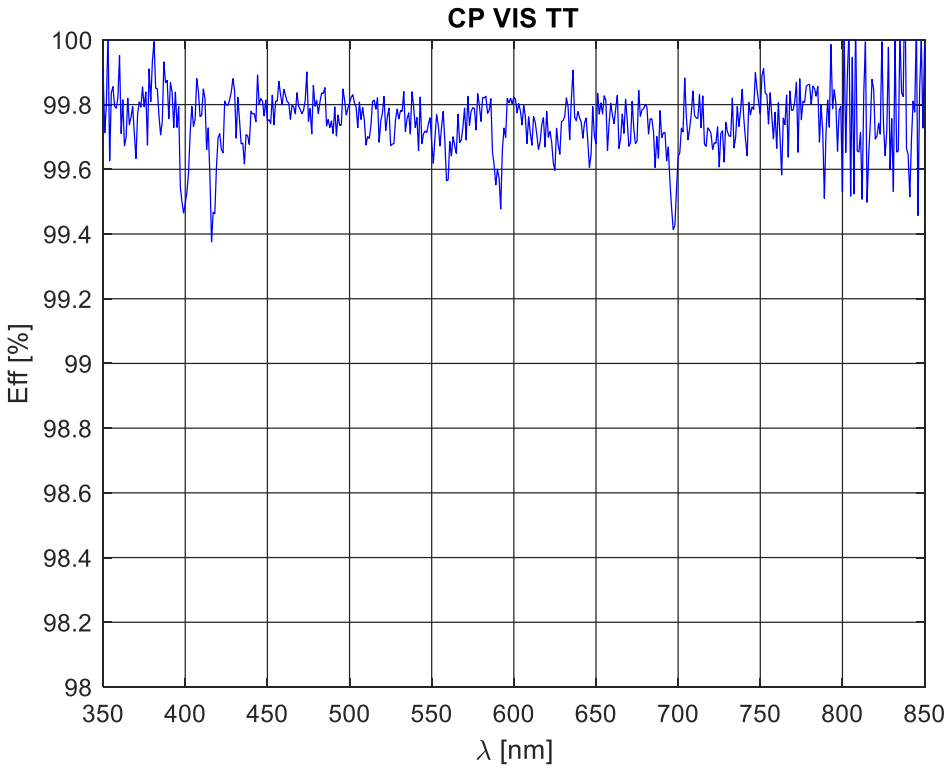

Interpolation from 350 to 850 nm, with 1nm step. This is the curve used in the global CP-VIS efficiency.

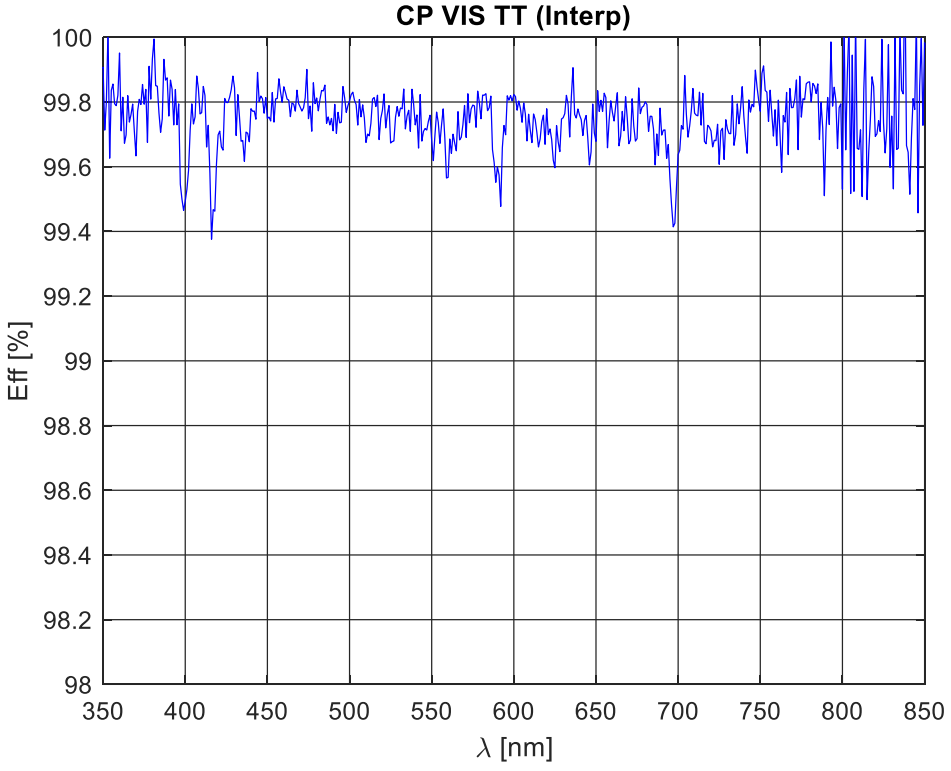

Figure 73. Common-Path UV-VIS tip-tilt mirror interpolated reflectivity profile used in the overall transmission computation.

5.1.8 Field Lens VIS (CP_LVIS_03)

The lens is in silica 1.5mm thick. The AR-coating data for both surfaces are given by PECCHIOLI report.

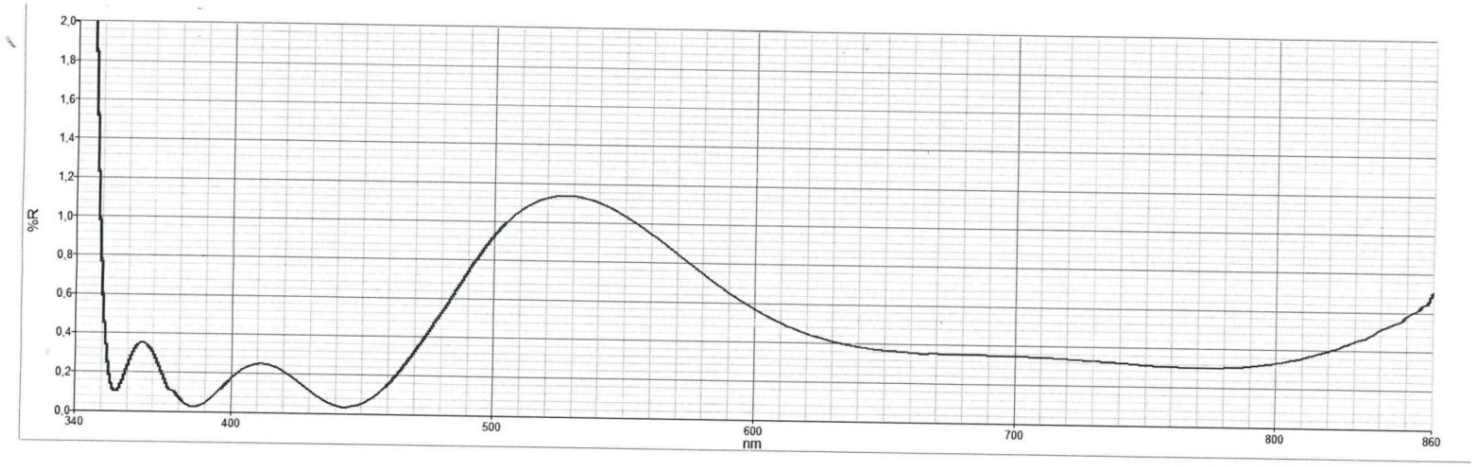

Extracted data with MATLAB.

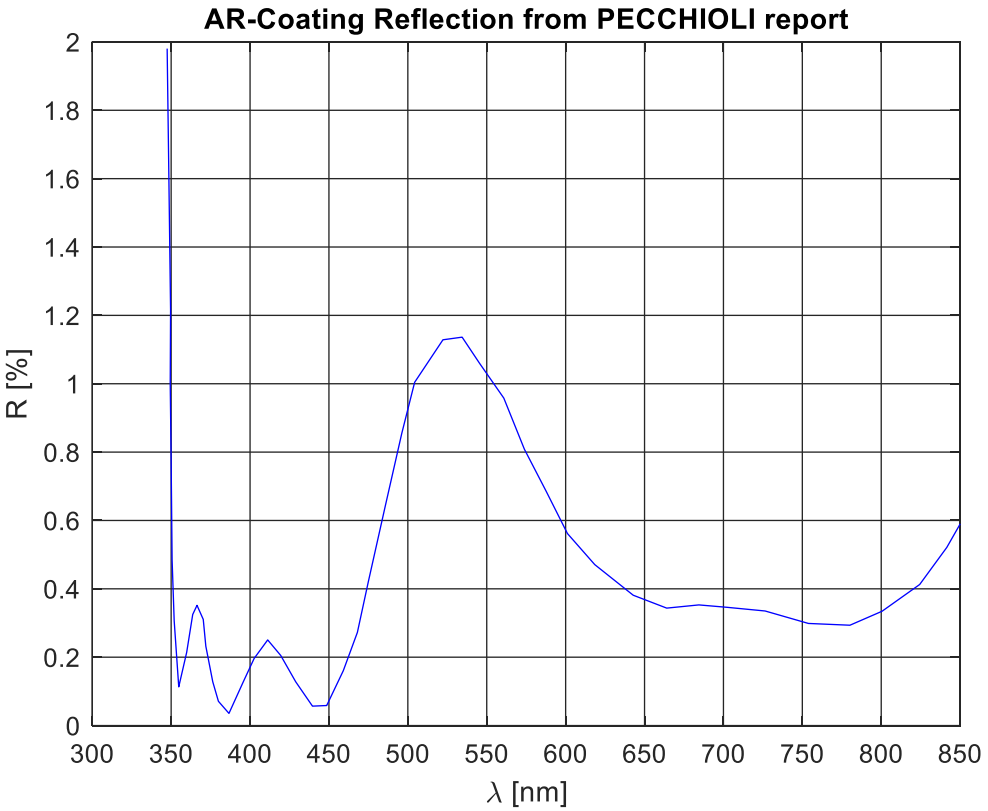

Figure 74. Common-Path UV-VIS field lens AR-coating curve data from producer (PECCHIOLI) report.

The Silica internal transmission is assumed to be 0.995.

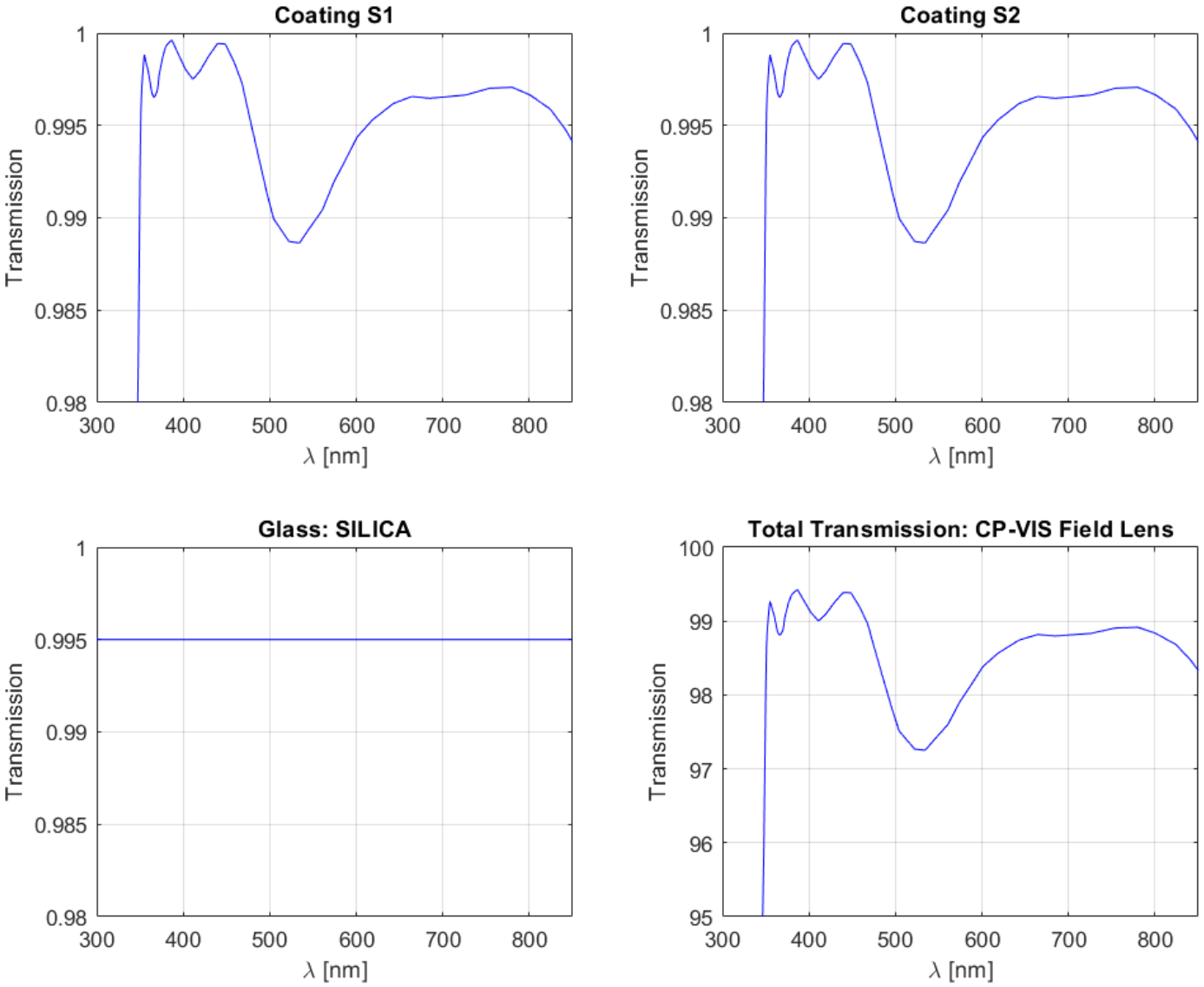

Figure 75. Common-Path UV-VIS field lens total transmission (bottom right panel) computed from AR coating on surfaces (top row panels) and silica glass.

5.1.9 UV-VUS Common-Path total efficiency

The total CP-UVVIS transmission efficiency is built from the:

- Dichroic transmission
- Folding mirror (CP_FM_VIS) reflection
- ADC total transmission (product of ADC-1, i.e. CP-LVIS_01, and ADC-2, i.e. CP-LVIS_02)
- Tip-tilt mirror (CP_TT_VIS) reflection
- Field lens (CP-LVIS_03) transmission

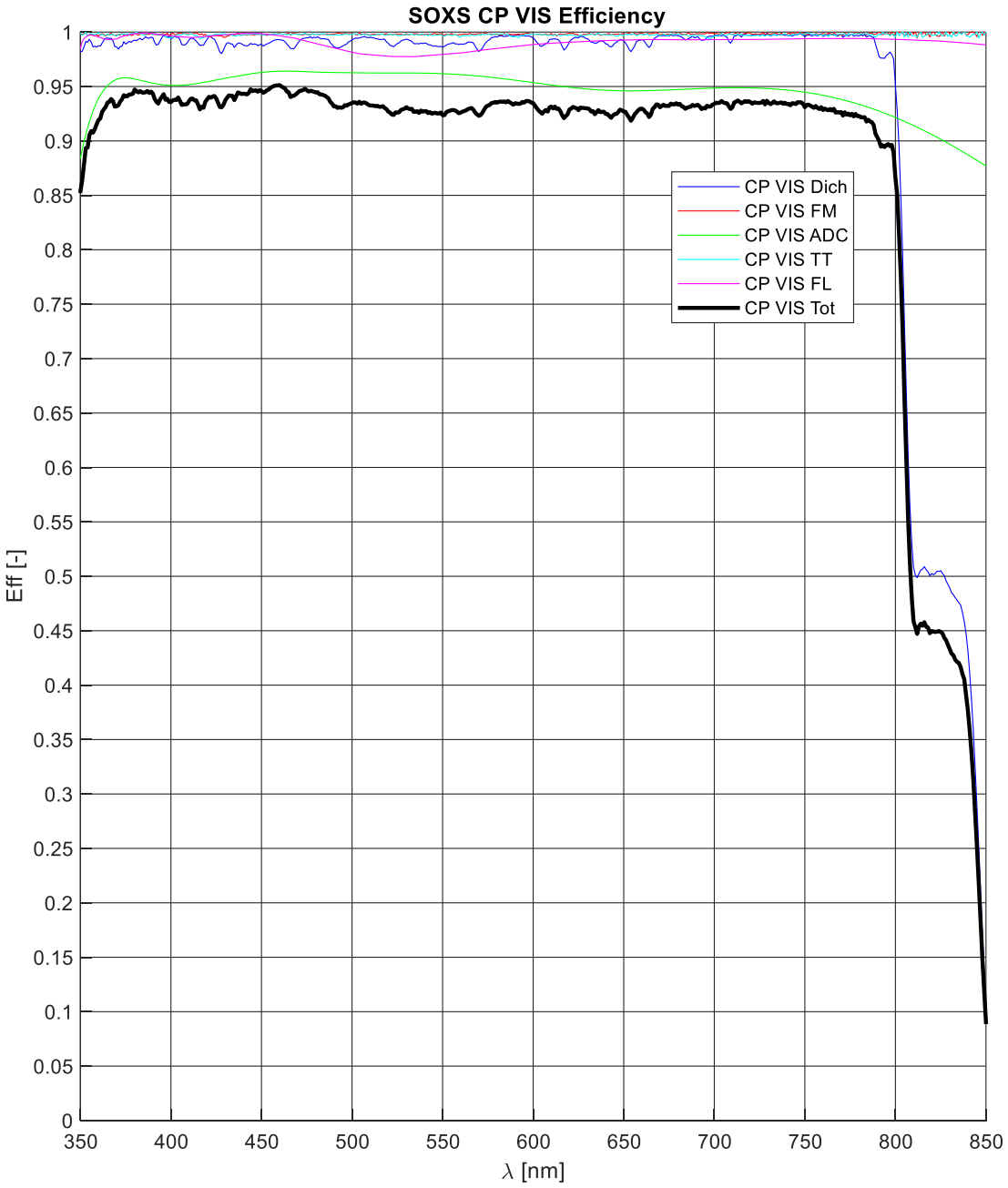

Figure 76. Common-Path UV-VIS total efficiency and single optical element curves.

5.2 NIR Common-Path Efficiency

5.2.1 Overwiev

The SOXS NIR Common-Path is composed by the following optical elements:

- Dichroic
- Folding Mirror
- Tip-tilt mirror
- Refocuser doublet
- Window
- Field lens

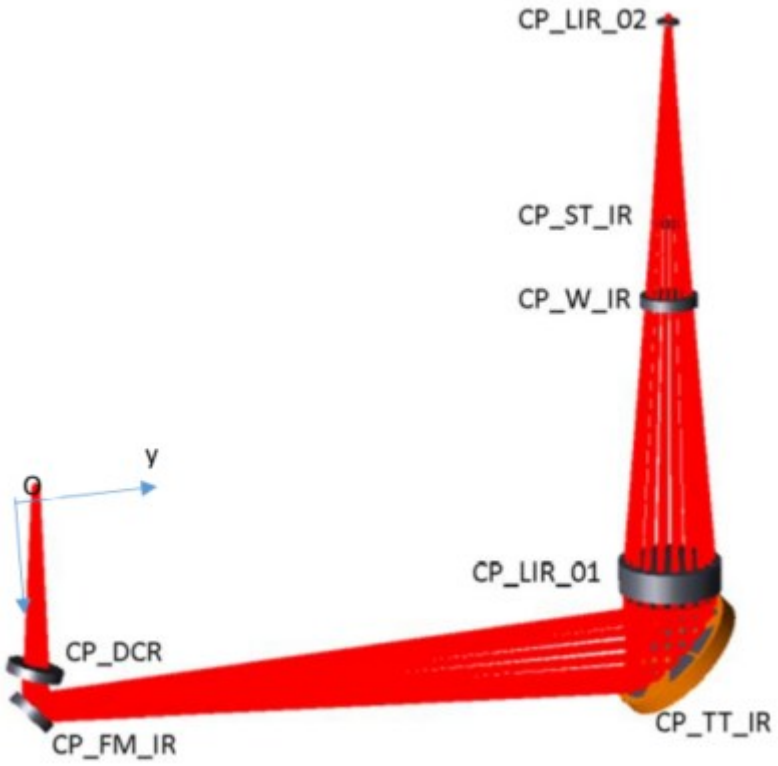

Figure 77. NIR Common Path optical layout.

5.2.2 Dichroic (CP_DCR)

The data for the dichroic transmission come from ASAHI-SPECTRA measure reports. From ASAHI mail confirmation:
" the attached Excel data is equal to the actual dichroic performance."
We assume that the dichroic full transmission is the following one from the excel measure-data.

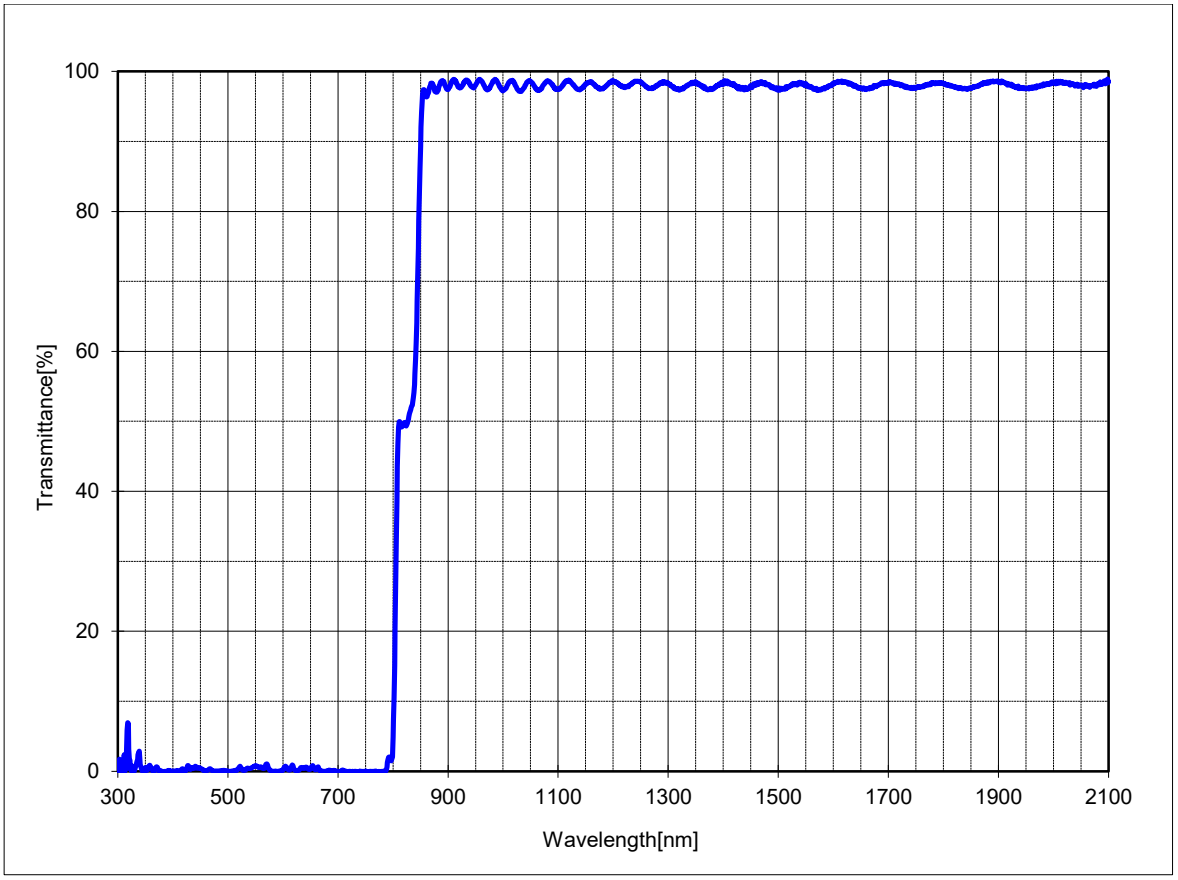

Figure 78. Common-Path Dichroic NIR transmission curve. Data from ASAHI manufacturer.

Extracted data with MATLAB.

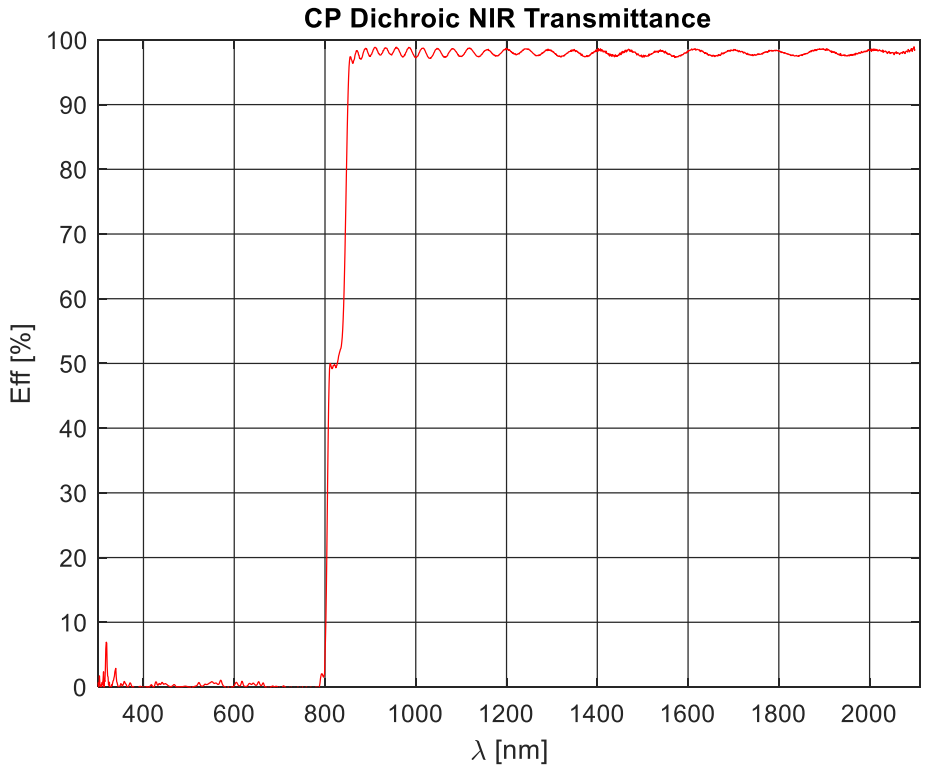

Interpolation from 780 to 2100 nm, with 1nm step. This is the curve used in the global CP-NIR efficiency.

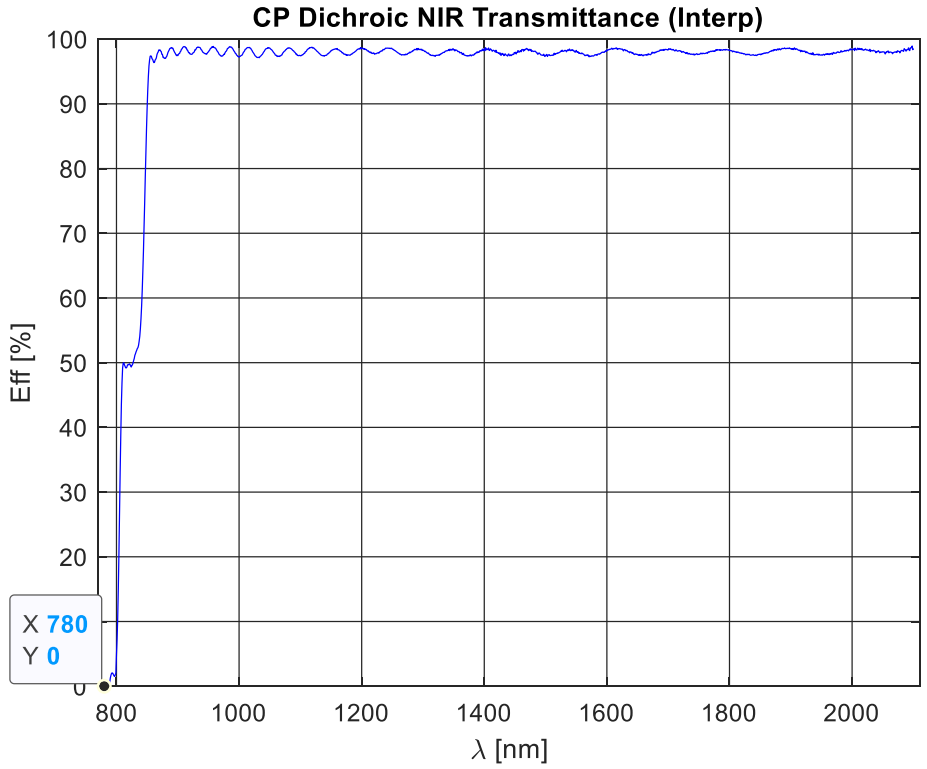

Figure 79. Common-Path Dichroic transmission curve interpolation used for the total CP NIR transmission.

5.2.3 Folding Mirror (CP_FM_IR)

PDF plot and excel data from ASAHI-SPECTRA. See the zoomed plot of data in 780-2100 nm.

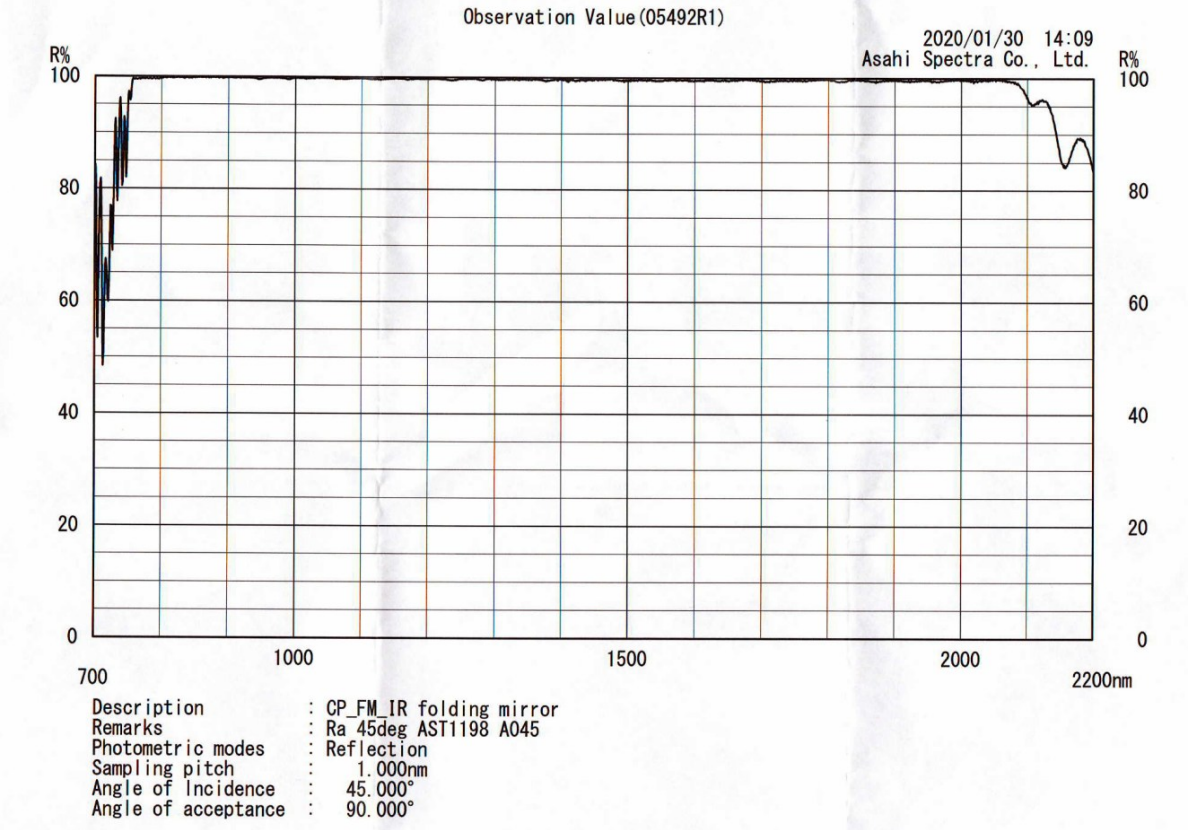

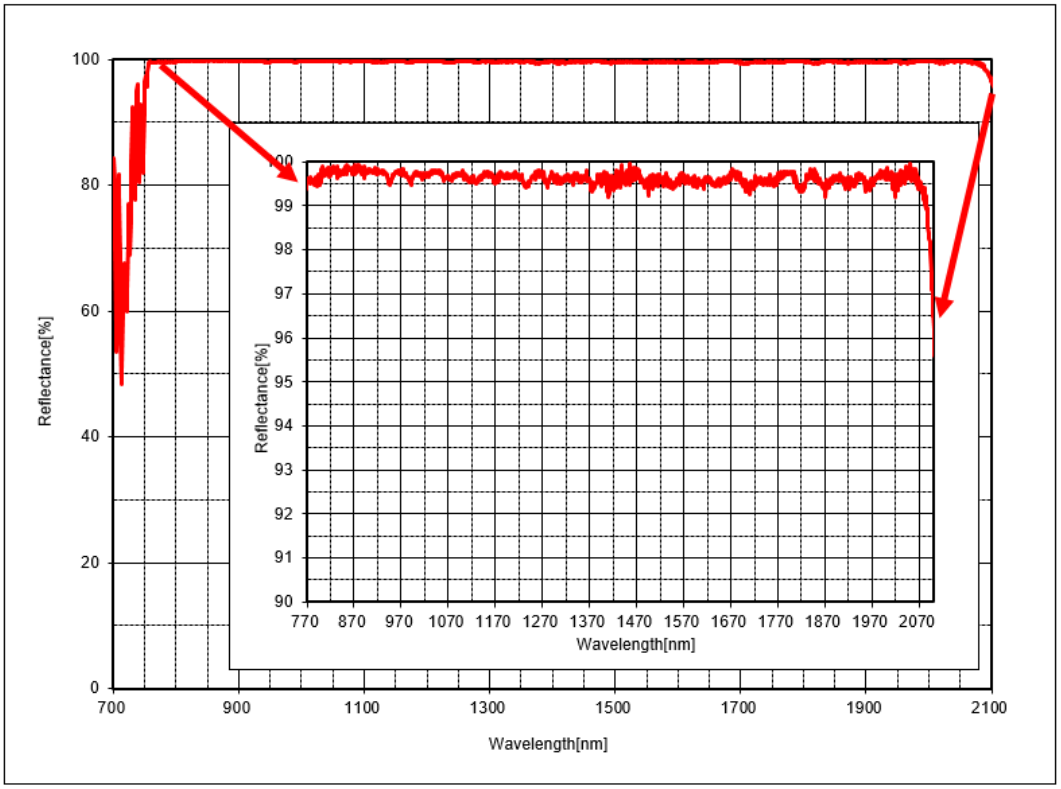

Figure 80.Common-Path NIR folding mirror reflectivity profile. Top panel: PDF data. Bottom panel: excel data with zoom view.

Extracted data with MATLAB.

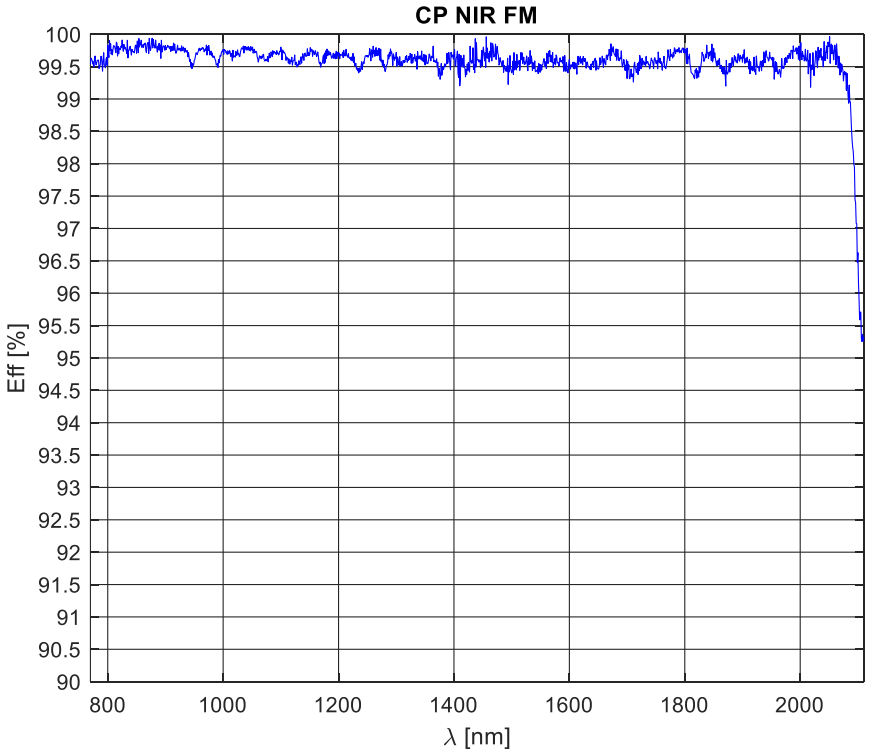

Interpolation from 780 to 2100 nm, with 1nm step. This is the curve used in the global CP-NIR efficiency.

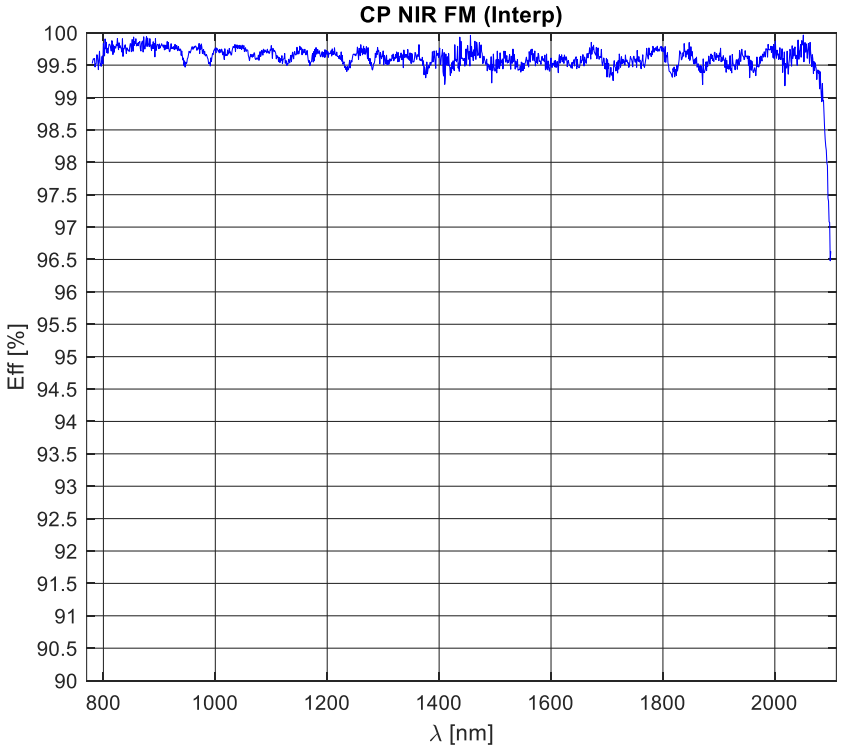

Figure 81. Common-Path NIR folding mirror interpolated reflectivity profile used in the overall transmission computation.

5.2.4 Tip-Tilt Mirror (CP_TT_IR)

PDF plot and excel data from ASAHI-SPECTRA. See the zoomed plot of data in 780-2100 nm.

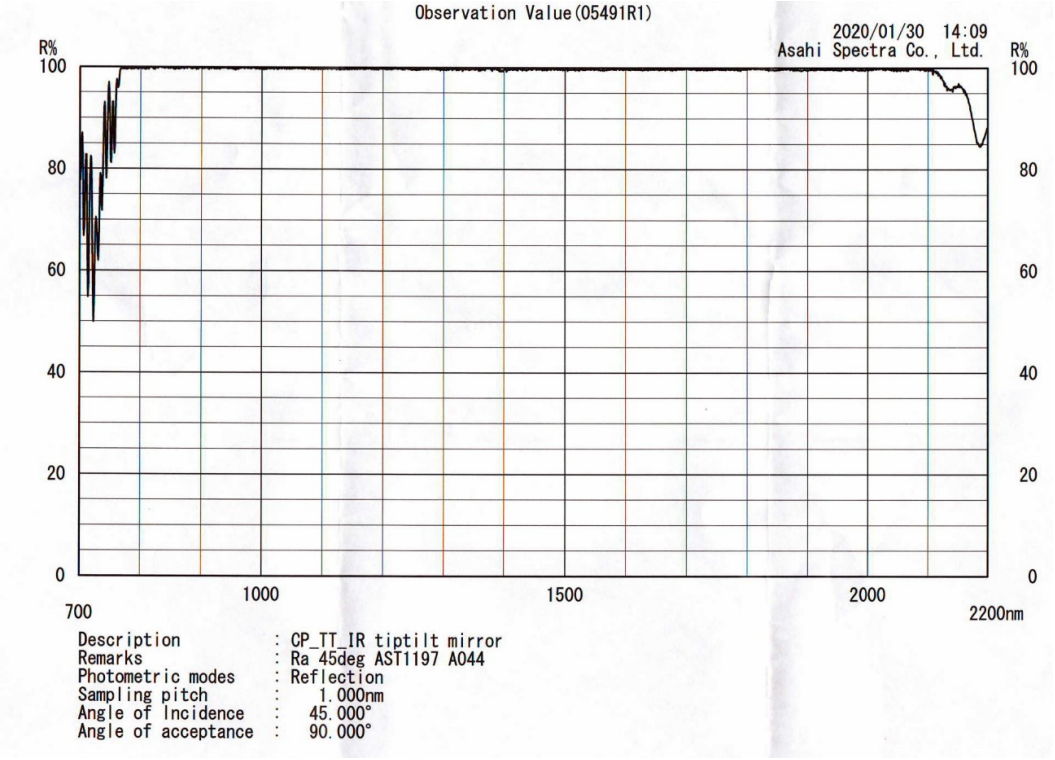

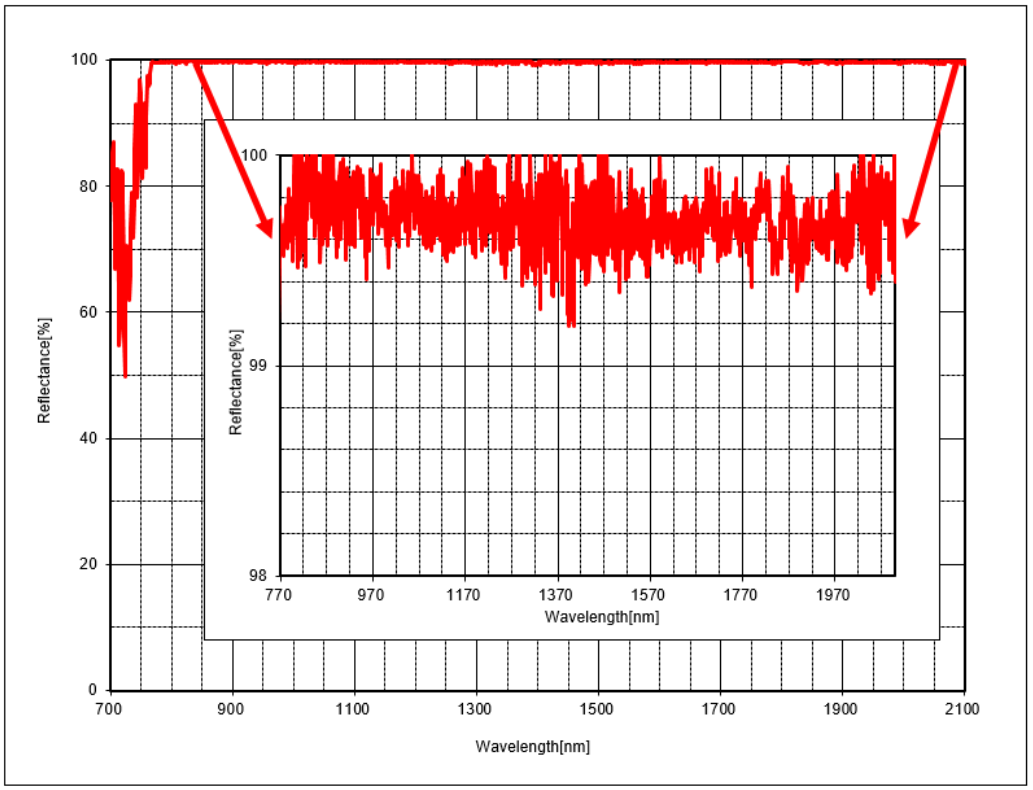

Figure 82. Common-Path NIR tip-tilt mirror reflectivity profile. Top panel: PDF data. Bottom panel: excel data with zoom view.

Extracted data with MATLAB.

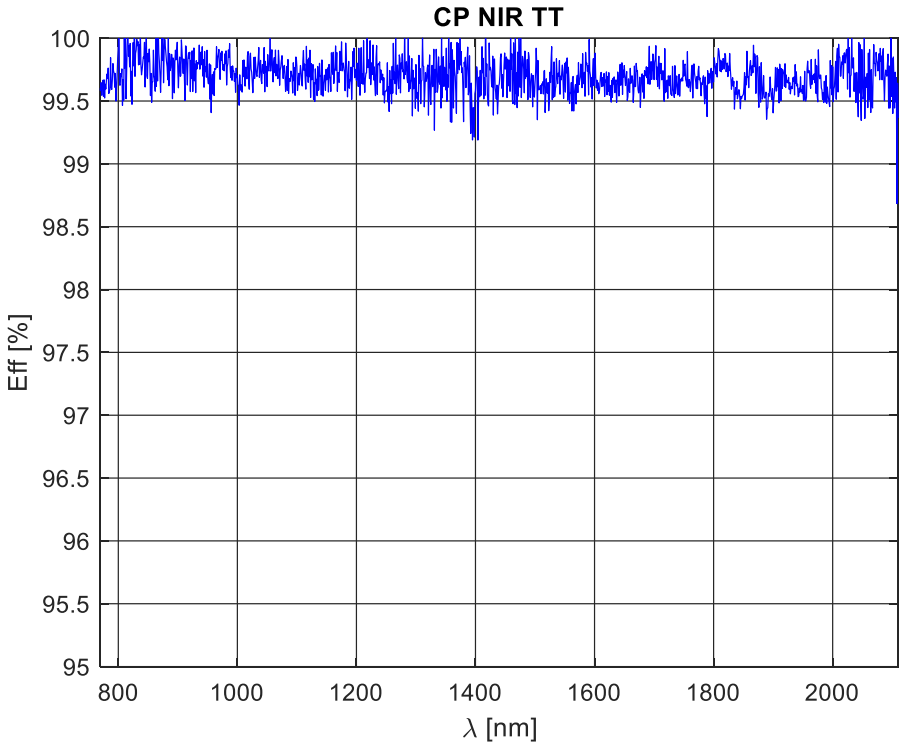

Interpolation from 780 to 2100 nm, with 1nm step. This is the curve used in the global CP-NIR efficiency.

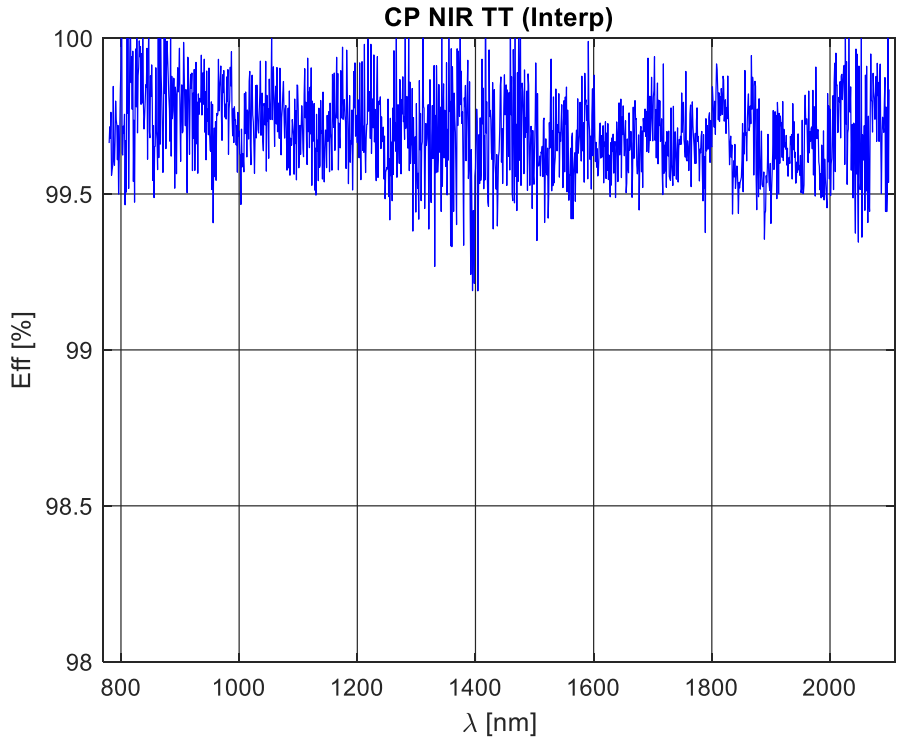

Figure 83. Common-Path NIR tip-tilt mirror interpolated reflectivity profile used in the overall transmission computation.

5.2.5 Refocusing doublet (CP_LIR_01)

For the ARC the data are taken from report-Plot OPTIMAX.

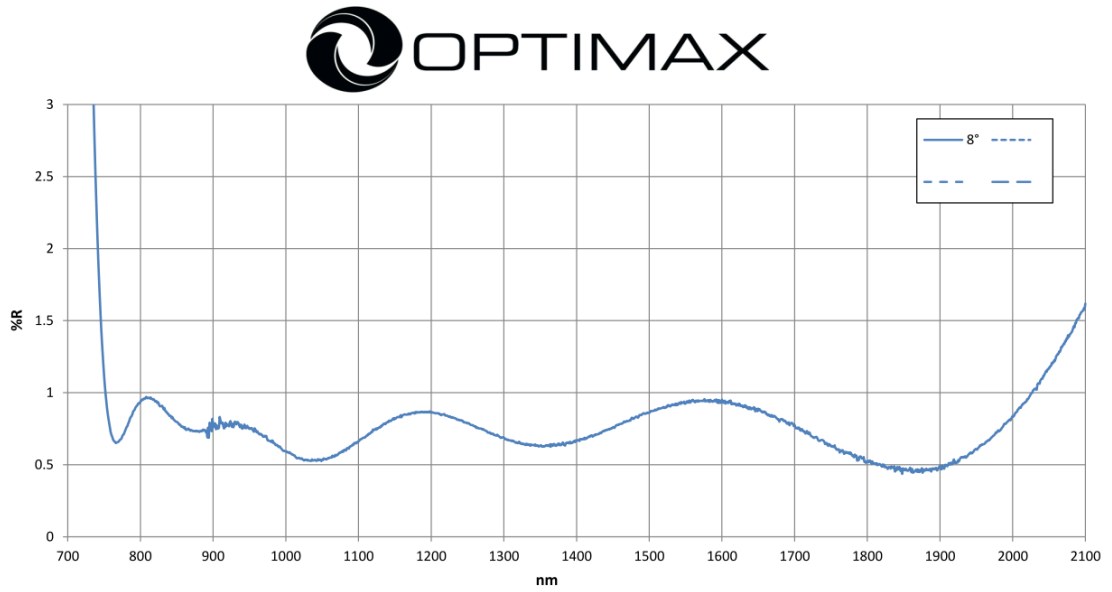

Customer: INAF
Run #: I-1300C
Job #: MRP32421 ASM:1
P/N: NTT-DWG-SOXS-CP-010104a
Serial #/Surface: 1-2/S1

Coating Requirements: Ravg< 1.5% from 800-2000nm

Measurements: 8°: Ravg=0.72%

Coating Date: 3/6/20 **Generated By:** JF

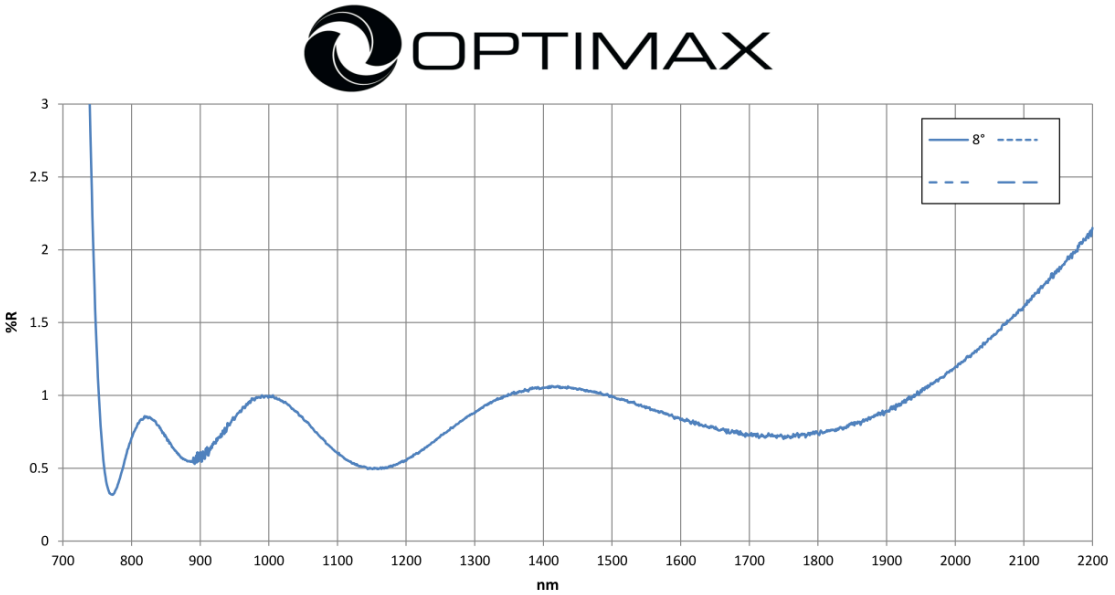

Customer: INAF
Run #: I-1289C
Job #: MRP32421 ASM:2
P/N: NTT-DWG-SOXS-CP-010104b
Serial #/Surface: 1-2/S1

Coating Requirements: Ravg< 1.5% from 800-2000nm

Measurements: 8°: Ravg=0.82%

Coating Date: 3/3/20 **Generated By:** MR

Figure 84. Common-Path NIR refocusing doublet. AR-coating data from producer (OPTIMAX) report.

The doublet is made by S-TIM2 (5mm central thickness) and CAF2 (12 mm central thickness). For what concern CAF2, in absence of data, we considered a 0.99 internal transmittance.
For S-TIM2 the OHARA catalogue internal transmittance data are considered, and to be conservative they are not rescaled to a thickness of 5mm instead of 10mm.

S-TIM 2

Code(d) **620363**
Code(e) **624360**

Refractive Index	n_d	**1.62004** 1.620041	Abbe Number	ν_d	**36.26**	Dispersion	n_F-n_C **0.017099**
Refractive Index	n_e	1.624088	Abbe Number	ν_e	35.99	Dispersion	$n_{F'}-n_{C'}$ 0.017339

Refractive Indices		
λ(μm)		
n_{2325}	2.32542	1.58240
n_{1970}	1.97009	1.58806
n_{1530}	1.52958	1.59435
n_{1129}	1.12864	1.60041
n_t	1.01398	1.60260
n_s	0.85211	1.60663
$n_{A'}$	0.76819	1.60952
n_r	0.70652	1.61225
n_C	0.65627	1.61502
$n_{C'}$	0.64385	1.61581
n_{He-Ne}	0.6328	1.61655
n_D	0.58929	1.61989
n_d	0.58756	1.62004
n_e	0.54607	1.62409
n_F	0.48613	1.63212
$n_{F'}$	0.47999	1.63315
n_{He-Cd}	0.44157	1.64081
n_g	0.435835	1.64218
n_h	0.404656	1.65100
n_i	0.365015	1.66728

Constants of Dispersion Formula	
A_1	1.42193846E+00
A_2	1.33827968E-01
A_3	1.45060574E+00
B_1	1.07291511E-02
B_2	5.72587546E-02
B_3	1.45381805E+02

Chemical Properties	
Water Resistance(Powder) Group RW(P)	1
Acid Resistance(Powder) Group RA(P)	1
Weathering Resistance(Surface) Group W(S)	2
Acid Resistance(Surface) Group SR	1.0
Phosphate Resistance PR	1.0

Mechanical Properties		
Young's Modulus E (10^3N/m^2)	776	
Rigidity Modulus G (10^3N/m^2)	315	
Poisson's Ratio σ	0.230	
Knoop Hardness Hk[Class]	550	6
Abrasion Aa	150	
Photoelastic Constant β (nm/cm/10^3Pa)	2.86	

Partial Dispersions	
n_C-n_t	0.012426
$n_C-n_{A'}$	0.005500
n_d-n_C	0.005017
n_e-n_C	0.009064
n_g-n_d	0.022135
n_g-n_F	0.010053
n_h-n_g	0.008822
n_i-n_g	0.025105
$n_{C'}-n_t$	0.013213
$n_e-n_{C'}$	0.008277
$n_{F'}-n_e$	0.009062
$n_i-n_{F'}$	0.034131

Relative Partial Dispersions	
$\theta_{C,t}$	0.7267
$\theta_{C,A'}$	0.3217
$\theta_{d,C}$	0.2934
$\theta_{e,C}$	0.5301
$\theta_{g,d}$	1.2945
$\theta_{g,F}$	0.5879
$\theta_{h,g}$	0.5159
$\theta_{i,g}$	1.4682
$\theta'_{C',t}$	0.7620
$\theta'_{e,C'}$	0.4774
$\theta'_{F',e}$	0.5226
$\theta'_{i,F'}$	1.9685

Deviation of Relative Dispersions Δθfrom "Normal"	
$\Delta\theta_{C,t}$	0.0099
$\Delta\theta_{C,A'}$	0.0019
$\Delta\theta_{g,d}$	0.0051
$\Delta\theta_{g,F}$	0.0051
$\Delta\theta_{i,g}$	0.0468

Thermal Properties		
Strain Point StP (℃)		551
Annealing Point AP (℃)		576
Transformation Temperature Tg (℃)		598
Yield Point At (℃)		634
Softening Point SP (℃)		703
Expansion Coefficients	(-30~+70℃)	81
α (10^{-7}/℃)	(+100~+300℃)	95
Thermal Conductivity k (W/m·K)		1.39

Temperature Coefficients of Refractive Index							
Range of Temperature (℃)	dn/dT relative (10^{-6}/℃)						
	t	C'	He-Ne	D	e	F'	g
-40~-20	1.7	2.3	2.3	2.5	2.8	3.4	4.2
-20~ 0	1.8	2.3	2.4	2.6	2.9	3.6	4.4
0~20	1.8	2.4	2.5	2.7	3.0	3.7	4.6
20~40	1.9	2.5	2.6	2.8	3.1	3.9	4.8
40~60	1.9	2.6	2.6	2.9	3.2	4.1	5.0
60~80	2.0	2.7	2.7	3.0	3.4	4.2	5.2

Coloring			
λ_{80}	390	λ_5	355
λ_{70}			

Internal transmission			
$\lambda_{0.80}$	385	$\lambda_{0.05}$	359

CCI		
B	G	R
0.00	1.20	1.19

Internal Transmittance	
λ(nm)	τ 10mm
280	
290	
300	
310	
320	
330	
340	
350	
360	0.08
370	0.44
380	0.73
390	0.87
400	0.942
420	0.978
440	0.987
460	0.990
480	0.992
500	0.994
550	0.997
600	0.997
650	0.996
700	0.997
800	0.999
900	0.999
1000	0.999
1200	0.999
1400	0.995
1600	0.995
1800	0.984
2000	0.971
2200	0.930
2400	0.914

Other Properties	
Bubble Quality Group B	
Specific Gravity d	2.69
Remarks	

OHARA 17-04

Extracted data with MATLAB.

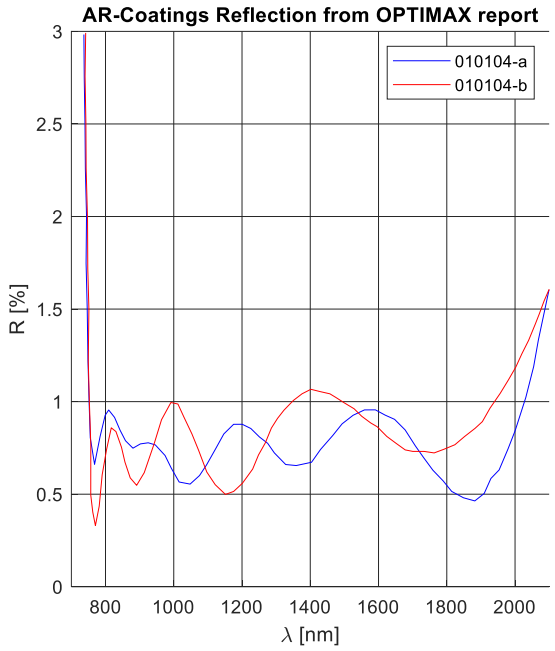

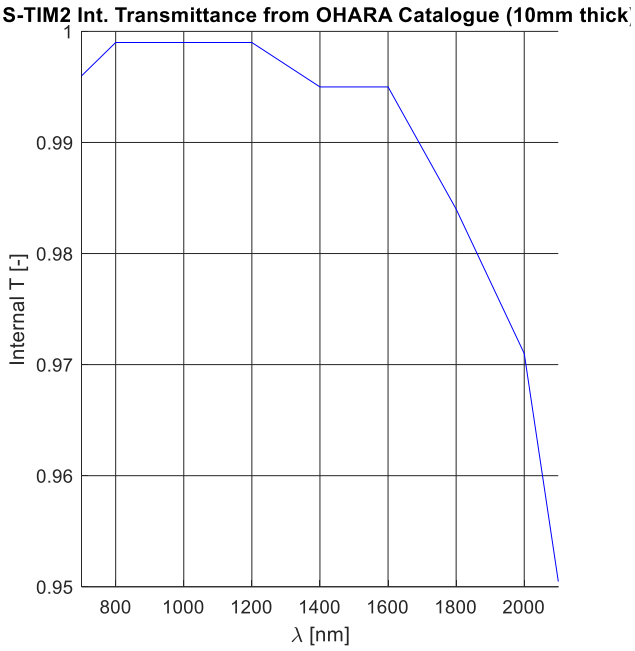

From the AR-Coating in %, the surfaces transmission is calculated, then by multiplying these by the internal transmission of the two glasses, the completed doublet transmission is evaluated.

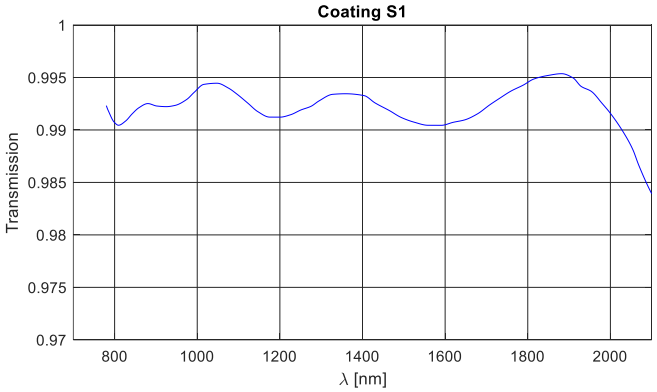

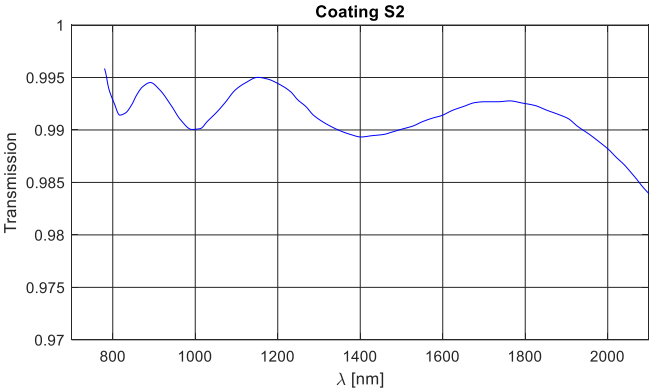

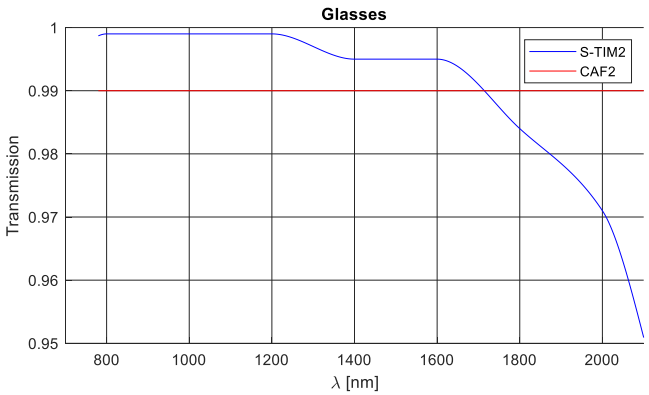

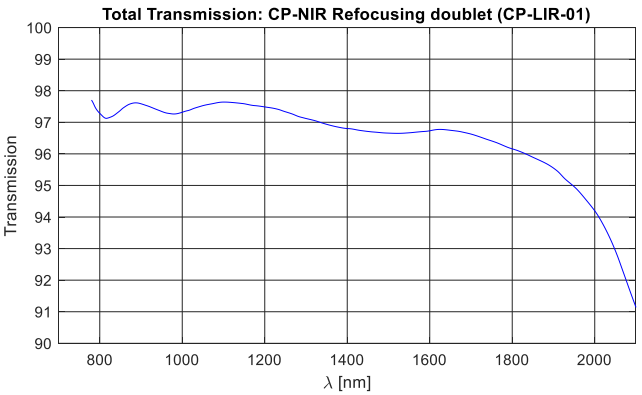

Figure 85. Common-Path NIR refocusing doublet total transmission (bottom right panel), computed from AR coating data (top row panels) and glasses internal transmission profile (bottom left panel).

5.2.6 Window (CP_W_IR)

The window is in silica 5mm thick. The AR-coating data for both surfaces are given by PECCHIOLI report.

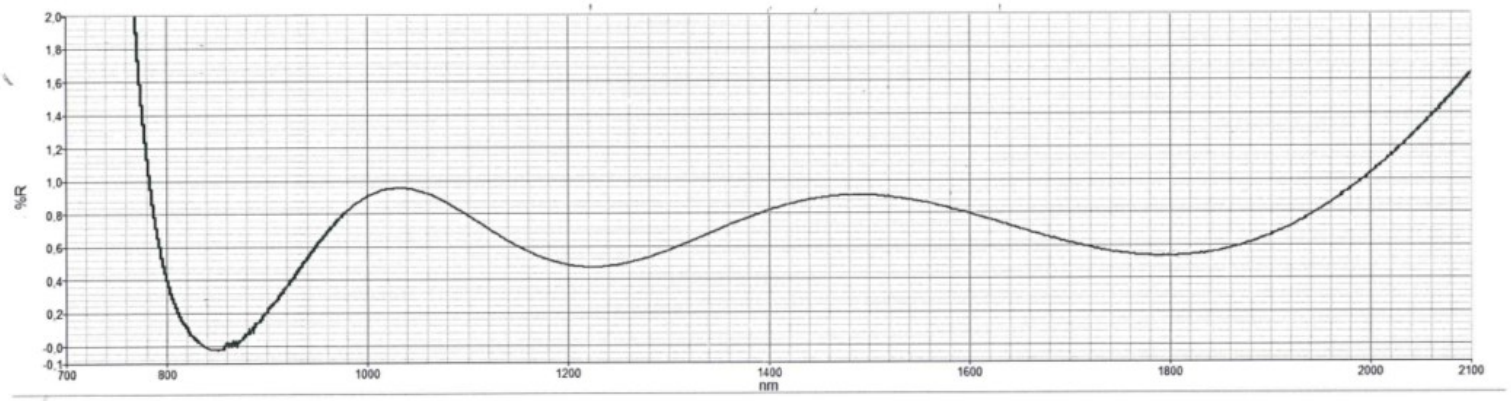

Extracted data with MATLAB.

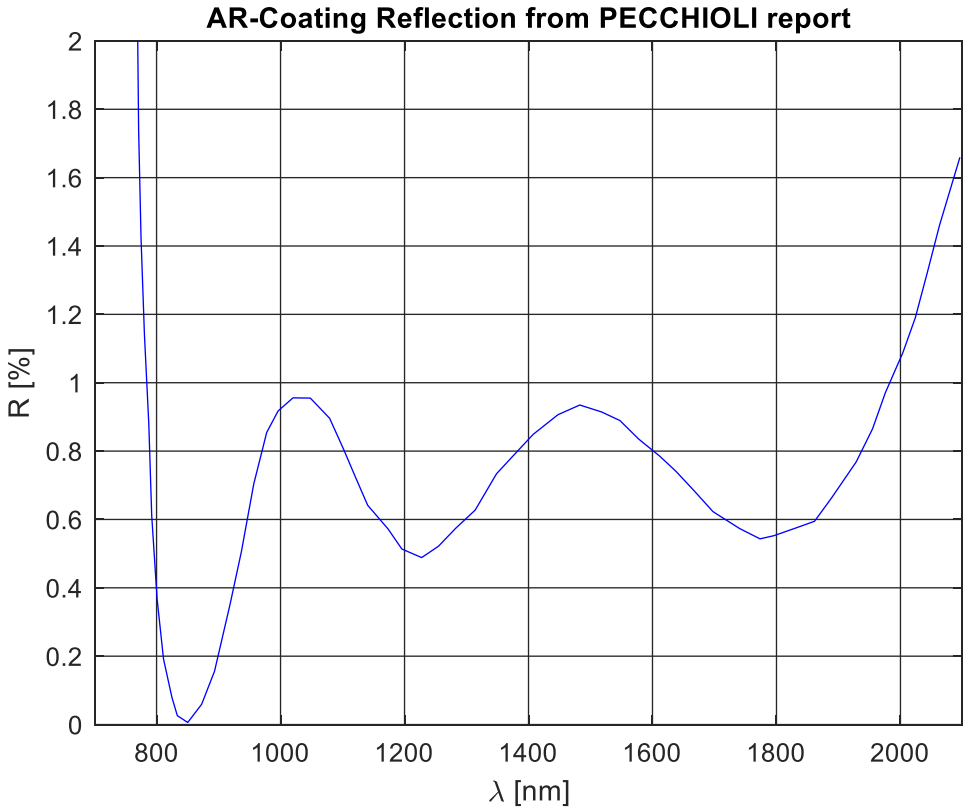

Figure 86. Common-Path NIR window AR-coating curve data from producer (PECCHIOLI) report.

The Silica internal transmission is assumed to be 0.995.

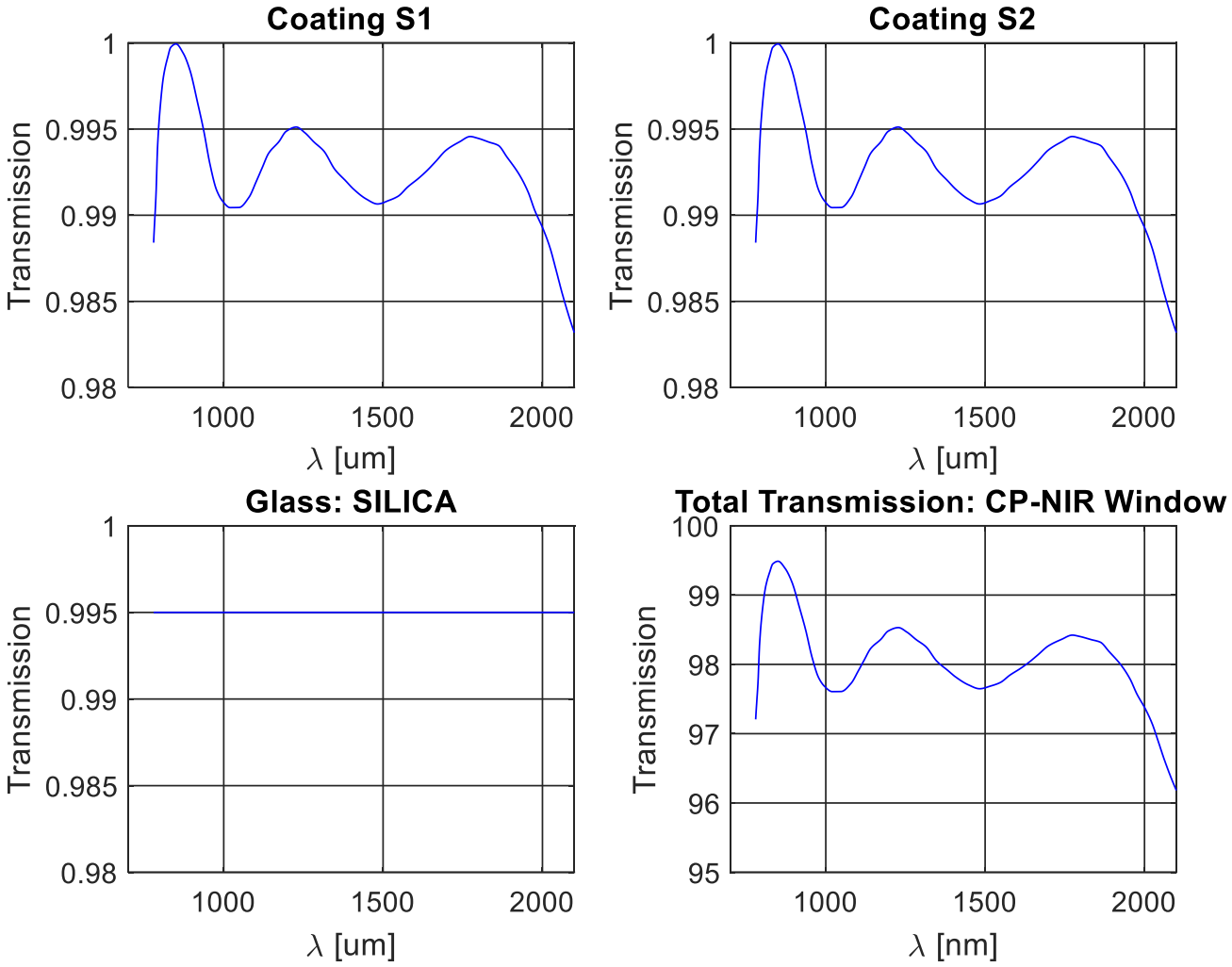

Figure 87. Common-Path NIR window total transmission (bottom right panel) computed from AR coating on surfaces (top row panels) and silica glass.

5.2.7 Field Lens (CP_LIR_02)

The lens is in silica 1.5mm thick. The AR-coating data for both surfaces are given by PECCHIOLI report.

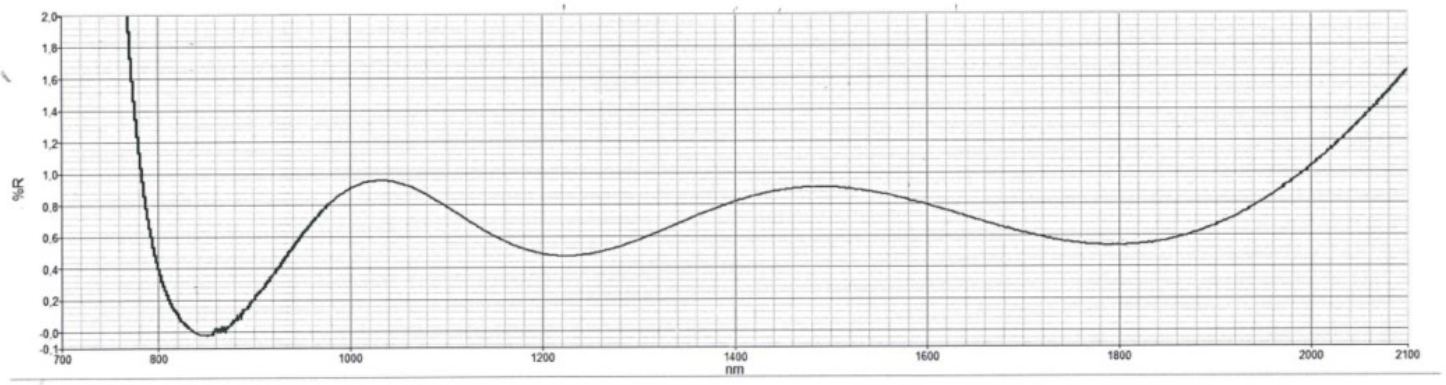

Extracted data with MATLAB.

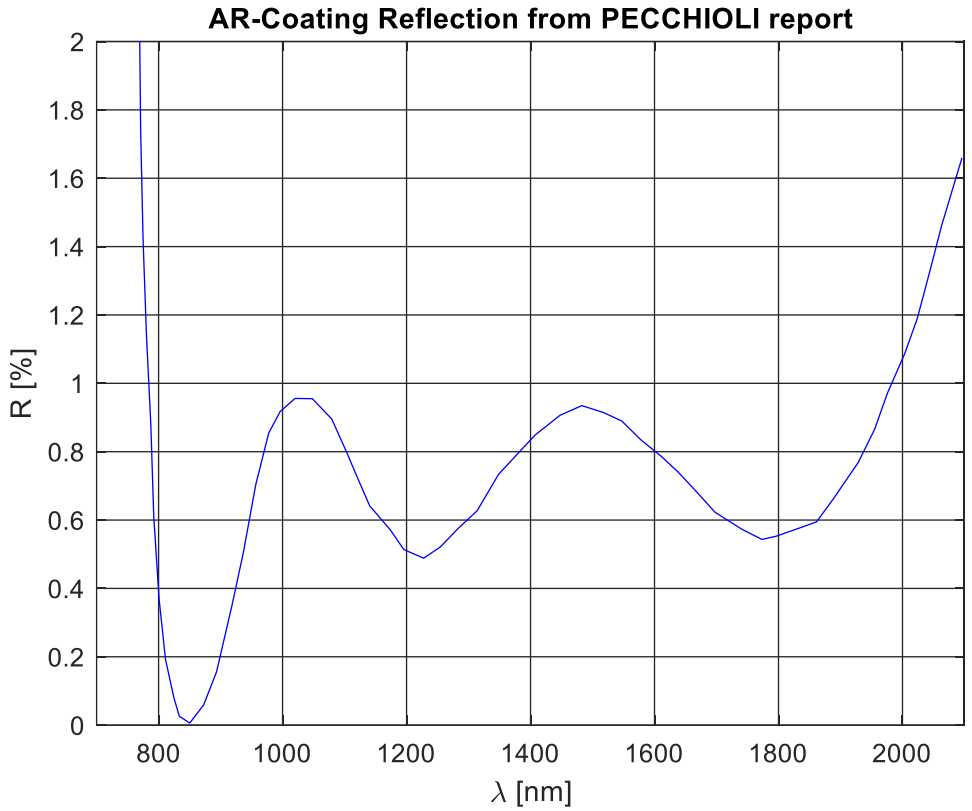

Figure 88. Common-Path NIR field lens AR-coating curve data from producer (PECCHIOLI) report.

The Silica internal transmission is assumed to be 0.995.

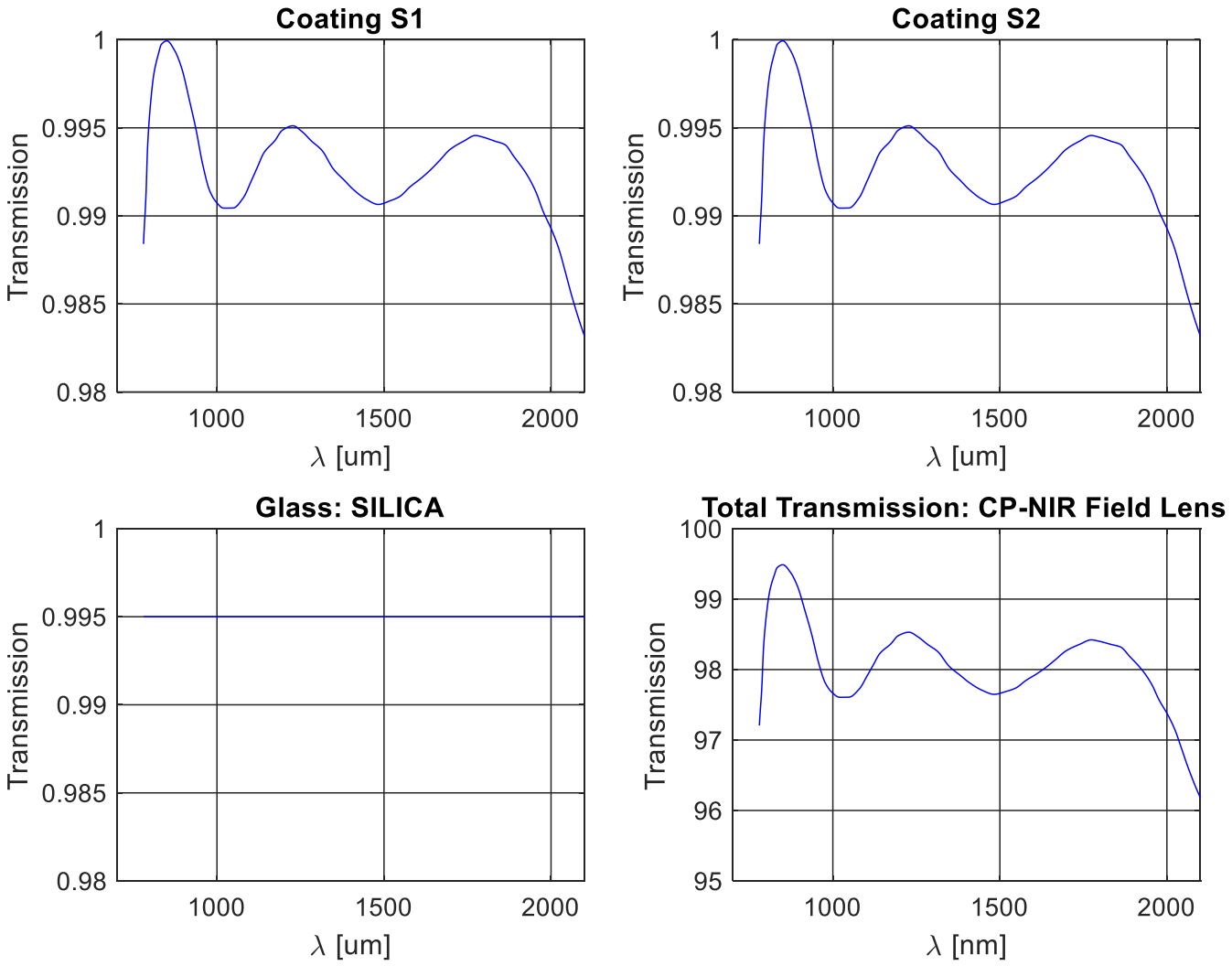

Figure 89. Common-Path NIR field lens total transmission (bottom right panel) computed from AR coating on surfaces (top row panels) and silica glass.

5.2.8 NIR Common-Path total efficiency

The total CP-NIR transmission efficiency is built from the:

- Dichroic transmission
- Folding mirror (FM) reflection
- Tip-tilt mirror (TT) reflection
- Refocuser (CP-LIR_01) transmission
- Window transmission
- Field lens (CP-LIR_01) transmission

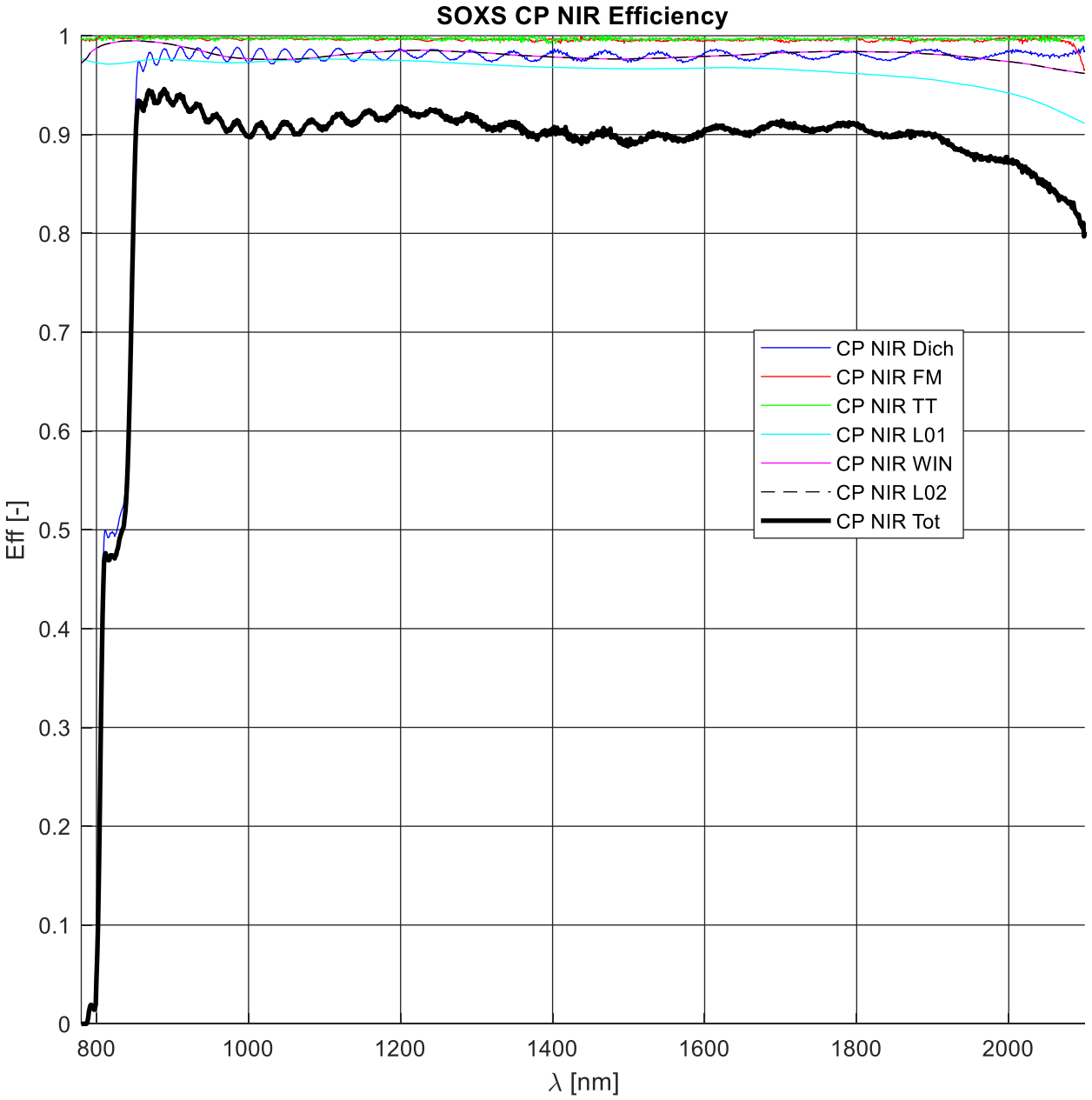

Figure 90. Common-Path NIR total efficiency and single optical element curves.

6 APPENDIX 2: Spectrographs Efficiency estimation

Purpose of this appendix is to provide the data that are considered to compute the Efficiency of the SOXS UVVIS and NIR spectrograph arms (from slit to detector excluded).

6.1 UV-VIS Spectrograph Efficiency

The UV-VIS Spectrograph is composed in its 4 arms, by the following optical elements:

- A, Fold mirror
- B, collimating OAP
- C, D, G dichroic mirrors
- E, F, H, dielectric mirrors
- I transmission gratings

As shown in the next figure, blue, green, red and yellow represent u, g, r, i bands respectively.

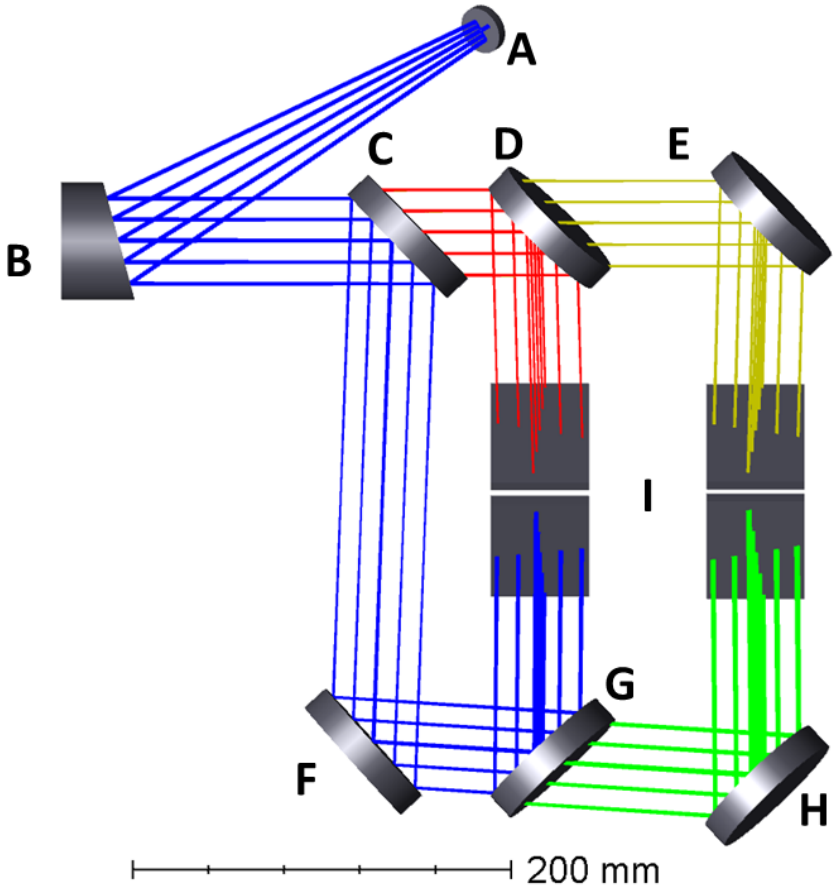

Figure 91. SOXS UV-VIS spectrograph arm optical layout.

The data, considered for the transmission/efficiency calculation of dichroics, dielectric mirrors and gratigns can be found on:
https://owncloud.ia2.inaf.it/index.php/apps/files/?dir=/SOXS/SharingFolder/Weizmann/VIS/Efficiency&fileid=160120254

6.1.1 A, Fold Mirror

Plot from the excel file, available in owncloud link.

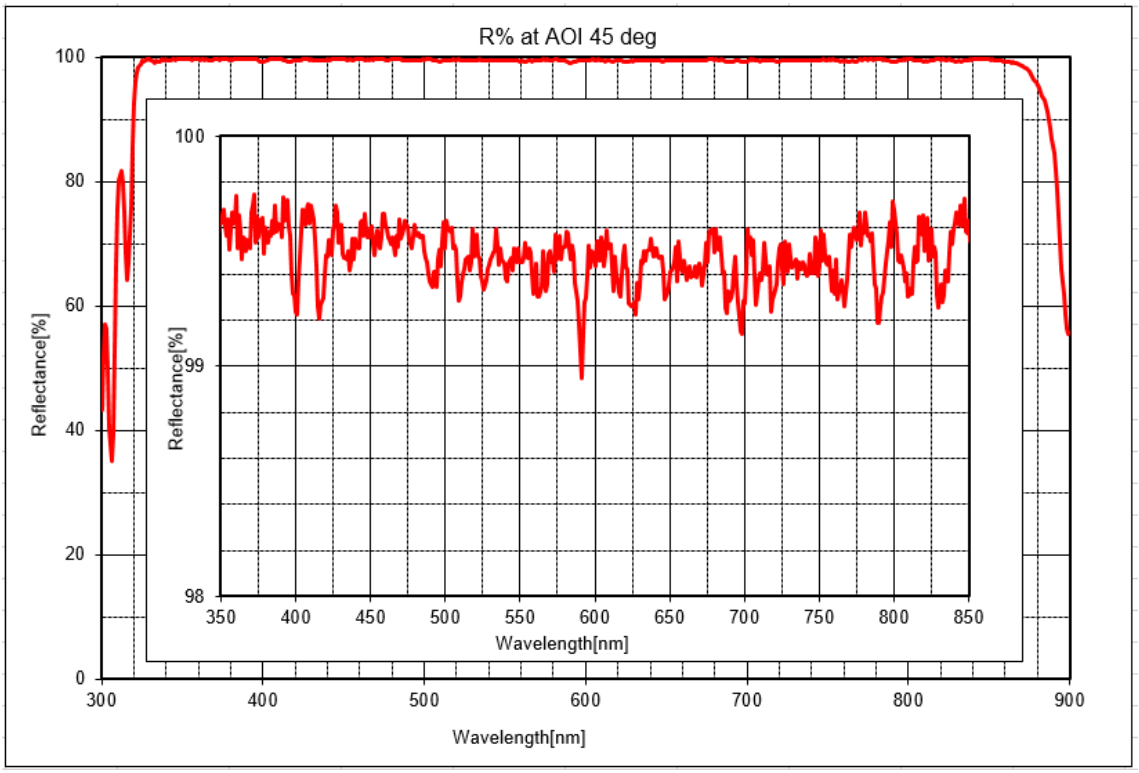

Figure 92. UV-VIS Spectrograph element A reflectance curve.

Extracted data with MATLAB. This is the curve used in the global VIS Spectrograph efficiency.

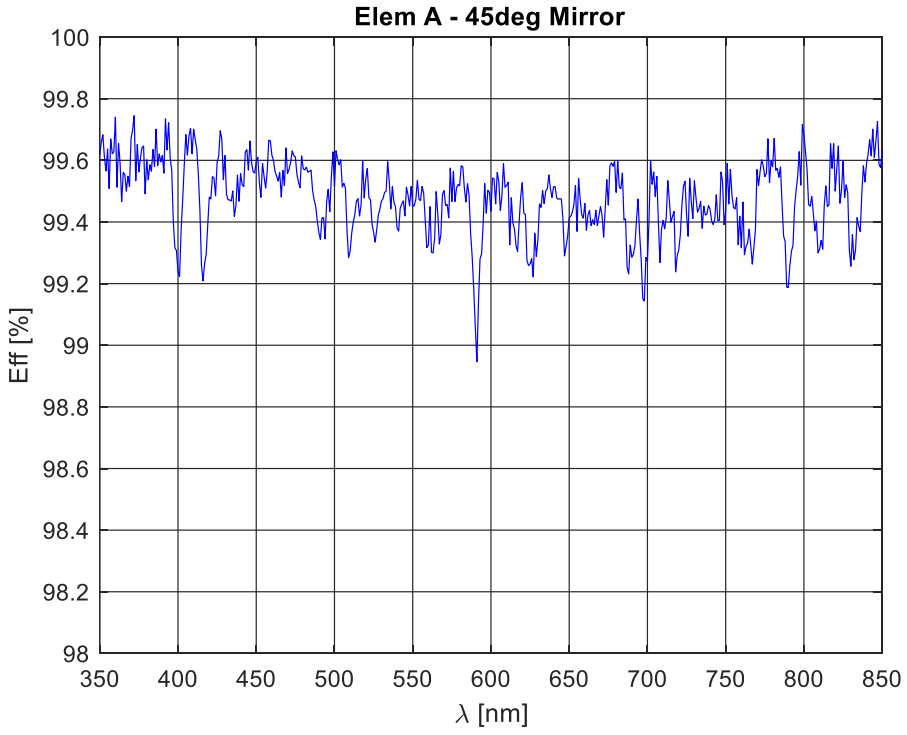

Figure 93. **UV-VIS Spectrograph element A reflectance extracted curve, used in the UV-VIS spectrograph overall efficiency.**

6.1.2 B, Collimating OAP

Measurement done by WinLight System, taken from Inspection Report.

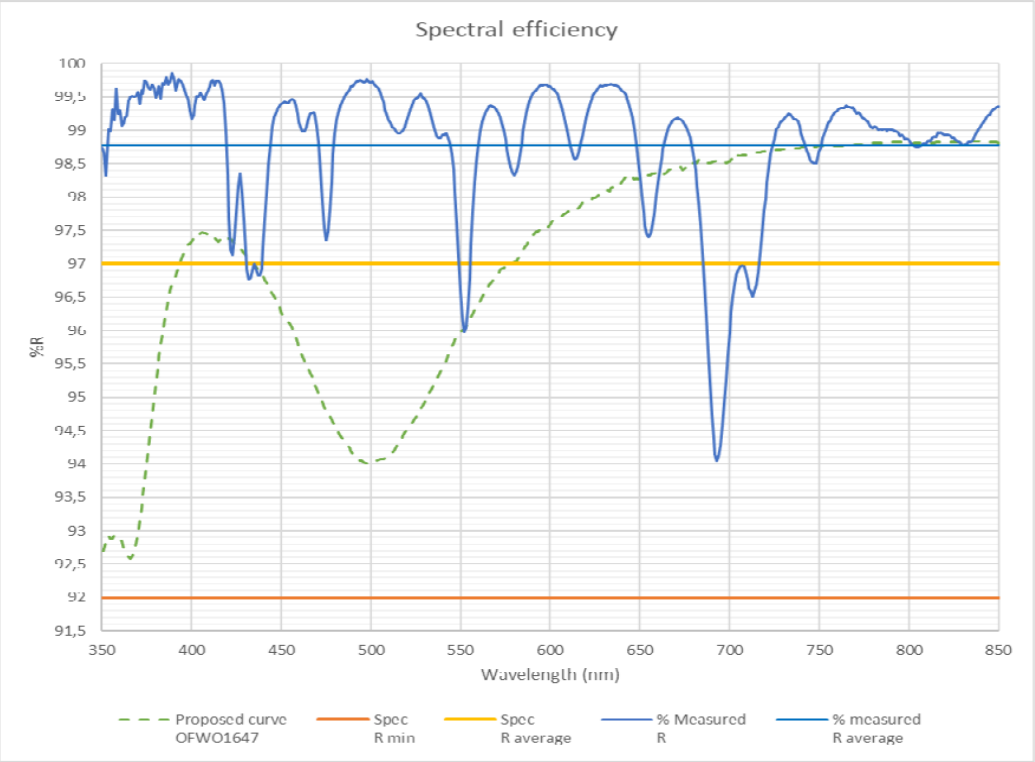

Figure 94. UV-VIS Spectrograph element B, off-axis parabola, reflectance data from producer (Winlight System) report.

Extracted data with MATLAB. This is the curve used in the global VIS Spectrograph efficiency.

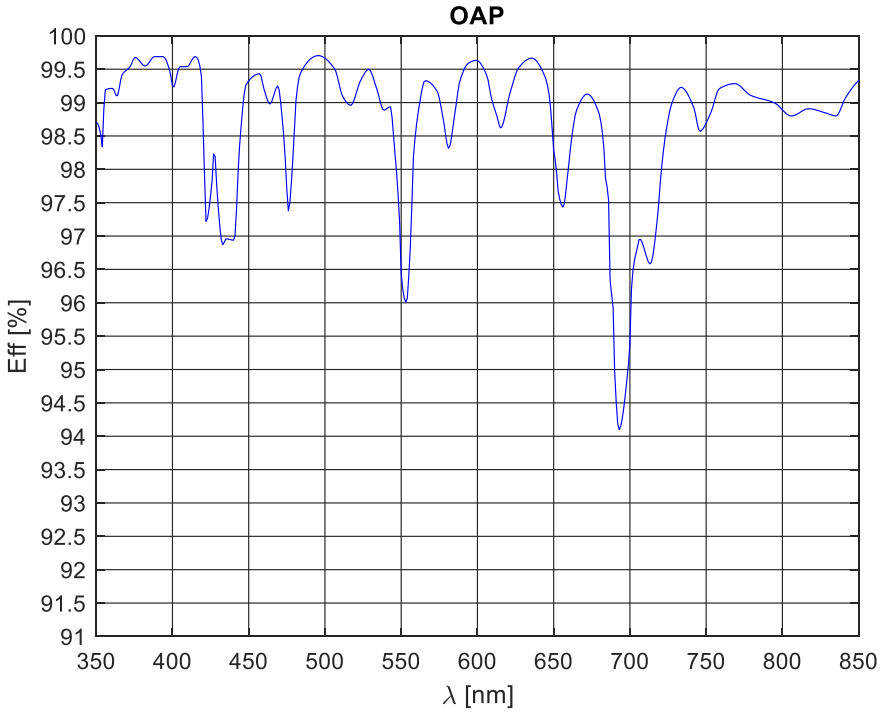

Figure 95. UV-VIS Spectrograph element B, off-axis parabola, reflectance data from producer (Winlight System) report. Extracted curve.

6.1.3 C, dichroic

This dichroic works in reflection for u and g bands, while in transmission for r and I bands.
REFLECTANCE (u, g bands). Zoomed view in the range of u,g bands.

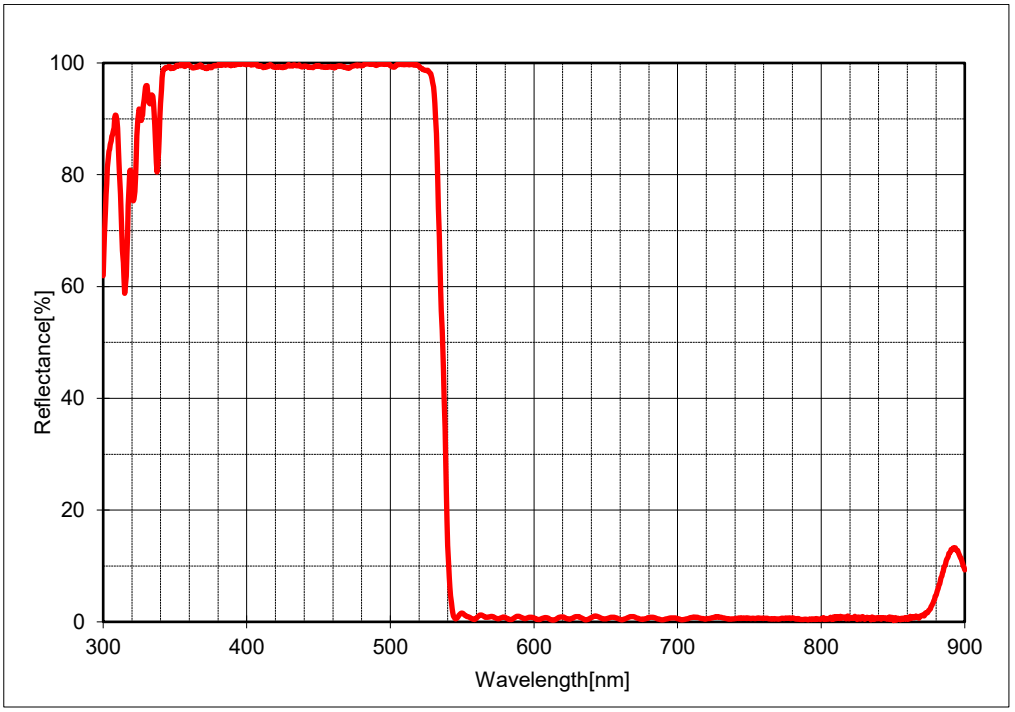

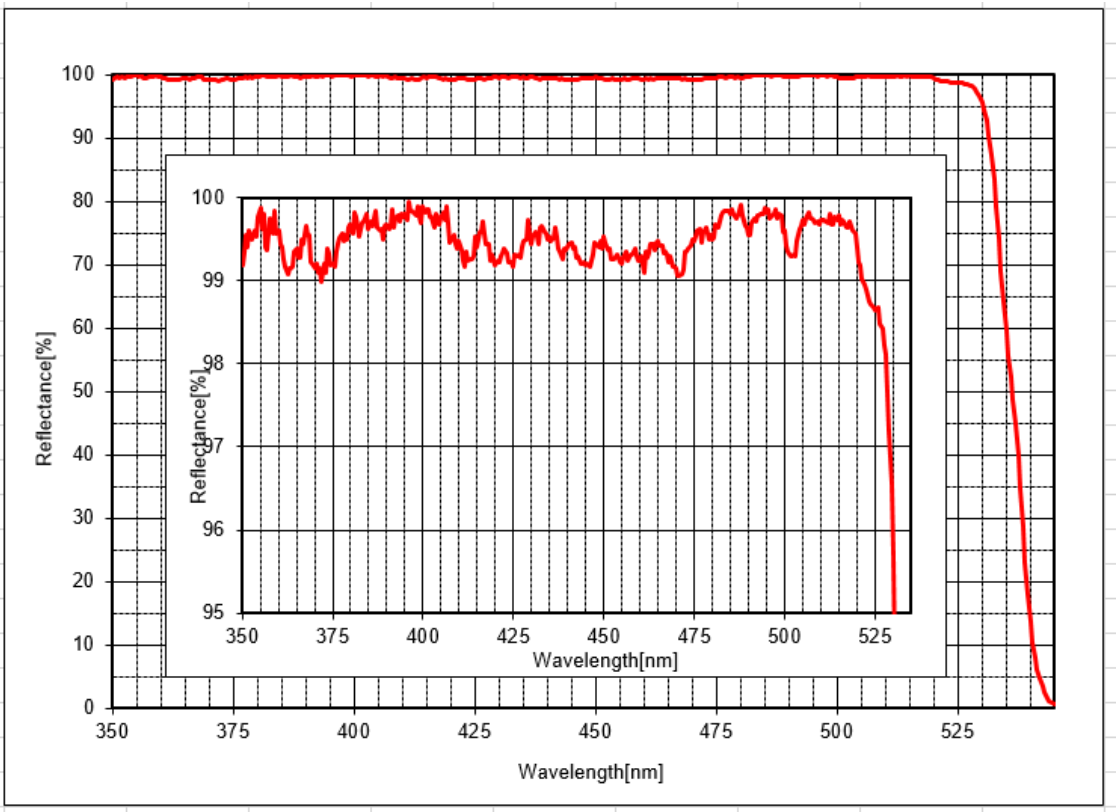

Figure 96. UV-VIS Spectrograph element C, Dichroic, reflectance curve (top panel) and zoomed view in the u,g bands (bottom panel).

Extracted data with MATLAB. This is the curve used in the global VIS Spectrograph (u, g) efficiency.

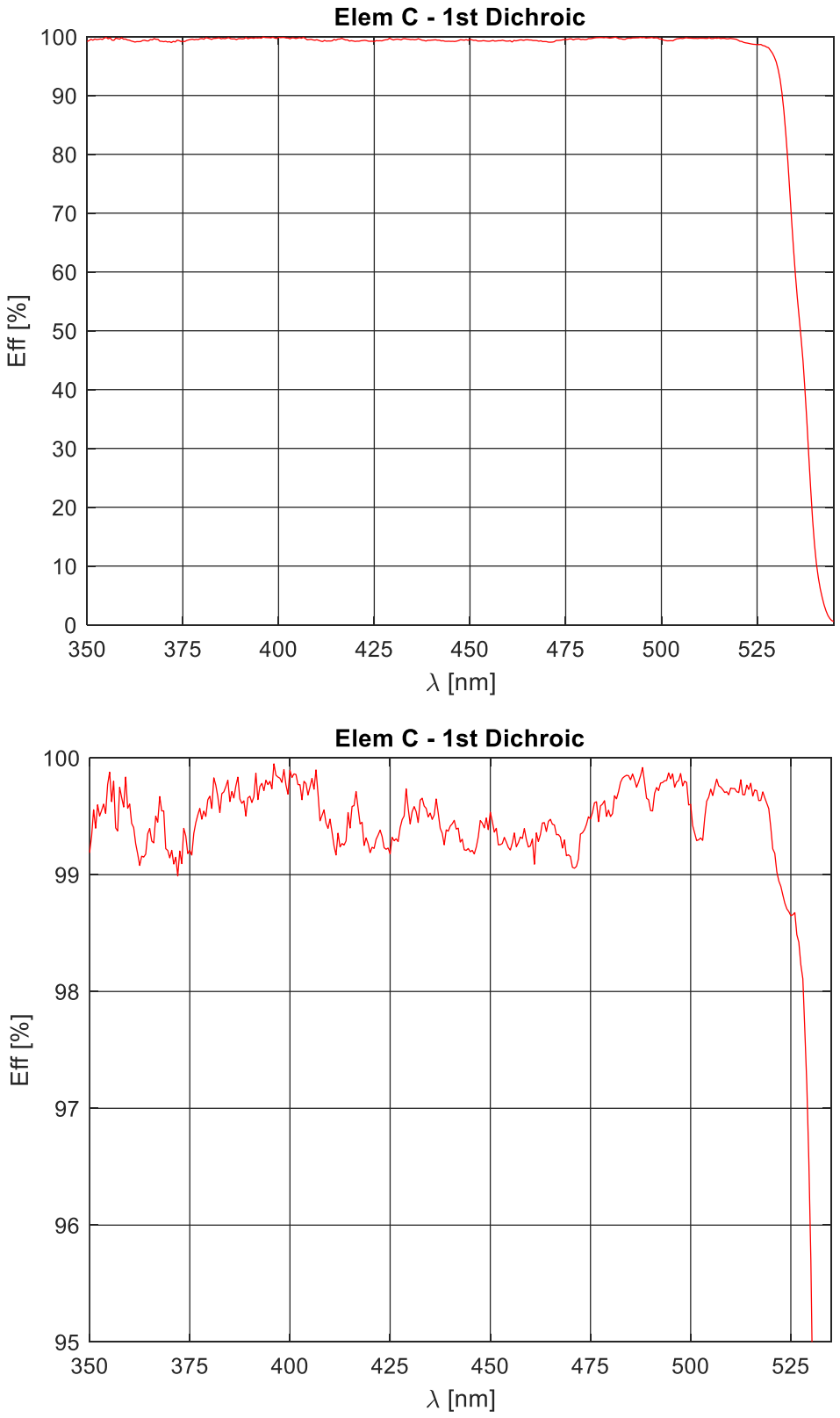

Figure 97. UV-VIS Spectrograph element C, Dichroic, reflectance curve (top panel) and zoomed view in the u,g bands (bottom panel). Extracted data used in the total VIS spectrograph efficiency computation.

TRANSMITTANCE (r, I bands). Below Zoomed view in the range of r, i bands.

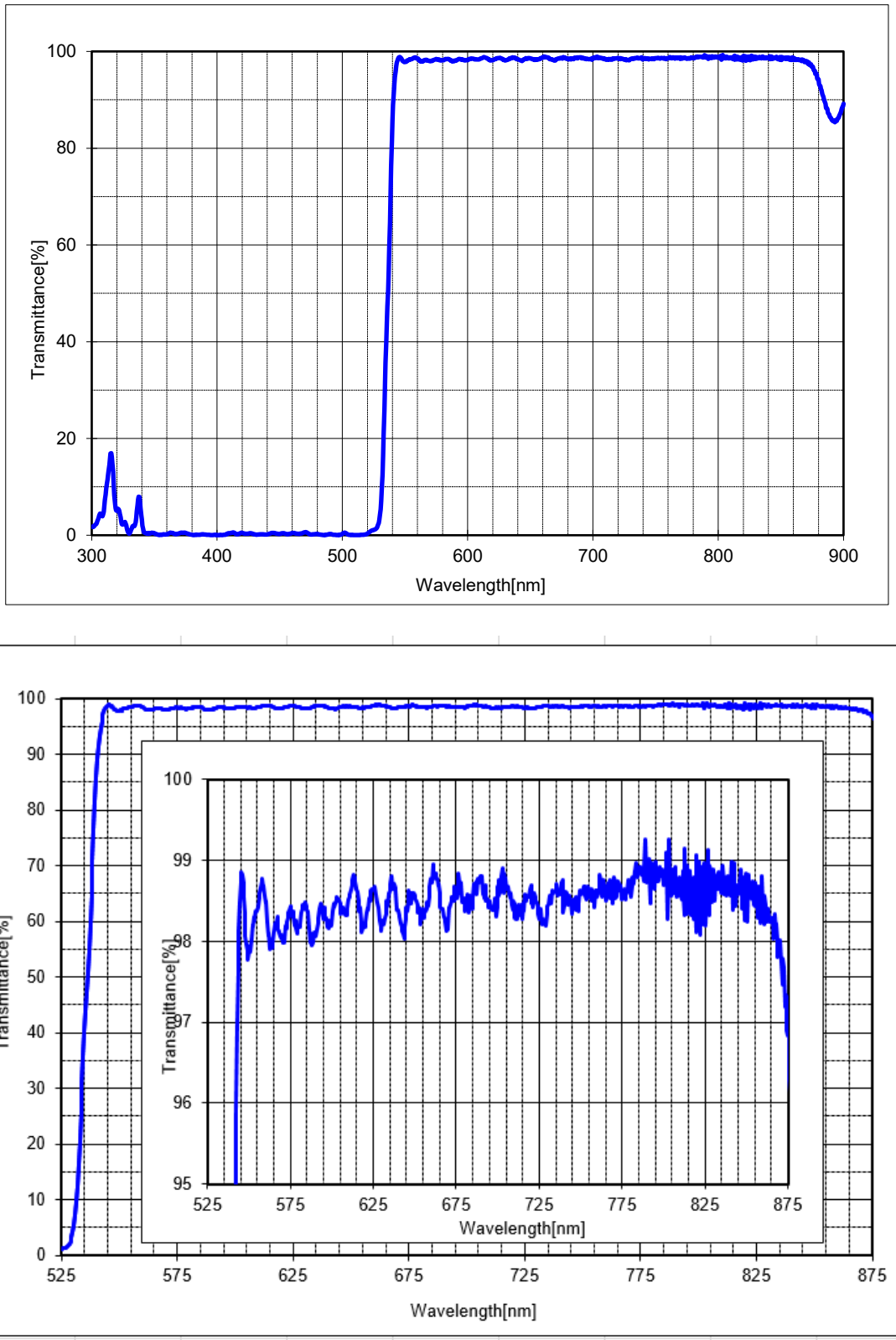

Figure 98. UV-VIS Spectrograph element C, Dichroic, transmission curve (top panel) and zoomed view in the r,i bands (bottom panel).

Extracted data with MATLAB. This is the curve used in the global VIS Spectrograph (r, i) efficiency.

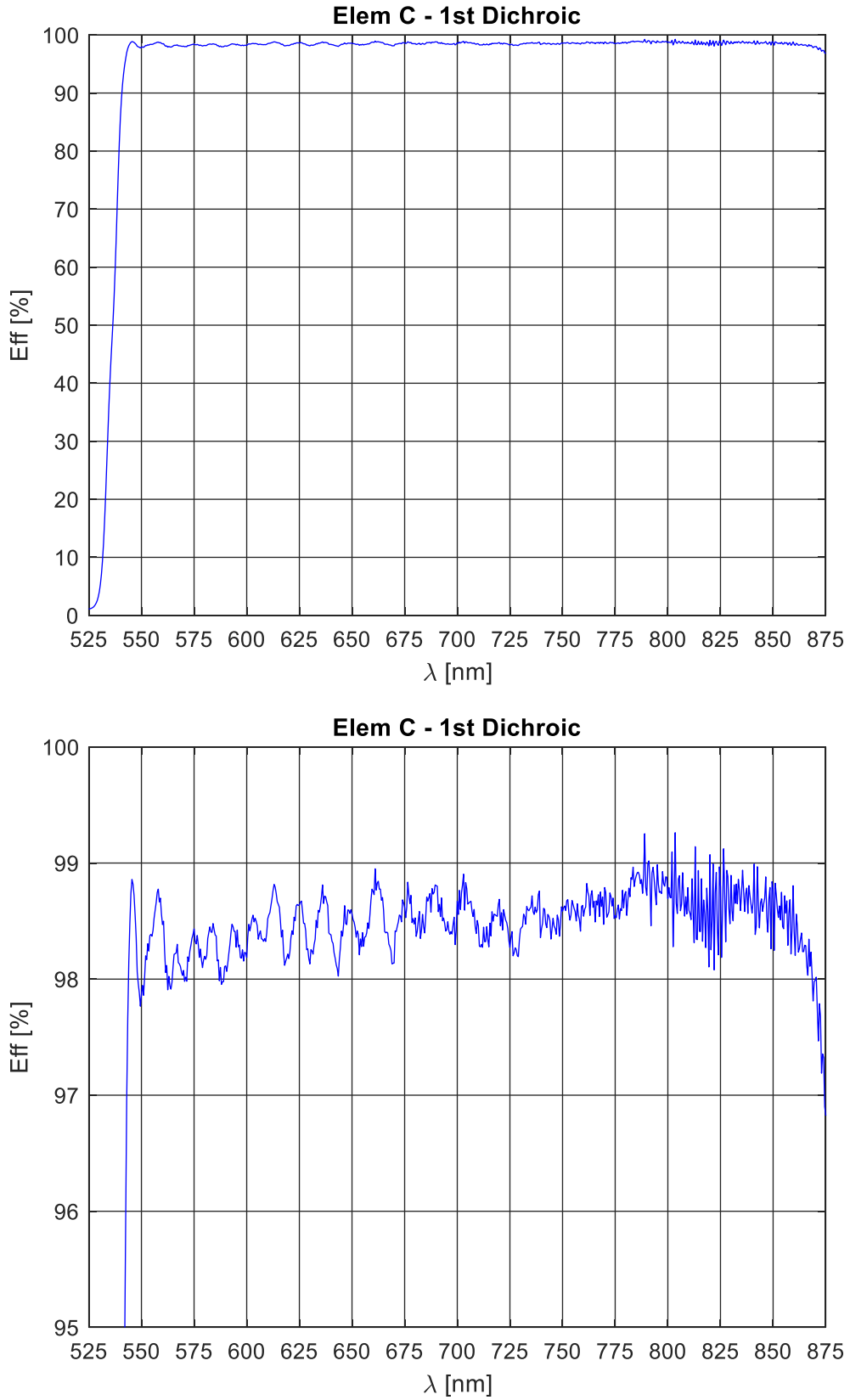

Figure 99. UV-VIS Spectrograph element C, Dichroic, transmission curve (top panel) and zoomed view (bottom panel). Extracted data used in the total VIS spectrograph efficiency computation.

6.1.4 D, dichroic – r-i bands

This dichroic works in reflection for r band, while in transmission for I band.

REFLECTANCE (r band).

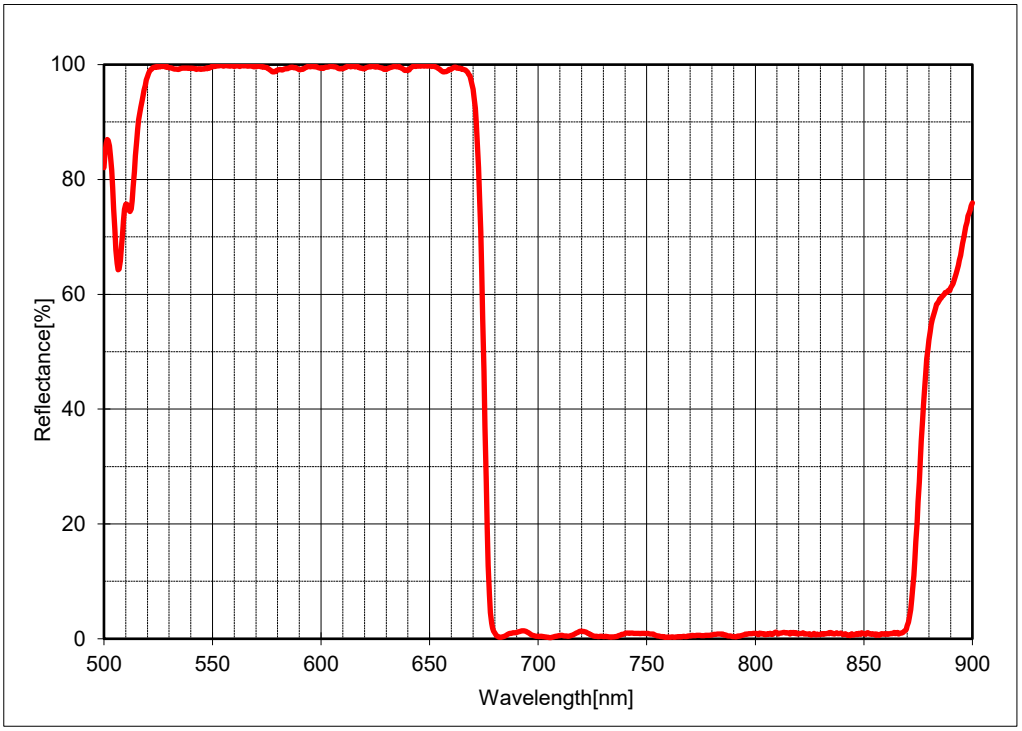

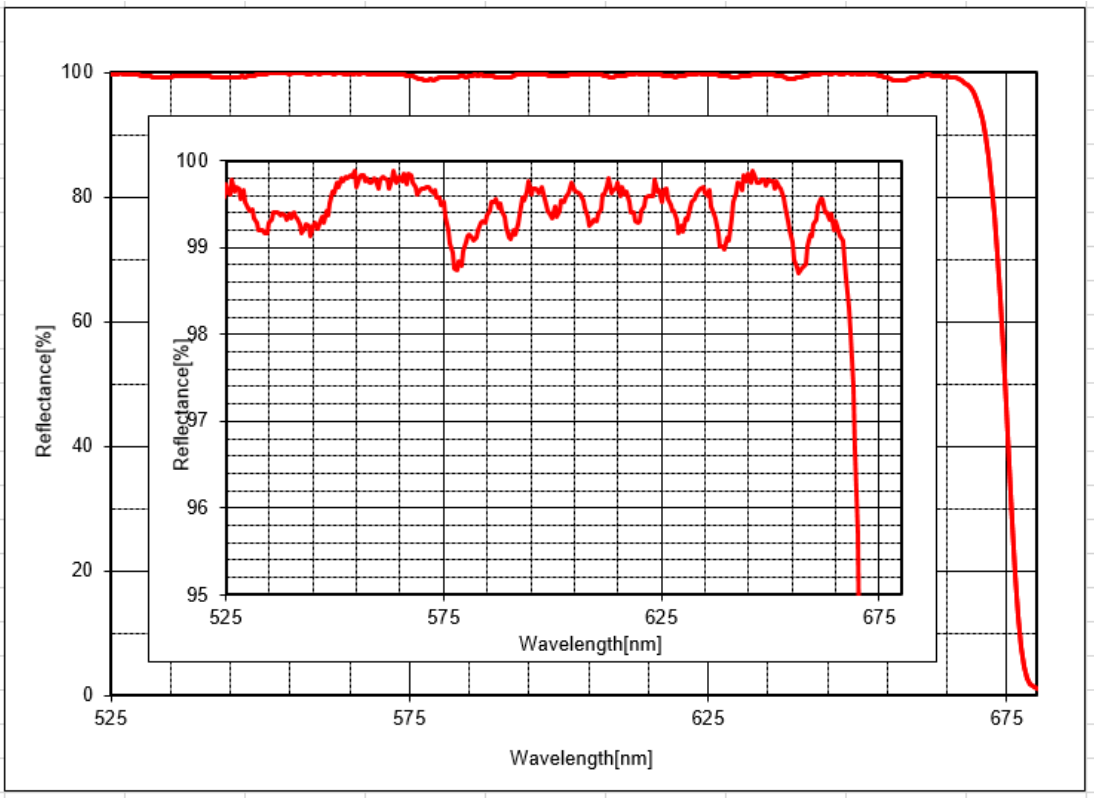

Figure 100. UV-VIS Spectrograph element D, Dichroic, reflectance curve (top panel) and zoomed view in the r band (bottom panel).

Extracted data with MATLAB. This is the curve used in the global VIS Spectrograph (r) efficiency.

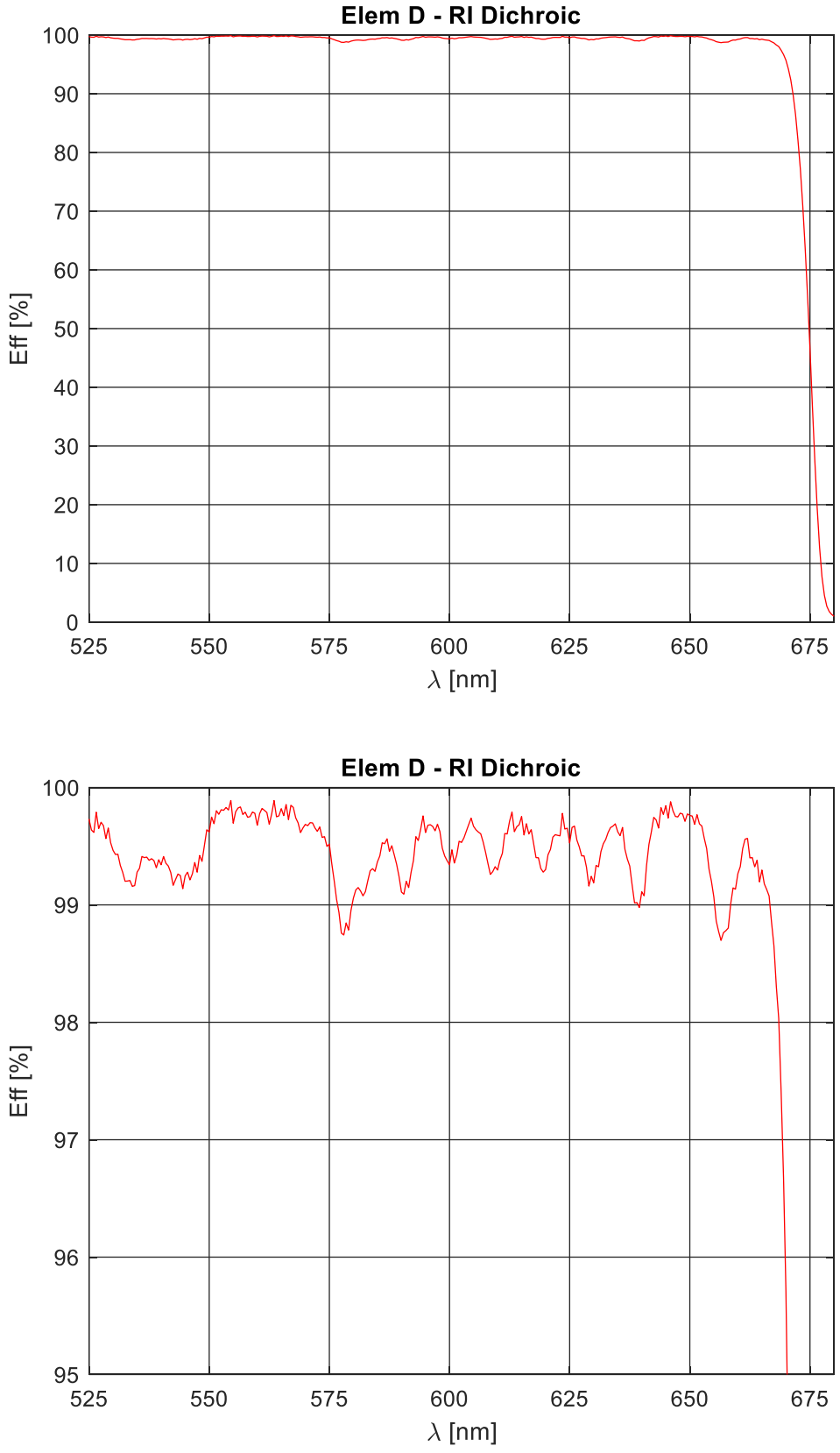

Figure 101. UV-VIS Spectrograph element D, Dichroic, reflectance curve (top panel) and zoomed view (bottom panel). Extracted data used in the total VIS spectrograph (r-band) efficiency computation.

TRANSMITTANCE (I band), and Zoomed view in the range of i band.

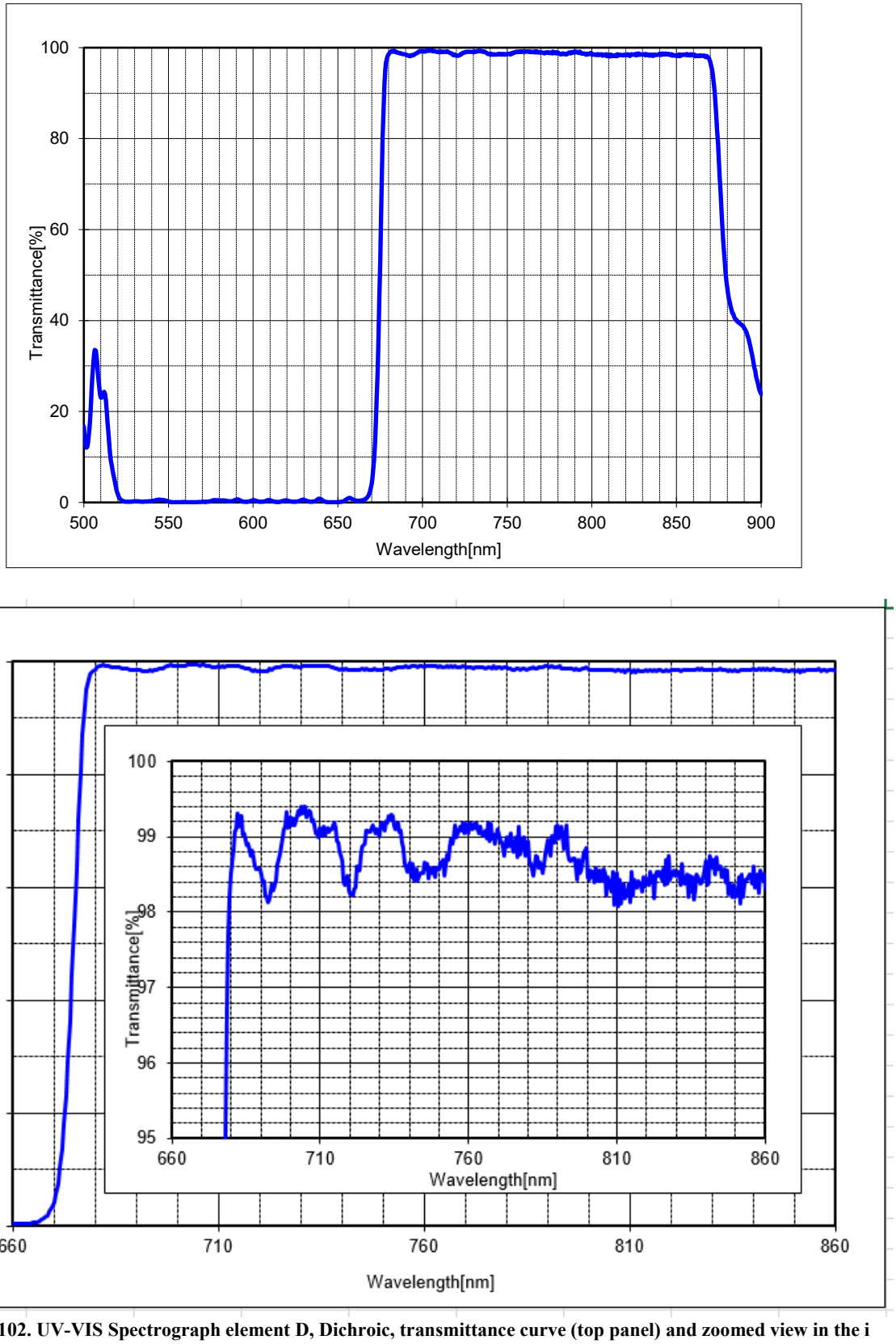

Figure 102. UV-VIS Spectrograph element D, Dichroic, transmittance curve (top panel) and zoomed view in the i band (bottom panel).

Extracted data with MATLAB. This is the curve used in the global VIS Spectrograph (i) efficiency.

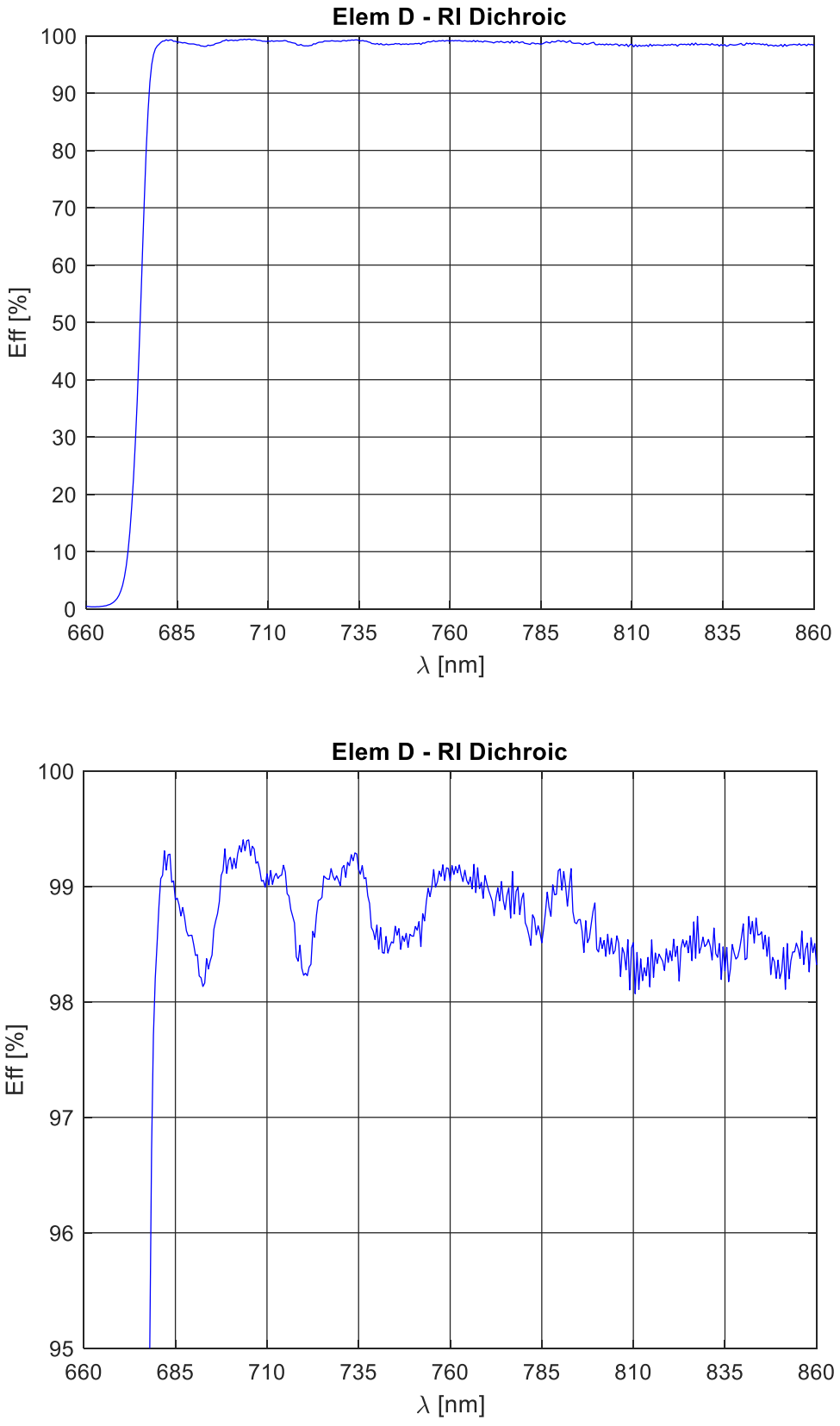

Figure 103. UV-VIS Spectrograph element D, Dichroic, transmission curve (top panel) and zoomed view (bottom panel). Extracted data used in the total VIS spectrograph (i-band) efficiency computation.

6.1.5 E, dielectric mirror i band

This mirror is present only for the I-band. Below, the rxtracted data with MATLAB. This is the curve used in the global VIS Spectrograph (i) efficiency.

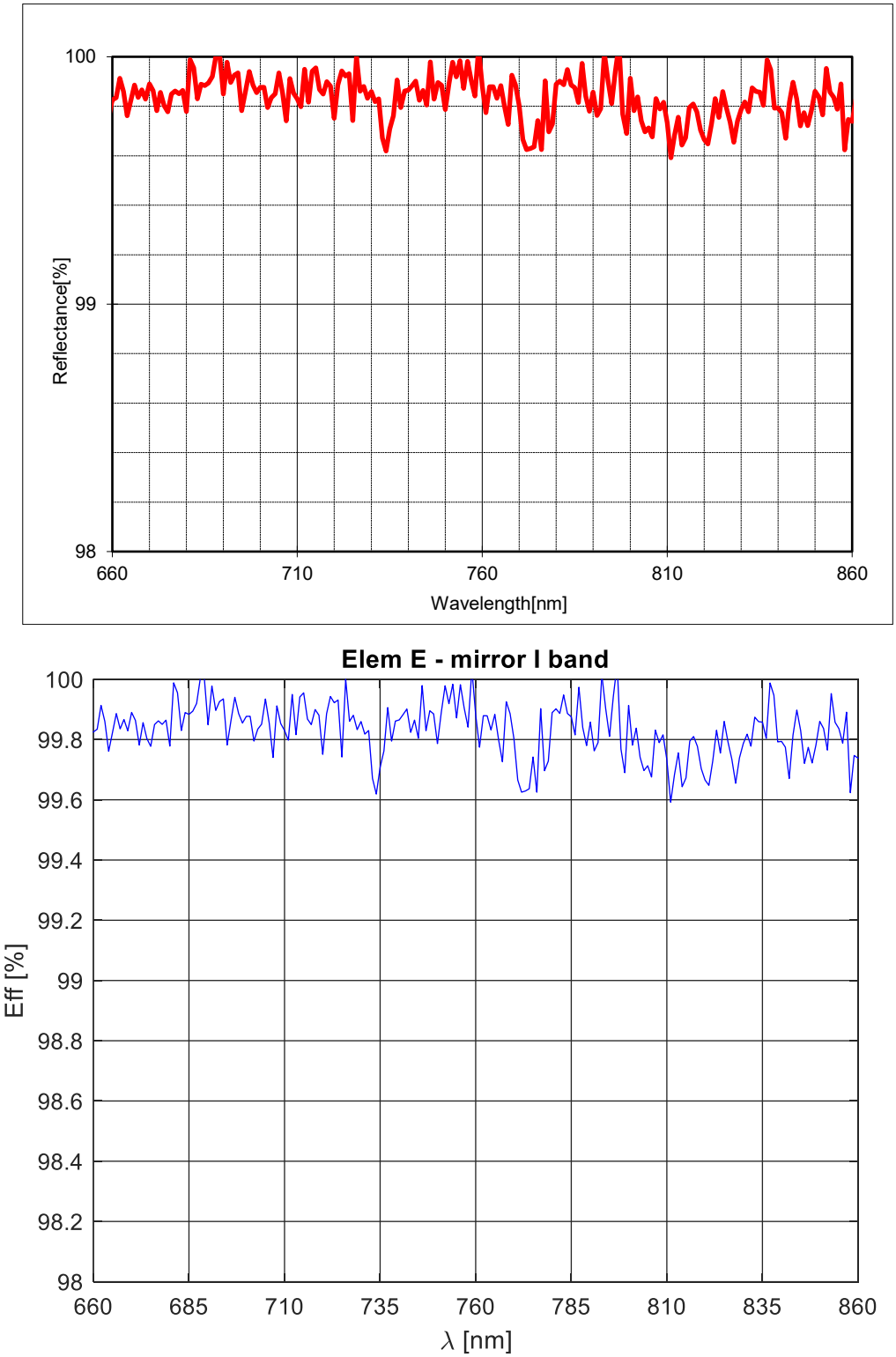

Figure 104. UV-VIS Spectrograph element E, dielectric mirror for I band. Top panel: data from measurement. Bottom panel: extracted curve used for the computation.

6.1.6 F, dielectric mirror u, g bands

This mirror is present only in both the u, g bands. Below, the extracted data with MATLAB. This is the curve used in the global VIS Spectrograph (u, g bands) efficiency.

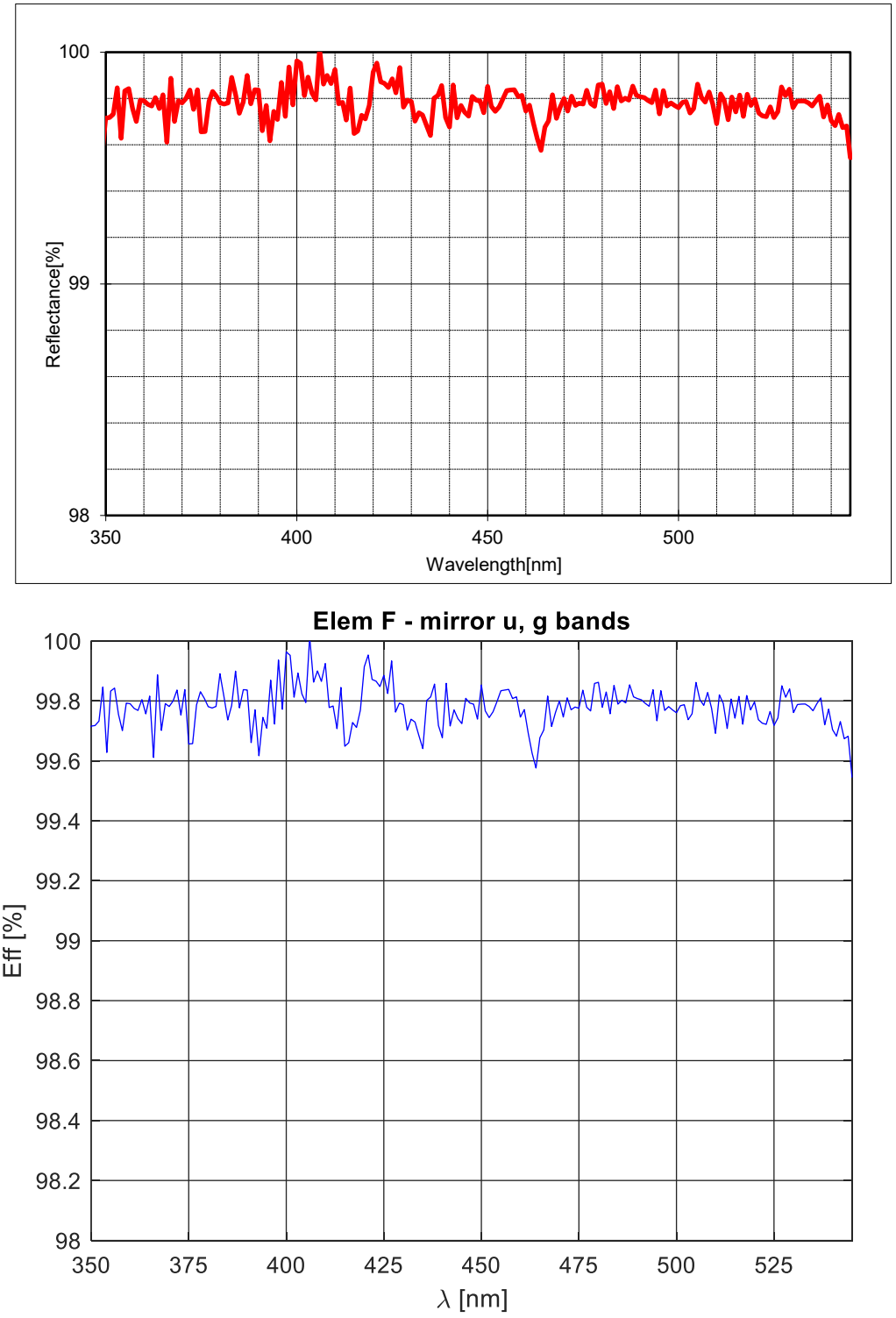

Figure 105. UV-VIS Spectrograph element F, dielectric mirror for u-g bands. Top panel: data from measurement. Bottom panel: extracted curve used for the computation.

6.1.7 G (lot-A), dichroic – u-g bands

This dichroic works in reflection for u band, while in transmission for g band. Excel file available on owncloud.

REFLECTANCE (u band)

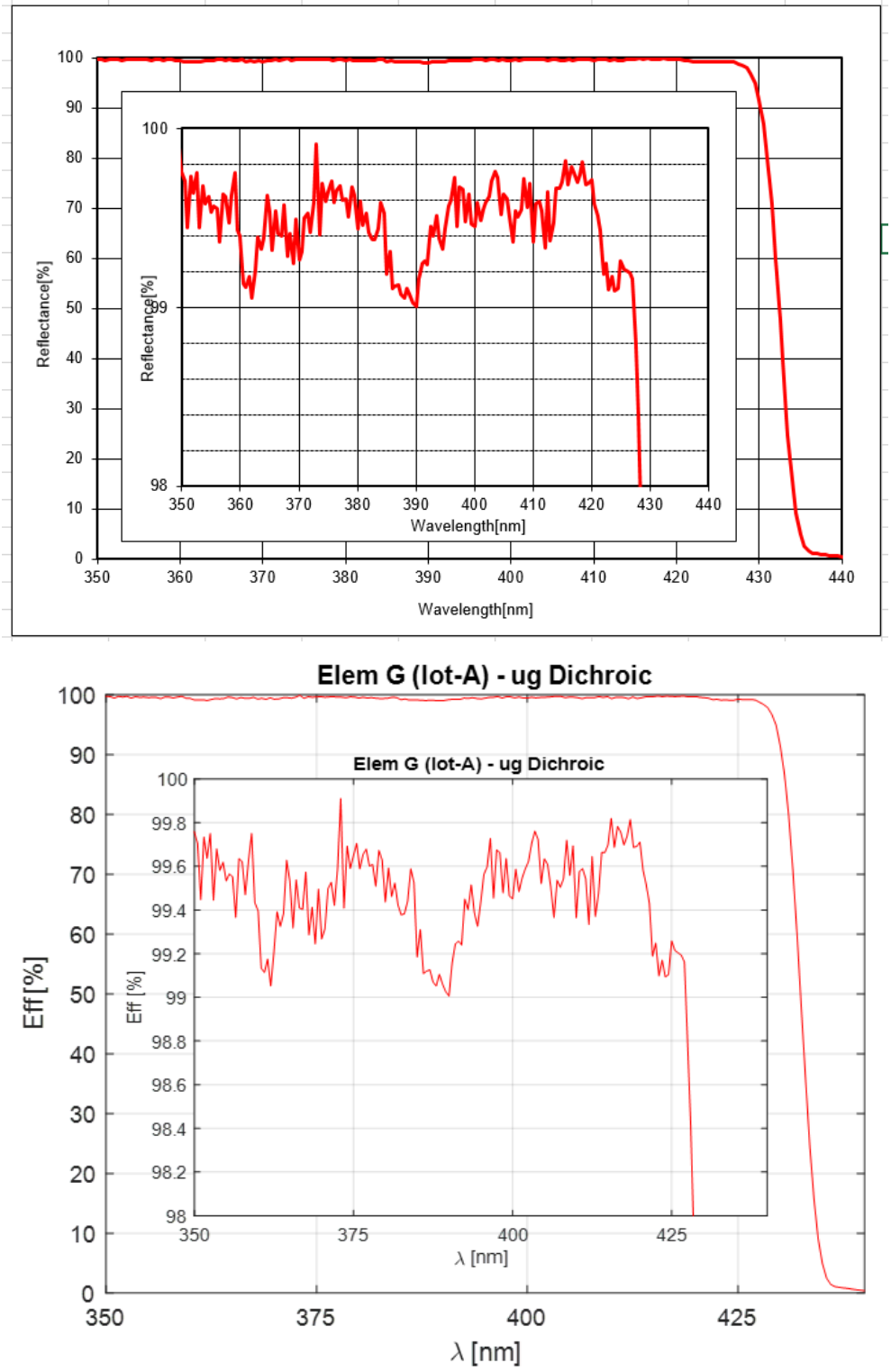

Figure 106. UV-VIS Spectrograph element G, dichroic for u-g bands, working in reflection for u-band. Top panel: data from measurement. Bottom panel: extracted curve used for the computation.

TRANSMITTANCE *(g band)*

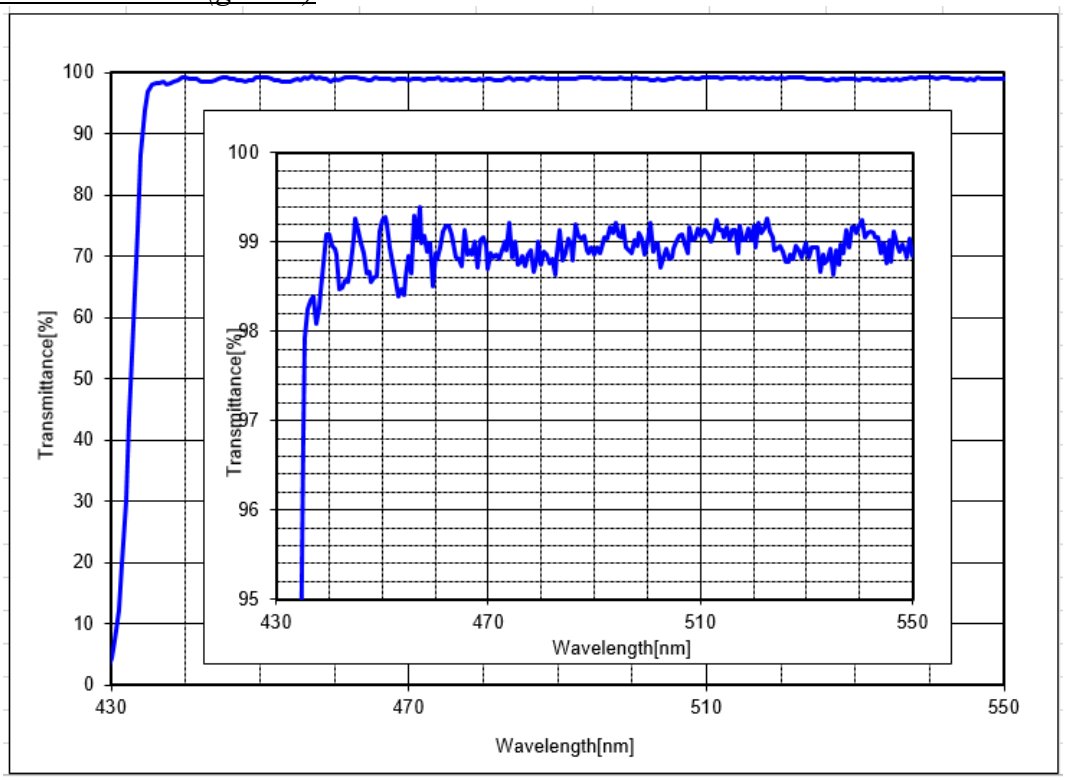

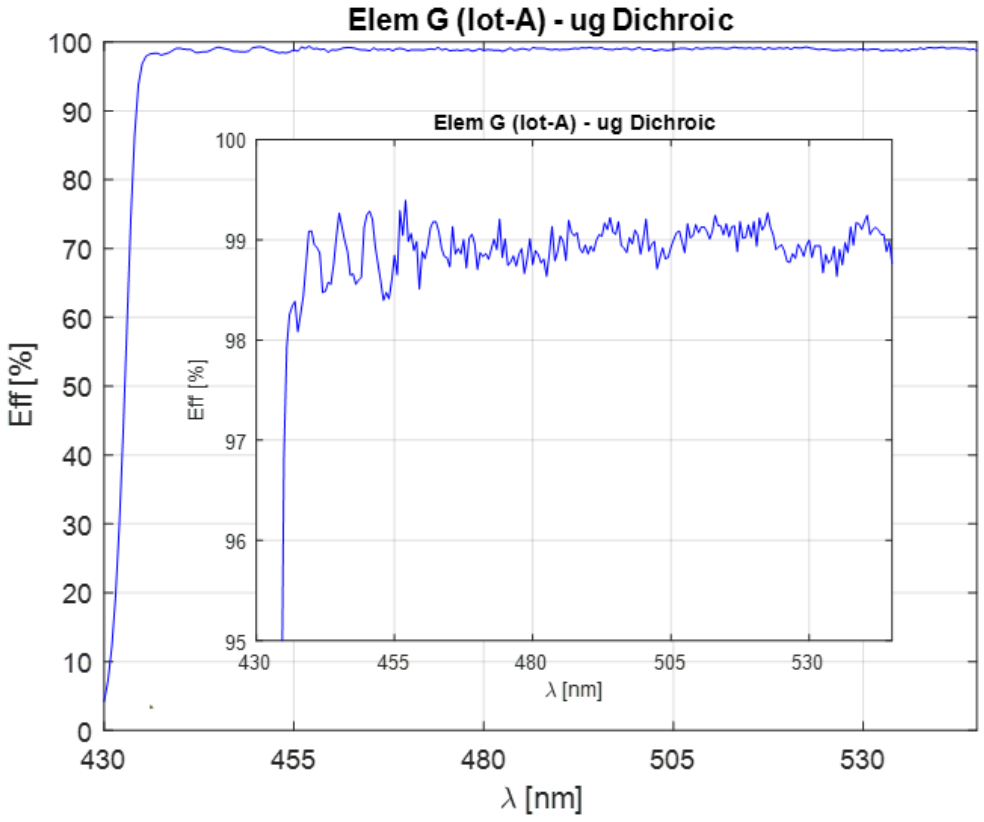

Figure 107. UV-VIS Spectrograph element G, dichroic for u-g bands, working in transmission for g-band. Top panel: data from measurement. Bottom panel: extracted curve used for the computation.

6.1.8 H, dielectric mirror g band

This mirror is present only for the g-band. Below, the extracted data with MATLAB. This is the curve used in the global VIS Spectrograph (g band) efficiency.

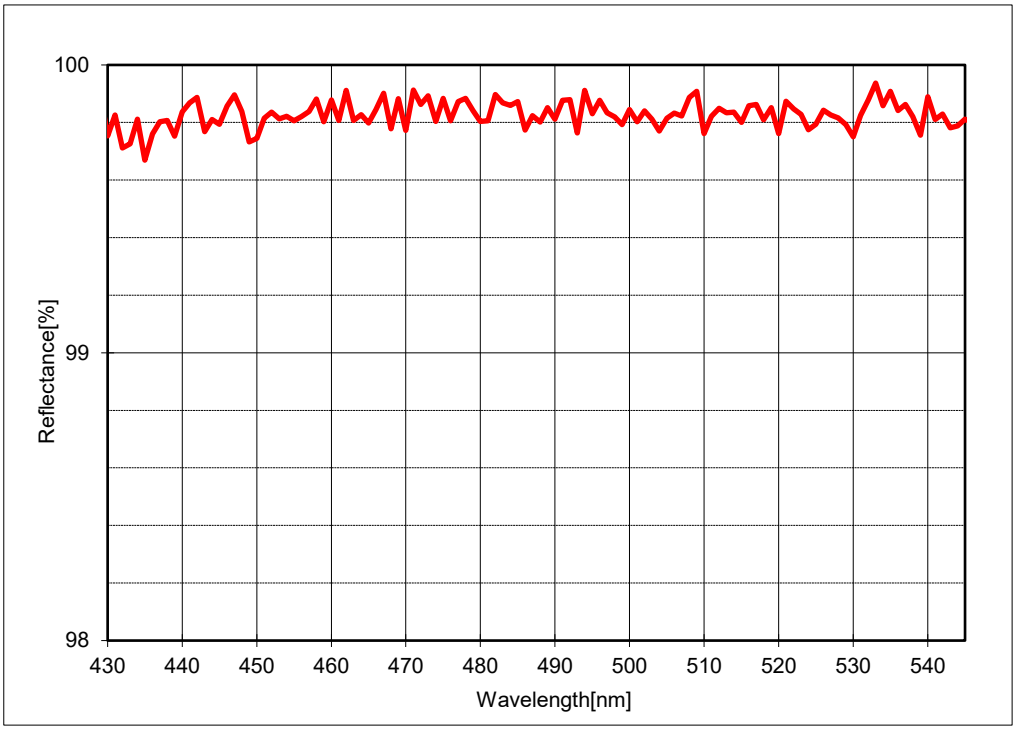

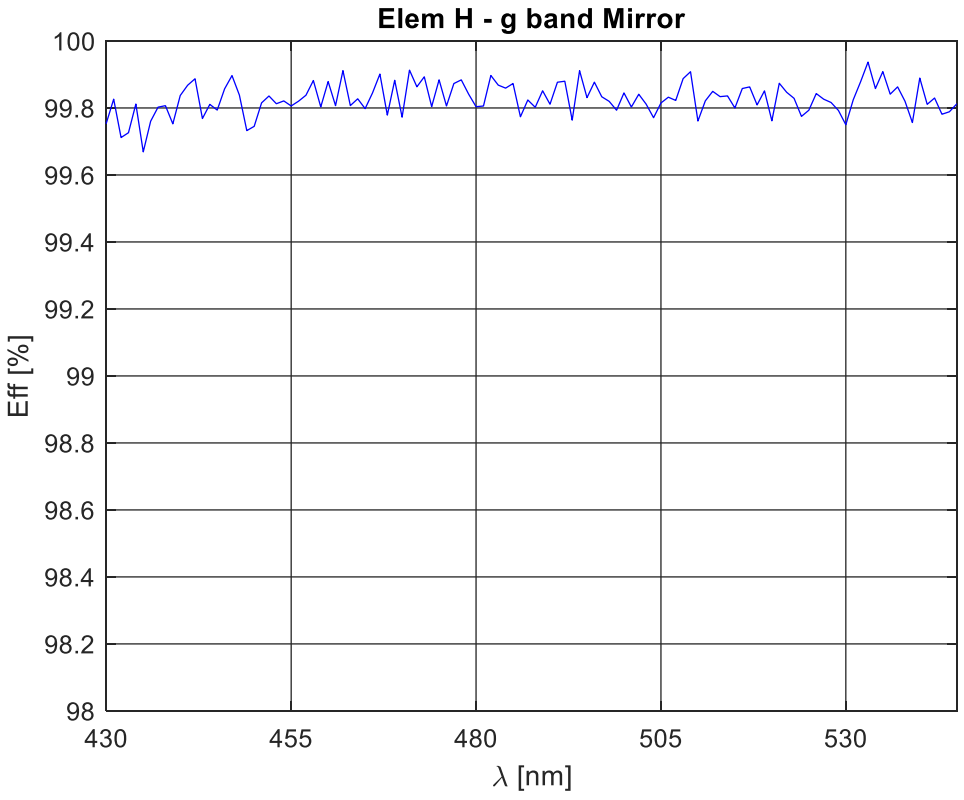

Figure 108. UV-VIS Spectrograph element H, dielectric mirror for g-band. Top panel: data from measurement. Bottom panel: extracted curve used for the computation.

6.1.9 VIS GRATINGS

6.1.9.1 u-band

Plot of design efficiency and measure data-points from IOF report. Extracted data with MATLAB. This is the curve used in the global VIS Spectrograph (u band) efficiency.

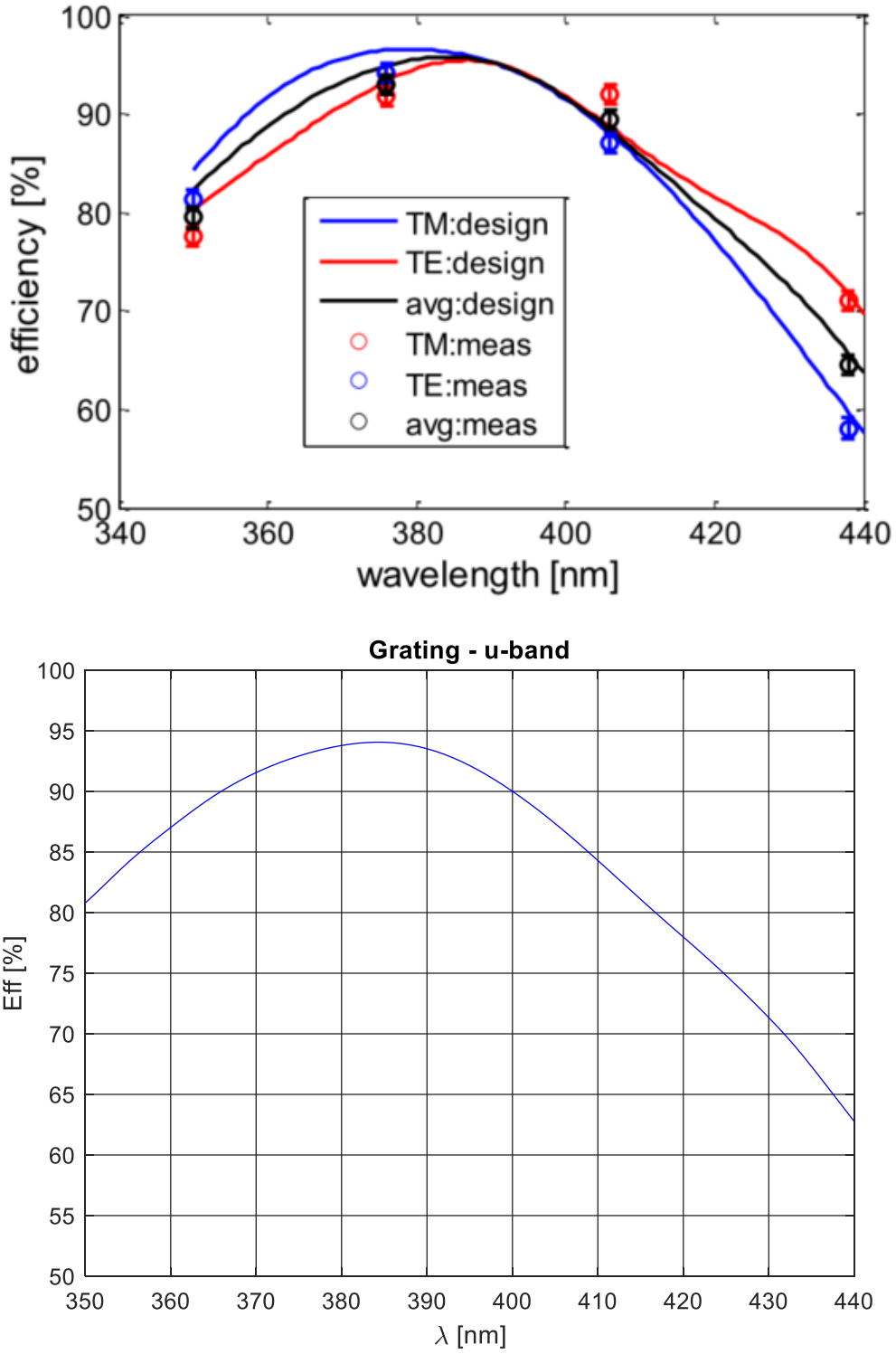

Figure 109. UV-VIS Spectrograph, u-band grating efficiency. Top panel: data from measurement. Bottom panel: extracted curve used for the computation.

6.1.9.2 g-band

Plot of design efficiency, the curve is rescaled for measure data points from IOF report. Extracted data with MATLAB. This is the curve used in the global VIS Spectrograph (g band) efficiency.

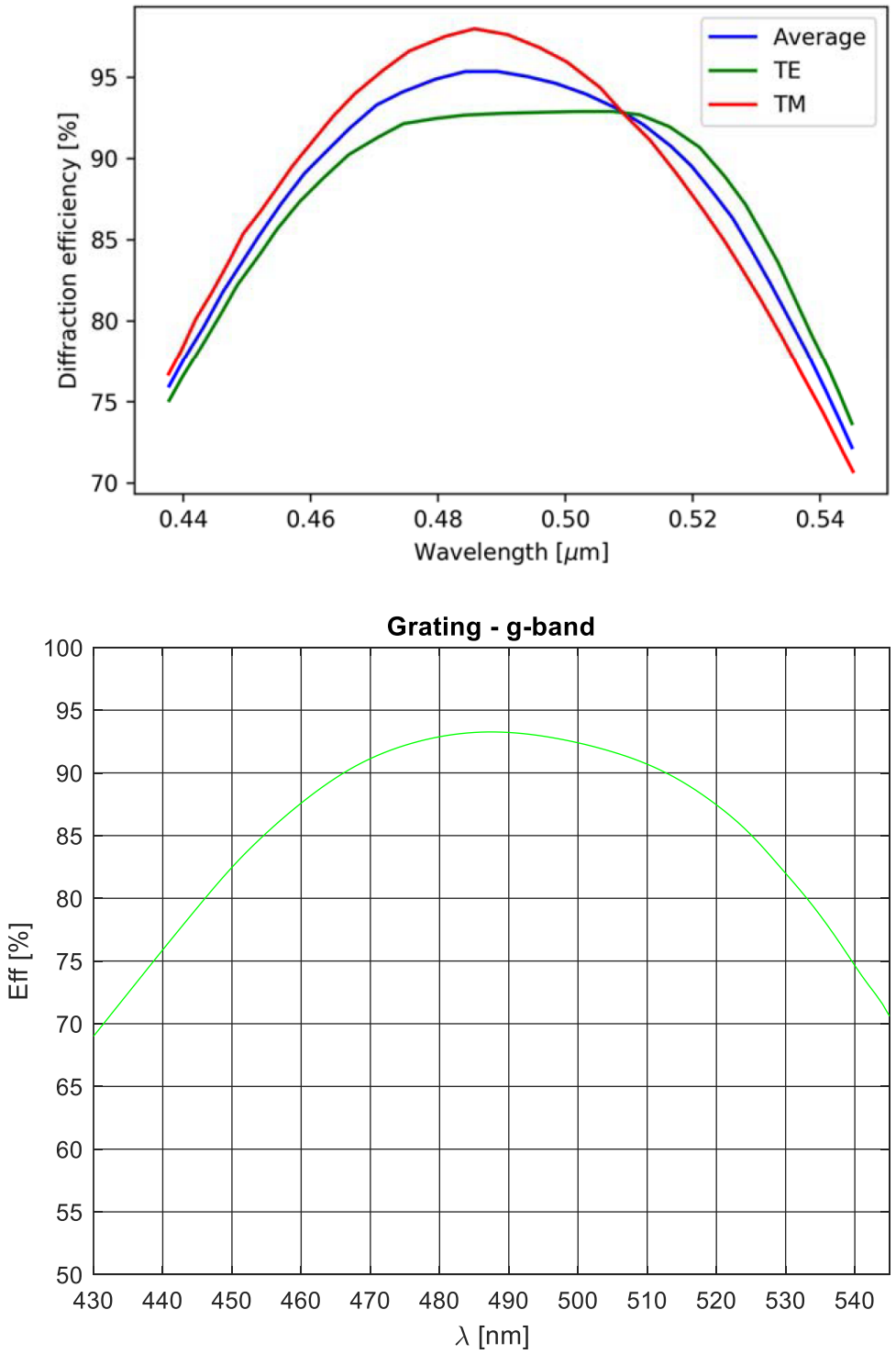

Figure 110. UV-VIS Spectrograph, g-band grating efficiency. Top panel: data from measurement. Bottom panel: extracted curve used for the computation.

6.1.9.3 r-band

Plot of design efficiency and measure data-points from IOF report. Extracted data with MATLAB. This is the curve used in the global VIS Spectrograph (r band) efficiency.

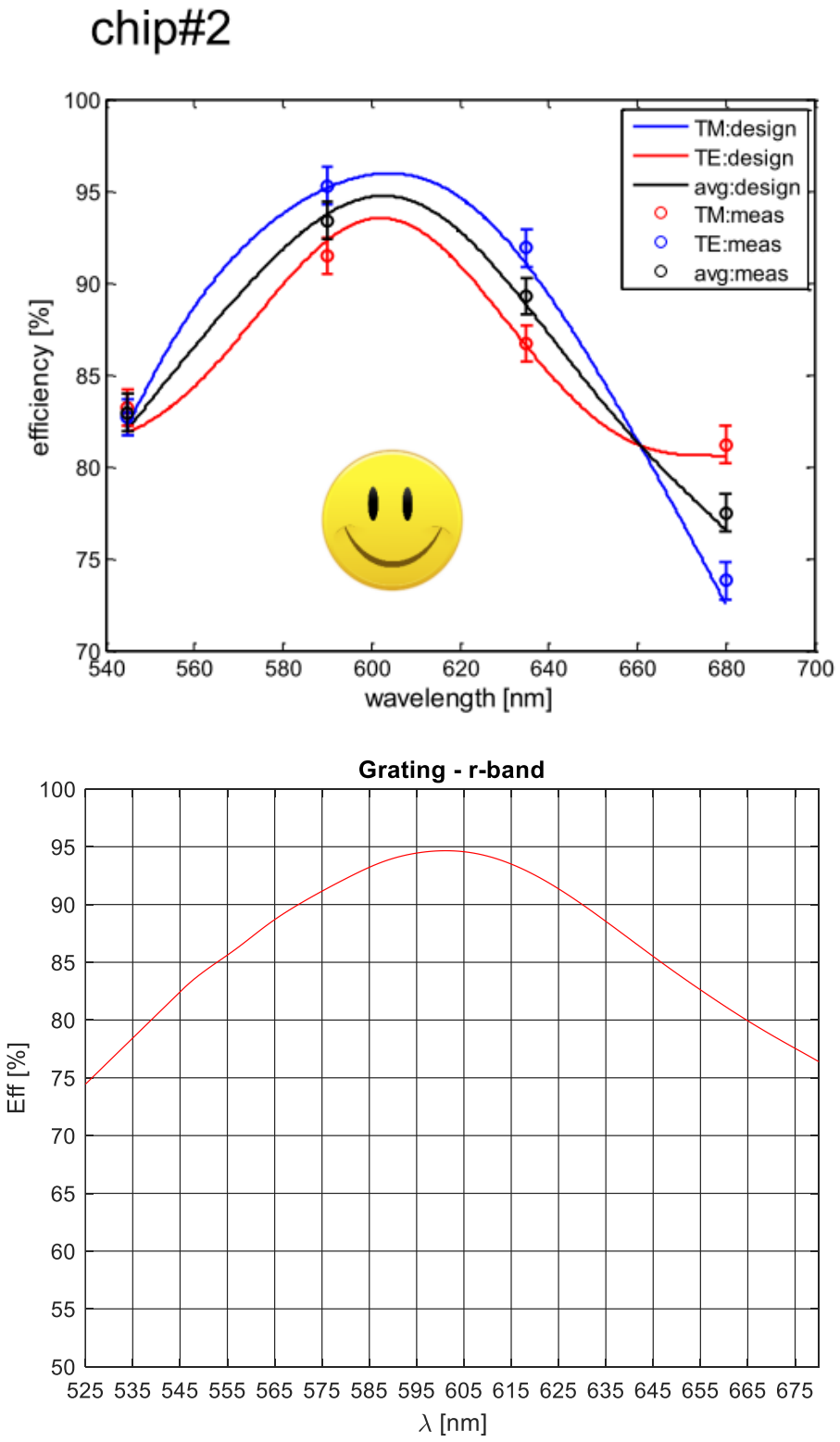

Figure 111. UV-VIS Spectrograph, r-band grating efficiency. Top panel: data from measurement. Bottom panel: extracted curve used for the computation.

6.1.9.4 i-band

Plot of design efficiency and measure data-points from IOF report. Extracted data with MATLAB. This is the curve used in the global VIS Spectrograph (i band) efficiency.

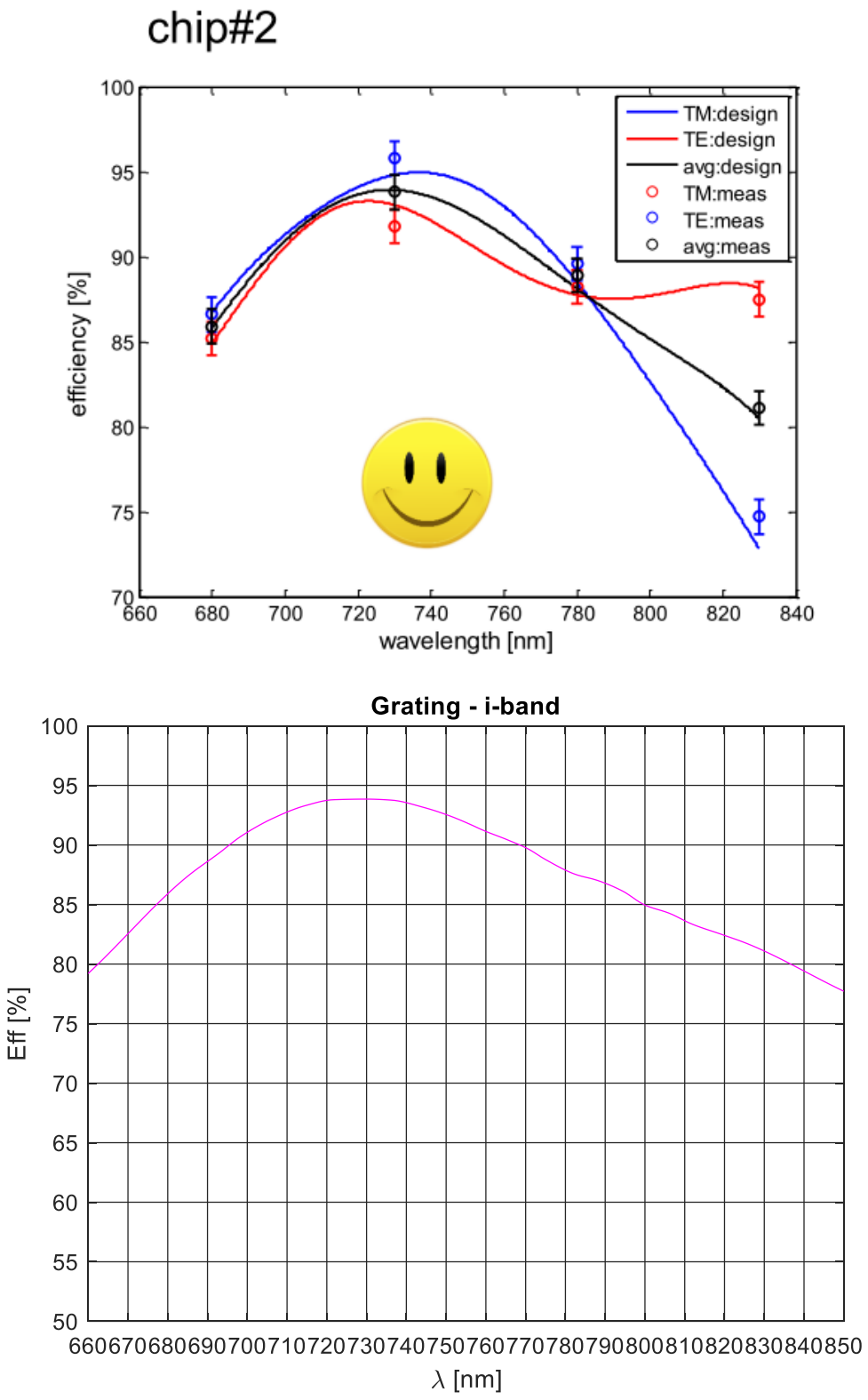

Figure 112. UV-VIS Spectrograph, i-band grating efficiency. Top panel: data from measurement. Bottom panel: extracted curve used for the computation.

6.1.10 Camera

The camera transmission is computed from the model of the reflection and refraction surfaces provided.

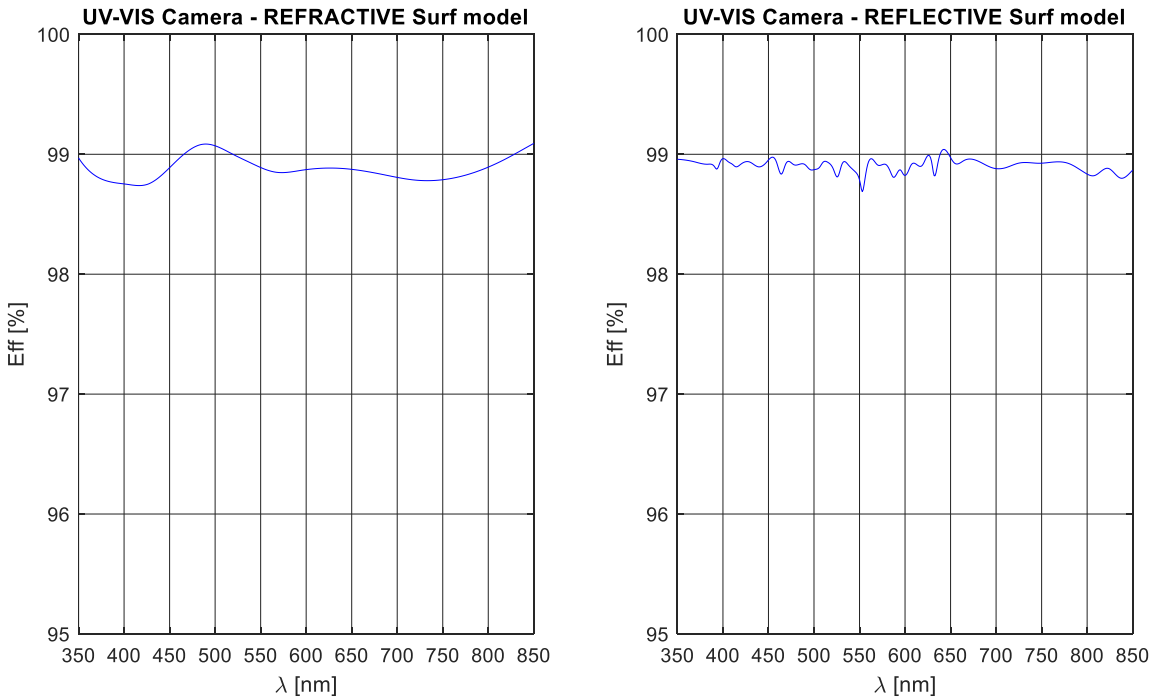

Figure 113. UV-VIS arm camera. Refractive and reflective model for optical element surfaces.

The camera design foresees 2 elements in transmission and 1 in reflection. Thus the total camera efficiency is computed by considering 4 refractions and 1 reflection.

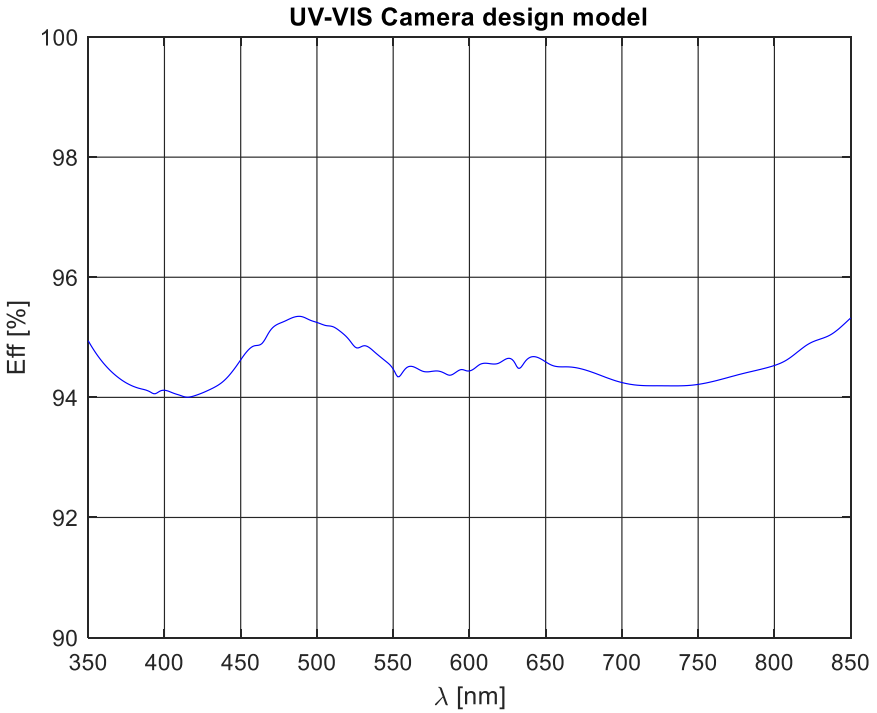

Figure 114. UV-VIS arm camera total efficiency.

6.1.11 UV-VIS Spectrograph efficiency

6.1.11.1 u-band

The u-band spectrograph efficiency (so, no telescope, no CP, no CCD-QE) is computed by multiplying the data of the following elements:

- A, Fold mirror
- B, collimating OAP
- C, dichroic in reflection
- F,mirror
- G, dichroic in reflection
- u-band transmission grating
- Camera

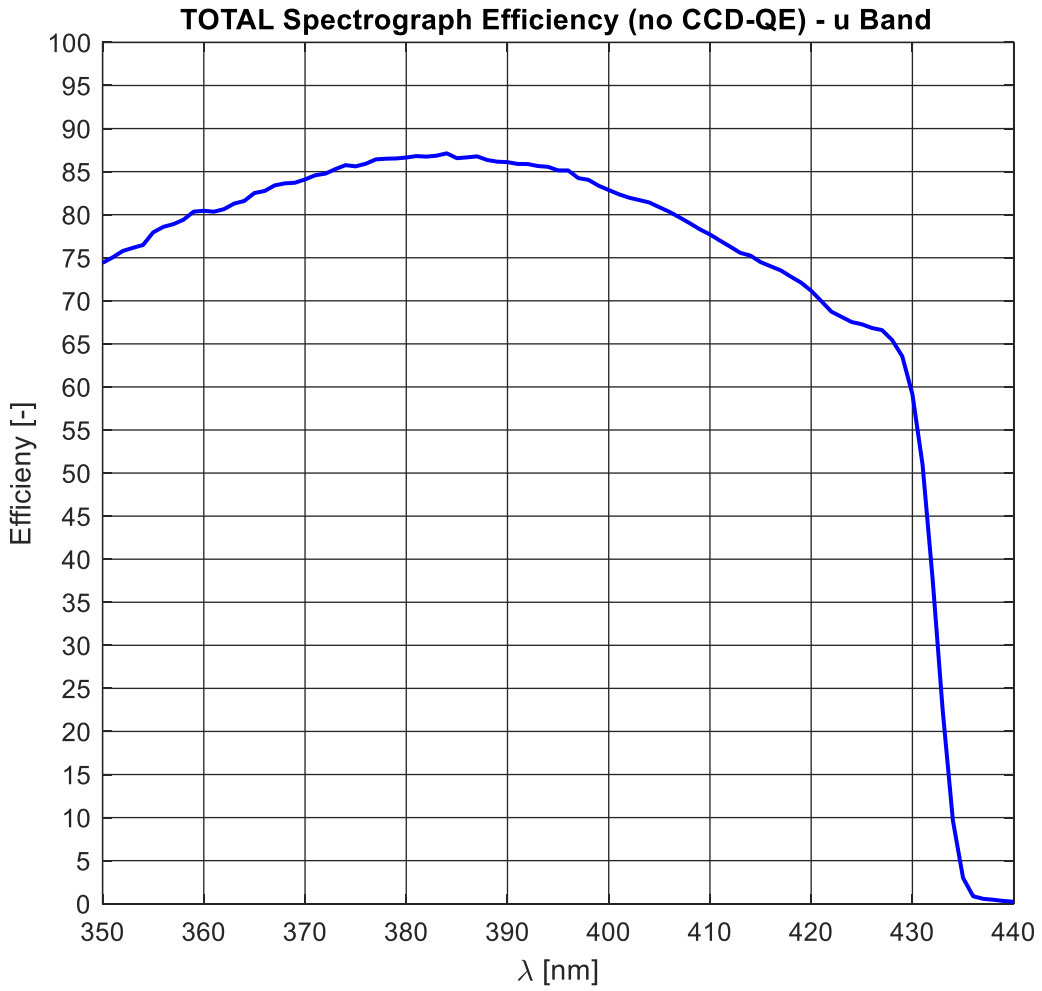

Figure 115. UV-VIS u-band total efficiency. No CCD-QE included.

6.1.11.2 g-band

The g-band spectrograph efficiency (so, no telescope, no CP, no CCD-QE) is computed by multiplying the data of the following elements:

- A, Fold mirror
- B, collimating OAP
- C, dichroic in reflection
- F,mirror
- G, dichroic in transmission
- g-band transmission grating
- Camera

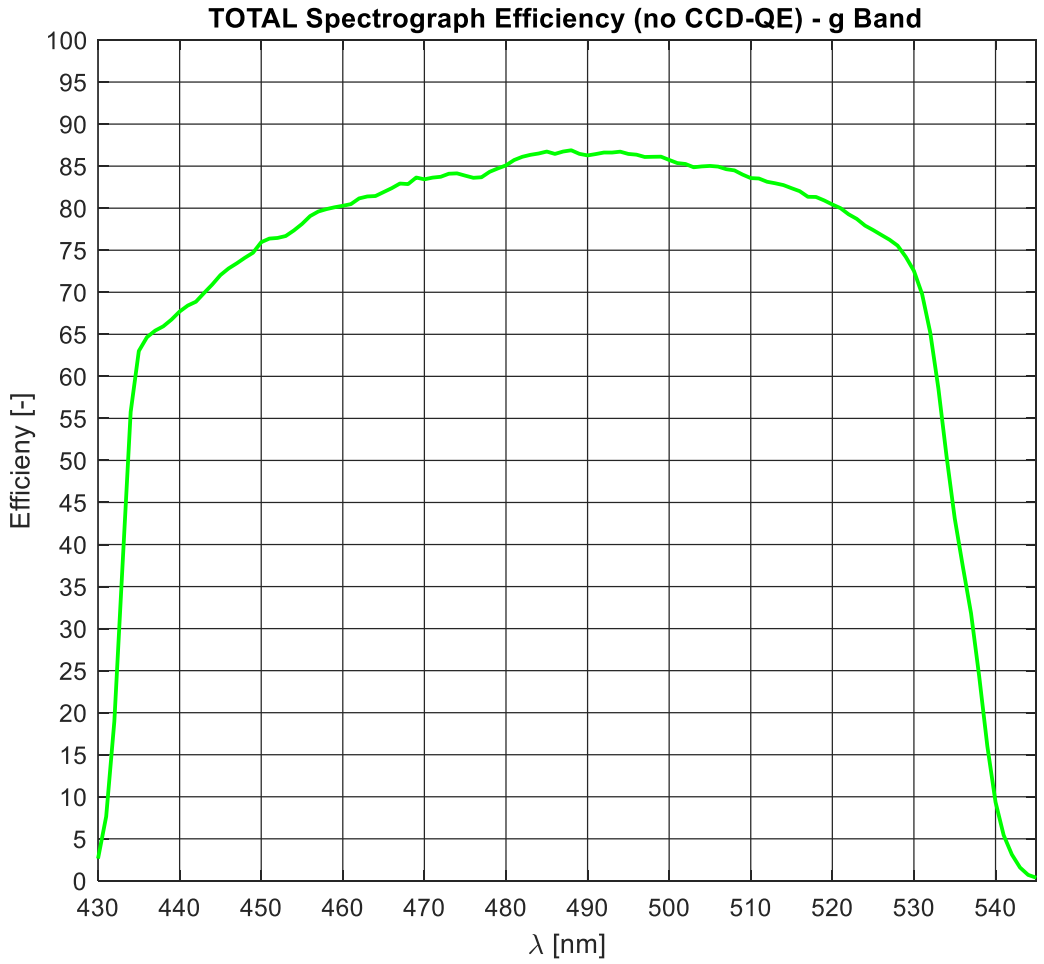

Figure 116. UV-VIS g-band total efficiency. No CCD-QE included.

6.1.11.3 r-band

The r-band spectrograph efficiency (so, no telescope, no CP, no CCD-QE) is computed by multiplying the data of the following elements:

- A, Fold mirror
- B, collimating OAP
- C, dichroic in transmission
- D, dichroic in reflection
- r-band transmission grating
- Camera

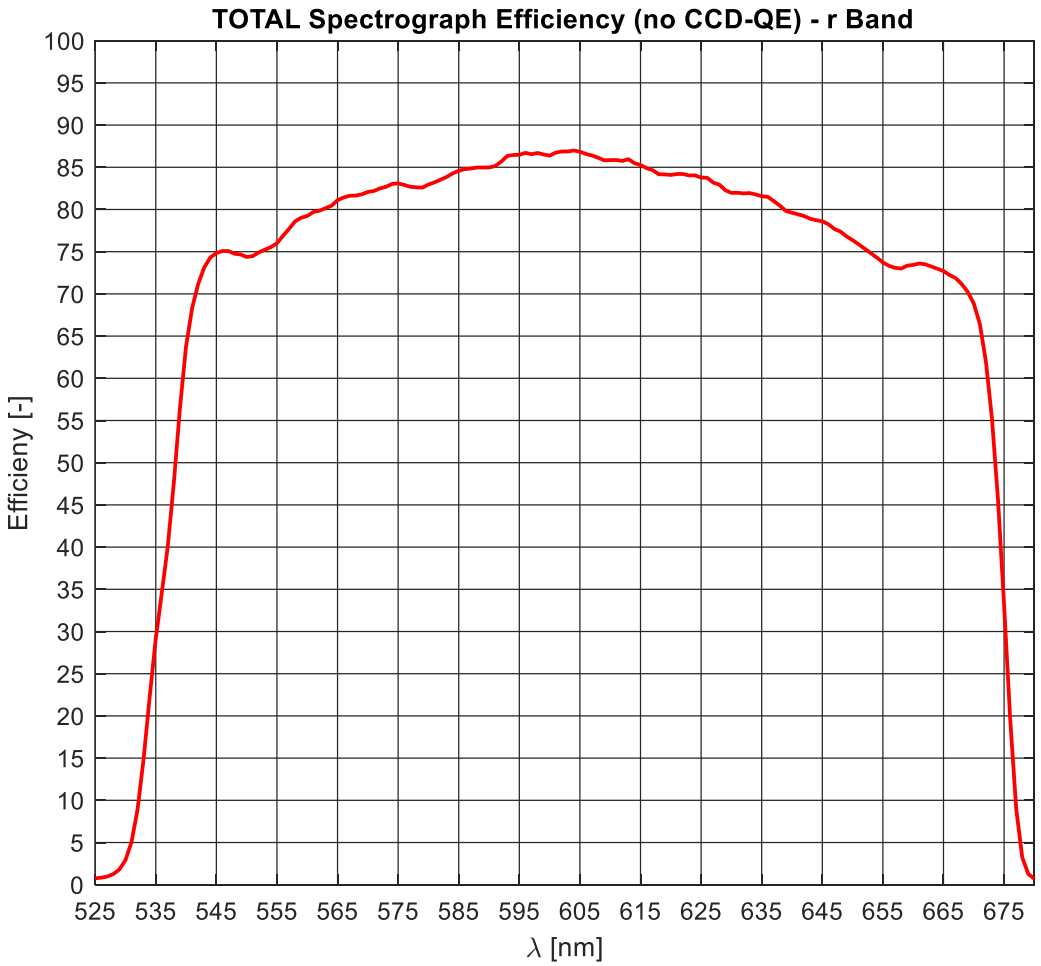

Figure 117. UV-VIS r-band total efficiency. No CCD-QE included.

6.1.11.4 i-band

The i-band spectrograph efficiency (so, no telescope, no CP, no CCD-QE) is computed by multiplying the data of the following elements:

- A, Fold mirror
- B, collimating OAP
- C, dichroic in transmission
- D, dichroic in transmission
- E, mirror
- i-band transmission grating
- Camera

Figure 118. UV-VIS i-band total efficiency. No CCD-QE included.

6.2 NIR Spectrograph Efficiency

The NIR Spectrograph is composed by the following optical elements:

- Folding mirror
- Collimator (in double pass)
- Echelle Grating
- Cross-disperser prisms (3 in double pass)
- Field Mirror
- Camera (3 lenses)

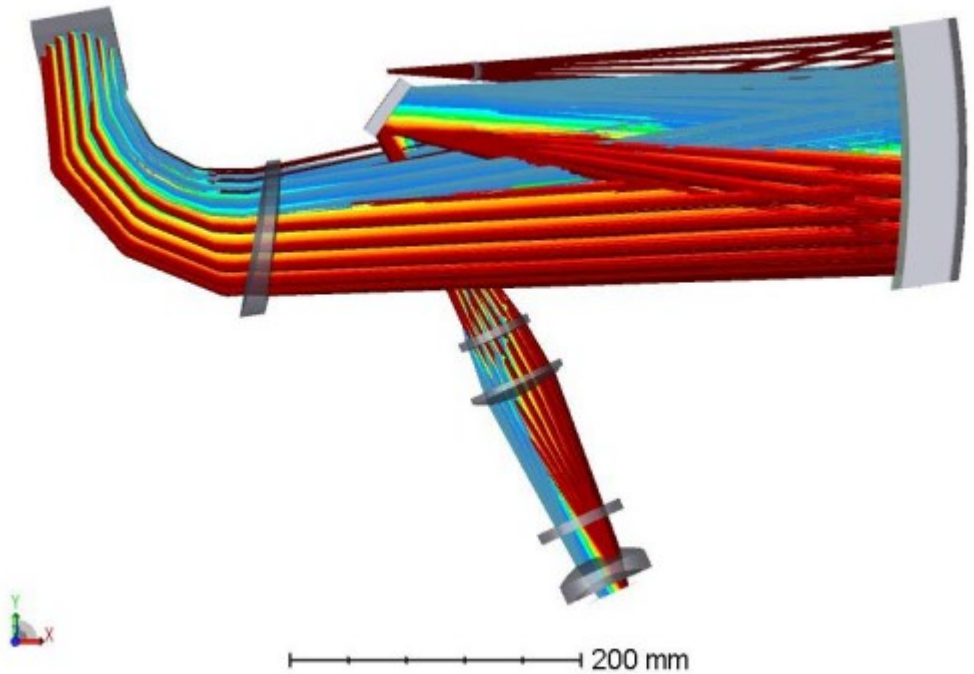

Figure 71: SOXS-NIR Spectrograph Layout.

Figure 119. SOXS NIR spectrograph arm optical layout.

6.2.1 NIR Folding Mirror

The NIR folding mirror, as the other bare gold coated mirrors in the NIR arms, has the following reflectance profile measured by the manufacturer (ASTRON). Below, the extrapolated data in the SOXS-NIR range.

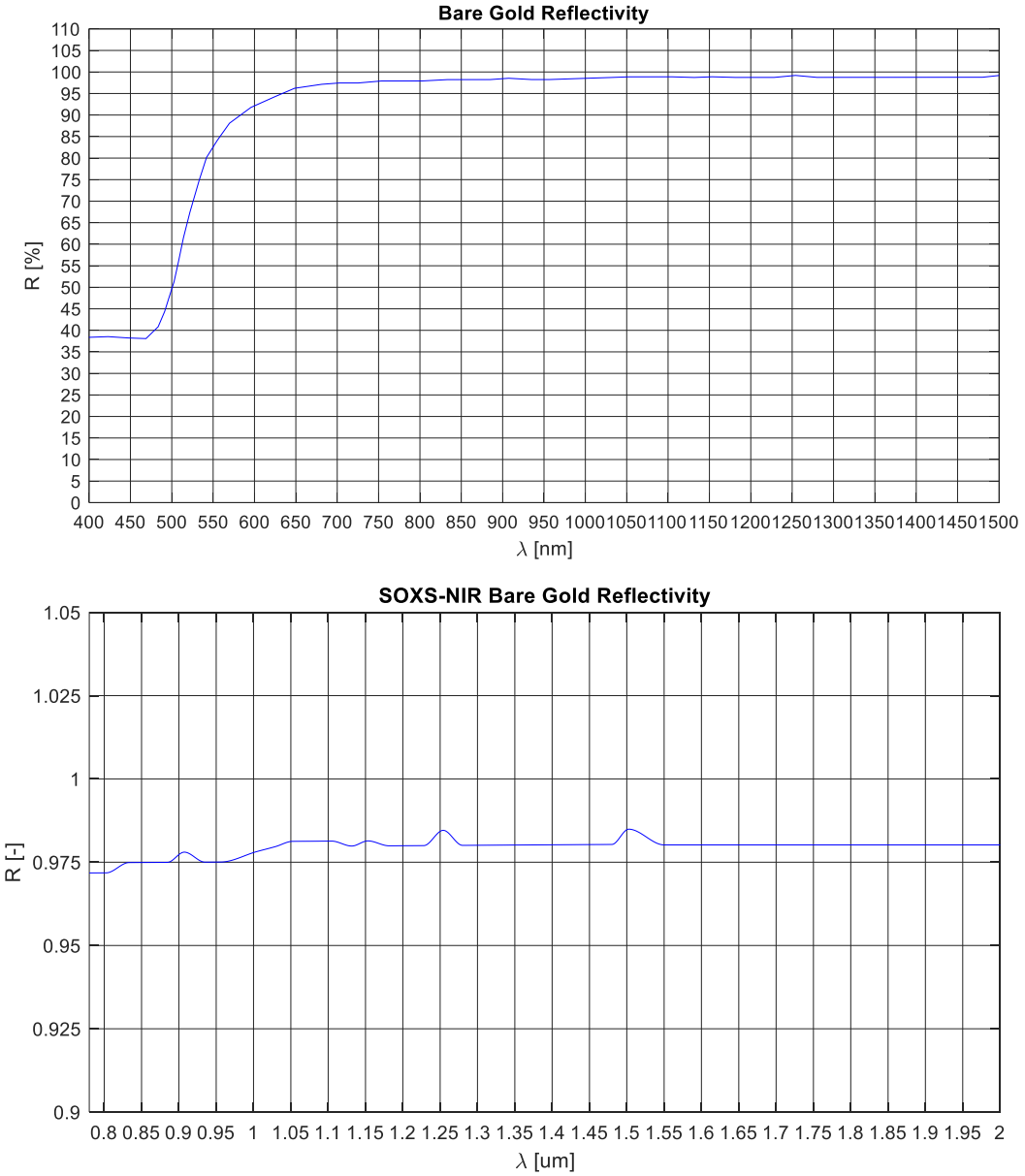

Figure 120. NIR folding mirror reflectivity curve. Top panel: data from manufacturer. Bottom panel: extracted curve used for the computation.

6.2.2 NIR Collimator

The collimator is made by the collimator-mirror and corrector-lens in double pass. The data for the bare gold mirror are the same as for the folding mirror (see previous sub-section); while the AR coating measurement for the corrector lens were provided by the lens manufacturer (Officina Stellare).

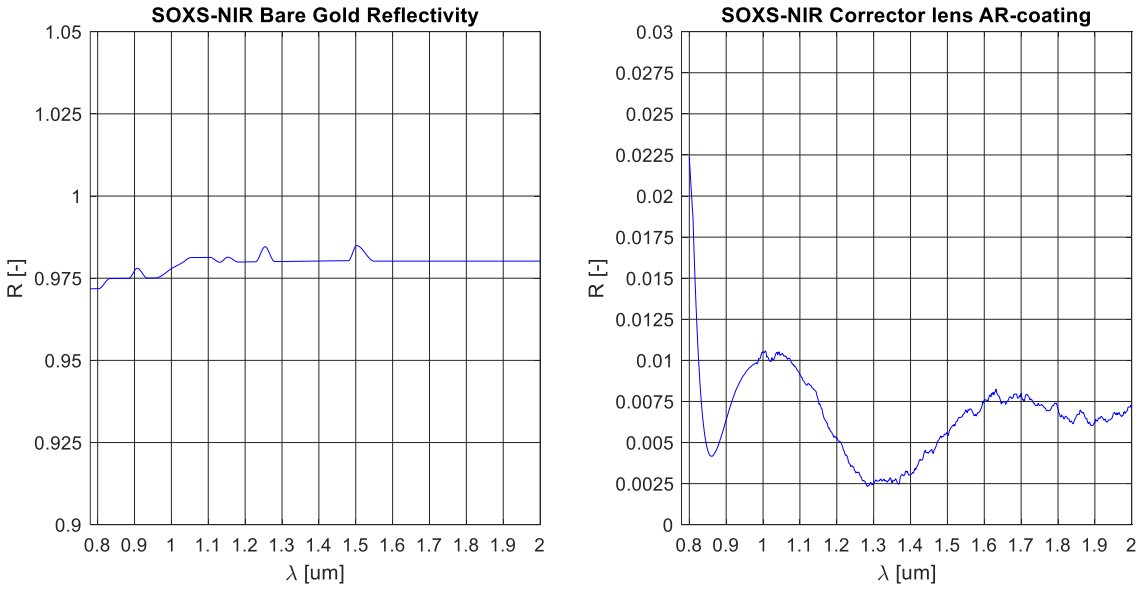

Figure 121. NIR collimator measurement data from manufacturers. Left panel: Collimator mirror reflectance. Right panel: Corrector lens AR coating reflectance.

The total collimator transmission in double pass is computed considering the mirror refelctance and lens transmission (AR coating on both surfaces plus the glass, INFRASIL 302, internal transmission considered as a constant value = 0.9925 for 10 mm thickness)

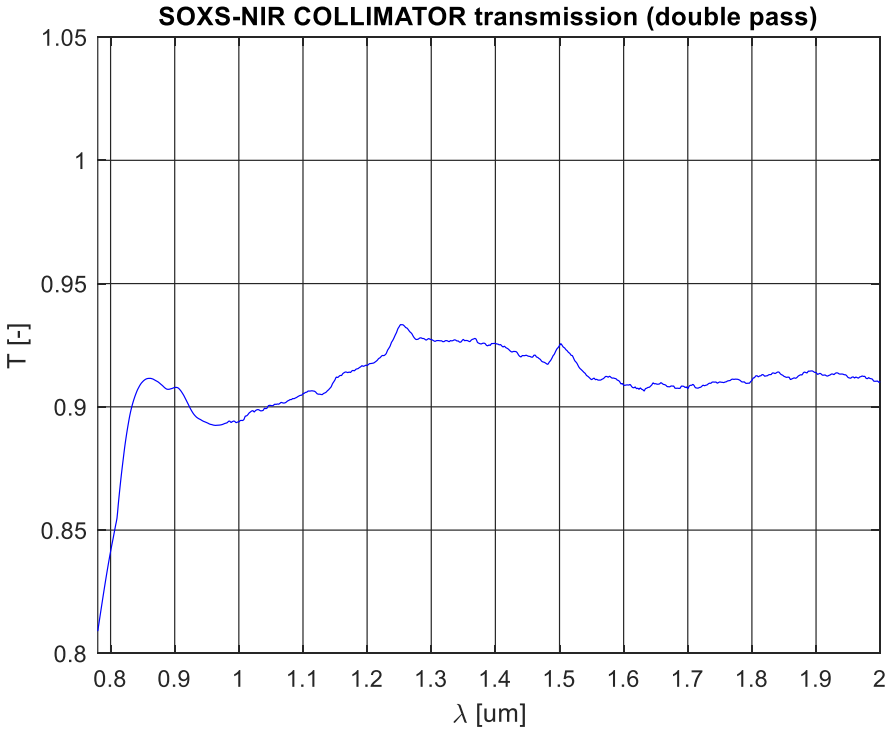

Figure 122. NIR Collimator computed transmission curve in double pass. This is the curve used for the NIR arm total instrumental efficiency.

6.2.3 Echelle Grating

The echelle grating has been manufactured by Richardson-Gratings. A report with measured diffraction grating efficiency of some orders has been delivered, an example is shown here.

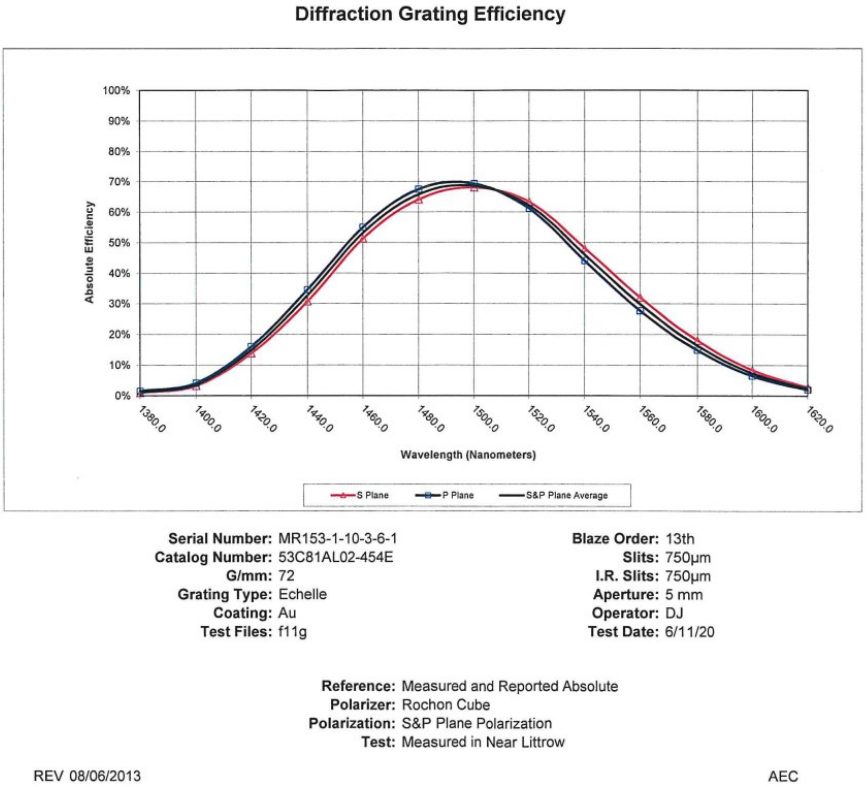

Figure 123. NIR Echelle grating diffraction efficiency from Richardson-Gratings. Example of a single order (13).

The extrapolated data curve for all diffraction orders is the following, and the one used for the estimation of the total NIR spectrograph efficiency.

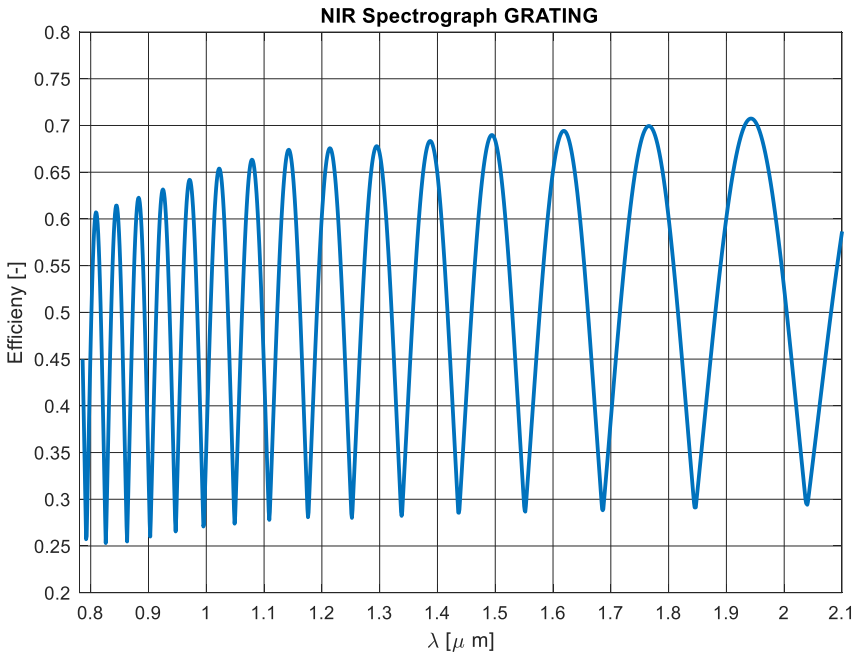

Figure 124. NIR Echelle grating diffraction efficiency curve for the whole NIR range.

6.2.4 NIR Cross-Disperser

The NIR cross-disperser is composed by 3 prisms in double pass. The 3 prisms are made in CLEARTRAN. The manufacturer delivered the measures for the AR-Coatings on both sides of the prisms, at two different AOI according to the working angle of the prisms.

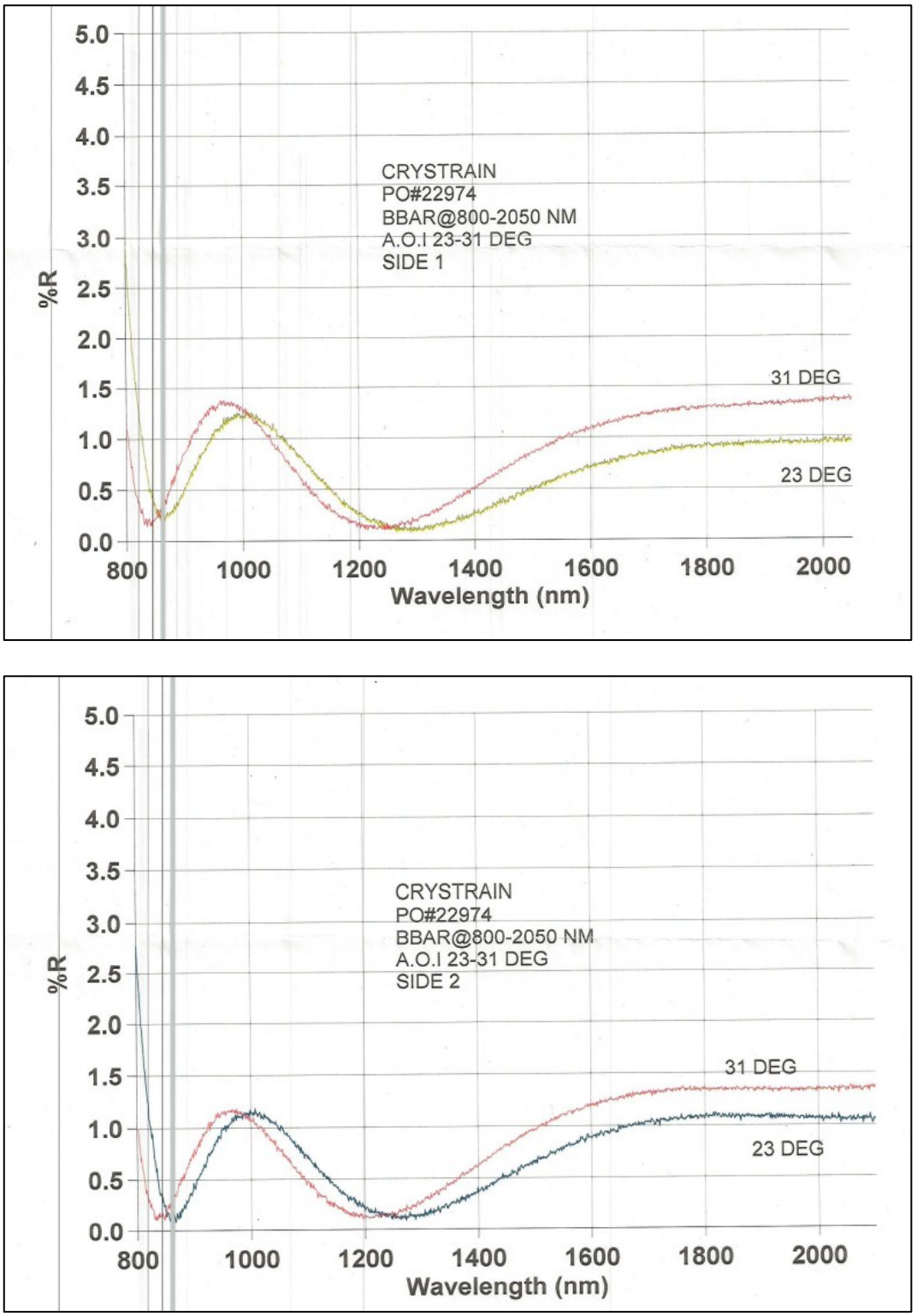

Figure 125. NIR prisms cross disperser AR coating curves delivered by the manufacturer (Crystran). Plot of the two extreme working AOI at prisms surfaces.

According to the optical path, the 1st and 2nd prisms work at 23 deg AOI in the first pass, while the 3rd one works at 31 deg. In the second pass all the prisms work at different angles according to the diffraction order and wavelengths along each diffraction order, but considering all the prisms at 31 deg is a good compromise to simulate the prisms behavior (even though it does not fully match the real one).
For the glass, CLEARTRAN, internal transmission a model with a medium thickness of 18 mm is implemented for the total single prism efficiency calculation.
In the following the prisms transmission in first pass.

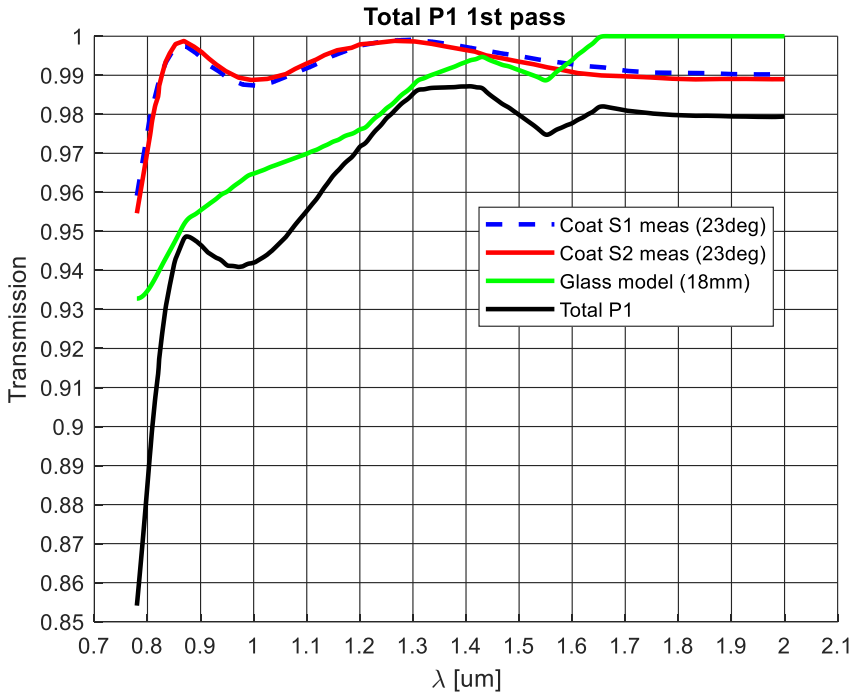

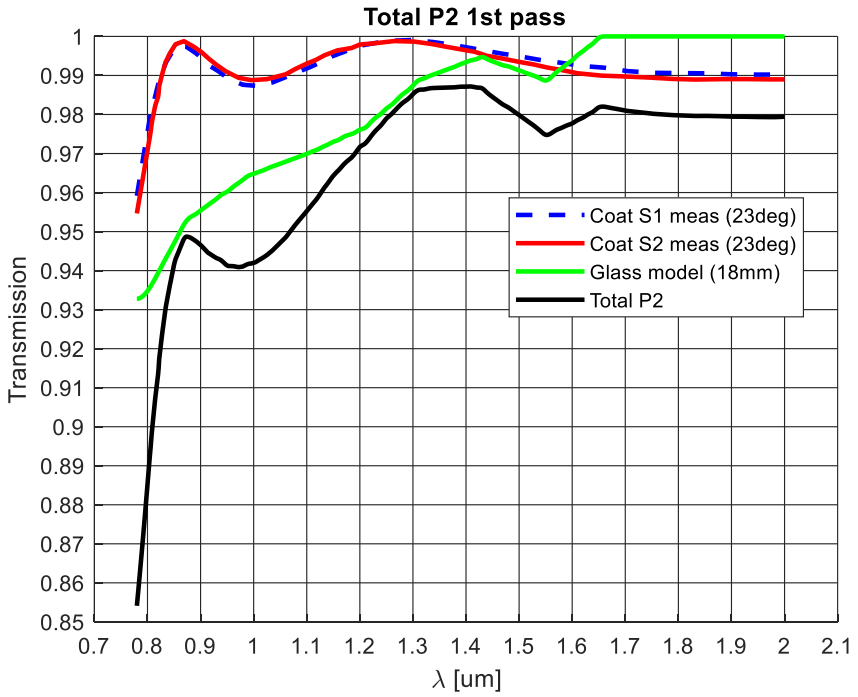

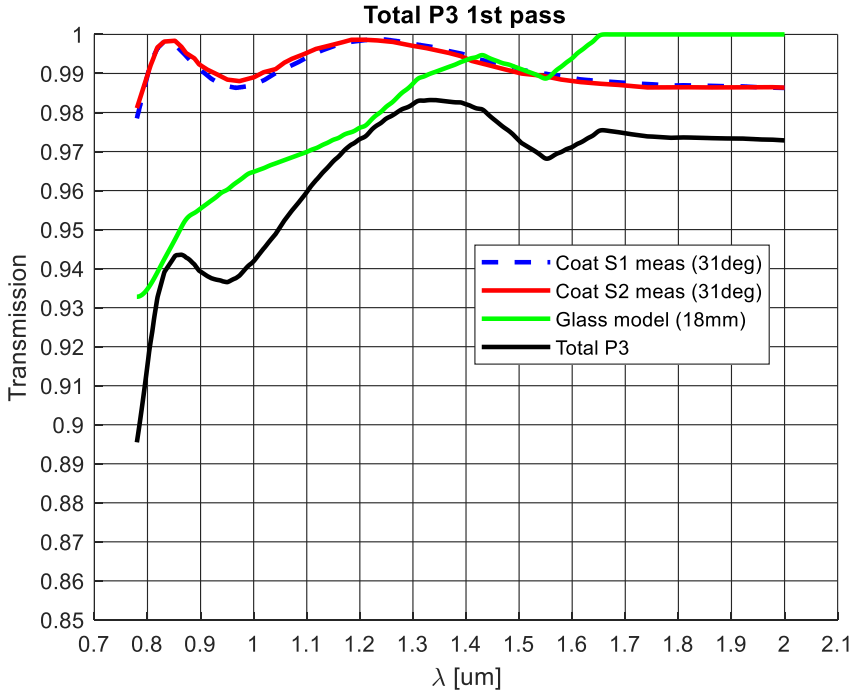

Figure 126. NIR prisms total transmission plot for the single prisms in single pass. The legend in the plots explain the different curve meaning.

In the following the prisms transmission in second pass.

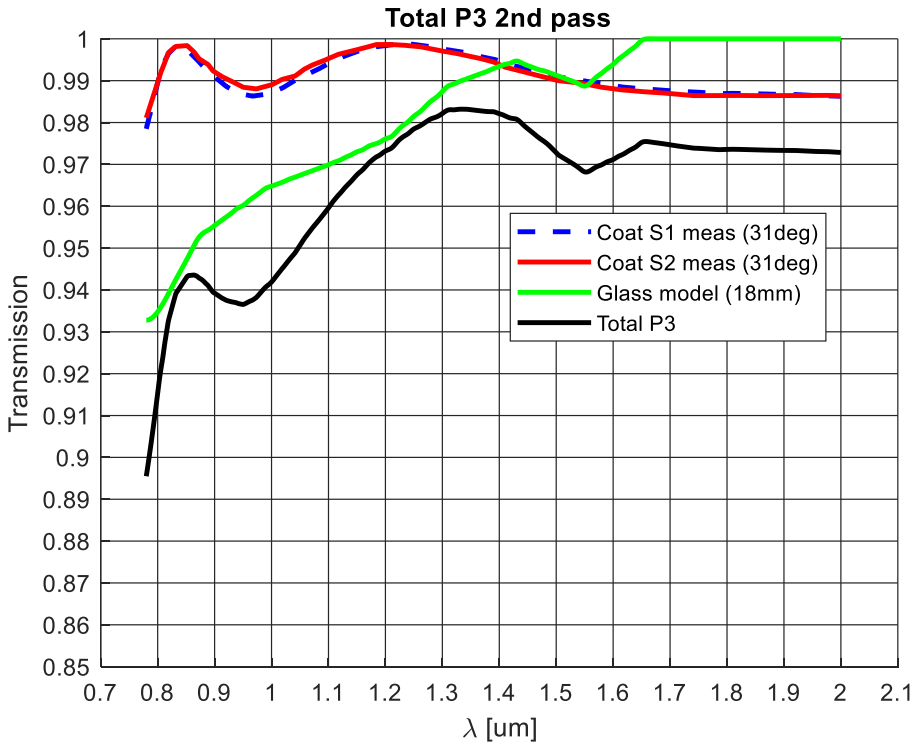

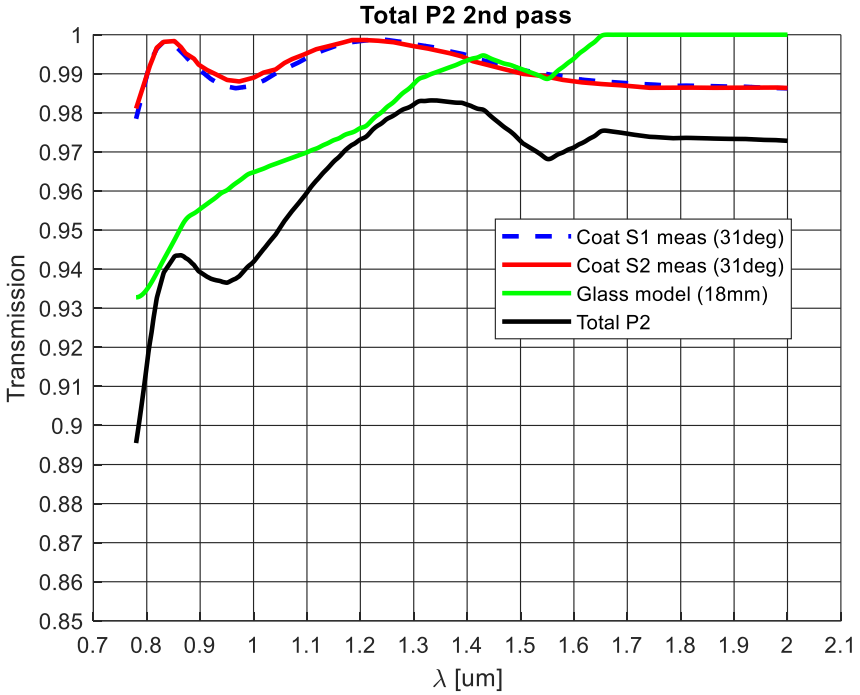

Figure 127. NIR prisms total transmission plot for the single prisms in *double pass*. The legend in the plots explain the different curve meaning. These ones are the curves used for the total cross-disperses transmission calculation.

The total Cross-Disperser transmission is the product of the six curves, it is shown in the next plot. This is the curve considered for the total NIR spectrograph efficiency computation.

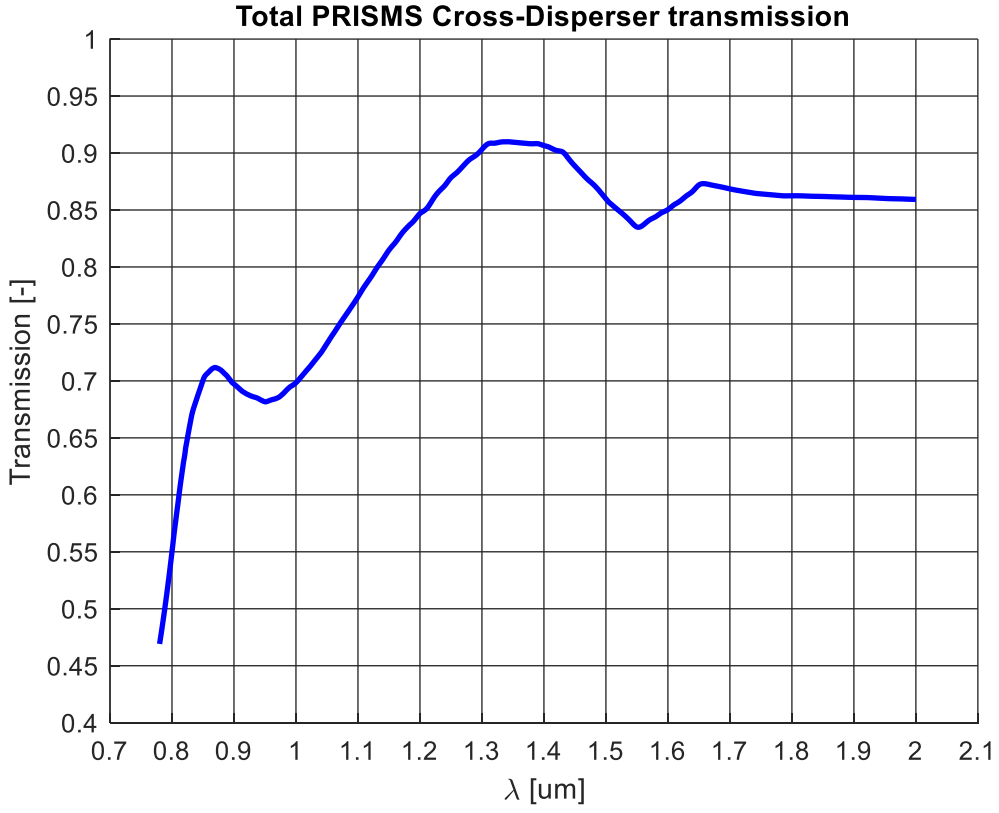

Figure 128. NIR prisms cross-disperser unit total transmission. This is the curve considered for the total NIR spectrograph efficiency computation.

6.2.5 NIR Field Mirror

The NIR folding mirror has the same reflectivity of the NIR folding mirror. (See also sec. 6.2.1).

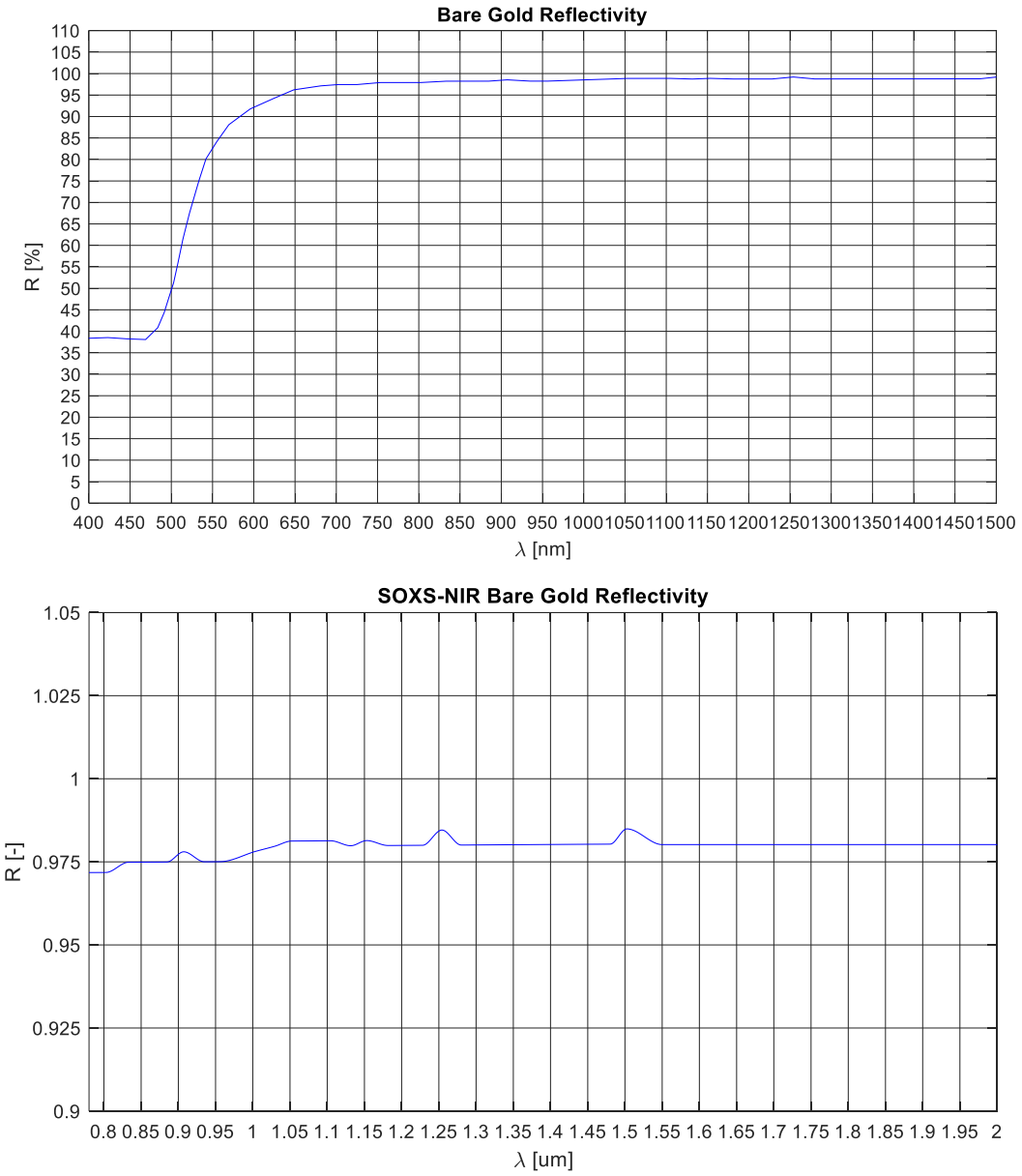

Figure 129. NIR field mirror reflectivity curve. Top panel: data from manufacturer. Bottom panel: extracted curve used for the computation.

6.2.6 NIR Camera

The camera is composed by 3 lenses, 2 in CLEARTRAN, 1 inCAF2. The data of AR-Coatings are provided by the lenses manufacturer, OPTIMAX.
For the lenses in CLEARTRAN, the surfaces has the following ARCoatings

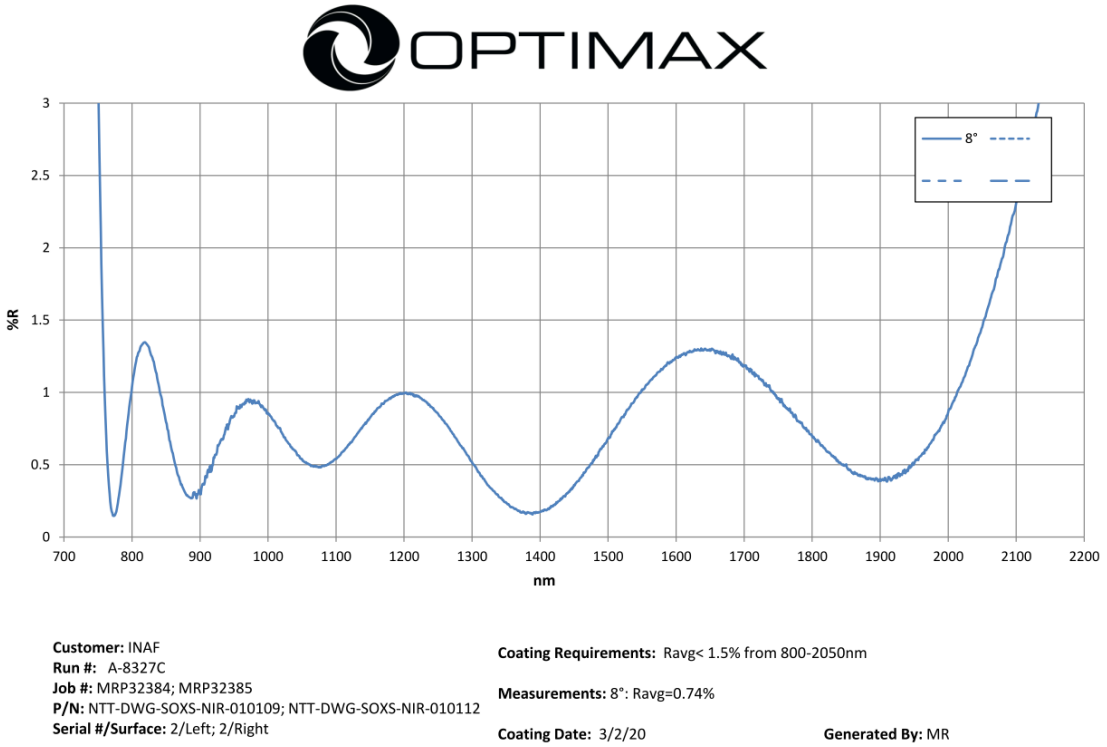

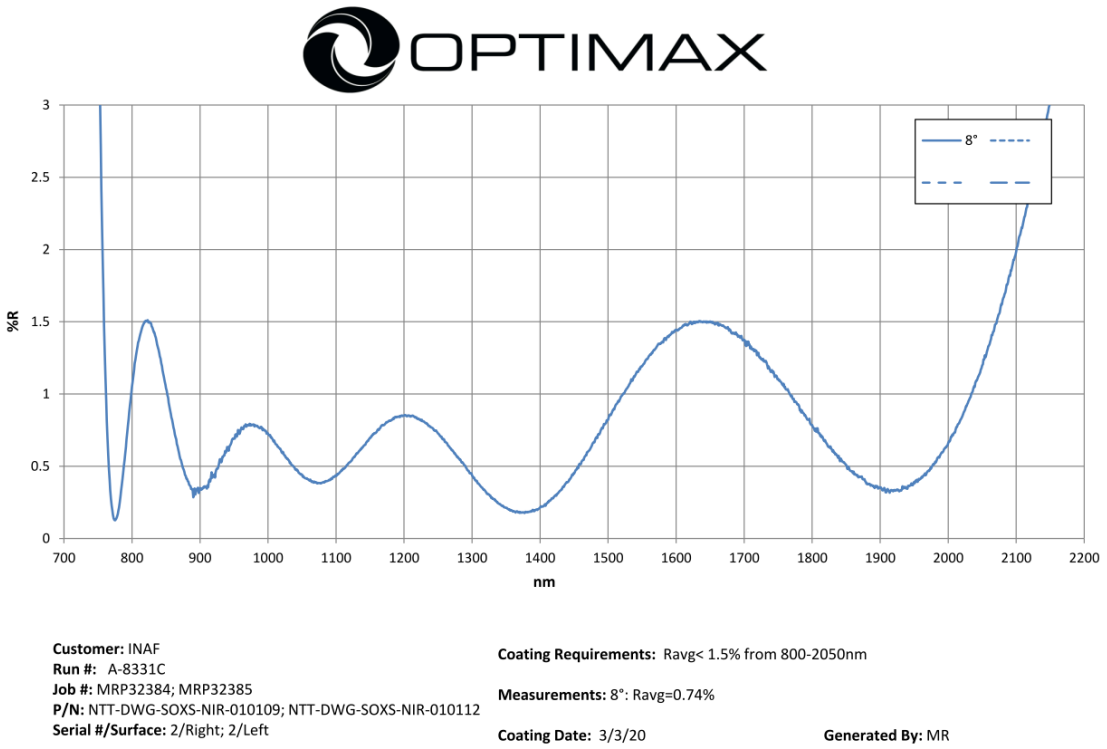

Figure 130. NIR Camera AR coatings curves for the CLEARTRAN lenses. Data provided by the manufacturer (OPTIMAX).

The lens in CAF2 has the following AR-Coatings:

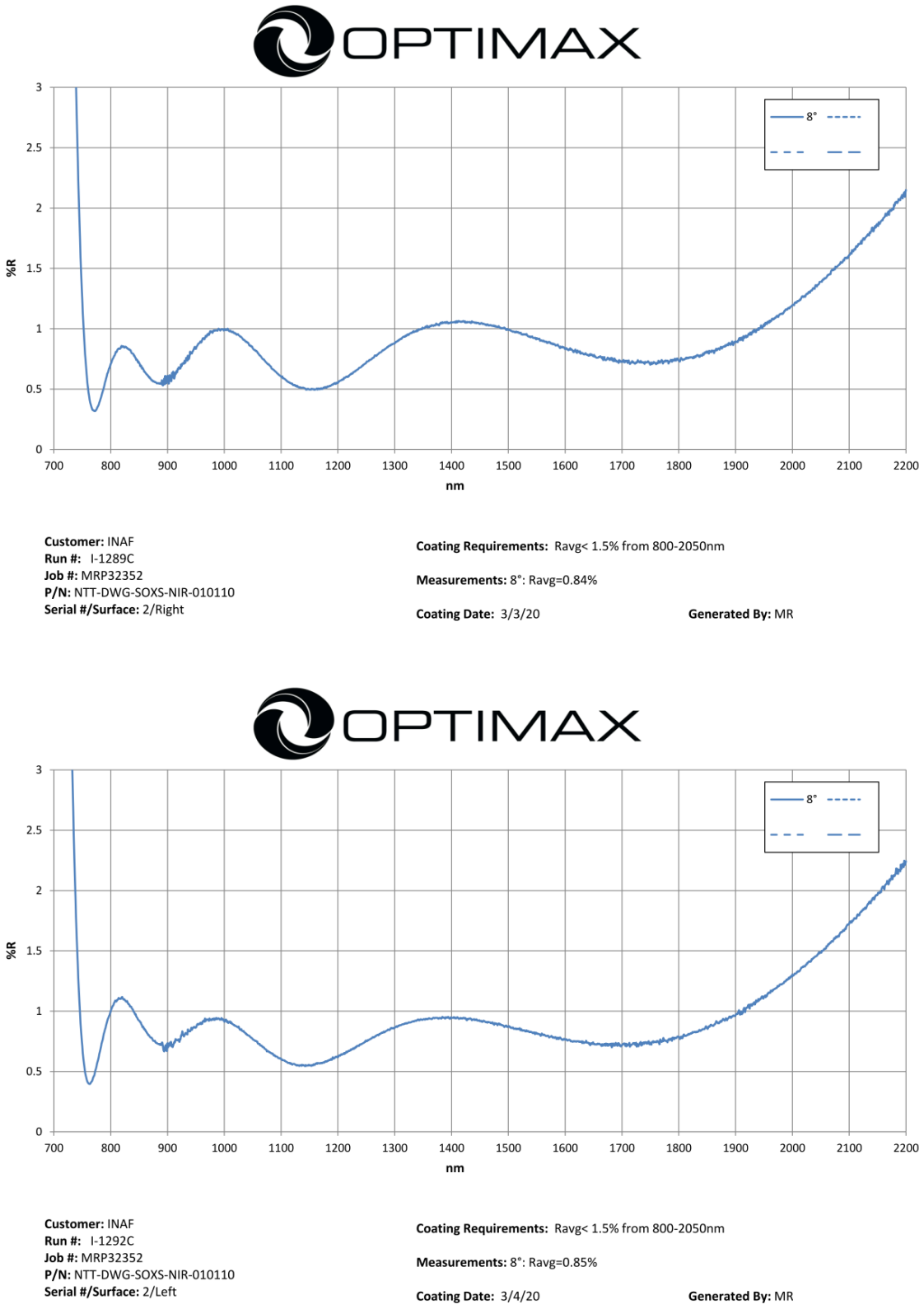

Figure 131. NIR Camera AR coatings curves for the CAF2 lens. Data provided by the manufacturer (OPTIMAX).

From these AR-Coatings data and a model of the glasses (CLEARTRAN and CAF2), we estimated the transmission of each lens and compare this estimation with lab-measurements.

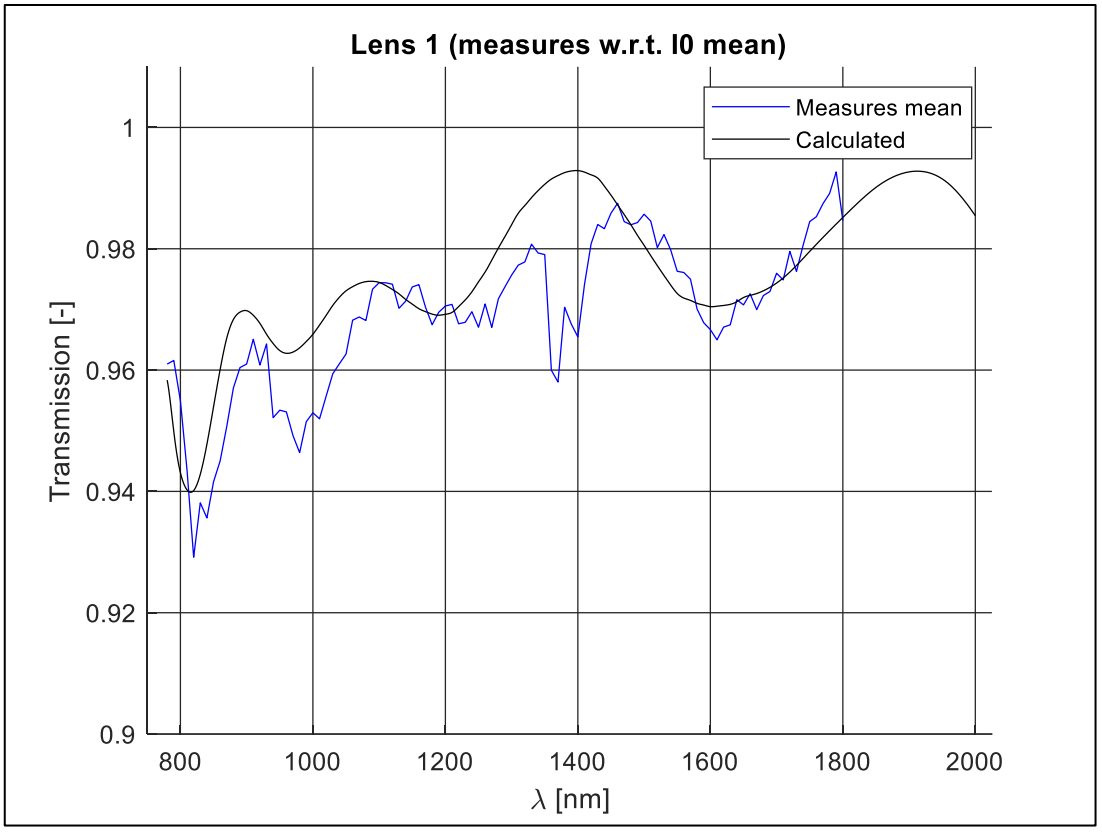

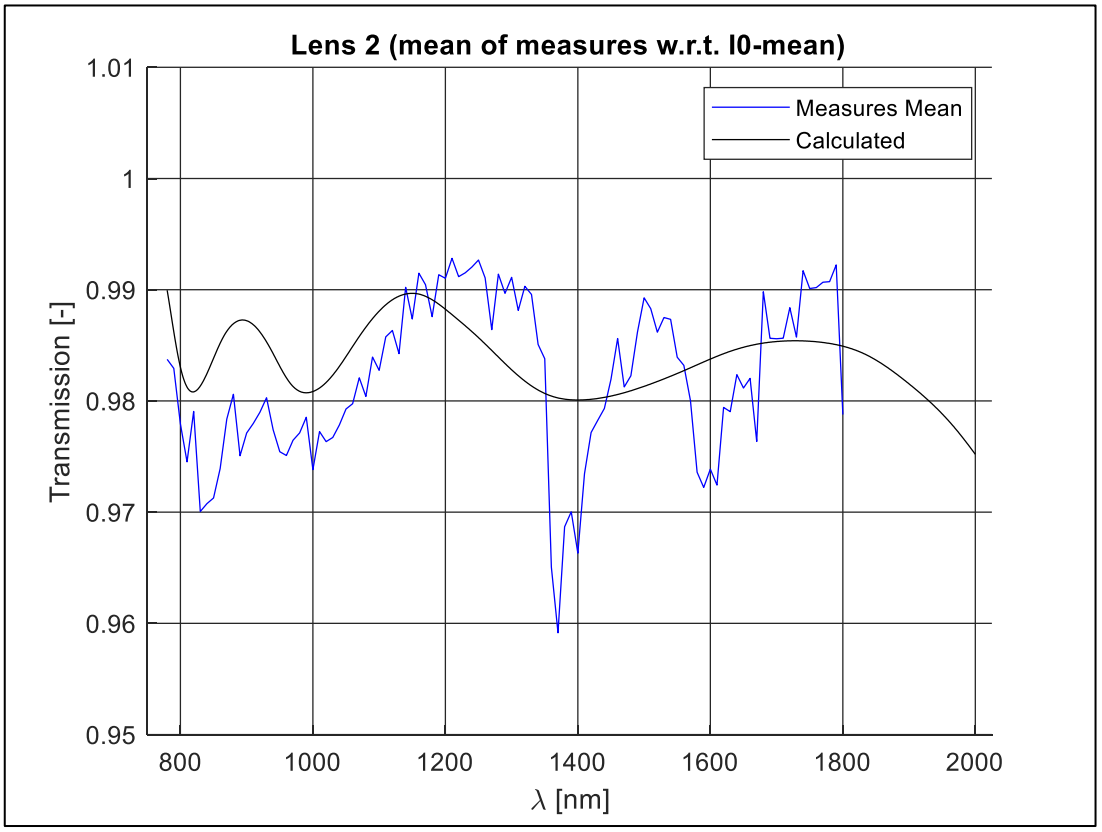

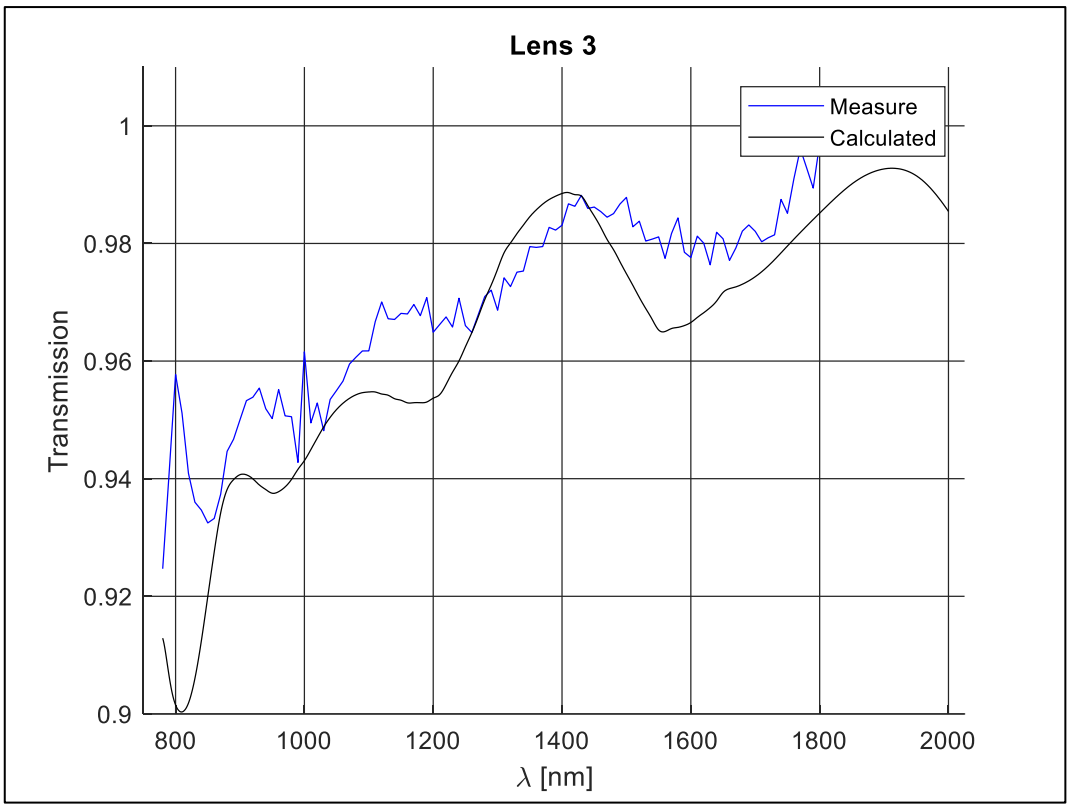

Figure 132. NIR camera single lenses transmission curves. Comparison between calculation (AR data and glasses internal transmission models) and measurements taken in laboratory.

The total NIR Camera transmission is derived from the calculation compared with measures. This is the curve considered for the total NIR spectrograph efficiency computation.

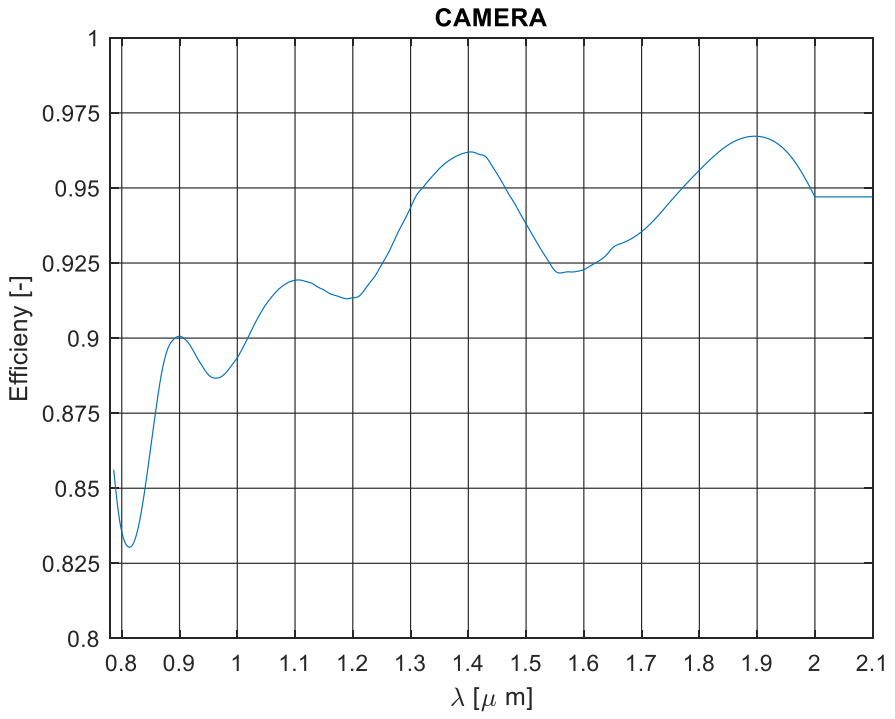

Figure 133. NIR Camera total transmission curve. This is the one used for the NIR arm total instrumental efficiency.

6.2.7 NIR Spectrograph efficiency

The total NIR spectrograph efficiency is computed by multiplying all the elements transmission.

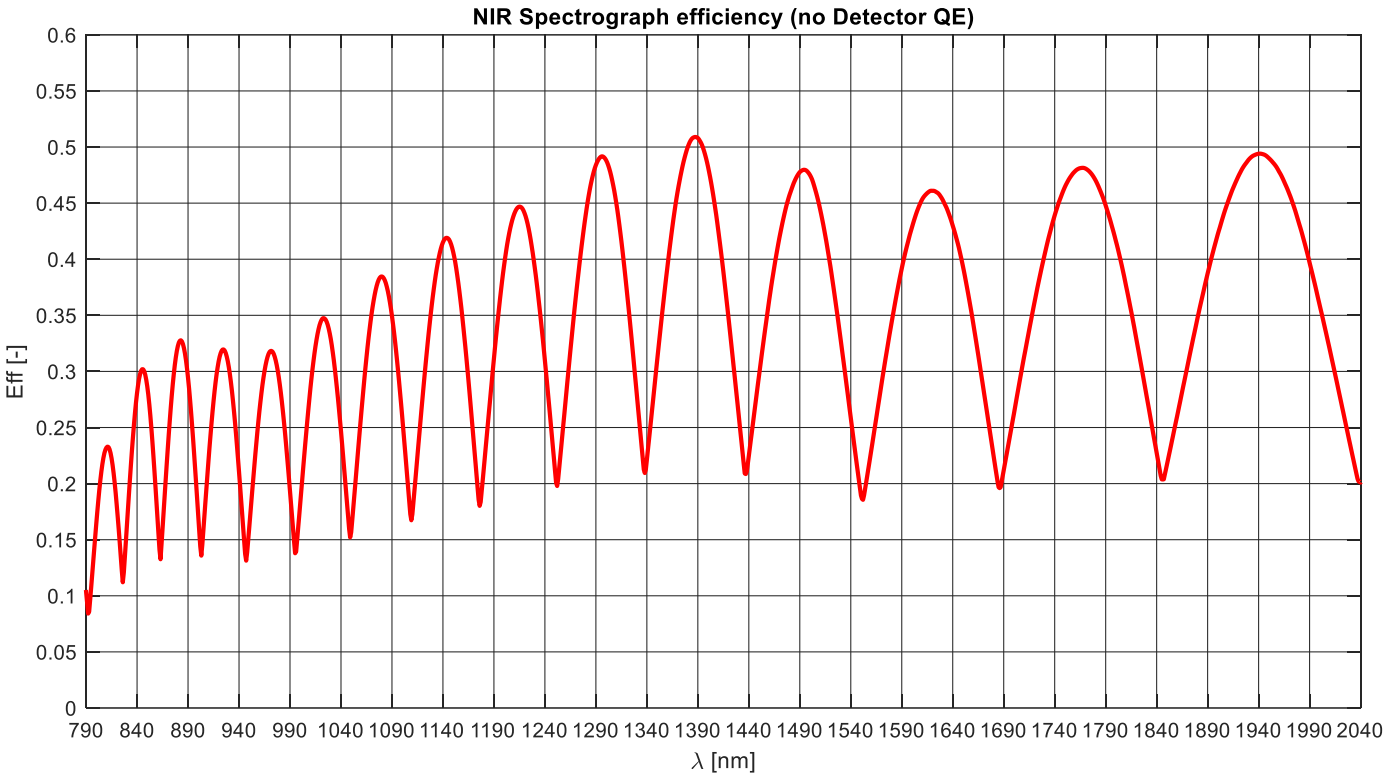

Figure 134. SOXS NIR spectrograph total instrumental efficiency (from slit to detector excluded).

Abbreviations and Acronyms

AD	Applicable Document
AI	Action Item
CP	Common Path
DRD	Document Requirement Description
DFS	Data Flow System
DRS	Data Reduction Software
ETC	Exposure Time Calculator
ESO	European Southern Observatory
FDR	Final Design Review
FITS	Flexible Image Transport System
FOV	Field Of View
HW	HardWare
ICD	Interface Control Document
ICS	Instrument Control Software
MoU	Memorandum of Understanding
NGC	New Generation Controller
NTT	New Technology Telescope
PAC	Provisional Acceptance Chile
PAE	Preliminary Acceptance Europe
PDR	Preliminary Design Review
PDP	Preliminary Design Phase
QTH	Quartz Thorium
RD	Reference Document
RON	Read Out Noise
S/N	Signal-to-Noise ratio
SNR	Signal-to-Noise ratio
SRE	Spectral Resolution Element
SoW	Statement of Work
SOXS	Son Of X-Shooter
SW	SoftWare
TBC	To Be Confirmed
TBD	To Be Defined
TCS	Telescope Control System
TLR	Top Level Requirements
TRS	Technical Requirements Specifications
UT	Unit Telescope (of the VLT)
VIC	VLT Instrument Consortium
VLT	Very Large Telescope
WP	Work Package